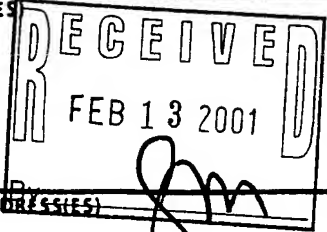


REPORT DOCUMENTATION PAGE

Form Approved
OMB No. 0704-0188

Public reporting burden for this collection of information is estimated to average 1 hour per response, including the time for reviewing instructions, searching existing data sources, gathering and maintaining the data needed, and completing and reviewing the collection of information. Send comments regarding this burden estimate or any other aspect of this collection of information, including suggestions for reducing this burden, to Washington Headquarters Services, Directorate for Information Operations and Reports, 1215 Jefferson Davis Highway, Suite 1204, Arlington, VA 22202-4302, and to the Office of Management and Budget, Paperwork Reduction Project (0704-0188) Washington, DC 20503.

1. AGENCY USE ONLY (Leave blank)		2. REPORT DATE	3. REPORT TYPE AND DATES COVERED
		June 30, 1997	FINAL 9/1/92-6/30/97
4. TITLE AND SUBTITLE		5. FUNDING NUMBERS	
Enhancing Clark Atlanta University Participation in Defense Research		DAAL03-92-G-0380	
6. AUTHOR(S)		7. PERFORMING ORGANIZATION NAME(S) AND ADDRESS(ES)	
Kofi B. Bota, Ph.D.		 Clark Atlanta University 223 James P. Brawley Drive, SW Atlanta, GA 30314 FEB 13 2001	
8. PERFORMING ORGANIZATION REPORT NUMBER		9. SPONSORING/MONITORING AGENCY NAME(S) AND ADDRESS(ES)	
ARO 30231.1-MA- HDR		U.S. Army Research Office P. O. Box 12211 Research Triangle Park, NC 27709-2211	
10. SPONSORING/MONITORING AGENCY REPORT NUMBER		11. SUPPLEMENTARY NOTES	
12a. DISTRIBUTION/AVAILABILITY STATEMENT		12b. DISTRIBUTION CODE	
Approved for public release; distribution unlimited.			
13. ABSTRACT (Maximum 200 words)		<p>The Army-supported research program focused on interdisciplinary research areas in environmental technologies: flow, structures and materials, and software engineering. The program aimed at enhancing CAU's research capabilities, through development of resources and facilities (including equipment and personnel) in areas relevant to the Department of Defense. Several projects were executed to develop expertise and research programs that fall within the mission goals and program objectives of the Department of Defense.</p> <p>20010223 100</p>	
14. SUBJECT TERMS		15. NUMBER OF PAGES 213	
		16. PRICE CODE	
17. SECURITY CLASSIFICATION OF REPORT UNCLASSIFIED	18. SECURITY CLASSIFICATION OF THIS PAGE UNCLASSIFIED	19. SECURITY CLASSIFICATION OF ABSTRACT UNCLASSIFIED	20. LIMITATION OF ABSTRACT UL



**ENHANCING CLARK ATLANTA UNIVERSITY
PARTICIPATION IN DEFENSE RESEARCH**

VOLUME I

**FINAL RESEARCH PROJECT REPORT
PROJECT DIRECTOR: DR. KOFI B. BOTA**

SEPTEMBER 1, 1992 – JUNE 30, 1997

CONTRACT NUMBER DAAL03-92-G-0380

**CLARK ATLANTA UNIVERSITY
223 JAMES P. BRAWLEY DRIVE, SW
ATLANTA, GEORGIA 30314**

TABLE OF CONTENTS

SECTION 1: EXECUTIVE SUMMARY.....	4
1.1 Objectives.....	4
1.2 Research Programs.....	4
SECTION 2:	
2.1 Groundwater Modeling and Contaminant Transport.....	6
2.2 Development of Pulsating Medical Waste Incinerator	12
2.3 Study of the Effects of Ambient Conditions Upon the Performance of Fan Powered, Infrared, Natural Gas Burners.....	24
2.4 Development of a Two Stage, Pulse Combustion, VOC Destruction Technology.....	29
2.5 Preliminary Study of Droplet Behavior Under Various Pressures.....	34
2.6 Waste Form Development for Use with ORNL Waste Treatment Facility Sludge	42
2.7 The Application of Plasma ARC Torch in the Vitrification of Hazardous and Simulated Radioactive Mixed Waste.....	51
2.8 The Application of Geographic Information Systems (GIS) in Environmental Assessment, Restoration, Modeling and Management	57

TABLE OF CONTENTS (Continued)

2.9	Atlanta Electronic Commerce Resource Center Integrating Computer-Based Distance Learning.....	66
2.10	Turbulent Premixed Methane-Air Combustion	70
2.11	Optimization of Non-Thermal Discharge (NTD) Electrochemical Systems	75

SECTION 1: EXECUTIVE SUMMARY

1.1 Objectives

The Army-supported research program entitled "Enhancing Clark Atlanta University Participation in Defense Research" (Grant #DAA203-92-9-03890), focused on interdisciplinary research areas in environmental technologies: flow, structures and materials; and software engineering. The program aimed at enhancing CAU's research capabilities, through development of resources and facilities (including equipment and personnel) in areas relevant to the Department of Defense. Several projects were executed and several faculty members were supported to develop expertise and research programs that fall within the mission goals and program objectives of the Department of Defense.

1.2 Research Programs

This final report is organized into two volumes. Below is a listing of the research projects covered by each volume:

Volume I

- Groundwater Flow and Contaminant Transport Modeling
- Development of a Pulsating Medical Waste Incinerator
- Study of the Effects of Ambient Conditions Upon the Performance of Fan Powered, Infrared Natural Gas Burners
- Development of a Two Stage, Pulse Combustion, VOC Destruction Technology
- Preliminary Study of Droplet Behavior Under Various Pressures
- Waste Form Development for Use with ORNL Waste Treatment Facility Sludge
- The Application of Plasma ARC Torch in the Vitrification of Hazardous and Simulated Radioactive Mixed Waste
- The Application of Geographic Information Systems (GIS) in Environmental Assessment, Restoration, Modeling and Management
- Atlanta Electronic Commerce Resource Center Integrating Computer-Based Distance Learning
- Turbulent Premixed Methane-Air Combustion
- Optimization of Non-Thermal Discharge (NTD) Electrochemical Systems

Volume II

- Health Monitoring of Concrete Structures Using Distributed Time Domain Reflectometry (ETDR) Sensors
- Elastically Tailored Composite Design

- Long term durability of polymer matrix composites for high temperature applications
- Blended-wing-body structural technology study
- Finite element and analytical cross-sectional, analysis of composite rotor blades for nonclassical beam formation
- Finite deformation response of unsymmetric composite laminates in the presence of damage
- High performance computing techniques in fluid structure interaction problems
- Constitutive modeling and testing of polymer matrix composites incorporating physical aging at elevated temperature
- Modeling and testing of hybrid titanium composite laminates at normal and elevated temperatures
- Low density, low conductivity PAN ablative optimization and nozzle fabrication
- Compressive creep of IM7/K3B composite and the effects of physical aging on viscoelastic behavior
- Characterization and mechanical testing of a polarization maintaining optical fiber - Phase II
- Micromechanics modeling of fiber reinforced composites incorporating distinct interface properties
- Sol-gel based mullite ceramics
- Zirconia-toughened alumina ceramics
- Mechanical and physical testing of a polarization-maintaining optical fiber
- Superconducting materials processing
- Investigation of front frame failure in high performance aircraft engines
- Research in structural dynamics and control and aeropropulsion
- Unsteady aerodynamics of rotor-stator interactions
- An adaptive flow solver for air-borne vehicles undergoing time-dependent motions/deformation
- Unsteady aerodynamics of airfoils undergoing large amplitude motion/deformations: Parallel implementation of incompressible viscous flows
- High frequency response of a new fiberoptic probe for temperature fluctuation measurements
- Experimental investigation of flow disturbances in constricted arteries
- Thermal analysis of a novel axial power monitor for nuclear reactors
- Model studies of heart valve motion under pulsatile flow

2.1 GROUNDWATER MODELING AND CONTAMINANT TRANSPORT

Investigators: D. Chen, L. Moeti, B. Vona and Y. Yeboah

Collaborators: Robert Carsel, EPA, Athens, GA

INTRODUCTION

Nationwide, Superfund sites are located in many diverse hydrogeologic environments (e.g., multiple aquifer systems, fractured and/or karst systems, and systems with wide variations in depth to the water table). In addition, recharge can vary widely because of hydromodifications and/or climate. Also, domestic and irrigation wells, which pump at different and varying rates, are commonly located throughout these sites. Therefore, the ability to model transient flow conditions (i.e., transient recharge, a fluctuating water table, and transient pumping from a variety of points in x, y, z space) for a wide variety of hydrogeologic conditions is important.

Contamination scenarios within Superfund sites must consider multiple point and nonpoint source loadings which vary both spatially and temporally. Chemical loadings to the subsurface are affected by surface processes and source control management practices. Most of these processes require detailed modeling of subsurface flow and transport.

Several models are capable of simulating the transport and transformation of chemicals in the soil subsurface. None of these models, however, has been linked together in such a way as to yield a complete simulation package that provide consistent set of linked unsaturated zone models that have the flexibility to handle a wide variety of hydrogeologic soils, climate, and source control scenarios. The formulation of the risk analysis problem, however, requires more than a simple, deterministic evaluation of potential exposure concentrations. The inherent variability of force, capacitance and resistance in natural systems, combined with the inability to exactly describe these attributes of the system, suggest that exposure concentrations cannot be predicted with certainty. Therefore, the uncertainty associated with the predictions must be quantified.

Numerical models provide the greatest flexibility and accuracy in representing complex environments and can be applied to nearly all types of hydrogeologic settings. The models can also be used to predict the dynamic aspects within a Superfund site, such as changes in the size of the chemical plume resulting from natural or man-made effects.

Disadvantages for this method include costs that are high relative to other methods and the need for considerable technical expertise in hydrogeology and modeling.

OBJECTIVES

Exposure assessment and remedial investigation are required at Superfund sites to address groundwater contamination under the Comprehensive Environmental Response, Compensation and Liability Act (CERCLA), as amended by the Superfund Amendments and Reauthorization Act (SARA). Prediction of spatial and temporal movement of contaminant potential migration using a three-dimensional groundwater and solute advective-dispersive-sorptive transport model is an important issue in the overall evaluation of groundwater assessment and remedial design at Superfund sites. The particular objective of the groundwater and solute transport modeling was to find out if two-plumes at Site-38 merge together and migrate to the Pensacola Bay in five years. During this period, the remedial design for the site will be completed and remedial performance will start.

APPROACH

A three-dimensional finite element model of density-dependent flow and transport through saturated-unsaturated porous media (FEMWATER) was applied to simulate the subsurface system at the Superfund site. FEMWATER was developed by G. T. Yeh at Pennsylvania State University and interfaced with the US Corp of Engineers Waterways Experimental Station Groundwater Modeling System (GMS), a pre- and post-processing software for data manipulation and data analysis. The GMS includes a Geographic Information System (GIS) link and model input/output (visualization) technology. A modeling practice always starts from conceptual model development and proceeds to parameter identification, mesh generation and boundary condition assignment, model calibration and sensitivity study, routine simulation, and presentation of predictive results. Initial work was conducted on databases from the Florida Superfund site with the GIS software package ARC/INFO to develop the necessary data to support conceptual model development and provide spatial, temporal and hydrogeological input parameters. Visualization technology provided by both GIS and GMS greatly enhanced the modeling application through each modeling step.

ACCOMPLISHMENTS

Technical Results and Discussion

Development of a Conceptual Model

The NAS Pensacola is located in the Gulf Coast lowlands on a peninsula bounded by Pensacola Bay to the south and east and Bayou Grande to the north. Three main regional hydrogeologic units have been defined with the stratigraphy beneath the Florida Panhandle: The Surficial/Sand-and-Gravel Aquifer, The Intermediate System, and the

Floridan Aquifer System. The Surficial zone is contiguous with land surface and contains groundwater under water table or perched conditions. The Surficial zone is approximately 30 to 40 feet thick and is generally composed of a poorly graded quartz sand. Depth to groundwater ranges from 0 to 20 feet depending on ground surface elevation. Aquifer tests have yielded high hydraulic conductivities, on the order of 10^1 to 10^2 feet/day. Shallow groundwater flow is generally influenced by topography, usually resulting in flow toward and discharge to, the nearest surface water body such as ditches.

A plume of VOC and SVOC contaminants was detected in the soil and groundwater at Building 71 centered beneath the building and extending into the west yard and to the seawall. A chlorinated hydrocarbon plume was detected extending southward from the former underground storage tank at Building 604. Inorganic contaminants were detected over a broader area of the site. Current receptors are the Surficial zone and Pensacola Bay. The risk assessment considered the Surficial/Sand-and-Gravel Aquifer as exposure media.

Figure 1-1 is a NAS Pensacola location map for the Site 38 study area. The map was produced by GIS ARC/INFO. The Pensacola GIS databases that we obtained covered a large area of about 7.35×5.85 square miles and contained over 200 megabytes of data on topography, well characteristics and geochemical sampling. The topographic database contained GIS files for displaying topographic contours, roads, buildings, hydrologic characteristics, and vegetation. This database was used to delineate the physiographic boundaries, estimate the groundwater divides, and to provide boundary condition assignments. The GIS software was also used in the project to support a variety of investigation and evaluations using the data query and analysis capabilities. Procedures were developed to summarize information in a variety of forms. For example, to revise and update interpretations of the extent and magnitude of contamination, geochemical database was queried for data on specific contaminants, at specific locations, from a specific time period, and output the information using a table or predetermined symbology on maps that are used as a base on which interpretations are made. Date input procedures were used to upload information from GIS to GMS through converting a GIS file to DXF file format and importing a DXF file into GMS. DXF is a standard file format specified by AutoDesks AutoCAD.

GIS applications, as mentioned above, was employed to mimic manual map-processing techniques, such as map reclassification, overlay and simple buffering around features. The new wave of GIS applications concentrates on *data mining* employing advanced analytical operation, which uses the GIS and GMS to discover relationships among mapped variables. A variety of interpolation schemes are supported by both GIS and GMS including kriging. We attempted to correlate between vegetation parameter and infiltration/evapotranspiration at the site. Unfortunately, there was not enough quantitative vegetation data in the GIS database for analysis. The correlation was then intuitively perceived through visual observation. However, we found that the site is almost entirely covered with concrete or asphalt and only a very limited vegetation area was needed to assign an infiltration/evapotranspiration rate. Secondly, we used the two-

dimensional interpolation module in GMS to interpolate the concentration data from scatter points to obtain a graphical representation of the contaminant plume. In our case, the linear scheme was the preferred procedure.

With the aid of GIS, the regional flow model has been conceptualized as a heterogeneous, three-dimensional, isotropic unconfined aquifer. Neither the transient behavior of the groundwater flow system, nor the tidal effects were presently considered. The solute transport, however, is transient and the simulated period was five years. The aquifer system was represented by an irregular, finite-element mesh consisting of 4752 nodes and 7721 elements, and having eight-layers and horizontal dimensions of about 800 m \times 700 m. The model boundaries along the east and south sides were assigned constant heads (mean sea level). The northern and western boundaries were also established as constant head nodes in accordance with observed water table elevations map. The impermeable bottom of the aquifer was assumed to be no flow, whereas at the top a recharge was infiltrated as 0.00354 m/day with evapotranspiration rate of 0.00066 m/day.

Groundwater modeling of natural phenomena is made complex and difficult by characteristics such as spatial and temporal variability and dominating mechanisms that vary with environmental circumstances. GIS technologies offer powerful tools to deal with some of these problems.

3D Mesh Construction

The finite-element analysis associated with the solution of partial differential equations over the simulated domain were performed using generalized numerical analysis procedures which approximate the continuous problem in terms of a discrete system. A key aspect of the finite element method is the construction of the finite element mesh used to represent the domain over which the analysis technique will be applied. Consideration of the type and distribution of finite elements in the mesh is key because (1) the accuracy and computational efficiency of the finite element method is dictated by type and distribution of finite elements; (2) the generation of the finite element mesh dominates the cost of application of the finite element method. Its construction typically represents 70-80% of the total cost; and (3) the finite element mesh is the approximate representation of the domain to which solution results and visualization processes will be tied (Shephard and Schroeder, 1995).

In the early application of the finite element method, finite element meshes were manually drawn and converted into the computer by creating input "decks" defining each and every finite element entity. This can be particularly tedious and time-consuming in the case of an irregular three-dimensional mesh. The GMS interface is composed of a number of separate modules such as TIN (Triangulated Irregular Network) module, solid modeling module, 3D mesh module, 3D grid module etc. Finite element meshes can be generated in several different ways. Also, the generated meshes can be edited and renumbered. For 3D models, mesh and/or grid generation modules are the comprehensive and core part of the GIS interface.

Since the hydrogeological stratigraphy at this site is fairly uniform, we used a very simple mesh generation technique. Steps for generating a 3D finite element mesh are: (1) import a DXF file converted from GIS formatted file showing site extension and topography, (2) create a two-dimensional mesh covering the modeling area, (3) input a set of boreholes which define the elevations of interfaces between the stratigraphic units at scattered locations throughout the modeling domain, and (4) construct a 3D mesh by a 2D mesh and automatically interpolate surfaces using the borehole data which represent the interfaces between the stratigraphic units. Each element in the 2D mesh was extruded into a vertical column of 3D elements. Figure 1-2 is a constructed 3D mesh for the simulation of groundwater and solute transport at the site.

Model Calibration

Calibration is the process of adjusting model inputs until the resulting predictions give a reasonably good fit to observed data. It is an iterative and very much time-consuming process. The GMS can overlay contours produced from observed water-level data onto contours generated by predicted water-level output; thus the two sets of water level contours can be compared directly on the screen. Use of GMS eliminates the need for extensive printing associated with comparing hard copy results in conventional calibration techniques. This visualization capability provides rapid analyses and saves on manual manipulation of data.

Input/Output Visualization

Visualization techniques, when used in conjunction with numerical modeling, is providing the most meaningful means to view both the 'input' and 'output'. A large number of visualization tools have been provided in GMS. Highly realistic images of all objects can be displayed in a 3D oblique view and rotated interactively. Contours, color fringes and iso-surfaces can be generated from scattered data or 3D meshes and grids. An animation sequence can be generated to represent a moving contaminant plume. The growth of computer hardware has spurred numerical analysis and computer visualization which have developed along separate yet interrelated paths, particularly as they became cost-effective for a wide range of applications.

EDUCATION and TRAINING

The following students were involved in the groundwater modeling project:

Name	Classification	Status
Michelle Houston	B.S./M.S. Mathematics	Graduation May 1996
Nicole Wright	B.S./M.S. Mathematics	Graduated May 1995

Florida Superfund Site

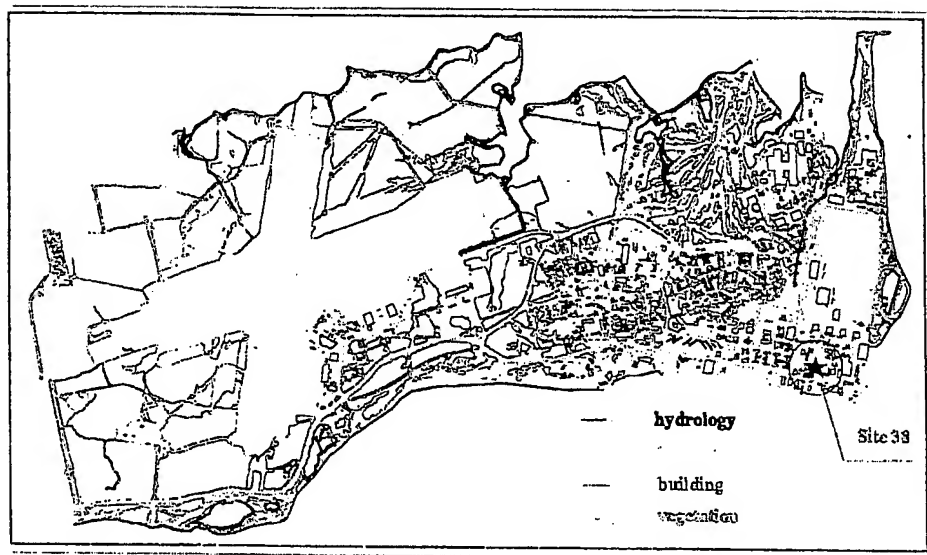


Figure 1.1 Site location

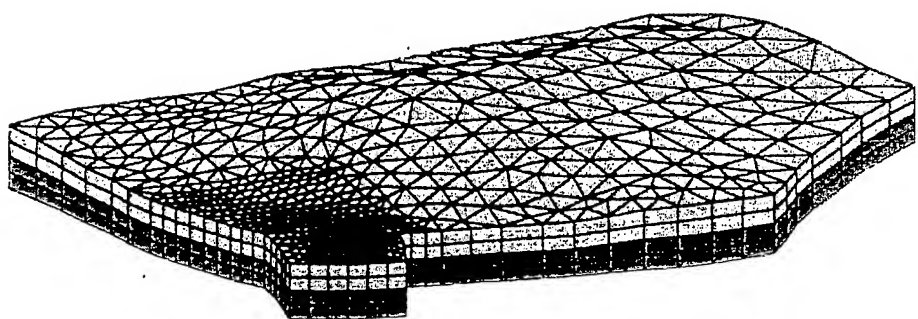


Figure 1.2 Finite element mesh

PUBLICATIONS AND PRESENTATIONS

1. "Enhanced Groundwater Flow and Solute Transport Analyses Using GIS at a Florida Superfund Site", D. Chen, J. Winkie, R. Carsel, L. Moeti, and B. Vona. XI International Conference on Computational Methods in Water Resources, accepted.

REFERENCES

Brigham Young University, (1994a) "GMS, Groundwater Modeling System Reference Manual," Engineering Computer Graphic Laboratory, Provo, UT.

EnSafe/Allen & Hoshall, (1994). "Draft Remedial Investigation, NAS Pensacola Site 38."

Lin, H.C., and G. T. Yeh (1995). "User's Manual for the FEMWATER Groundwater Computer Program: A Three-Dimensional Finite Element Model of Density-Dependent Flow and Transport through Saturated-Unsaturated Porous Media," U.S. Army Corps of Engineers Waterways Experiment Station, Vicksburg, MS.

Shephard, M. S. and W. J. Schroeder, (1995) "Analysis Data for Visualization", in Computer Visualization: Graphics Techniques for Scientific and Engineering Analysis. edited by R.S. Gallagher, CRC Press, 1995, pp. 61-87.

2.2 DEVELOPMENT OF A PULSATING MEDICAL WASTE INCINERATOR

Investigators: T. Bai, K. B. Bota and Y. D. Yeboah

INTRODUCTION

The study investigates the effect of pulsating combustion upon the incineration of wastes, especially medical wastes. These wastes are generated by hospitals, laboratories, animal research facilities, and other institutional sources. The disposal of these wastes is under severe public scrutiny. Incineration offers a highly attractive approach for eliminating hazardous medical waste (Green, 1992). It is the only commercially available method of treatment which destroys the organisms associated with these wastes completely and effectively (Green, 1992; Brunner, 1991; Barton et al, 1989).

The medical waste stream contains paper and cardboard, plastics, aqueous and nonaqueous fluids, anatomical parts, animal carcasses, and bedding, glass bottles, clothing, and many other materials (Bulley, 1991). Much of this waste is combustible. Medical waste incinerators are generally small, in the range of 2 to 10 tons/day, which is much smaller than average central disposal, municipal waste incinerators (Brunner, 1988).

There exist various types of incinerator designs, which include rotary kiln systems, conveyer furnaces, fluidized bed combustors, cyclonic furnaces, and agitated hearth (Green, 1992 and Brunner, 1991). Generally, the incineration process utilized in the existing medical waste incinerators can be classified into starved air and excess air combustion processes.

In a starved air incineration process, an oxygen-deficient atmosphere is provided in the primary chamber, and temperatures are controlled in the range of 1450 to 1750 °F. Additional air is provided in the secondary chamber to complete combustion, at temperatures from 1700 to 1900 °F. Starved air combustion process has been preferred in the past practice. The main advantage of the starved air incineration is the low air requirement in the primary chamber. With the lower airflow, fans, ducts, flues, and air emissions control equipment can be sized smaller than in excess air systems, and more importantly, the air pollution control system is simpler because the emissions are less (Brady, 1991).

However, starved air incineration results in incomplete ash burnout, lower combustion efficiency and lower destruction rate of the wastes. This is mainly due to the fact that with little air passing through the waste there is less turbulence within the incineration chamber. Generally, the performance of incinerators is controlled by the rate of mass, momentum (i.e., mixing) and heat transfer. For example, the rate of heat transfer from the gas to the waste controls the rate at which the waste is dried and pyrolyzed; the rate of mixing controls the rate at which the pyrolyzed fuel molecules mix with available air; and the rate of mass transfer controls the rates at which reactants and combustion products diffuse to and from reactive pockets. A new technology has to be developed to increase the turbulence within the incineration chamber, and at the same time maintain the starved air operation. By finding effective means for increasing the turbulence level and, therefore, the rates of the transport processes within incinerators, it would be possible to increase the incineration rate of the waste and reduce the size of the required incineration system.

The rates of transport processes within incinerators can be increased by the excitation of large amplitude acoustic waves. It has been demonstrated that such large amplitude acoustic waves can be excited within a chamber by use of a pulse combustor (Bai, et al, 1993). In a pulsating combustor, the combustion process occurs under oscillating conditions. The oscillation of the flow improves the mixing and increases the rates of heat and oxygen transfer from the gas to the fuel. Thus, difficult-to-burn fuels burn faster and more completely in pulsating combustors. This prevents or minimizes incomplete combustion and lowers the emissions of hydrocarbons, CO and soot into the environment. In addition, the scrubbing-like action of the oscillating gases reduces or eliminates fuel deposits on the combustor walls.

OBJECTIVE

The primary objective of this investigation is to study the effect of pulsating combustion upon the incineration of wastes, especially medical wastes, and to develop a laboratory scale experimental pulsating combustion medical waste incinerator.

APPROACH

The project is mainly an experimental investigation. It aims to develop a waste incineration system by using a pulse combustor to heat the waste and excite pressure oscillations in the incineration chamber. It is believed that the performance of medical waste incinerators (both old and new) can be considerably improved by retrofitting them with a pulse combustor that excites large amplitude, resonant, pulsations within the incinerator.

ACCOMPLISHMENT

The major tasks being conducted under this program are: Task 1-Development of the laboratory facilities; Task 2-Development of the pulse combustion medical waste incinerator experimental setup; and Task 3-Investigation of the incineration performance of the pulse combustion medical waste incinerator.

Task 1, the development of the laboratory facilities, started in early 1994, and proceeded smoothly. At present, most of the needed laboratory equipment and instruments have been acquired and installed in the lab. These include power supply, cooling water supply, natural gas supply to the lab, the measurement systems that measure temperature and pressure, and the gas analysis station that determines the emissions of CO, O₂, CO₂, NO_x, SO_x and THC.

Specifically, the research facilities in the CAU Combustion Laboratory include:

- **CO, CO₂, SO₂, NO_x, O₂, and Total Hydrocarbon Measurement in Exhaust Flow**

The gas analysis station consists of sampling probe, sample conditioning unit, and analyzers for CO, CO₂, SO₂, NO_x, O₂, and Total Unburned Hydrocarbon (THC).

The CO, CO₂, and SO₂ analyzers are Horiba VIA-510 series non-dispersive infrared analyzers. The NO_x analyzer is a Horiba CLA-510S chemiluminescence analyzer. The O₂ analyzer is a Horiba MPA-510 magnetopneumatic analyzer

and the THC analyzer, Horiba FIA-510, is based on the principle of hydrogen flame ionization.

- **Pressure Measurement**

Various pressure gauges and piezoelectric transducers for static, dynamic, and acoustic pressure measurement.

- **Temperature Measurement**

Various thermocouples and IR thermometers for temperature measurement.

- **Flow Rate Measurement**

Various flow meters including rotameters for flow rate measurement.

- **Flow Visualization by Laser Sheet**

60"x60" and 60"x120" optical tables.

Coherent 5W Argon Ion laser.

Fiber optic based laser sheet projector

- **High Speed Multi-Channel Data Acquisition System**

Intel 80486 66MHz processor with 12 bit, 4 channel 1 million samples per second data acquisition board. IEEE488 interface for testing and process monitoring and control.

- **Pressurized Air Supply**

10 SCFM/100 PSI air supply

- **Fuel Supply**

Installed natural gas supply line; LPG and other fuel cylinders.

The objective of Task 2, development of the pulsating incinerator experimental setup, is to develop a pulsating combustor which will later be integrated into the incineration system. It has been decided that a Rijke type pulse combustor with a tangential reactant injection system will be used in this study. This type of pulse combustor is well known for its simple geometry, low maintenance, and good performance. However, a key issue in developing such a pulsating combustor is the combustion timing, which states, as Rayleigh's criterion, that the heat release must be in phase with the pressure oscillation in order to maintain the pulse combustion operation. This combustion timing is largely controlled by the mixing process of the air and the fuel.

To gain a better understanding of the mixing process and its effects upon the combustion efficiency and pollutant emissions, a small scale combustor that has a tangential injection configuration has been designed and built. This combustor is a premixed, open flame burner. The body of the burner consists mainly of the mixing chamber and the reactants injection ports. The open flame is stabilized by the swirling flows which are generated by the tangential injection of the combustion air. On the mixing

chamber there are four axial fuel injection ports and four tangential air injection ports. The openings of the axial injection ports are located immediately downstream of the tangential injection ports. This configuration forms impinging jets of the fuel and air, ensuring quick and complete mixing of the two. In addition, the tangential injection of the air generates a strong swirling flow which will further enhance the mixing process. The mixture of the fuel and air leaves the mixing chamber through the orifice on the top of the burner. As a result of the strong swirling, a toroidal vortex will be generated at the downstream of the orifice to stabilize the flame.

This combustor has been installed in the lab. The performance of the combustor has been characterized. The results obtained from these experiments have shown excellent performance of the combustor. The combustor provided high combustion efficiency and reached extremely low CO and NO_x emissions under certain operating conditions. The visualization of the flames also revealed that the combustor can work under distinctively different operating modes. These different operating modes provided the flexibility for the combustor to be used in different applications. These results are discussed as follows:

The Operating Modes and the Flame Shape

The operating conditions of the Twin Swirl Burner (TSB) combustor have been studied to determine the flame shape, stability, operating range. It has been observed that the TSB can operate under distinctively different operating modes, which include diffusion flame, partially premixed flame, and premixed flame. When the combustor is operated under different modes, the flame shape is drastically different. Photographs showing the flame shape at different operating modes are presented in Figures 2-1 to 2-5. It has been shown that when the combustor is operated at diffusion mode, a long diffusion flame is formed at the downstream of the mixing chamber exit. When the combustor is operated under partial mixing mode, compared with the diffusion mode, the flame is shortened and an intense blue flame zone and a dark red soot forming region can be observed. Further increase of the swirling air shortens the flame even further. Most interestingly, the injection of the secondary swirling air produced a unique flame shape of thin flame sheet "tornado".

It is believed that the change of the flame shape is due to the interaction between combustion and the swirling flow. Swirling has large-scale effects on flow fields. Jet growth, entrainment and decay and flame size, shape, stability and combustion intensity are all affected by the degree of swirl imparted to the flow. Swirling intensity can be measured by the Swirling number S . The swirling number S is a nondimensional number representing axial flux of swirl momentum divided by axial flux of axial momentum, times the equivalent nozzle radius. The swirling number under above discussed TSB operating modes are being calculated based upon the fuel and air flow rates, the geometry of the combustor, and other information. The effects of swirling flow on the flame shape, stability limits, and other performance will be further studied.

Figure 2.1 The flame shape of the twin swirl burner when operated under diffusion mode.

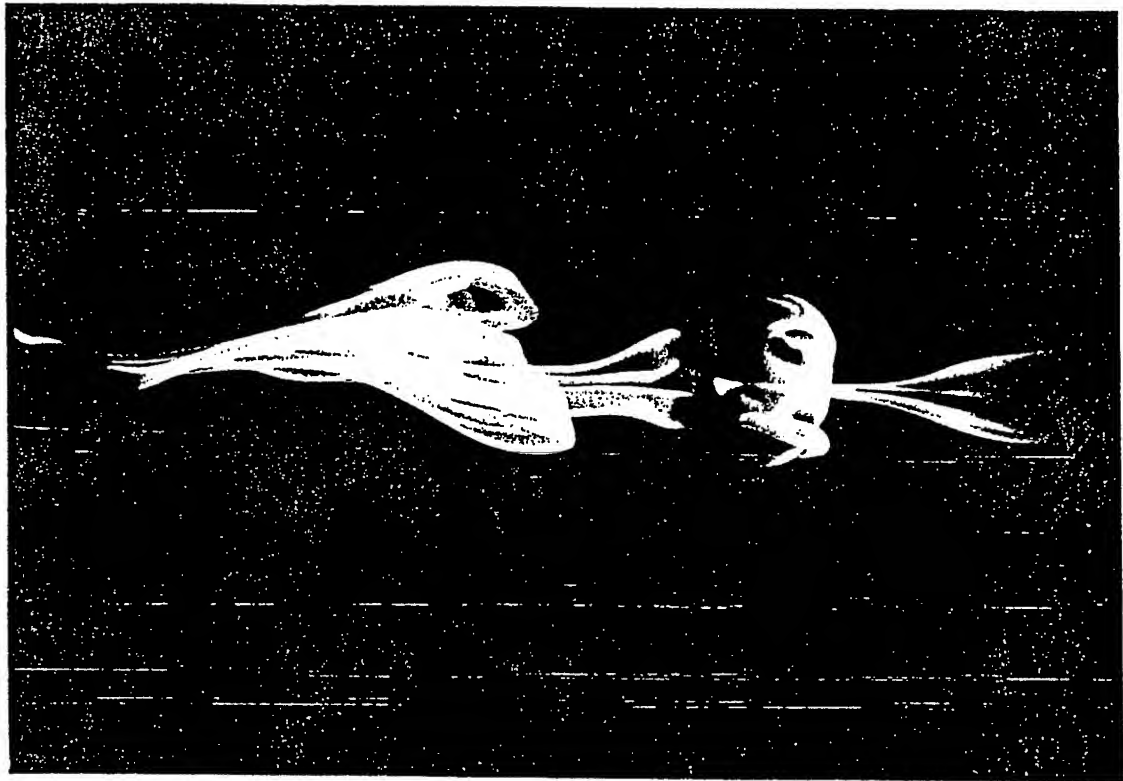
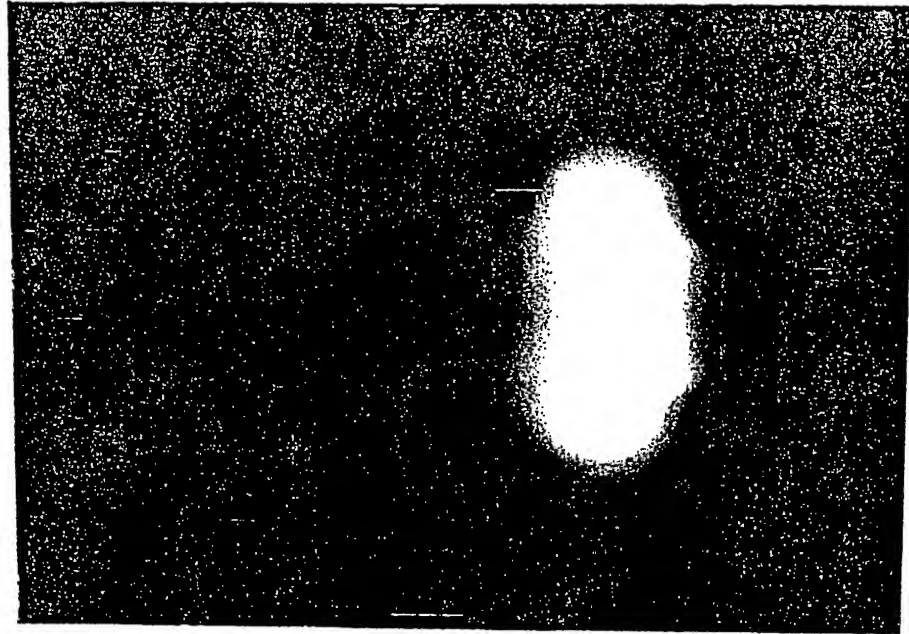
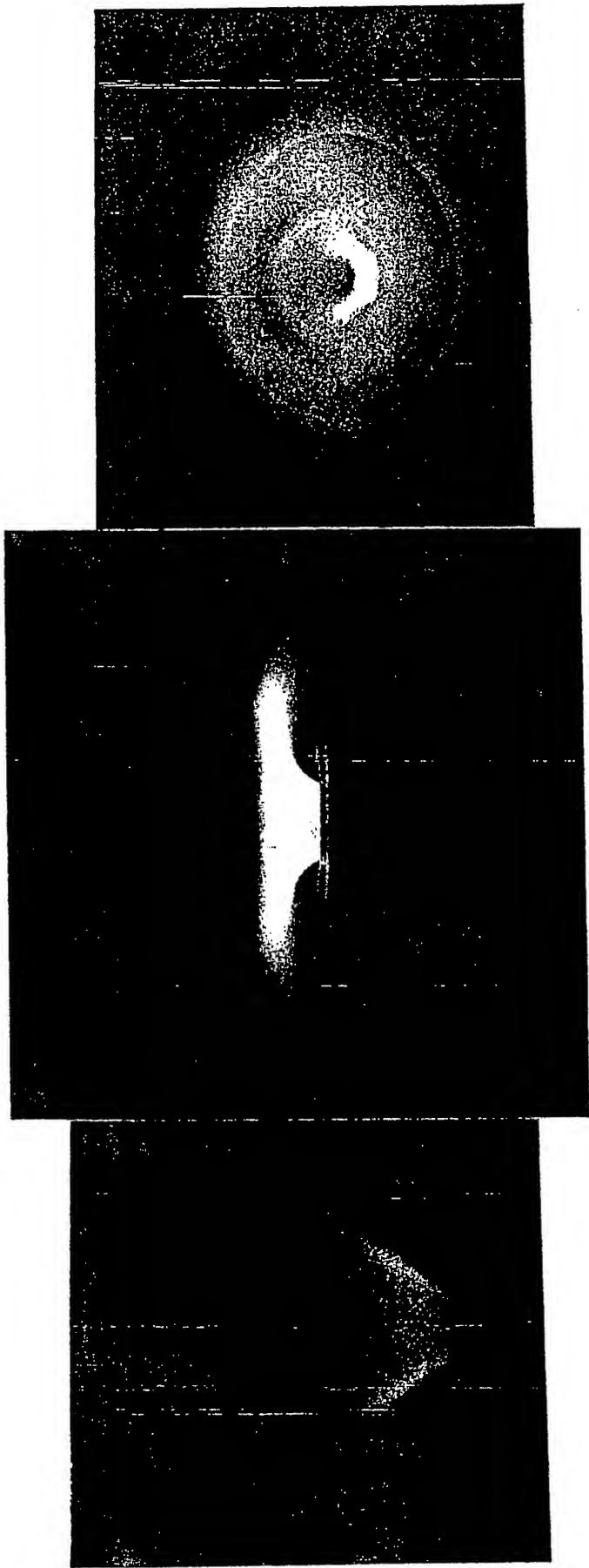


Figure 2.2 The flame shape of the twin swirl burner when operated under partial premixing mode.





The flame shape of the twin swirl burner
Figure 2.3 when operated under premixing mode.

Figure 2.4 The side view of the flame of the TSB when operated
under premixing mode with secondary swirling air.

Figure 2.5 The top view of the flame of the TSB when operated
under premixing mode with secondary swirling air.

The Effects of the Center Body Height

The design of the combustor includes a center body that is located in the center axis of the mixing chamber and its height can be adjusted. The purpose of the design is to provide capability to change the passage area of the exit orifice so that the exit flow velocity can be adjusted to facilitate flame stabilization. To evaluate the function of the center body, tests with different center body heights have been conducted.

Four components of the exhaust measurement were obtained, namely, CO, CO₂, NO_x and SO₂. An examination of the results indicates that the change of the center body height has little effect on the emissions. It showed a general trend of increasing emissions while the center body height is increased. However the change is minimal. In addition, from visual observation, the flame stability has not become a problem in the entire range of the center body height. Therefore, it is concluded that the center body does not play an important role in the emission production and flame stabilization (at least in the tested operating range).

The Pollutant Emissions

The emission measurements focused on the NO_x, CO, and Total Hydrocarbon (THC) emissions under various air/fuel ratios. CO, CO₂, SO₂, NO_x, O₂, and THC in exhaust flow were measured. The gas analysis station consists of sampling probe, sample conditioning unit, and analyzers of CO, CO₂, SO₂, NO_x, O₂, and THC. The CO, CO₂, and SO₂ analyzers are Horiba VIA-510 series non-dispersive infrared analyzers. The NO_x analyzer is a Horiba CLA-510S chemiluminescence analyzer. The O₂ analyzer is a Horiba MPA-510 magnetopneumatic analyzer. And the THC analyzer, Horiba FIA-510, is based on the principle of hydrogen flame ionization.

Measurements have been conducted for three fuels which include natural gas, methane, and propane. Typical results showing the dependence of CO and NO_x concentrations in the exhaust flow upon the nondimensional air/fuel ratio are presented in Figures 2-6 and 2-7 for city line natural gas, methane, and propane, respectively. It is found that the NO_x emissions from this combustor were below 10 ppm when the combustor was operated under fuel lean premixed conditions. The NO_x concentration reached its maximum near the stoichiometric ratio. It dropped quickly in the fuel rich conditions. However, the equivalence ratio where minimum NO_x emissions were obtained varied upon different operating conditions. For example, when secondary air is injected, the equivalence ratio for the low NO_x emission was significantly different from the results obtained when only the primary air was used. The CO concentrations in the exhaust gas were found to be between 10 ppm to 30 ppm for a small range of equivalence ratios where low NO_x emissions were obtained. These extremely low CO concentration data clearly indicate that the combustion efficiencies of this combustor is nearly 100 percent within this range of operating conditions. However, it should be noted that the CO emissions are significantly higher under other operating conditions and exceeded the configured measurement range of the CO analyzer (1000ppm).

Emission performance characterization will be continued. Detailed results, analysis, and interpretation of the results will be provided in future publications.

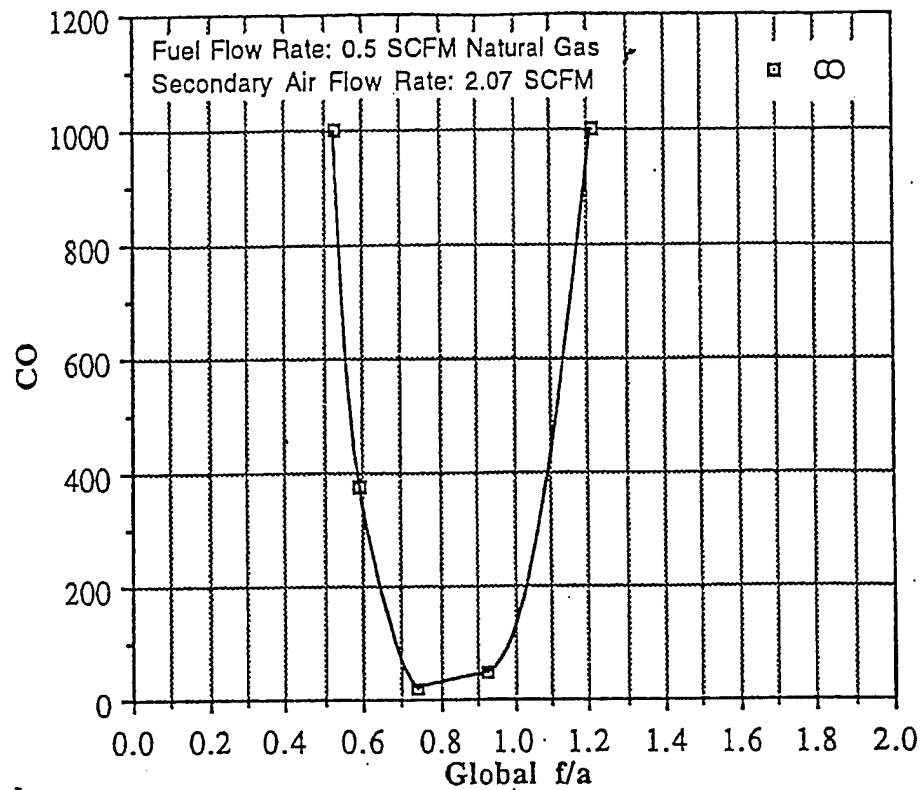


Figure 2.6 CO concentration in the exhaust gas. The operating conditions are given in the figure

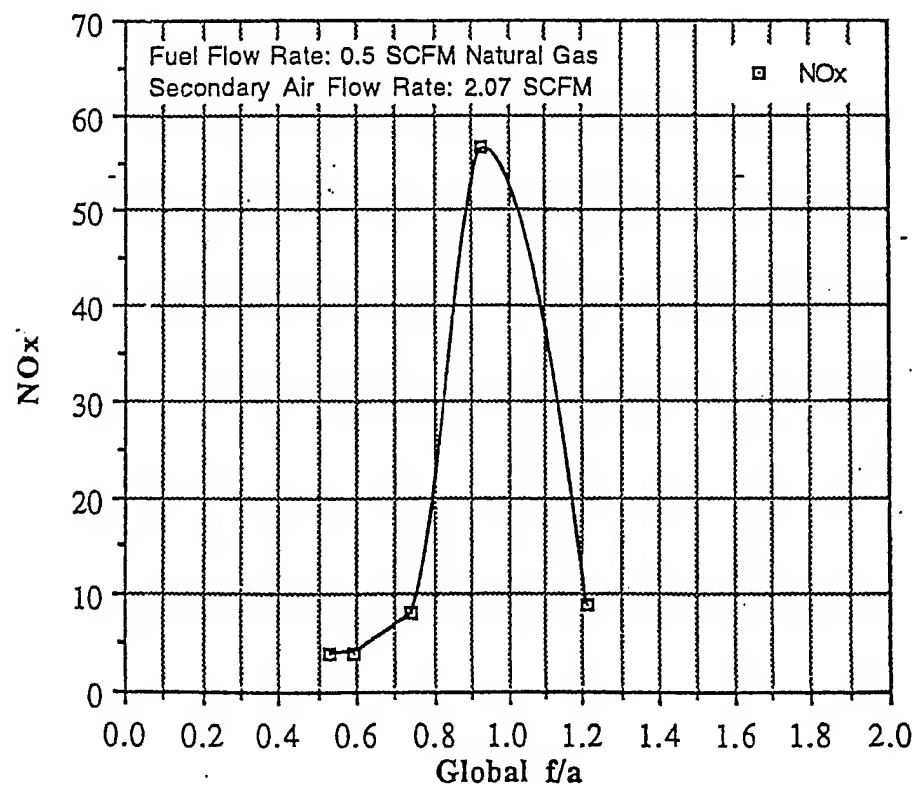


Figure 2.7 NOx concentration in the exhaust gas. The operating conditions are given in the figure

Task 3 is currently being undertaken. The pulsating combustor developed in Task 2 is used as a driver to excite the acoustic pressure oscillations inside the chamber of the incinerator. The remaining parts of the incineration system has been designed, fabricated, and installed. These remaining parts include the feeding mechanism, the incineration chamber, and the disposal mechanism. The effect of pulsations upon the incineration of the wastes are being determined by comparing the efficiency of the incineration process under steady and pulsating conditions.

To determine the performance of the developed system, certain parameters are being investigated. These parameters are either most likely changed in practice or, based upon experience, are known to strongly influence the system's performance in terms of exhaust gas emission and the waste destruction rate. These parameters are:

The Fuel Feed Rate

The performance of the pulsating combustor is expected to depend upon the fuel feed rate. To determine this dependence, the maximum acoustic pressure excited and the pressure distribution, the steady temperature distribution and the exhaust flow chemical composition will be measured under several fuel feed rates.

The Air/Fuel Ratio

For each fuel feed rate, tests will be conducted at several air/fuel ratios corresponding to fuel rich and fuel lean conditions. The fuel feed rate will be the total fuel that includes the combustible waste and the necessary fuel for the operation of the pulse combustor.

To determine these parameters, the following measurements will be conducted: (1) dynamic pressure measurements; (2) steady temperature distribution measurements; and (3) exhaust gas emission measurements.

Pressure Measurements

Acoustic pressure will be measured at various locations in the combustor using piezoelectric pressure transducers. Since these transducers are highly heat sensitive, steps must be taken to prevent heat damages and performance drifting. Each transducer will be mounted on a "semi-infinite" tube at a distance of 2 feet from the combustor wall. These pressure measurements will characterize the excited acoustic oscillations in the combustor by determining the frequencies, amplitudes, spatial dependencies and phases of the excited acoustic pressure oscillation.

Steady Temperature Distribution Measurements

The steady temperature will be measured at various locations in the pulsating combustor. Nickel-chromium/nickel-aluminum thermocouples will be used to perform the steady temperature measurements. The steady temperature distribution measurements will reveal the location of the intensive chemical reaction and heat release zone. This

information will be used to qualitatively determine the variation of the combustion intensity and the heat transfer rate.

Exhaust Gas Emissions Measurements

A chemical analysis station will be used to measure the concentrations of Total Unburned Hydrocarbon(THC), CO, CO₂, O₂, SO₂, and NO_x in the exhaust gases of the incineration system. The gas sampling line will use a dual head diaphragm vacuum pump to pump the sampled gas from the exhaust pipe through a heated stainless steel pipe and a permeation/distillation type dryer. It will then feed the pumped gas sample into the THC, CO, CO₂, O₂, SO₂, and NO_x analyzers. A personal computer with adequate software and an analog to digital converter (A/D) will be used to acquire the signals and analyze data.

EDUCATION AND TRAINING

During this report period, three(3) students (one graduate and two undergraduates) worked on the project. They participated in the installation of the combustor, the calibration and checkout of the analyzer systems, the performance testing, and data acquisition and analysis. Reading material was provided to the students to strengthen their background in combustion theory. The students trained on the project were:

Name	Classification	Status
Mr. Z. Wang	Ph.D Chemistry	Started Thesis Research
Ms. Amy Arthur	B.S. Chemistry/Chemical Engineering	Graduated Sept 1996
Mr. LaShanda James	B.S. Chemistry/Chemical Engineering	Graduating May 1998

PUBLICATIONS AND PRESENTATIONS

"Waste Incineration through Pulsating Combustion, Part I- Combustor Characterization," Proceeding of the International Conference on Nuclear and Hazardous Waste Management SPECTRUM 1996, Seattle, Washington, August 18-23, 1996, pp 456-461.

"Numerical Simulation of a Twin Swirl Burner," the 34th AIAA Aerospace Sciences Meeting, Reno, NV, January, 1996.

"Driving of Different Modes in a Rijke-Like Pulse Combustor," Proceedings of the 3rd Asia-Pacific International Symposium on Combustion and Energy Utilization, Hong Kong, Dec. 11-16, 1995

"Performance of a gas burning Rijke type pulse combustor with tangential air/fuel injection," Special Issue on Pulse Combustion, Combustion Science and Technology, Vol. 94, pp 1-10, 1993.

"Vortex shedding and periodic combustion processes in a Rijke type pulse combustor," Special Issue on Pulse Combustion, Combustion Science and Technology, Vol. 94, pp 245-258, 1993.

"Low NOx Emission by Lean, Premixed Combustion" 2nd Annual HBCU Private Sector Fossil Energy Research and Development Technology Transfer Symposium, April, 1994

"Experimental Study of the Effect of Fuel and Air Feed Rate Modulation Upon Pulse Combustion in A Rijke Type Pulse Combustor," AIAA 94-0216, 32nd Aerospace Sciences Meeting and Exhibit, Reno, Nevada, Jan., 1994.

"Combustion of Fossil Fuels in Rijke Type Pulse Combustors," 1st Annual HBCU Private Sector Fossil Energy Research and Development Technology Transfer Symposium, May, 1993

REFERENCES

1. Green, A.E.S., *Medical Waste Incineration and Pollution Prevention*, 1992, Van Nostrand Reinhold.
2. Brunner, C.R., *Handbook of Incineration Systems*, 1991, McGraw-Hill, inc.
3. Barton, R.G., Hassel, G.R., Lanier, W.S., and Seeker, W.R., "State-of-the-art Assessment of Medical Waste Thermal Treatment," Report for Risk Reduction Engineering Laboratory, U.S. EPA Contract #68-03-3365 and California Air Resources Board Contract #A832-155, Energy and Environmental Research Corporation, Irvine, CA, 1989.
4. Bulley, M.M., "Incineration of Medical Waste: Treating the Cause rather than the Symptoms," *Clean Air*, May, 1991, pp 51-53.
5. Brunner, C.R., "Hospital Waste Disposal by Incineration," *Journal of the Air Pollution Control Association*, Vol. 38, No. 10, Oct. 1988, pp. 1297-1309.
6. Brady, J.D., "Recent Developments in Pollution Control Systems for Chemical and Infectious Waste Incinerators," Mid-West American Institute of Chemical Engineers Meeting, St. Louis, MO, February, 1991.
7. Bai, T, Cheng, X.C., Daniel, B.R., Jagoda, J.I., and Zinn, B.T., "Performance of a gas burning Rijke type pulse combustor with tangential air/fuel injection," Special Issue on Pulse Combustion, *Combustion Science and Technology*, 1993, Vol. 94, pp 1-10.

2.3 STUDY OF THE EFFECTS OF AMBIENT CONDITIONS UPON THE PERFORMANCE OF FAN POWERED, INFRARED, NATURAL GAS BURNERS

Investigators: T. Bai, Y. Yeboah, and R. Sampath

Collaborator: Craig A. Farnsworth, American Gas Association Research Division

INTRODUCTION

The fan powered infrared burner is a technology introduced more recently in the residential and commercial markets. It is a surface combustor that elevates the temperature of the burner head to a radiant condition. A variety of metallic and ceramic materials are used for the burner heads. It has been demonstrated that infrared burners produce low CO and NO_x emissions in a controlled geometric space [Sathe et al, 1990]. As environmental regulations become more stringent, infrared burners receive increasing attention.

However, the performance of natural gas-fired infrared burners is strongly dependent on ambient conditions and natural gas composition. In the United States, ambient temperature, pressure, and relative humidity vary significantly by location and season. Also, natural gas compositions supplied by local gas distribution companies exhibit seasonal and regional variations. These variations can cause reliability and performance problems of this type of burner. In service, IR burners have had reliability and performance problems, especially when exposed to various gas compositions, operating altitudes, and other ambient conditions like temperature and humidity. These parameters also affect the composition of the gaseous emissions from these burners. Burning characteristics will also differ in important respects, one of these being speed of flame propagation. It is the responsibility of the manufacturers to design appliances capable of performing more satisfactorily under reasonable wide variations in gas composition while retaining desirable efficiencies and operation.

There have been very limited studies to investigate the effects of gas composition upon the performance of radiant burners. Due to the lack of data and fundamental understandings, the IR burner product development in the industry is empirical in nature, and is conducted with one gas composition. This project characterizes the operation of IR burners at various gas compositions and ambient conditions and develops a baseline theoretical analysis to predict the behavior of these burners to the change in fuel compositions.

OBJECTIVE

The objective of this investigation is to characterize the operation of a fan powered infrared burner (PIR) at various gas compositions and ambient conditions and develop design guidelines for appliances containing PIR burners for satisfactory performance.

APPROACH

In this program, an experimental setup has been devised and built. The experimental rig is capable of measuring the combustion product output, as well as providing a means by which the radiant heat output can be measured. The burner is selected from an existing commercial appliance that is compatible with the laboratory facilities in the Combustion Laboratory at Clark Atlanta University. The theoretical basis for the behavior of PIR burners to the changes in ambient conditions and fuel compositions is being established through analysis of the heat transfer between the burner and gas. The model is then modified and improved through comparison with experimental results.

ACCOMPLISHMENT

Technical Results and Discussion

The infrared burner has been installed in the CAU combustion laboratory and proper instrumentation including fuel/air flow rate measurement, exhaust gas emission measurement, and radiation measurement have been developed. Since accurate IR radiation measurement plays a critical role for the success of this project, various instrumentation to measure the radiant output from the infrared burner have been evaluated. An FTIR, System 2000 from Perkin Elmer, has been selected and installed for its complete emission spectrum measurement capability and its potential applicability to future combustion projects. A black body (to calibrate the FT-IR), and associated optics have also been installed for calibration. Theoretical analysis of the performance of the IR burner is being conducted and various analytical models to predict the heat output were examined. A detailed test matrix has been determined. Experimental measurements are being taken. These accomplishments are described as follows:

Development of the Experimental Facilities

Sathe et al. [1990] used a pyroelectric detector (Oriel Model) connected to an Oriel radiometer to measure the radiation from the porous radiant burner. Sheridan [1994] used a thermopile (Eppley Model) connected to a radiometer to measure the radiant output from a tube heater. Williams et al. [1992] employed an optical pyrometer to measure the total radiation output from surface burners. Though these techniques are inexpensive, they do not provide a detailed spectrum of intensity versus wavelengths. Such a spectrum will indicate at which wavelength a load best absorbs heat and how much energy is available at various wavelengths. Also, it will help to match the burner emission to load absorption for optimum process efficiency.

An FTIR spectrometer such as System 2000 FT-IR from Perkin Elmer provides such spectrum measurement capability. Solomon et al.[1986] demonstrated the use of FT-IR technique in the measurement of emission output and concentration of gaseous species in their coal combustion experiments. They validated the FT-IR measurements with independent thermocouple measurements made at the same point. System 2000 with a KBr detector will provide a wavelength range of about 1 to 25 micrometer. Further, it can be upgraded for any range of wavelength as necessary in the future. Furthermore, System 2000 is versatile that it's use can be expanded and configured with a GC-IR interface, TG-IR interface, FT-IR microscope, and NIR FT-Raman accessory. A blackbody with a temperature range of 50 to 1200 degree C (model IR-564 from Graseby Infrared) is used to calibrate the FTIR. The IR burner is a modified commercial deep fat fryer that has a window to allow in-situ radiation measurements on the surface of the infrared burner via the view port through the oil vat. A set of Horiba gas analyzers are used to measure the emissions from the burner. Experiments are being conducted for an extensive test matrix of fuel gas mixtures that represent the complete range of gas compositions usually encountered in the United States. Methane is used as the baseline fuel. Mixtures of methane/propane, methane/hydrogen, and methane/nitrogen along with two propane-air peak shaving gas mixtures were designed to study sooting, flashback, and lift-off conditions. The performance of the burner is being examined for stability limits, radiant efficiency (ratio of radiative flux escaping the burner to the heat released by combustion), and gaseous emissions at each gas composition and air/fuel ratio.

Experimental Results and Discussion

An extensive test matrix of fuel gas mixtures was prepared to represent the complete range of gas compositions found in the United States. In this matrix methane is the baseline fuel. Mixtures of methane/propane (sooting), methane/hydrogen (lightback), and methane/nitrogen (flame lift) along with two propane-air peak shaving gas mixtures have been designed to simulate variations in gas compositions. The air/fuel ratio in terms of theoretical combustion air (TA) was designed to vary between 90% -170% for each fuel mixture. The baseline TA was set at 130%.

Test results for methane/propane/air mixtures were obtained for TA ranging from 80% to 170%. Experiments were performed for various methane/propane mixtures (82/18, 88/12, 91/9, 94/6, and 97/3). For any mixture in general, radiant efficiency, CO₂ and NO_x emissions showed a steady increase up to stoichiometric and decreased through air/fuel ratio of 1.7. Unburned hydrocarbon emission continued to increase as air/fuel ratio decreased from 1.

A fuel gas mixing station was designed and constructed to supply a continuous flow of repeatable, accurate fuel gas mixtures to the fryer during the fuel composition variability testing. This mixing station consisted of four rotometers with different flow ranges connected in parallel to a mixing manifold. The constituents for the fuel mixtures, supplied by compressed gas cylinders, were mixed together in the desired volumetric ratios via the mixing station, and piped to the fryer for continuous operation. By

continuously mixing the fuel mixtures from inexpensive gas constituents, the high cost for specially mixed gases would be avoided and test durations would not be limited.

The remaining experiments planned in the test matrix covering methane/hydrogen, methane/nitrogen, and peakshaving gases are in progress. Data analysis and the evaluation of the effect of fuel blends on the performance of the burner and its associated behaviors will be completed.

Environmental chamber test runs and experiments will be conducted at AGAR, Cleveland, Ohio.

PIR Burner Performance Model Development

Applications of the radiant burners include boilers, air heaters, deep fat fryers, process heaters, and immersion heaters. One main reason for the present interest in this type of burner is its low NO_x emissions. This is attributed to the fact that a large proportion of the heat of combustion is given out as radiation from the burner surface. This results in relatively low gas temperature in the combustion zone compared to that of a conventional free-flame burner. As a consequence, such burners produce less NO_x mainly by the so called prompt-NO mechanism [Williams et al, 1992].

The principle of the infrared burner is as follows: A mixture of air and natural gas enters a highly porous ceramic or metal layer of approximately 10 mm thick; the mixture is gradually heated inside the layer and combusted, while it is flowing through the layer. The combustion takes place within the layer at some 5 mm thick. The enthalpy of combustion released in the gas phase heats the porous matrix which then emits thermal radiation to a heat load.

The above situation has been modeled by numerous researchers using conduction, convection, radiation, combustion (heat generation), and premixed flame model for one or more outputs such as surface temperature, gas temperature, temperature within the porous layer, flame speeds/flame locations, radiant output, efficiency, and emissivity [Kawaguchi et al, 1990; Sthe et al, 1990; Andersen, 1992; sathe et al, 1990 and Yoshizawa et al, 1988].

The physical mechanism and theoretical analysis of the combustion process of the PIR burner were formulated. The numerical modeling and implementation of a burner code at CAU's computing faculty is in progress. Modification of a heat transfer model to predict the burner behavior to the change in fuel compositions will be completed.

In summary, the project is progressing well. The scheduled tasks for this period of time were conducted smoothly. Specifically:

1. The infrared burner has been installed in the CAU combustion laboratory and proper instrumentation including fuel/air flow rate measurement, exhaust gas emission measurement have been developed. Preliminary tests

for the proper operation of the burner have been conducted. The installation of the radiation measurement system has been completed.

2. Theoretical formulation and analysis of the PIR burner performance model continued. The review and evaluation of the literature in this area was completed.

EDUCATION AND TRAINING

Students actively participated in the research program. They conducted experiments, analyzed the data, drafted laboratory reports, and presented the research progress at professional meetings. Four students worked on this project. Their names and classifications are as follows:

1. Amy Arthur (Graduated, 1996, Chemistry/Chemical Engineering)
2. Zhicheng Wang (Graduate, Chemistry)
3. LaShanda James (Junior, Chemical Engineering)
4. Regina Malloy (Sophomore, Engineering)

PUBLICATIONS AND PRESENTATIONS

An abstract for the paper entitled "An Experimental Study of the Effects of Natural Gas Composition Variations on Fan Powered Infrared (PIR) Burners" was published at the 1996 American Flame Research Committee (AFRC) International Symposium, September 30 - October 2, 1996, Baltimore, Maryland.

A student paper was presented in a poster session at the Fourth Annual HBCU/Private Sector Energy Research and Development Technology Transfer Symposium, 1996.

REFERENCES

1. Sathe, S. B., Kulkarni, M. R., Peck, R. E., and Tong, T. W., An Experimental and Theoretical Study of Porous Radiant Burner Performance. Twenty-Third Symposium (International) on Combustion/The Combustion Institute, 1990/pp. 1011-1018.
2. Sheridan, R., Determination of Radiant Output from Infrared Tube Heaters, GRI Topical Report, May 1994.
3. Williams, A., Woolley, R., and Lawes, M., The Formation of NO_x in Surface Burners, Combustion and Flame 89: 157-166 (1992).

4. Solomon P. R., Serio, M. A., Carangelo, R. M., and Markham, J.R., Very Rapid Coal Pyrolysis, 1986, Fuel 65, 182.
5. Kawaguchi, O., Otoh, T., Nakamura, S., Todoroki, A., and Murayama, Y., Premixed Combustion at a Fiber Mat, Twenty-Third Symposium (International) on Combustion/The Combustion Institute, 1990/pp. 1019-1024.
6. Sathe, S. B., Peck, R. E., and Tong, T. W., Flame Stabilization and Multimode Heat Transfer in Inert Porous Media: A Numerical Study, Combust. Sci. and Tech., 1990, vol.70, pp. 93-109.
7. Andersen, F., Heat Transport Model for Fibre Burners, Prog. Energy Combust. Sci., 1992. Vol. 18, pp. 1-12.
8. Sathe, S. B., Peck, R. E., and Tong, T. W., A Numerical Analysis of Heat Transfer and Combustion in Porous Radiant Burners, Intl. J. Heat and Mass Transfer, Vol. 33, No. 6, pp. 1331-1338, 1990.
9. Yoshizawa, Y., Sasaki, K., and Echigo, R., Analytical Study of the Structure of Radiation Controlled Flame, Intl. J. Heat and Mass Transfer, Vol. 31, No. 2, pp. 311-319, 1988.

2.4 DEVELOPMENT OF A TWO STAGE, PULSE COMBUSTION, VOC DESTRUCTION TECHNOLOGY

Investigators: T. Bai and Y. Yeboah

Collaborator: Robert Barat, New Jersey Institute of Technology

INTRODUCTION

Innovative volatile organic compounds (VOCs) treatment technologies must be developed to significantly reduce the direct discharge of VOCs and to meet the increasingly stringent regulations on VOC emissions.

The efficiency of burning gaseous fuels critically depends upon the efficiency of mixing processes. Consequently, the performance of VOC incineration systems could be drastically improved by improving their mixing processes. One way to accomplish this efficiently is by the excitation of large amplitude acoustic waves within the incineration systems. Such acoustic waves are excited spontaneously within pulse combustors,

resulting in an extremely efficient combustion process. This suggests that VOCs could be incinerated effectively by injecting them directly into a pulse combustor.

This project aims to develop a combined, thermal and catalytic, VOC destruction technology that relies upon the unique characteristics of pulse combustion to achieve high Destruction and Removal Efficiency(DRE). Pulse combustion and the associated increases in the rates of mixing, mass transfer, and heat transfer are expected to produce the following benefits: 1) higher thermal destruction efficiencies due to high combustion intensity, enhanced mixing, and heat transfer from combustion product to the VOCs, and 2) higher catalytic destruction efficiencies due to significantly increased mass transport to the catalyst material by the excited acoustic oscillations of pulse combustion.

OBJECTIVE

This effort consists of basic research and engineering development. The goal is to develop an advanced, two stage, pulse combustion VOC destruction technology to incinerate VOCs more efficiently. Specifically, the proposed system will be built upon a Rijke type pulse combustor that utilizes a tangential reactant injection system and a staged combustion design.

APPROACH

The project is jointly conducted with researchers at the Northeast Hazardous Substance Research Center. Collaborations between Drs. Tiejun Bai and Yaw Yeboah at CAU and Dr. Robert Barat at NHSRC brings the expertise of CAU faculty in pulse combustion and Dr. Barat's expertise in hazardous substance treatment together in this well focused research project. In addition to providing technical consultation, Dr. Barat conducts comparable experiments on his two zone turbulent flow reactor facility, which is operating under steady state. The results from NHSRC group's tests are used by the CAU group to compare with the results obtained in the pulse combustor and elucidate the effect of pulsations on VOC destruction.

The major tasks to be conducted consist of (1) development of the experimental facilities, (2) study of pulsating combustion VOC destruction mechanisms, (3) parametric study of the VOC destruction system, and (4) system optimization.

ACCOMPLISHMENT

Experimental Setup Development

The pulsating VOC incineration experimental setup consists of a mixing chamber, a tangential fuel injection system, a primary combustion chamber, a secondary combustion chamber that also serves as a resonant tube, and decoupling chambers that are installed at the inlet and exit of the combustor. The tangential injection system is located at $1/4$ L from the entrance, where L is the total length of the combustor tube. The catalytic destruction section is located at $3/4$ L from the combustor entrance, where high amplitude oscillations of both pressure and velocity exist when a half-wave-length standing wave is established in the combustor tube. A metered stream of hexane is used to represent the VOCs and is injected into the mixing chamber, where the hexane mixes with air and fuel (natural gas). Then the mixture is injected into the primary combustion chamber. A design that is similar with the "dump" combustor is used so that the reactant jet experiences a sudden expansion when it enters the primary combustion chamber. Part of the combustion product flows towards the corner and is entrained by the jet, forming a large vortex at the corner. In the shear layer between the jet and the recirculating flow, rapid mixing and heat transfer occurs between the combustion product and the fresh reactants. Since the primary combustion chamber is tangentially attached to the secondary combustion chamber, the combustion product is forced to enter the secondary combustion chamber tangentially. By this arrangement a strong swirling flow is formed that dramatically increases the turbulence and, therefore, the mixing and combustion rates.

The project started with the development of the reactant injection system and the primary combustion chamber. Initially, the experimental setup was then characterized. Of special concern is the determination of the effect of the VOCs upon the performance of the pulse combustor. Subsequent studies will determine the effect of the pulsations upon the VOC incineration by comparing the efficiency of the incineration process under steady and pulsating conditions. Finally, parametric studies will be conducted and the system will be optimized based upon the results.

TECHNICAL RESULTS AND DISCUSSION

The measurement method and instrumentation has been completed. A test matrix was determined. To determine the performance of the developed system, certain parameters will be investigated. These parameters are either most likely changed in practice or, based upon experience, are known to strongly influence the system's performance. These parameters are:

The Fuel Feed Rate of the Pulsating Combustor

The performance of the pulsating combustor is expected to depend upon the fuel feed rate. To determine this dependence, the maximum acoustic pressure excited and the pressure distribution, the steady temperature distribution and the exhaust flow chemical composition will be measured under several fuel feed rates.

The Air/Fuel Ratio of the Pulsating Combustor

For each fuel feed rate, tests will be conducted at several air/fuel ratios corresponding to fuel rich and fuel lean conditions. In addition, for several feed rates, diagnostics in the combustion regions will be conducted near the rich and lean limits of the combustor operation.

The Distribution of the Primary and the Secondary Air Feed Rates

The distribution of the primary and secondary air feed rates will determine the air/fuel ratios in the primary combustion chamber and the secondary combustion chamber. This will also have a direct influence on the NO_x reduction effect of the combustion staging. The performance of the combustion system will be determined at several air feed rates to the primary combustion chamber for each fixed air feed rate to the secondary combustion chamber. By doing this, the dependence of the combustion system's performance upon the distribution of the air feed rates will be determined so that the NO_x reduction effect of the combustion staging can be optimized. To determine these parameters, the following measurements will be conducted: (1) dynamic pressure measurements; (2) steady temperature distribution measurements; and (3) exhaust gas emissions measurements.

Pressure Measurements

Acoustic pressure will be measured at various locations in the combustor using piezoelectric pressure transducers. Since these transducers are highly heat sensitive, steps must be taken to prevent heat damages and performance drifting. Each transducer will be mounted on a "semi-infinite" tube at a distance of 2 feet from the combustor wall. These pressure measurements will characterize the excited acoustic oscillations in the combustor by determining the frequencies, amplitudes, spatial dependencies and phases of the excited acoustic pressure oscillation.

Steady Temperature Distribution Measurements

The steady temperature will be measured at various locations in the pulsating combustor. Nickel-chromium/nickel-aluminum thermocouples will be used to perform the steady temperature measurements. The steady temperature distribution measurements will reveal the location of the intensive chemical reaction and heat release zone. This information will be used to qualitatively determine the variation of the combustion intensity and the heat transfer rate.

Exhaust Gas Emissions Measurements

A chemical analysis station will be setup to measure the concentrations of Total Unburned Hydrocarbon(THC), CO, CO₂, O₂ SO₂, and NO_x in the exhaust gases of the combustion system. The gas sampling line will use a dual head diaphragm vacuum pump to pump the sampled gas from the exhaust pipe through a heated stainless steel pipe and a permeation/distillation type dryer. It will then feed the pumped gas sample into the THC, CO, CO₂, O₂, SO₂, and NO_x analyzers. A personal computer with adequate software and an analog to digital converter (A/D) will be used to acquire the signals and analyze data.

EDUCATION AND TRAINING

Students are actively participating in the research. They work in a research environment and gain hands-on environmental protection research experience. This experience will encourage their matriculation to graduate environmental engineering programs and provide a smooth transition from undergraduate to graduate school. Following students contributed in this research:

1. Amy Arthur (Chemistry/Chemical Engineering; Graduated, 1996)
2. Zhicheng Wang (Graduate, Chemistry)

OUTREACH AND TECHNOLOGY TRANSFER

Through this project, faculty and students at CAU are developing research capabilities and expertise to meet the needs of the EPA. It will also help the CAU research group to develop linkages with researchers at EPA Northeast Hazardous Substance Research Center (NHSRC) for future research collaborations.

The results of this study will be used to develop guidelines that could be used in the development of full scale, highly efficient, VOC incineration systems. It is also expected that the results of this study will indicate how pulsations could be used to improve the performance of existing VOC incinerators.

PUBLICATIONS AND PRESENTATIONS

An invited seminar was given at New Jersey Institute of Technology in October, 1995 by Dr. Tiejun. The seminar focused upon pulsating combustion and its application in environmental protection.

A presentation of project progress and preliminary results was also given at MIT in the Technical Review Meeting for the EPA Northeast Hazardous Substance Research Center (NHSRC) in November, 1995.

REFERENCES

1. Bai, T., "Combustion of Liquid Fuels in a Rijke Type Pulse Combustor," Ph.D. Thesis, Georgia Institute of Technology, June, 1992.
2. Hermia, J., and Vigneron, S., "Catalytic incineration for Odor Abatement and VOC Destruction," *Catalysis Today*, v17 n1-2 p 349-358, May 1993.

3. Palazzolo, M. A., and Tichenor, B. A., "Destruction of Volatile Organic Compounds via Catalytic Incineration" Environmental Progress, v6 n3 p172-176, Aug., 1987
4. Zinn, B. T., "Pulsating Combustion," in "Advanced Combustion Methods," edited by Weinberg, F. J., Academic Press, 1986, pp. 113-181.

2.5 PRELIMINARY STUDY OF DROPLET BEHAVIOR UNDER VARIOUS PRESSURES

Investigators: T. Bai

Collaborator: Jada Mo, Memphis State University

INTRODUCTION

The phenomena associated with the evaporation of a single droplet and the methods of predicting its evaporation rate are important in the analysis of engineering operations involving the process of spray cooling, drying, absorption, deposition, humidification, and combustion. Extensive literature, concerning both experimental and theoretical research, is available on the subject of single droplet evaporation in a stagnant environment or under forced convective conditions at atmospheric or near atmospheric pressures. However, in many applications, droplet evaporation at elevated pressures and temperatures is important, especially when the elevated level of the pressure and temperature gets close to and beyond the critical point. The behavior of liquid droplets in the environments at supercritical pressures and temperatures has long been a topic of intense interest because of the direct relation to practical spray combustion devices and environmental protection processes. A number of industrial applications have to deal with or purposely make use of these processes. In fact, the droplet behavior is considered to be a major contributor to the spray combustion dynamics in liquid rockets, advanced gas turbines, and diesel engines, as well. Its potential importance is so well-recognized that studies aimed at improving the basic understanding of the physics have been pursued.

The previous research efforts have resulted in certain plausible explanations for experimentally observed behavior which provides a somewhat rational basis for anticipating the influence on and interaction with spray combustion dynamics in practical devices. However, considerable uncertainties still remain. These uncertainties include the fundamental basis on which any theoretical formulations were established. In order to develop a rational theoretical model, a comprehensive understanding of the physics of the vaporization process of the droplet is necessary.

OBJECTIVE

The objective of this project is to develop the necessary experimental apparatus and numerical model so that theoretical and experimental investigation of the vaporization history for a single liquid droplet vaporizing in subcritical, critical and supercritical environments can be conducted in the second phase of this program.

APPROACH

This project is the first phase of a larger effort. The major task in this project is to design, fabricate, install, and test an experimental apparatus so that a desirable range of droplet combustion tests under controlled temperature and pressure can be conducted. Another important task under this project is to develop numerical models to calculate the temperature history of the droplet and the ambient flow velocities.

ACCOMPLISHMENTS

Experimental Facility Development

It is apparent that experimental vaporization histories in supercritical environments are necessary either to verify existing theories or to formulate an improved theory. These experimental vaporization histories would necessarily include the mass, radius, and temperature-time variation for a single droplet in a varying temperature and pressure environment. Realizing the complexity of such an experimental apparatus required to obtain these time dependent parameters, the more fundamental and less complex problem of droplet evaporation in a stagnant environment is thought to be a first step in the understanding of the supercritical vaporization phenomena encountered in various advanced engines. Limited by the availability of experimental equipment and instrumentation, experimental work can be grouped as 1) droplet staying in a stagnant environment, 2) droplet experiencing a forced convection; and 3) droplet undergoing a forced convection and chemical reaction.

To simplify the experiments to the bare essentials, a single component liquid phase and a single component gas phase has been considered. Based on these considerations, a high pressure and temperature test chamber has been designed. This experimental facility consists of pressure gas supply, electrical heating, and pressure vessels. Its major components are made of stainless steel. Quartz glass windows are installed in the walls of the test section for observation and optical flow visualizatoin and flow velocity measurement. The conceptual design was conducted by CAU researchers. The engineering design and fabrication was carried out by Ralph L. Jackson Company, a high pressure vessel fabricator located in Memphis, Tennessee. The apparatus will be installed in the CAU Combustion Laboratory, where further experimental investigation under extended funding will be conducted. A schematic drawing of the test chamber is shown in Figure 5-1.

Numerical Analysis

Many theoretical investigations of droplet vaporization at elevated pressures and temperatures have been published. These investigations used different levels of models. For example, Wieber et al. (1963) investigated the attainment of droplet critical state conditions in rocket engine chambers. The results of his film theory calculations employing low pressure assumptions showed that oxygen and heptane droplets would approach their critical temperatures during vaporization in a high temperature and pressure environment. Manrique and Borman (1973) investigated high pressure vaporization by performing detailed numerical calculations for the steady state vaporization of carbon dioxide drops in a nitrogen environment. For the case of a spherically symmetric boundary layer, they included the effects of thermodynamic non-idealities, property variations through the boundary layer and high pressure liquid-vapor equilibrium. They found that at sufficiently high pressures steady state conditions can not be obtained. They focused their attention on the state of the gas mixture at the liquid-vapor interface and pointed out that this mixture could reach its critical state at pressures above the pure liquid critical pressure but at temperatures below the pure liquid critical temperature. If the droplet interface conditions reach the mixture critical point during the heating up period, all subsequent heat transfer to the droplet will result in sensible droplet heating since the latent heat vanishes at the mixture critical point. All these models provided realistic results to some extent. However, no models currently available could avoid all of the following assumptions:

- (1) the droplet temperature is uniform at any instant because of the internal mixing;
- (2) steady state heat and mass transfer correlation's are applicable to non-steady conditions;
- (3) average film properties and spherical symmetry can be assumed in obtaining the corrections for high mass transfer rates;
- (4) property values can be based on the mean temperature and composition in the film assuming ideal gas and ideal mixture behavior;
- (5) the effects of surface regression velocity can be neglected;
- (6) the mole fraction of droplet vapor at the droplet surface can be calculated from the vapor pressure of the pure droplet liquid;
- (7) properties such as thermal conductivity, viscosity coefficient, specific heats and latent heat of vaporization are independent of pressure.
- (8) no ambient gas is absorbed in the liquid phase.

Besides concerns about these fundamental assumptions, another essential prerequisite for any realistic handling of droplet behavior in analysis is the evaluation of thermodynamic and transport properties and the constituent species over a broad range of fluid thermodynamic states. For subcritical droplet vaporization, the conventional

approach which treats separately liquid droplet and the surrounding gases works well, and property evaluation schemes developed for these two distinct phases can be effectively used. However, the situation with supercritical fluids becomes quite different. Owing to the continuous variations of fluid properties in the entire domain, classic techniques dealing with liquids and gases individually may lead to erroneous results of droplet behavior and computational difficulties. Until today, this remains one of the unsolved problems.

The proposed numerical analysis aims to develop a unified model which will describe the droplet behavior when passing from subcritical, across critical, and finally into supercritical regimes. To precisely predict these physical processes, the model will be eventually calibrated with the experimental data.

Governing Equations

The basic equations employed in this study to describe a general flowfield are the axisymmetric, multi-component conservation equations. A generalized form of these equations written in curvilinear coordinates is given by

$$\frac{1}{J} \frac{\partial r q}{\partial t} = \frac{\partial}{\partial x_i} \left[-r U_i q + G_q G_{ij} \frac{\partial q}{\partial x_i} \right] + S_q \quad (1)$$

where J , U_i and G_{ij} represent the Jacobian of the coordinate transformation, contravariant velocities and diffusion metrics, respectively. μ_e is the effective viscosity when the turbulent eddy viscosity concept is employed to model the turbulent flows. S_q is the source term. The equation of state for an ideal gas is used to close the above system of equations.

Grid Generation

To be consistent with the governing equation formulation and efficient in numerical solution, an elliptic three-dimensional grid generation has been implemented into this computer modeling. An ADI/SOR method is employed for the numerical solutions of the elliptic Poisson equations for the grid network. Through the specification of proper boundary conditions, a favorable grid network is obtained which is smooth and close to be orthogonal.

Numerical Scheme

A pressure based solution method is selected so that a wide range of flow speeds and multi-phase fluid could be analyzed with the same code. To solve the system of nonlinearly coupled partial differential equations, control volume approximations are used to establish a system of linearized algebraic equations. A relaxation solution procedure is employed to couple the governing equations. A simplified momentum equation is combined with the continuity equation to form a pressure correction equation. The pressure correction equation exhibits elliptic behavior for low speed flow and becomes continuously more hyperbolic as flow speed increases. To solve the system of linear algebraic equations, a semi-implicit matrix solver is utilized. This matrix solution algorithm is a modified Stone's method. This method has been reported to be very efficient for matrix systems resulting from

complex curvilinear coordinates systems including high aspect ratios and high grid skewness. However, this method does require a large amount of memory.

Preliminary results

The computational model of the droplet is taken from a practical consideration. For this stage of the study, the droplet is considered as a sphere and to be isothermal. The droplet has a diameter of 0.1 (cm). The calculations were made on INDIGO R4000. The convergence of the solution is monitored using a global residual of the conservation variables.

Figure 5-2 shows the flow velocity vector plots. Though there is no forced flow from the ambient fluid around the droplet, a flow is developed by the temperature difference between the droplet and far field ambient fluid temperature under the action of gravity. Currently, the droplet temperature is set as 300 K and the ambient temperature is taken as 450 K. The selection of the parameter is only for the testing of the numerical model. Eventually, the physical conditions will match with the experimental conditions. This flow is well known as natural convection. The flow plot clearly indicates a recirculation in the test chamber. Figure 5-3 shows the temperature distribution. It is obviously noticeable that the natural convection plays significant roles on the resulting temperature distribution. Therefore, we can conclude that the computer model has to couple the flow system with the temperature.

EDUCATION AND TRAINING

One graduate student actively participated in the research: Zhicheng Wang (Graduate, Chemistry)

PUBLICATIONS

Two technical presentations have been give at the combustion physics branch at NASA Marshall Space Flight Center.

A paper has been presented in a technical conference:

J.D. MO, Qingwei Zhao, T. Bai, and Alan S. Chow, "Numerical Simulation of A Twin Swirl Burner," 34th Aerospace Sciences Meeting & Exhibit, January 15-18, 1996, Reno, NV.

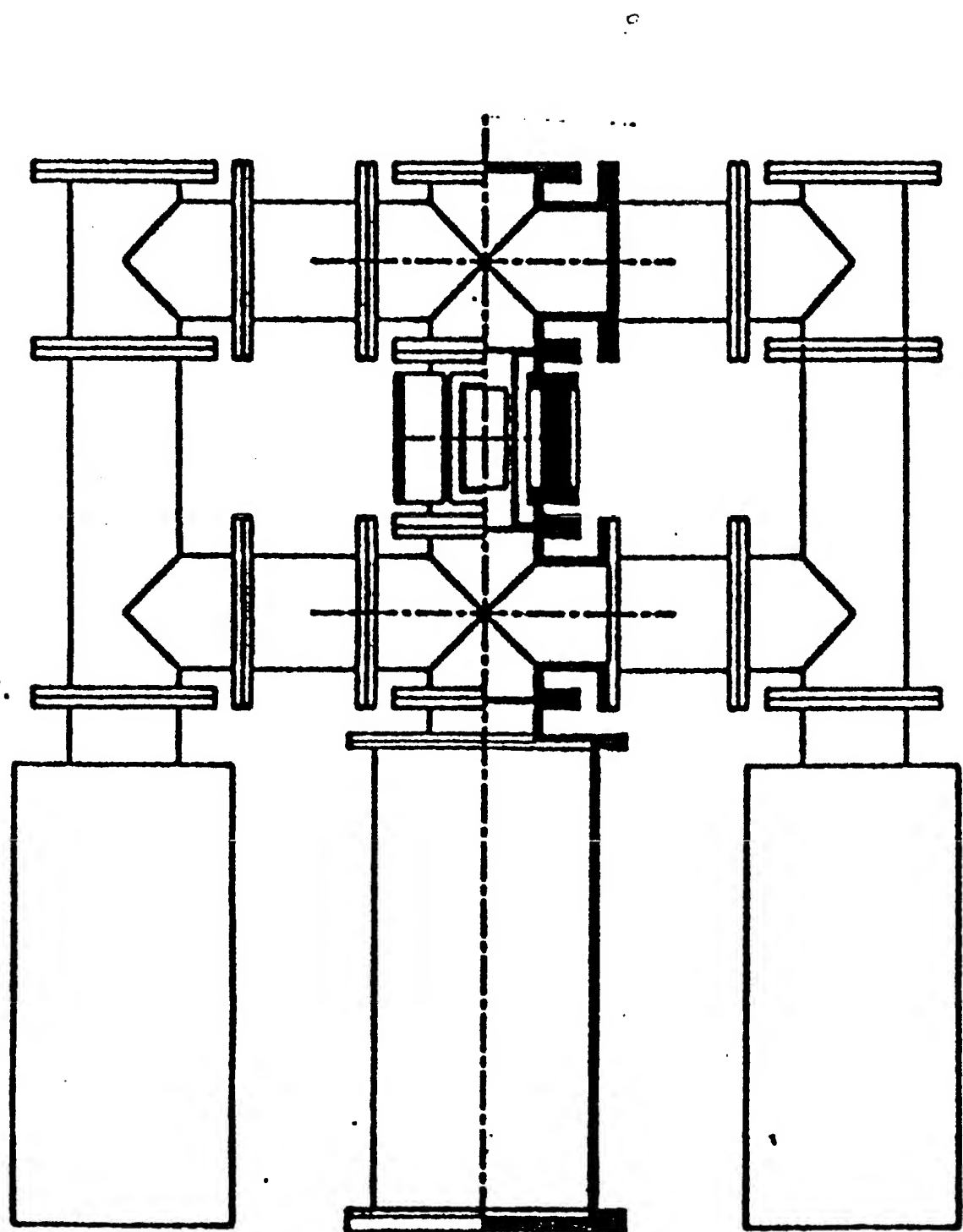


Fig. 5.1 Schematic of the test section of the droplet experiment apparatus

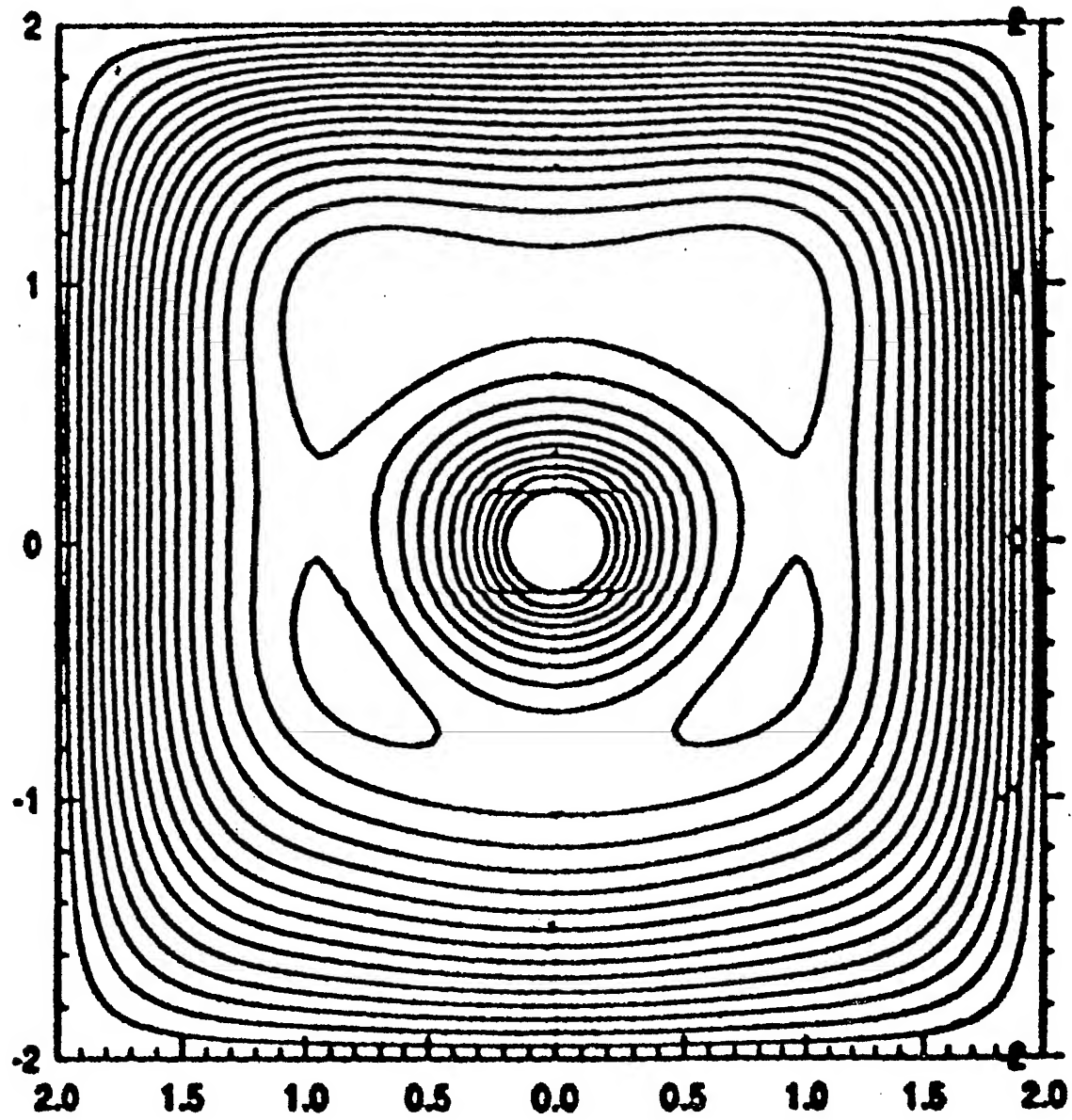


Fig. 5.2 Temperature distribution around a single droplet.

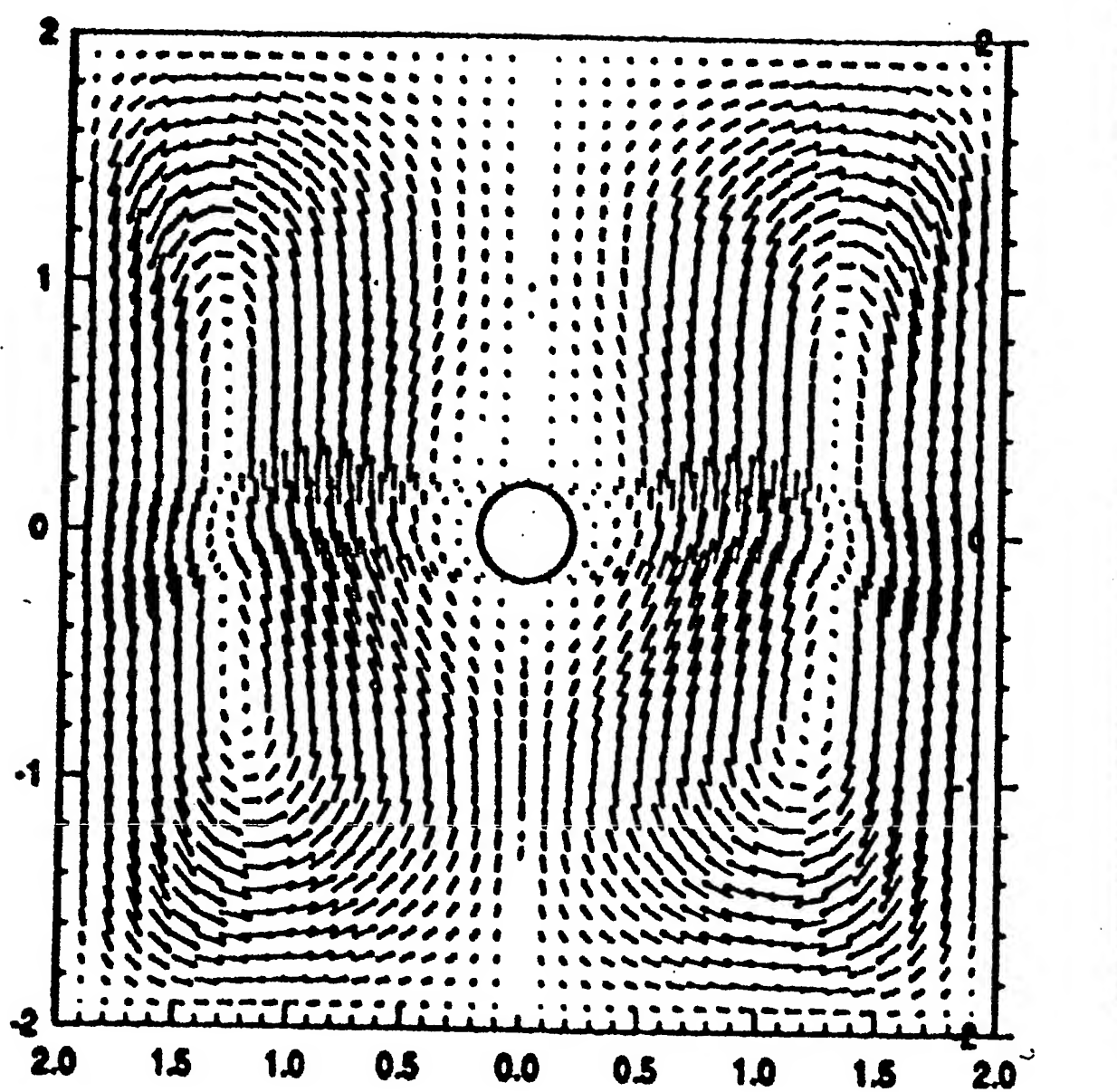


Fig. 5.3 Natural convection velocity distribution surrounding a droplet.

REFERENCES

1. Brzustowski, T. A. and Natarajan, R., "Combustion of Aniline Droplets at High Pressures," *Can. J. Chem. Eng.*, Vol. 44, No. 4, Aug. 1966, pp. 194-201.
2. Daou, J. Haldenwang, P., and Nicoli, C. "Supercritical Burning of Liquid (LOX) Droplet with Detailed Chemistry," *Combustion and Flame*, Vol. 101, 1995, pp. 153-169.
3. Dwyer, H. A. "Calculations of Droplet Dynamics in High Temperature Environments," *Progress in Energy and Combustion Sciences*, Vol. 15, 1989, pp. 131-158.
4. Faeth, G. M. "Current Status of Droplet and Liquid Combustion," *Progress in Energy and Combustion Sciences*, Vol. 3, 1977, pp. 191-224.
5. Ingebo, R. D. "Vaporization rates and heat transfer coefficients for pure liquid drops," *NACA TN 2368*, 1951.
6. Ingebo, R. D. "Study of Pressure Effects on the Vaporization Rate of Drops in Gas Stream," *NACA TN 2850*, 1953.
7. Law, C. K. "Recent Advances in Droplet Vaporization and Combustion," *Progress in Energy and Combustion Sciences*, Vol. 8, 1982, pp. 171-201.
8. Litchford, R. J., Parigger, C. And Jeng, S. M., "Supercritical Droplet Gasification Experiments with Forced Convection," *AIAA paper 92-3118*, 1992.
9. Manrique, Jose A. and Borman, Gary L., "Calculation of Steady State Droplet Vaporization at High Ambient Pressures," *Intern. J. Heat Mass Transfer*.
10. Matlosz, R. L., Leipziger, S., and Torda, T. P., "Investigation of Liquid Droplet Evaporation in a High Temperature and High Pressure Environment," *Int. J. Heat Mass Transfer*, Vol. 15, pp.831-852, 1972.

2.6 WASTE FORM DEVELOPMENT FOR USE WITH ORNL WASTE TREATMENT FACILITY SLUDGE

Investigators: G. M. K. Abotsi

Collaborators: William D. Bostick, Oak Ridge National Laboratory

INTRODUCTION

The potential use of grout as a stabilization/solidification medium for hazardous and radioactive wastes has been extensively investigated by D. Cul (1993), Morgan and Bostick (1992), Gilliam and Spence (1990), Spence (1990) and Osborne (1992) and McDaniel et al (1989). Bostick et al (1993) have shown that strong-base anion exchange resins derived from polyvinylpyridine are more effective in removing soluble pertechnetate

ion (TcO_4^-) from aqueous solution than standard quaternary ammonium resins. They have also shown that the sorbed technetium forms a strong bond with the resin and can only be desorbed to an appreciable extent by very strong reagents such as perchloric acid. Solidification in grout has been suggested as a possible final waste form for the disposal of the spent resin. Similar studies on the application of ion-exchange resins and grout to nitrate ion disposal have been conducted by Morgan and Bostick. Addition of granulated blast furnace slag to portland cement has been shown to enhance the integrity of the solidified waste forms containing nitrogen.

It has also been shown that mixed low-level radioactive and hazardous wastes can be stabilized by solidification in cement-based grout. Hydrolyzable metals such as cadmium, lead, nickel and uranium have been shown to be effectively retained in grouts formulated from portland cement and fly-ash. However, the ability of the grouts to retain technetium is low due to the existence of the radioactive metal (^{99}Tc) as highly mobile pertechnetate anion. Significant improvement in the retention of technetium was achieved by addition of blast furnace slag to the grout. This enhancement has been attributed to the ability of the slag to reduce $Tc(VII)$ to the less aqueous soluble $Tc(IV)$ species. Cement-based waste forms have also been suggested as viable media for final disposal of sludge.

McDaniel et al (1989) have shown that the leach rates of cesium-137 can be significantly reduced by the addition of various inorganic substances to the cement. It has been shown that incorporation of conasauga shale into cement reduced the Cs-137 release rates by almost three orders of magnitude after leaching in distilled water for 120 days. Indian red pottery clay reduced the leachability by about two orders of magnitude. Grundite also reduced Cs-137 extraction from the cement, although the effect was less than those for conasauga and pottery clay. The mechanism for the improved retention of cesium is attributed to ion-exchange and sorption to the inorganic media.

GOALS AND OBJECTIVES

The above discussion shows that there are several methods of treating radioactive wastes for disposal and the selected treatment option will depend on the nature of the waste. The main objective of this project is to evaluate treatment options for safe storage or disposal of water softening sludge (WSS # 5, filtercake) generated at ORNL. However, for safety, a nonradiological sludge that simulates WSS #5 sludge at ORNL was used in this project to help define and demonstrate several treatment options. The waste form performance undertaken included: water elimination, radionuclide stabilization, volume reduction relative to the reference surrogate material, leachability of nonradiological cesium (Cs) and strontium (Sr) from the waste forms prepared from the surrogate material and waste form compressive strength.

APPROACH

Preparation of WSS #5 Surrogate Sludge

Simulated ORNL water softening sludge No. 5 (WSS #5) was prepared from in-house precipitated CaCO_3 and other ingredients shown in Table 6-1:

Table 6-1. Composition of WSS #5 Surrogate Sludge

<u>Chemical used</u>	<u>Chemical Formula</u>	<u>Amount, g</u>	<u>Nominal Conc'n, %wt.</u>
Calcium carbonate	CaCO_3	240.5	63.3
Hematite	Fe_2O_3	20.85	5.5
Magnesium carbonate	MgCO_3	59.0	15.5
Aluminum hydroxide	$\text{Al}(\text{OH})_3$	11.8	3.1
Diatomaceous earth	SiO_2	48.0	12.6

Calcium carbonate, the major constituent of the filtercake, was prepared by slow addition of equimolar solution of sodium nitrate (NaNO_3) to calcium chloride (CaCl_2) solution. The pH of the slurry was checked periodically until the final pH was 8.9. The sample was then filtered and rinsed with five volumes of tapwater to remove the excess sodium chloride. The wet sample was then weighed and dried in an oven at about 100°C . The dry solids (380.2g) were blended and 234.5g of water was added to yield a wet filtercake (614.7 g) which contained 38.2 %wt. moisture. The water was spiked with 75 mg/L of strontium (using nonradiological $\text{Sr}(\text{NO}_3)_2$) to obtain 92 mg Sr/g of dry solids.

Thermal Analysis of the Sludge

The effects of thermal treatment on the surrogate waste was determined using a Seiko Thermogravimetric/Differential Thermal Analyzer (TG/DTA 320). Approximately 3.36 mg of the filtercake was placed in a platinum pan of the instrument and the sample was heated in ultra pure nitrogen to a maximum temperature of $\sim 1200^\circ\text{C}$. A thermogram of the changes in the sample weight was obtained.

Waste Volume Reduction by Calcination

To determine the volume reduction of the calcium carbonate and the surrogate sludge as a result of heat treatment, samples of these materials were placed in a Coors ceramic boat and calcined at 850°C for 4 hours in a Lindbergh tube furnace with an

Eurotherm 818S controller. A heating rate of 20°C/min. was used to raise the temperature from ~25°C to 850°C. The samples were allowed to cool to 100°C and then removed from the furnace and cooled to room temperature in a dessicator. The initial weight of the calcium carbonate used was 1.2221g and the weight after the calcination was 0.6793g, giving a weight loss of 44.4%.

Compaction of the Calcined and Uncalcined Wastes

To further reduce the volume of the wastes, samples of the calcined and the uncalcined calcium oxide and the surrogate wastes were compressed at 4000, 6000 or 8000 psi for 10 minutes using a Buehler Specimen Mount Press. The effects of paraffin addition on the strength of the compressed wastes were also studied. The weight of each sample before compression was 14.0 g. The dimensions of the cylindrical molds produced were measured shortly after the compaction and repeated for several days to determine the stability of the compressed wastes.

Compressive Strength Analysis

The compressive strengths of selected samples were determined by Quantachrome Corporation, Boynton Beach, Florida, using a Quantachrome Crush Strength Analyzer and the ASTM standard test procedure D4179. A copy of the analysis is attached. The samples were compressed diametrically since the compressed test samples were too large to fit into the instrument grips for the commonly applied axial crush strength tests.

Surface Area Measurements

The BET surface area of the calcined calcium carbonate was measured using nitrogen as the adsorbate and a Micromeritics Gemini 2360 Surface Area Analyzer. The surface areas were determined using five N₂ adsorption values.

ACCOMPLISHMENTS

Results and Discussion

The results of the TGA studies are shown in Figure 6-1. The initial rapid weight loss (indicated by A) up to about 100°C is attributed to loss of moisture. Beyond this temperature, changes in the TGA profile are also noted at about 197, 347 and 637°C, as shown by B, C, and D, respectively. The slight weight loss around 200°C could be due to loss of water of hydration. The changes in the thermogram at 347°C and 637°C are ascribed to the decomposition of MgCO₃ and Al(OH)₃, respectively, and was confirmed by literature data Weast et al (1986), Gates et al, (1979). The total weight loss due to the thermal treatment to 1200°C was approximately 44 % and it is in good agreement with

TG/DTA
 <Sample> OAKRIDGE-FILCAK
 3.364 mg
 (3.364 mg)
 <Name> OAKRIDGE1
 <Reference> EMPTY PT PAN
 95/06/05 10: 44
 0.000 mg <Sampling>
 0.5 sec

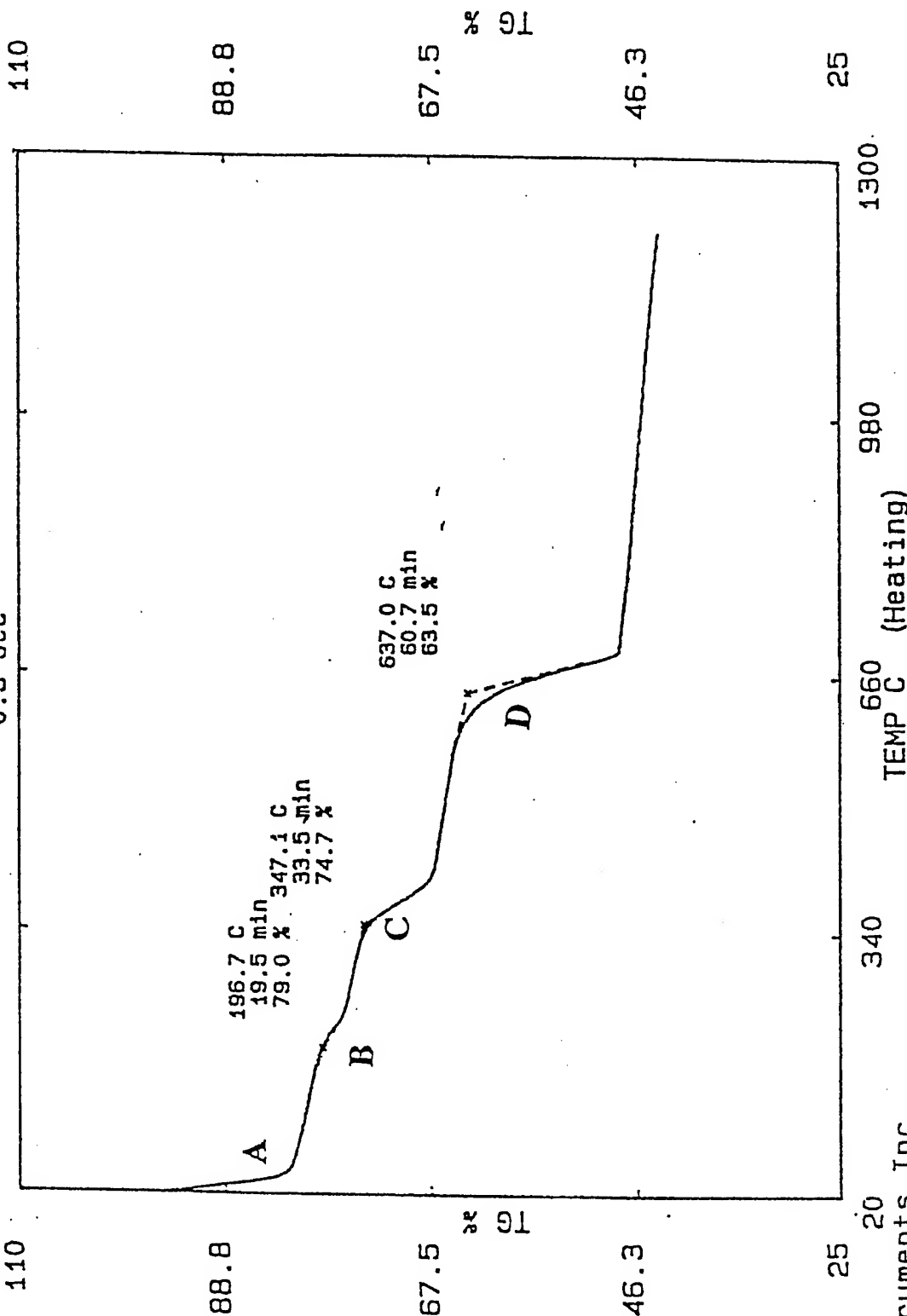


Figure 6.1 Thermogravimetric analysis of surrogate filtercake (WSS #5).

the value of 44.4% obtained when the sample was calcined at 850°C. This confirms the moisture content of the sample to be about 44%. Since the amount of water added to the synthetic sludge constituted 38.2%, the difference in moisture content (i.e., 38 versus 44%) is attributed to moisture in the starting materials used to prepare the surrogate waste. The thermogram for the CaCO₃ indicated that this sample decomposed at ~900°C and it is in agreement with the decomposition temperature of 898.6°C for calcium carbonate reported in the literature (Weast et al (1988)).

The compaction results and the dimensional changes of the molds after three days of exposure to atmospheric conditions are summarized in Table 6-2.

Table 6-2. Compaction and dimensional changes for the calcium oxide produced by calcination of calcium carbonate and the surrogate sludge.

Waste	Paraffin Added, % wt.	Compaction		Dimensional Change, %.
		Pressure, psi		
CaO	0	4000		31.3
CaO	0	6000		40.6
CaO	0	8000		15.6
CaO	15	8000		16.7
CaO	50	8000		25.0
Uncalcined Surrogate	15	8000		16.7
Calcined Surrogate	15	8000		8.3

The initial diameter of the CaO compressed at 4000 psi was 3.2 cm and the height was 1.2 cm. However, after 3 days, the diameter of the cylindrical mold expanded to 4.2 cm and it started to disintegrate. The diameters of the CaO samples that were pressed at 6000 and 8000 psi expanded from 3.2 cm to 4.5 and 3.7 cm, respectively after 3 days of exposure to laboratory conditions. Like the sample that was compressed at 4000 psi, the latter two samples were also unstable, although the specimen that was compressed at 8000 psi was slightly more stable. The diameters of the samples compressed at 4000, 6000 or 8000 psi expanded by 31.3, 40.6 and 15.6 %, respectively. After 3 days, the height of the uncalcined surrogate-15% paraffin cylinder was 1.4 cm, while that of the calcined surrogate-15% paraffin mold was 1.3 cm. These values represent expansions of 16.7 and 8.3 %, respectively. Compared to the paraffin-based samples, more crumpling occurred in the paraffin-free CaO after about one week of exposure to the atmosphere. Addition of

35% paraffin to the surrogate sludge increased the strength of the compacted material as shown in Tables 6-3. The stability of this sample was monitored for 39 days.

Table 6-3. Dimensions of the surrogate sludge containing 35% paraffin compressed at 8000 psi.

<u>Time, Days</u>	<u>Diameter, cm</u>	<u>Height, cm</u>
0	3.2	1.50
14	3.2	1.50
21	3.2	1.55
28	3.2	1.55
35	3.2	1.55
39	3.2	1.55

As the results in Table 6-3 show, the dimensions of this sample were essentially constant within the time period investigated and indicates insignificant moisture uptake by the sample. However, a slight increase of 3% in the height of the sample was noted after 14 days of exposure to the laboratory environment.

The results provided in Table 6-4 show that the compressive strengths of the waste forms that were evaluated ranged from 49 to 172 lb/in². The data also show that the compressive strength increased with increase in the paraffin content of the surrogate wastes.

Table 6-4. Compressive strengths of selected paraffin-containing samples.

<u>Sample</u>	<u>Compressive Strength, (lbs/in²)</u>
15% paraffin + calcined surrogate sludge compressed at 8000 psi.	49
35% paraffin + calcined surrogate sludge compressed at 8000 psi.	172
15% paraffin + calcined CaCO ₃ compressed at 8000 psi	139

The data in Table 6-5 show that the surface area of the calcined calcium carbonate is 0.1 m²/g. This value is much lower than that obtained for the calcined surrogate sludge which had a surface area of ~13 m²/g. Thus, it appears that the sludge constituents, other than the calcium carbonate, are primarily responsible for the observed surface area results. Due to problems with the surface area instrument which were later detected and rectified,

the current results should be more valid than those (which were around 160 m²/g) reported earlier.

Table 6-5. Surface areas of the CaO and the calcined surrogate sludge.

<u>Sample</u>	<u>Surface Area, m²/g</u>
Calcined CaO	0.1
Calcined surrogate sludge	13.2

SUMMARY AND CONCLUSIONS

A synthetic sludge that simulates Water Softening Sludge #5 (WSS #5) at Oak Ridge National Laboratory has been successfully prepared and evaluated for its thermal behavior, volume reduction by calcination, stabilization, compressive strength properties and surface area. Thermogravimetric analysis of the filtercake resulted in a weight loss of 44%, which occurred between 100-640°C. The weight reduction is attributed to loss of moisture and the decomposition of the surrogate constituents, primarily magnesium and calcium carbonates and aluminum hydroxide.

Compaction of the surrogate waste and the calcium oxide (produced by calcination of calcium carbonate) in the presence of paraffin resulted in cylindrical molds with various degrees of stability. The most stable product was the calcined surrogate-35% paraffin mixture that was compressed at 8000 psi. This sample expanded by 3% after 14 days and it also gave the highest compressive strength of 172 lb/in². In contrast, dimensional expansions of 8.3 to 40.6% occurred in compressed CaO-paraffin and surrogate-paraffin mixtures after three (3) days of exposure to laboratory conditions. The surface areas of selected samples were ~0.1 to 13 m²/g. The low surface areas will have the advantage of reducing moisture uptake and promote binding of the filtercake with polymeric materials such as paraffin. Similar benefits can be obtained by removing the moisture by calcination of the sludge at temperatures around 640°C.

This work has successfully demonstrated that surrogate water softening sludge #5 at ORNL can be sufficiently stabilized by blending it with about 35% paraffin and compacting the mixture at 8000 psi. The material has a compressive strength of about 172 lb/in² which is sufficient for temporary storage of the waste while long-term storage waste forms are sought. Since the composition of the surrogate sludge is similar to that of the real filtercake at ORNL, the results of this project may be extrapolated to the real WSS #5 sludge.

EDUCATION AND TRAINING

Two undergraduate students, one in Engineering and the other in Chemistry, have been involved in this project. Their responsibilities included collection of experimental data and reading relevant literature on waste form development. The students are:

<u>Name</u>	<u>Year</u>	<u>Department</u>
Daren Danzy	Senior (undergraduate)	Chemistry
Jeraline Askew	Junior (undergraduate)	Engineering

OUTREACH AND TECHNOLOGY TRANSFER

This research is a collaborative effort between Clark Atlanta University and the Oak Ridge National Laboratory. It is expected that the results of the study will assist ORNL, the Department of Energy, other federal, state agencies and industry to identify durable waste forms for long-term radioactive waste disposal.

PUBLICATIONS AND PRESENTATIONS

Abotsi, G. M. K., Bostick, W. D., "Waste Form Development for use with ORNL Waste Treatment Facility Sludge," Technical Report No. K/TSO-7A, Oak Ridge National Laboratory, 1996.

REFERENCES

1. Del Cul, G. D., Bostick, W. D., Trotter, D. R., Osborne, P. E., 1993. Separation Science and Tech., 28(1-3), 551.
2. Morgan, I. L., Bostick, W. D., 1992. In "Stabilization and Solidification of Hazardous, Radioactive and Mixed Wastes, 2nd. Vol. ASTM STP 1123, T. M. Gilliam and C. C. Wiles, Eds., p.133.
3. Gilliam, T. M., Spence, R. D., 1990. J. Hazard. Mat. 24,189.
4. Spence, R. D., Osborne, S. C., 1992. "Literature Review of Stabilization/Solidification of Volatile Organic Compounds and the Implication for Hanford Grouts", personal communication.
5. McDaniel, E. W., Tallent, O. K., Sams, T. L., Delzer, D. B., Bostick, W. D., "Bases for Selecting Cement-Based Waste Forms for Immobilizing Radioactive Wastes," In: Scientific Basis for Nuclear Waste Management, XII. W. Lutz and R. C. Ewing, Eds., Materials Research Society, p. 421-430., 1989.

6. R. C. Weast, M. J. Astle and W. H. Beyer, Eds., 1986-87, p. B-79. *Handbook of Chemistry and Physics*, 67th Edition,
7. B. C. Gates, J. R. Katzer and G. C. A. Schuit, "Chemistry of Catalytic Processes," McGraw-Hill, New York, 1979, p. 250.

2.7 THE APPLICATION OF PLASMA ARC TORCH IN THE VITRIFICATION OF HAZARDOUS AND SIMULATED RADIOACTIVE MIXED WASTE

Investigator: M. Danjaji

Collaborator: Louis Circeo, Georgia Institute of Technology

INTRODUCTION

Wastes can be sorted in several classes according to their origin (municipal, hospital, industrial wastes, etc.), their nature (mineral, biological, chemical, nuclear), their state (solid, liquid, gaseous) and the level of pollution. Some are discharged to dumps which are classified according to the toxicity of the wastes stored, the others undergo a suitable treatment which can result into a complete destruction of the product. Satisfactory destruction solutions exist for "ordinary" wastes: one can incinerate without any problem household refuse and some industrial wastes. For more polluting wastes, the classical techniques brought into operation are the following: reconversion, recycling, biological treatment, chemical oxidation, confinement, incineration and the ultimate solution, the suppression of waste-generating processes. This situation however is not satisfactory, indeed today some wastes are inadequately treated or are not treated at all because of the lack of suitable means. Incineration remains the ultimate desirable solution when it does not give rise to uncontrolled transfer of pollution especially in gaseous phase; in any case the polluting compounds have to be trapped and the quality of the environment protected (no emission of toxic gases, no pollutants into the fumes).

Mixed waste (a mixture of hazardous and low-level radioactive waste) introduces a whole new dimension to the waste problem. For the past 50 years, national laboratories and nuclear industries have been producing mixed waste from different nuclear activities at an alarming rate. All around the nation, there are sites and laboratories that are contaminated with mixed waste. Such sites include Hanford Reservation site, Fernald, Idaho National Laboratory and Brookhaven National Laboratory. At the moment there are no technologies approved for use in remediating mixed waste instead they are now stored in drums, temporary on site awaiting disposal to the nuclear waste storage facility-Waste Isolation Pilot Plant (WIPP). Nonetheless there are several problems facing the

smooth transfer of these drums to WIPP. Opening of WIPP depends upon, among other things, a five-year period. Other problems facing mixed waste disposal is that on site space for storage is been exhausted and if mixed waste are to be stored at WIPP untreated, the space available at WIPP will fill in a short time without disposing all of the drums containing the mixed waste.

The fight against pollution goes along with the search of means adapted to efficiently treat wastes, especially the toxic, hazardous and radioactive ones. For this purpose, processes using plasma bring new solutions which are more efficient than traditional techniques. The interest of plasma is to provide very high temperatures and energy densities, together with an ionized and reactive medium which can increase the kinetics of some of the reactions. Plasma techniques can advantageously replace conventional burners in incineration plant which process hard and costly to eliminate waste.

Plasma arc technology was developed 30 years ago by NASA for the US space program to simulate re-entry temperatures on heat shields. Only recently has this technology begun to emerge as a commercial tool in several industries such as steelmaking, metallurgy, previous metal recovery, and waste disposal. A plasma arc torch is a device that converts electrical energy into thermal energy. A plasma is an ionized gas that is conditioned to respond to electromagnetic forces. The plasma arc is created when a voltage is established between two points. The plasma acts as a resistive heating element and maintains a temperature around $12,000^{\circ}\text{C}$. Plasma occur naturally in the form of lightning. This resistive heating element presents a distinct advantage over any solid heating element since it is a gas and cannot melt and fail. The plasma arc creates a "flame" that has temperatures ranging from 4000°C to 7000°C . Thus plasma torches operate at much higher temperatures, higher enthalpies and greatly increased efficiencies than fossil fuel burners. In addition, plasma torches require only about 5% of the gas necessary for fossil burners. Therefore, effluent gases are greatly reduced. A plasma torch generally employs a stainless steel cylinder several inches in diameter and several feet in length, the specific dimensions are related to the torch power levels. This cylinder integrates the electrodes, insulators, gas injectors, and water dividers into a functional torch. In a special design, the rear electrode acts as the anode while the front electrode acts as the cathode. This design is referred to as the reverse-polarity torch. The two electrodes are separated by an electrical insulator. Cooling water is circulated within the walls of the tube to prevent the metals (stainless steel and cooper) from melting under the high temperatures of the plasma arc. A gas is injected into the tube tangentially to its circumference at the insulator. The gas serves two purposes. First, it replenishes the gas for the plasma (which actually only consumes about 1% of the total gas flow). Second, the gas stabilizes the plasma arc column and allows the contact location of the arc to be varied by varying the gas flow rate. In this manner, the copper electrode surfaces can be consumed at a uniform rate. The type of gas has no great effect on the process and gases such as air, argon, nitrogen, oxygen, or helium can be used. Typically, air is the simplest and least expensive gas source.

OBJECTIVES

The objective of this project is to evaluate the feasibility of plasma arc technology at a bench scale for destruction and stabilization of hazardous and mixed wastes. This will augment existing and anticipated Department of Defense (DOD) and private sponsored research efforts in plasma arc technology. The focus is to assess the plasma arc technology capability for the complete destruction of organics in both the hazardous and mixed wastes and the vitrification of inorganics thereby rendering the radioactive material non-leachable in the slag.

APPROACH

The physical processes to be examined include partitioning and evaporation. The target chemical processes include examinations of the reaction occurring during the melting and destruction of the material. The melt environment will promote sufficient oxidation to maximize retention of the heavy metals in the glass product, and to oxidize organic materials contained in the waste. The transformation mechanisms and thermal effects involved with the processing will be determined. The following are controllable parameters from which changes during the vitrification process can be noted:

1. The power at which the plasma system is operating. Changes to the power directly affects the amount of heat available to melt the simulated mixed wastes.
2. The type of gas used in the plasma torch. The gas used will determine whether the melting process is taking place in an oxidation or reduction state.
3. The feed rate of the simulated mixed waste into the plasma furnace chamber. By altering the feed rate of the material introduced into the chamber, the effects of exposure time to the plasma will be examined.

Additional equipment which will provide insights into the physical and chemical processes which may be occurring within the chamber will include an infrared pyrometer. The pyrometer will be used to track the surface temperature of the charge materials. While additional thermocouples will provide further information about the temperature gradients occurring within the chamber during the run. Real time monitoring and data acquisition of these temperatures will be done through use of a computer. A continuous gas emission monitoring analyzer system will be used to measure sulfur dioxide, oxides of nitrogen, carbon monoxide, hydrogen chloride, and volatile organic compounds measured as total hydrocarbons in the exhaust gasses of the source. The above mentioned pollutants will be measured in the exhaust gas stream using instrumental analyzers according to EPA approved test methodology. Toxicity Characteristic Leaching Procedure (TCLP) will be carried out on the slag to determine the leacheability of the metals in the slag.

QA/QC

Data Collection

A pyrometer will be used to measure the surface temperature of the waste bath during the vitrification process. Type C thermocouples will provide information about the temperature gradients inside the chamber during a run. A control panel with the capability of converting alternating current to direct current will measure the voltage and current that is used by the torch. This information is needed to determine the power (product of voltage and current) at which the torch is operating.

Data Analysis

Toxicity Characteristic Leaching Procedure (TCLP) test will be carried out on the vitrified product. This test is a standard Environment Protection Agency (EPA) test. The procedures, detection limits, precision and bias for this test are set by EPA

Calibration

A list will be maintained of all instruments (pyrometers, thermocouples) serial numbers used on the task for taking data. The list is maintained current so that the equipment substitutions made during the course of the task are known to the Principal Investigator. This is necessary should the test be repeated for any reason. Instruments used for taking data critical to the test shall be calibrated and calibration will always be traceable to a nationally recognized standard measurement. All instrumentation used will fall within calibration during the time of test.

Standard Operating Procedures (SOP)

- The electrode in the plasma torch is checked for holes, this is necessary to avoid leakage of water into the system during vitrification. If there is any hole in the electrode it should not be used.
- The compressed air or gas that will be used is checked for the right pressure and flow level to guarantee the power level of operation before igniting the torch.
- Since the system is water cooled, the temperature of the water and its level is checked before igniting the torch.
- The voltage level knob on the control panel is set to 50% of the voltage at which the torch operates. This is needed for a smooth start up of the torch.

For safety reasons the following precautions are taken:

- Every personnel is required to wear a protective gas mask against chemicals and particulates.
- Ear protectors are used to reduce the noise level due to the torch during operation.
- During or immediately after operation no one is allowed to torch the crucible because of its high temperature.
- An eye protector should be used if anybody wants to observe the bath during or immediately after operation.

ACCOMPLISHMENTS

Technical Results and Discussion

An experiment was conducted at plasma torch power level of about 170kW, and at furnace temperatures above 1,300 °C. Twenty five pounds of pure chrysotile asbestos in metal canister were fed into the furnace over a 35 minute period. Tests for asbestos fibers were made on the vitrified asbestos residue, the metal canister residue, samples of residue found inside the furnace, and air samples inside and outside the process gas stream. Trace amount of asbestos found in the solid residue and gaseous effluent consisted of only scattered fibers. This amount of asbestos is considered negligible, and falls below current EPA asbestos exposure standards guidelines (i.e. less than 1 percent volume in the solid vitrified material and a maximum airborne concentration of 0.2 fibers per cubic centimeter in the workplace). If necessary, a small increase in furnace temperatures or residence time of the asbestos should readily eliminate even these trace amounts. In this experiment, plasma arc technology was demonstrated to be an efficient and effective method of destroying and vitrifying pure chrysotile asbestos in an environmentally safe manner.

Other tests were carried out at different times on simulated mixed wastes such as:

Trial 1. Crushed and shredded remnants of electronic circuit boards from Department of Defense projects. The boards are largely composed of glass reinforced thermoplastics containing residual electronic components, copper, noble metals, and iron.

Trial 2. Savannah River Site (SRS) soils contaminated with organic liquids or sludges. These soils would be typical of those found in certain seepage basins.

Trial 3. Tyvek filter paper with attached filtrate.

Trial 4. Used high efficiency particulate air (HEPA) filters. These filters are widely used at SRS for the removal of sub-micron particulates.

Trial 5. A composite mixed solid waste. A surrogate composite waste representative of the standard "Heterogeneous Debris" recipe was processed. Eighteen feed canisters were loaded with a distribution of the following materials:

Charcoal, cedar, PVC piping, steel shot, nuts and bolts, glass jars, uncurred concrete, aluminum oxide, diatomaceous earth, leaded gloves, aluminum foil, CrCl₃-6H₂O, NiCl₂-6H₂O, CeNO₃, CsCl, and Water.

For trial 1, the plasma system was allowed to cool overnight prior to disassembly and cleaning. The processed soil was not all localized in the graphite crucible, nor was it all fused. A fused core was located in the center of the graphite crucible. This fused portion represented about 30.2 weight % of the material fed to the plasma unit. It was glassy at the center of the fused region and more bricklike at the edges. Also in the crucible, was a large fraction (6,941 g) of burned soil, calcined, but not fused. Unfused soil was also found between the top chamber gasket and the graphite crucible (179g),

overflowing the graphite crucible (75g) and blown out of the crucible into the chamber (1,517 g).

For trial 2, when the processed circuit board material was later collected from the plasma unit, it yielded a diverse waste form. The material had a significant metallic fraction, there was also some evidence of incomplete destruction of individual circuit board components. The balance was fused blackened material, and a brittle, flaky residue. About 23.3% of the material fed to the plasma was recovered. As circuit boards are largely composed of plastics, and dense packing into the cardboard carrier tubes was not attainable (i.e. a lot of cardboard was also sent to the torch), it is not surprising that so much material was lost.

In trial 3, the Tyvek-loaded tubes were fed to the pre-heated plasma chamber. A steady state feed rate of 1 canister every three minutes was achieved. The Tyvek was indeed destroyed by the plasma torch, but very little solid material was recovered from the plasma chamber (only 7.2% of the material was accounted for). This waste stream was composed largely of organic material, and while it was destroyed, much of the material exited with the off-gases. A great deal of tar-like scum was captured by the off-gas system.

As for trial 4, the waste stream was quite well suited to plasma processing. The preloaded filter was melted using the plasma torch prior to feeding any additional material. This preload provided a molten bath which kept a higher fraction of the material in the graphite crucible itself, generating less "blowout." Also the fact that the waste stream was almost exclusively metal and glass meant there was less of an organic fraction to volatilize. The waste form recovered was a fused mass containing a significant metallic fraction.

In Trial 5, a total of 10,474g of "heterogeneous debris" feed material was processed in the plasma chamber. After initial processing a steady state feed rate of 1 canister every 5 minutes was achieved. The resultant waste form was a homogeneous fused mass. The waste was well vitrified after cooling. Due to the available scope of this effort, very little analytical information was gathered and/or performed as a results of these test. However, a wealth of physical observations were available. The plasma processing effectively destroyed the original waste and generated a fused waste form plus a residual.

OUTREACH AND TECHNOLOGY TRANSFER

When all feasibility studies are completed, the plasma arc technology can be transferred for immediate use to the Department of Defense, Department of Energy, Municipal Landfill owners, and the Steel Industry.

PRESENTATIONS

M. Danjaji, Circeo L.J., R.A. Newson, A. Applewhite-Ramsey, R.F. Schumacher, T.L. Spatz, "High Temperature Vitrification of Surrogate Savannah River Site (SRS) Mixed Materials" to appear in Proceedings of America Ceramic Society Conference 1995.

2.8 THE APPLICATION OF GEOGRAPHIC INFORMATION SYSTEMS (GIS) IN ENVIRONMENTAL ASSESSMENT, RESTORATION, MODELING AND MANAGEMENT

Investigator(s): H. O. Adeyemi, and M. Danjaji

Collaborator: United States Army Construction Engineering Research Laboratory (CERL), US EPA Region IV GIS Section (Office of Integrated Environmental Analysis), Georgia Institute of Technology, and Science Application International Corporation (SAIC)

INTRODUCTION

Geographic Information Systems (GIS) are computerized systems of hardware and software used for the storage, manipulation, managing, visualizing and analysis of spatial environmental data. It is a data integration tool which combines sophisticated mapping capabilities together with a large computing capacity. The vast volume of spatial data and its direct relationship and interaction with man, has become a critical and important concept for analysis to promote intelligent decisions in planning and utilization of human resources.

As a management tool it enables extensive multi-media analysis and evaluation in geographic areas in ways which were previously too time consuming or difficult to conduct. Additionally, the data integration capability is useful in the Superfund Accelerated Cleanup Model (SCAM) whose aim is to make the Superfund process timely and efficient. As different program areas of Superfund are integrated into SCAM, GIS can be used to integrate data collection and site characterization for a timely assessment of site-specified conditions. Coupled with a statistical package called S-PLUS, GIS has emerged as a powerful tool for modeling and analysis of environmental phenomena.

Some of the projects that were undertaken in the GIS laboratory are summarized below.

OBJECTIVE

The goal of GIS Laboratory at Clark Atlanta University (CAU) is to provide training in GIS technology and support research in environmental assessment, restoration, modeling and management. Some mathematics, science and engineering students have been trained in the GIS technology with the objective of increasing the minority math/science/engineering pool in environmental research. Through research we intend to contribute to advancement of GIS technology and demonstrate our capability by undertaking GIS projects for federal, state and local governments and agencies, and for industry and business concerns.

APPROACH/METHODOLOGY

Each project has its own unique approach as explained below.

“Utilizing Geographic Information Systems in the Analysis of Relationships Between the Environment and Endangered Species in the State of Alabama”

For this project eleven digit maps of hydrologic units and sub-watersheds of Alabama were digitized by using an Altek back-lit digitizer and an ARC/INFO environment. The digital map was made available by EPA Region IV.

“On the Estimation of the Black-Capped Vireo Territory Density Using Geographic information Systems Technology”

GRASS and the S-PLUS statistical package were used for this project. The data was given by USACERL.

“The Benefits of the Cultural Resources Information Systems in the XWindows(XCRIS) to Military Installations”

This project used different computer environments such as GIS, Data Base Management Systems(DBMSs), and Word Processing Systems(WPSs). The data used was given by USACERL.

“The Citing of Landfills in Habersham County, Georgia”

An ARC/INFO environment was used for this project and the data was submitted by EPA Region IV.

“Effects of Chlordane and Dursban on the Environment and its Inhabitants at Fort Polk, Louisiana via the Planning and Resources Integration Stewardship Module(PRISM)”

GRASS environment was used for the analysis of this project and the data was provided by USACERL.

“A Study of Clark Atlanta University Spatial Features for Future Security System Implementation Using Geographic Information Systems Technology”

For this project a number of methods were used in capturing the data into the computer for the analysis such as:

- ARC/INFO was used to capture the text data and also for retrieving, editing and plotting the different geographic data layers.
- PHOTOSTYLER, a PC-based computer software for scanning the buildings and aerial photographs.
- ERDAS, a UNIX based software for rectifying the images.

A number of agencies and units within and outside the university were consulted for the data needed for this project. Of these the main ones were:

- Georgia Aerial Survey and Metro Engineering Company for aerial photographs of CAU and surrounding areas.
- Atlanta City Council for map of geographic footprints for the area
- USGS Office for 7 1/2 inch quadrangle maps
- Facilities Office at CAU for information on trees, shrubs and buildings in the CAU main campus.
- Development Office at CAU for data on CAU property boundaries.

QA/QC

Digitization Error

A way to assure the quality of the digitizing process is using the 'check plot' method. In this method, the plot is placed on top of the original map being digitized. After the registration of the map, a few long lines could be digitized from the map data. These lines could then be plotted and used for comparison. If they exhibit noticeable distortion, then the registration is suspect. Otherwise, digitizing can continue using the proven registration points. Quality can also be assured by producing a scaled output during or after completion of digitizing and compared visually, often with the aid of a light table, to other paper maps, aerial photography, or remotely-sensed data.

Reporting and Calculations

Calculations for compliance tests above are based on basic statistical inference methods.

1. Select a sample of n points, where n is at least 20.
2. Evaluate the error (residuals) at each point in the x dimension as

$$e_{x_i} = \hat{x}_i - x_i$$

where \hat{x}_i is the encoded x -coordinate of point i and x_i is the reference x -coordinate for that point according to a source of higher accuracy.

3. Compute the mean error (residual) in the x dimension for all n sample points as

$$\bar{e}_x = \frac{1}{n} \sum_{i=1}^n e_{x_i}$$

4. Compute the standard error in the x dimension as

$$s_x = \left[\frac{1}{n-1} \sum_{i=1}^n (e_{x_i} - \bar{e}_x)^2 \right]^{\frac{1}{2}}$$

The following is often referred to as the root mean squared error (RMSE) of the residuals:

$$RMSE_x = \left(\frac{1}{n} \sum e_{x_i}^2 \right)^{\frac{1}{2}}$$

5. Compute the mean errors and standard errors in the y and z dimensions using analogous equations.

6. Compliance testing is performed by applying hypothesis tests for bias and precision. A test for bias in the x dimension is carried out by computing the statistic

$$t_x = \frac{(\bar{e}_x - e_{x_0})n^{\frac{1}{2}}}{s_x}$$

where e_{x_0} is the acceptable error (residual) in the x dimension. If the inequality

$$|t_x| < t_{n-1, \alpha/2}$$

is achieved, the map has achieved compliance with the standard. Note that $t_{n-1, \alpha/2}$ is defined as the percentile from the t-distribution with $n-1$ degrees of freedom corresponding to a two-tailed confidence level of $1-\alpha$.

7. Perform analogous compliance tests in the y and z dimensions.

8. Perform a test for precision in the x dimension by computing the statistic

$$\chi_x^2 = \frac{s_x^2(n-1)}{s_{x_0}^2}$$

where s_{x_0} is the acceptable standard error in the x dimension. If the inequality

$$\chi_x^2 < \chi_{n-1,\alpha}^2$$

is achieved, the map has achieved compliance with the standard. Note that $\chi_{n-1,\alpha}$ is defined as the percentile from the χ^2 distribution with $n-1$ degrees of freedom and corresponding to a confidence level of $1-\alpha$.

9. Perform the analogous tests for the y and z dimensions.

Detection Limits and Acceptance Criteria

EPA's Data Quality Objective (DQO): RMSE< 25 meters.
Locational Data Policy stipulates that horizontal accuracy is to be specified as a range within which there is 95% confidence that the true value falls.

NMAS : **Horizontal Accuracy** standard specifies that at most 10% of the sampled points may have an horizontal error greater than $1/30''$ (for map scales greater than 1: 20,000) or $1/50''$ (for map scales of 1:20,000 or less). Error is defined in terms of the discrepancy in the locations of the mapped and reference points. Note that the standard is expressed in map units.

The **Vertical Accuracy** standard specifies that at most 10% of the sampled points may have a vertical error greater than one-half the contour interval of the map. Discrepancies in the vertical dimension may be offset by allowing for a shift in the locations of points by an amount equal to the allowable horizontal error.

EMAS/ASPRS: Only if **Compliance and Precision** tests are confirmed.

USGS: Compliance Testing is based on the maximum error and RMSE computed for a Digital Elevation Map (DEM) database.

Accuracy Category for the DEM is based on the following criteria.

For Level I DEMs the maximum RMSE is 15m and the sample contains no points for which the vertical error is over 50m.

For Level II DEMs the maximum RMSE is 7m and the sample contains no points for which the vertical error is more than twice the contour interval of the source map

For Level III DEMs the maximum RMSE is 7m and the sample contains no points for which the vertical error is more than the contour interval of the source map.

Locational (Positional) Error

Perhaps the most serious error in GIS is locational or positional error. This is the discrepancy between the position of a point, line or polygon in a GIS and its actual geographic location. Digitized maps obtained from the EPA will be cross-checked for errors. One of the ways the maps will be checked is by comparing positions of known geographic locations on hard copy maps with those in the GIS. It will be ensured that the Data Quality Objective (DQO) of 25 meter positional accuracy is maintained. Furthermore, a Data Quality Assessment Summary (QAS) (James, 1993) will be required for any dataset that is used in environmental justice studies. QAS is designed to show compliance with DQO for positional accuracy.

Attribute Errors

Thematic attribute consists of all available data/information concerning a point, line or polygon in GIS. For purposes of accuracy assessment, thematic attribute can be nominal (e.g. land cover types), ordinal (referring to rankings, where numerical attribute values indicate relative quantities (such as suitability scores or interval/ratio (continuous scales for which a given interval or ratio has the same meaning for all values of the attribute, such as temperature and precipitation). Even when attributes in data input to GIS are correct, GIS may associate the attributes to wrong polygons. A thematic attribute consistency/accuracy test is required to identify this type of error.

Population Estimation Error

An accurate population estimate is very important in environmental justice studies. Risk assessment is frequently used to compare risks among exposed populations in order to set priorities for mitigating exposure. Information on the size of exposed populations is often essential to selecting appropriate regulatory options and concentrating limited resources on the most severe problems.

Population estimate errors occur because the affected population cuts across Census Block Groups (BG) and Enumeration Districts (ED) or it is located in rural sites where the population is sparse. In each of these scenarios any assumption of uniform population distribution will result in population estimate error. No one method has been found to be universally accurate although standard methods frequently used for estimating population include Photo count, Map count, Census centroid, Census Polygon/Land Use, Census Polygon/Uniform Density, Thiessen Polygon/Uniform Density and Thiessen Polygon/Land Use. Photo count and map count methods are manual methods. The last four methods employ GIS to combine census geographic and demographic data with land use data to obtain population estimates. Thiessen polygons are the polygons generated by the ARC/INFO Thiessen command.

ACHIEVEMENTS

Technical Results and Discussion

"The Benefits of the Cultural Resources Information Systems in the XWindows(XCRIS) to Military Installations"

Under the Federal Historic Preservation legislation, all federal lands must be surveyed for historic and prehistoric cultural resources. Much of the software available in aiding in the process of managing a military installation's cultural resources is both expensive and time consuming to learn. This process has commonly used separate, incompatible computer environments such as: Data Base Management Systems, and Word Processing Systems, making successful cultural resource management extremely arduous. The Cultural Resources Information System in windows(XCRIS) is a computer software that integrates DBMSs, WPSs and GISs letting users efficiently manage cultural resources in a user friendly environment.

XCRIS has proven to provide effective and efficient management of cultural resources on military installations. It reduces the existence of extremely expensive, yet under utilized spatial and relational data bases and their associated hardware. XCRIS lets the cultural resource manager use GIS to overlay archeological, historical and present training maps to help the installation locate cultural resources and protect them from over exposure to military training routines. In one particular case XCRIS had saved Ft. Riley an estimated 2 million dollars over a spread of eight months. The cultural resource manager at Ft. Riley has stated that his post-XCRIS work has been cut in half and made to be more efficient and less time consuming. Before, he was relying on several people to accomplish his tasks, now he is able to complete tasks without waiting on others.

"The Citing of Landfills in Habersham County, Georgia"

Habersham county, Georgia has a reputation for having numerous poultry farms. This county also has a total of three Superfund sites, four Toxic Release Inventory sites and five Resource Conservation and Recovery System sites. All of these sites are located in the southern and central regions of the county around the three major cities of Baldwin, Cornelia, and Clarkesville. The focal point of the project is to investigate possible toxic hazards to the human and animal populations of Habersham county.

The visual analysis, conducted using Geographic Information Systems, concluded that the vicinity of these hazardous sites leaves no doubt as to the contamination of the environment. The GIS overlayed maps of the hazardous sites, populated areas, bodies of water, chicken farms, etc. showed that these sites lie along rivers, streams and drinking wells which carry the water for the nearby population. GIS also showed that the hazardous sites were close to some residential areas as well. Not only are these sites harming the occupants of Habersham county but the rest of Georgia as well, for Habersham is a leading producer of poultry for the state.

"On the Estimation of the Black-Capped Vireo Territory Density Using Geographic Information Systems Technology"

Based on a 1994 study of the nesting and territory preferences of the Black-Capped Vireo, a small migratory songbird, it was declared that the bird was endangered. Using Geographic Information Systems(GRASS and S-Plus) maps of territory distribution of the vireo were produced. These maps were overlaid on the slope, aspect, soils,

elevation, vegetation, and military activities coverages. With the density estimate of the nesting success and the GIS maps, territory position preferences were identified, thus, helping in the land management plan for the preservation of the black-capped vireo on the Fort Hood military installation.

GIS and S-Plus were able to show that the 1994 black-capped vireo territory distribution was not independent of geographic bearing, rather the northwestern region seemed to be the preferred region of nesting. The map combining Fort Hood's military activities, positioned in the northwest region, and the 1994 vireo territory data shows that almost half of the successful vireo territories (106/225) lied within artillery impact areas. Therefore, to preserve the black-capped vireo, the northwestern region should be prohibited from further human development and interface.

"Effects of Chlordane and Dursban on the Environment and its Inhabitants at Fort Polk, Louisiana via the Planning and Resources Integration Stewardship Module(PRISM)"

In a cursory glance at the building maintenance files at Fort Polk, it was found that a tremendous amount of insecticides especially Dursban and Chlordane were used on a regular bases to rid the buildings of annoying pests. In an effort to sustain a healthy environment for living creatures a study was done as to how these chemicals, namely Dursban(which can affect the central nervous system) and Chlordane (which can cause cancer) can affect those who come into contact with them on a long and short term bases.

Geographic Information systems was used to identify the buildings on the installation that had been sprayed. A map of these buildings was created then overlayed on a map of soils then overlayed on a map of streams to show the geographic location of these chemicals to potential catalysts for expansion or transportation to the general public.

"Utilizing Geographic Information Systems in the Analysis of Relationships Between the Environment and Endangered Species in the State of Alabama"

Many government agencies have been created to aid in the process of sustaining a healthy relationship between humans and the environment we live in. When the relationship between the two becomes unhealthy and threatens the existence of one of the two constituents, something must be done to rectify the problem; especially in cases where the ecosystem is in danger of deterioration.

In an effort to show the relationship between endangered species and watershed regions in the state of Alabama, GIS was used to input, analyze, manipulate and store data collected through various government agencies. The first effort was directed at building the database for studying the habitats of the endangered and threatened species. Thus, a map of Alabama's hydrologic units regions and watersheds was digitized(a process of inputting raw data into a digital form), using Arc/Info. Also the data pertaining to the endangered species and their locations with respect to the hydrologic units and watershed regions had been collected.

"A Study of Clark Atlanta University Spatial Features for Future Security System Implementation Using Geographic Information Systems Technology"

The purpose of this study was to gather and represent CAU geographic data in a form which will assist the University Administration in making important decisions affecting the university. Decision of the expansion of the University, siting of facilities, implementing of security systems, are indeed dependent on the geography of the University. The scope of this study was limited to the spatial data for CAU main campus.

Data was collected from different agencies. Vertical and horizontal analysis of spatial data for CAU main campus were generated using ARC/INFO. Adequate database has been designed and built to cater for decision-making in regards to implementing security systems. This database can also be utilized in planning for future expansion programs within the University. A level of analysis for the terrain has been done with respect to projecting images (e.g. building) and aerial representation of CAU surface area into the computer system with the aid of photostyler and ERDAS.

EDUCATION AND TRAINING

The following students were trained in the GIS laboratory:

Jashed Fakhrid Deen (CAU graduate student);
Jada Polk (graduated, start on her PhD. in fall of 96 at North Carolina University);
Sadonna Upchurch (graduated); Asantewa Macintosh (CAU graduate student);
Rahman Pounds (CAU senior student); Booker Washington (graduated);
Clauzell McIntyre (CAU senior student); Kenyetta Sims (CAU senior student);
Keyna Williams (CAU graduate student);
Affiong Bassey (Engineering student at Georgia Tech);
Charlene Cummings (graduated); Michelle Houston (graduated)
Keva Vaughn (Junior); Nicole Wright (graduated); Lisa Hills (senior)
Erica Jackson (PhD student at Georgia state University)

The following were graduate research assistants in the GIS laboratory:

Agatha Gaisie-Nketsiah (now with AT&T)
Martin Asare Bekoe (now with Federal Express)
Regismary Ngessa
Simon Gikiri (Ph.D student at the University of Maryland).

The GIS Laboratory also provided training in ARC/INFO to *Desmear Systems, Inc.*, a minority-owned engineering company located in Decatur, Georgia. *Desmear Systems* continues to use our laboratory facilities to achieve project grade competence in the technology.

OUTREACH AND TECHNOLOGY TRANSFER

The GIS technology can be transferred for immediate use to the Department of Defense, Department of Energy other Federal agencies and industries.

PRESENTATION

The following presentations were made:

- EPA/NIEHS National Symposium of Health Research and Needs to Ensure Environmental Justice, Washington, DC (February 9-12, 1994).
- Presentation was done for Colonel John Neil, Army Research Office, CEPER program evaluator (September 21, 1994)
- Presentation was done for Enhancing CAU Participation in Defense Research Annual Program Evaluation by ARO (November 28-29, 1994)

REFERENCE(S)

James, D. E.,1993. *Spatial Data Quality Assessment Tools for Environmental Applications*. Lockheed Environmental Systems and Technologies, Las Vegas. Nevada.

2.9 ATLANTA ELECTRONIC COMMERCE RESOURCE CENTER INTEGRATING COMPUTER-BASED DISTANCE LEARNING

Investigators: K. Shujaee, O. Olatidoye, M. Danjaji, and S. Sarathy

Collaborators: Georgia Institute of Technology

BACKGROUND

The Atlanta Electronic Commerce Resource Center (AECRC) is part of a eleven-center network which has a primary mission to promote awareness and provide implementation of Electronic Commerce (EC) and related technologies for a competitive US industrial base. Each center focuses on education and training, consulting, and technical support services in Electronic Commerce and related technologies for businesses and government activities located in its region. The AECRC located in Atlanta, Georgia, is operated by the Clark Atlanta University (CAU) and Georgia Institute of Technology under contract with the National ECRC Program office which is operated by Concurrent

Technologies Corporation (CTC) in Johnstown, Pennsylvania. The AECRC is chartered to serve the southeastern states of Georgia, Alabama, Florida, and South Carolina. Operations in Atlanta began with a signed contract from the National ECRC Program Office on November 3, 1994, however the subcontract for CAU was not fully operational until January of 1995. In support of the activities and research of the CAU-AECRC different area of operation are assigned to staff and faculty with student support. The CAU-AECRC is coordinated by Dr. Olu Olatidoye the program director.

A key component of the AECRC is the Legacy Data Management and Distance Learning which is coordinated by Dr. Khalil Shujaee.

Legacy Data Management (LDM) is the process of identifying and evaluating historical information and implementing potential solution requirements for long-term storage and data processing in a cost effective manner.

Distance learning is a rapidly growing method to deliver education and information to a different part of the globe, in real time, to a dispersed audience.

OBJECTIVES

The mission of the AECRC is to assist small and mid-sized manufacturers in implementing EC and CALS related technologies. The program focuses on five key areas, namely: Education and Training, Consulting and Technical Support, Information Infrastructure, Legacy Data Management, and Program Management.

The goal of this project is to demonstrate the feasibility of real time computer-based distance learning technology in a classroom environment. The aim is to establish an affordable computer learning system which provides both desktop teleconferencing capabilities and access to multimedia instructional material on the Internet.

METHODOLOGY AND APPROACH

The approach which this project has adopted is using desktop computer teleconferencing technology, and making use of existing software and hardware. Video teleconferencing distance learning is not a new idea, and it has existed for a long time. The idea here is to use existing technology and make that more accessible to remote sites via computer desktop teleconferencing.

The approach we are using is to identify the simplest, but most efficient way to interact between student and teacher, between different virtual classrooms via desktop teleconferencing, and to develop appropriate techniques to improve the capability of teleconferencing distance learning. This desktop teleconferencing approach has been tested between offices at Clark Atlanta University.

ACCOMPLISHMENTS

Results and Discussions:

Legacy Data Management (LDM)

- Equipment funding authority was received and a revised equipment list was generated, consistent with funding level. The procurement process was initiated.
 - ◊ The interim Atlanta AECRC file server system was operational.
 - ◊ An HTTP server was installed and tested and Atlanta ECRC Home page was designed.
 - ◊ Installation of a database system was completed.
- Completed the development of an intelligent forms conversion demonstration for the legacy data lab. A user can scan an original document in either a handwritten or typed format, such as an invoice, bill or sale, etc., and extract the image data from the form and send it zone by zone to an OCR engine for conversion into a database.
- The program is now in the pending stages of using Distance Learning to implement it's course delivery

Distance learning

For the preliminary stage, we have installed the desktop teleconferencing between the Visualization, simulation and Design Laboratory (ViSiDeL) at CAU and Video Teleconferencing room (VITREC) room at CAU. The methodology described above was used with sufficient audio and video connections between two sites to create real time interaction between them. The computers used for the test sites were Silicon Graphics made Indy machine. The Indy machine was equipped with the appropriate build-in hardware and software, which included audio and video capabilities. The second Video teleconferencing test took place between Clark Atlanta University and Savannah State College. The audio and video capability of the sites was absorbed, and communication improvements are under study.

The third part of the project, planned to create a home page for ECRC at CAU. The home page has been created at CAU Site for ECRC with student assistance, and already all information regarding ECRC is available at this home page. Moreover, efforts are being made to create a home page for the Department of Engineering, with a majority of this project already having been completed.

EDUCATION AND TRAINING

We intend to foster a collaboration among universities, industries and the government to deliver quality distance learning education using state-of-the-art interactive visual communications technology, to enhance the learning needs of students in primary schools and college level institutions, and to provide public information services.

We have created a home page for the ECRC at CAU, and it is linked to the ViSiDeL home page. Of course, more features can be added to this home page.

Under this program, the following undergraduate students assisted in this work during the Spring semester of 1996:

- Leon Milligan has worked as an undergraduate student assistant to create home page for ECRC at CAU. He is a Junior student on the Electrical Engineering program. He has been involved on Robotics design since spring 1996.
- John Washington was trained in Robotics Design. He is a Junior student in Electrical Engineering.
- Fumilola Awoniyi was involved in robotics design and she also been directed in electrical circuit design. She is a Junior Electrical Engineering student, and she will be transferring to Georgia Tech in spring 1997.
- Curry A.Wynn has been mentored in the area of Circuit analysis and control design. He is a sophomore student in Electrical Engineering.

All the above students were working in collaboration with ViSiDeL.

OUTREACH AND TECHNOLOGY TRANSFER

We have already begun to have departmental and faculty level interaction at different universities and industries. It is intended to create virtual classrooms via desktop and video teleconferencing, and to offer different courses (such as graphics and Electrical Engineering design courses) at different sites. Universities and colleges, such as the University of North Carolina A&T, University of Minnesota, Georgia Institute of Technology, Savannah State College, Spelman College, and Morehouse College have all shown an interest in having distance-learning linkage with us.

We have visited University of North Carolina A&T, and met with Dean of College of Engineering, (Dr. Carolyn W. Meyers), Dean of School of Technology (Dr. Earl Yarbarough), Chairman of the Department of Management and Safety (Dr. Robert Pyle), Dr. Musibau A. Shofoluwe from Department of Manufacturing Systems, Professor

Reginald C. Whitsett and Professor Ronnie Bailey from the Department of Architecture, Mr. Denis Selby and Dr. Ron Smith Director of Continued Education at NC A&T State university. They have agreed to establish exchange technology between faculty members and students via Video teleconferencing and computer desktop teleconferencing. We have established relations between ViSiDeL and the University of Minnesota, and Dr. Gary Henderson, from University of Minnesota, has asked us to have full capabilities of computer desktop teleconferencing in order to be able to train students and faculty members on high-performance computing and many other related courses.

2.10 TURBULENT PREMIXED METHANE-AIR COMBUSTION

Investigator: Y. Yeboah

Collaborator: Howard Ross, Microgravity Combustion Program, NASA Lewis Research Center

INTRODUCTION

Many industries are now pursuing lighter hydrocarbon alternative fuels to reduce pollutant emissions. These fuels include natural gas which is composed of about 80% methane. This makes methane an important fuel for the future. In most industrial equipment, the characteristic dimensions and flow rates are often large enough for the flows to be considered as turbulent. As a result, turbulent reacting flows are very important in the combustion and chemical processing industries. Thus, a clear understanding of the turbulent combustion of methane-air flames, for example, is essential to most industries that use methane or natural gas as fuel. Methane-air flames are reasonably understood as a result of the extensive studies that have been carried on them. Also, research activities in the area of turbulent reacting flows have increased significantly over the years.

Based on the review of the available literature, the following statements may be made:

Effect of Turbulence

- Turbulence increases flame area through wrinkling of the flame front by fluctuating velocity field.
- Turbulence reduces flamelet burning velocity through flame structure.

Numerical Modeling and Simulation

- Reliability of available prediction models for turbulent reacting flows is very low.

Environmental Concerns

- Understanding of turbulence-chemistry interaction is essential, especially for NO_x and soot formation.
- Understanding combustion characteristics of chlorinated hydrocarbons is needed.

Chemistry

- Analysis of methane-air kinetics using multiple reactions is important and has been attempted by other researchers.

Effect of Pressure

- Few studies have been conducted at elevated pressure in the intermediate temperature regime.
- Effect of pressure on practical combustion systems ($P > 10 \text{ atm}$) is not clear.

OBJECTIVE

The broad objective of this study is to develop and establish a turbulent reacting flow combustion program within the Combustion Laboratory at Clark Atlanta University, that will:

1. Enhance, through experimentation and modeling of CH_4 -air combustion, the understanding of turbulent reacting flows, and
2. Enable Clark Atlanta University to develop expertise and facilities to train and educate minority scientists and engineers capable of assisting NASA and other US organizations and industries in the area of combustion.

The specific research objectives are to:

- a) Establish the effects of process variables such as injection speed or flow rate (i.e., degree of mixing), presence of chlorinated hydrocarbons, and fuel/air ratio on the emissions, flame shape, velocity, and temperature distribution during turbulent combustion of premixed methane and air.
- b) Develop a mechanistic model to explain the results and to improve the reliability of prediction methods for turbulent reacting flows.

The results from this study could serve as the comparative ground based experimental and modeling program for a future microgravity research study which will investigate the influence of gravity or buoyancy-driven convection on a turbulent reacting flow system of methane and air.

APPROACH

The study is being conducted within the Combustion Lab at Clark Atlanta University and involves both experimental and theoretical (numerical modeling) activities. The experimental phase involves the design and fabrication of a premixed burner and the use of the burner to study the effects of injection speed or flow rate, chlorinated hydrocarbon concentration and fuel/air ratio on the emissions, flame shape, velocity distribution (including streamlines and vorticity), and temperature distribution. The theoretical activities will involve the development of a mechanistic model that will further improve the understanding and ability to make predictions on turbulent reacting flows. Shown in Figure 10-1 is a schematic of the experimental set up.

ACCOMPLISHMENTS

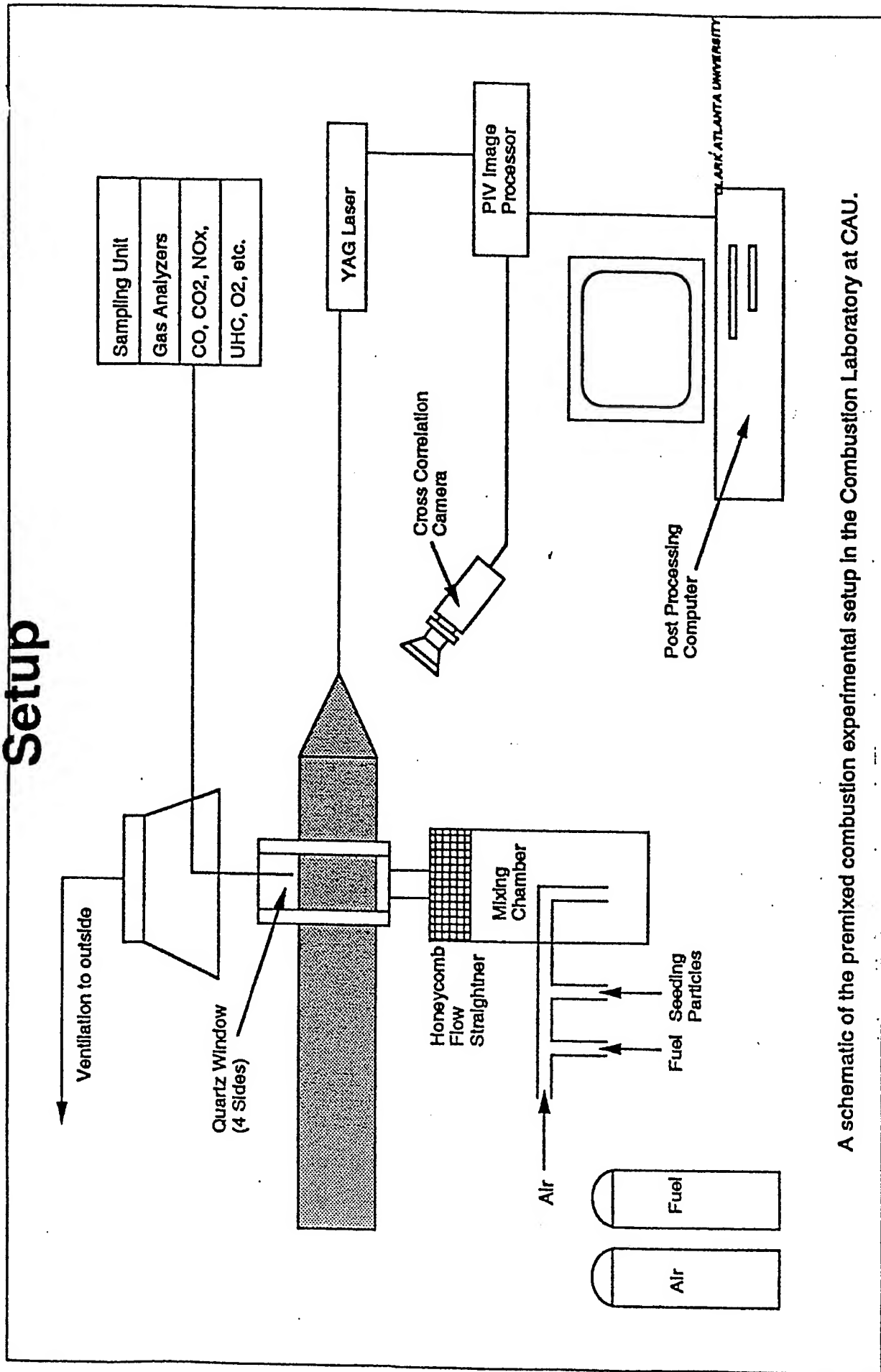
- Completed review of the literature on turbulent premixed methane-air combustion.
- Acquired and tested all necessary equipment. These include:
 - a) Horiba gas analyzers for CO, CO₂, SO₂, NO_x, O₂, and total hydrocarbons.
 - b) Perkin Elmer Model 2000 Fourier Transform Infra-red Analyzer.
 - c) Dantec Flow Map Particle Image Velocimeter (PIV) with a double image 700 PIV recorder, Spectra Physics 400 mj/pulse dual cavity YAG laser and dedicated PIV processor.
- Designed and Fabricated Premixed Burner (see Figure 10-1).
- Completed testing and calibration of equipment, instruments and sensors (including gas analyzer, thermocouples, etc.).
- Initiated preliminary data collection.
- Presented status report at 3rd HBCU Research Conference in Cleveland, Ohio.
- Submitted annual report at the end of July, 1996.

EDUCATION AND TRAINING

The following students continue to be educated and trained in this project as student research assistants:

- 1) Ms. Anny Ojekwe; Graduate student, Computer Science
- 2) Ms. LaShanda James; Junior, Engineering

Schematic Diagram of Experimental Setup



A schematic of the premixed combustion experimental setup in the Combustion Laboratory at CAU.

Figure 10.1

PUBLICATIONS AND PRESENTATIONS

The principal investigator and the graduate research assistant participated in the 3rd Annual NASA-Supported HBCU Research Conference held at Cleveland, Ohio on April 10-11, 1996. A paper with the same title as the project was presented at the Conference.

FUTURE PLANS

Future Activities will include:

- Parametric and optimization studies;
- Development of mechanistic model; and
- Analysis and Presentation of Result

2.11 OPTIMIZATION OF NON-THERMAL DISCHARGE (NTD) ELECTROCHEMICAL SYSTEMS

Investigators: Y. D. Yeboah, T. Bai and K. B. Bota

Collaborators: Jad Batteh, G. Rolader and J. Rogers, Science Applications International Corporation (SAIC), and W. C. Neely, Auburn University

BACKGROUND

With the passage of the Clean Air Act Amendment (CAAA) of 1990, federal agencies/departments and other major emitters must reduce their emissions of hazardous chemicals. Non-Thermal Discharge (NTD) is one of the most promising innovative technologies to destroy hazardous air pollutants (HAPs) and criteria pollutants contained in gas streams prior to atmospheric dispersion. Our research team has demonstrated destruction of eleven compounds: ethyl acetoacetate, dimethyl methylphosphonate, soman, formaldehyde, malathion, benzene, hydrogen cyanide, carbon monoxide, carbon tetrachloride, freon 12, and trichloroethylene. Other compounds successfully destroyed with an NTD include DCB, toluene, p-cumene, TCA, CFCs, methylene chloride, CFC-113, dioxin, acetone, isopropyl alcohol, and hydrogen sulfide.

The primary problem with NTD destruction is that the efficiency is not high enough. In other words, too much electrical energy is required for each hazardous compound destroyed. It is believed that this energy inefficiency stems from the free electrons exciting various non-useful molecular vibrational modes. To overcome this problem, a better understanding of the fundamental electron-impact and subsequent chemical kinetics is needed. The purpose of this research is to address, both theoretically and experimentally, this lack of fundamental understanding.

NON-THERMAL DISCHARGE (NTD) TECHNOLOGY

A schematic of a generic NTD system is shown in Figure 11-1, and its operation can be explained as follows. A reaction tube is comprised of electrodes separated, in the case of dielectric barrier discharges, from the working gas by dielectrics. A high-voltage power supply provides the required energy (Step #1). This high voltage, and the corresponding high electric field, is applied to the electrodes. As the gas flows through the reactor tube, between the dielectrics, it is exposed to an alternating high-voltage. This

high voltage, and the corresponding high electric field, breaks down the gas, stripping electrons from the gas molecules and creating a partially ionized plasma (Step #2). At atmospheric pressures, this breakdown results in a multitude of current filaments, or breakdown channels, called microdischarges. The input energy is efficiently transferred to the electrons. The dielectrics limit the duration of the discharges. The diameter of each of these discharge channels has been found to be on the order of 100 microns and the lifetime of each is on the order of a nanosecond. Because of the short time duration of the discharges, the electrons and heavy particles do not thermally equilibrate and the electrons are excited to temperatures on the order of 50,000-100,000 K while the bulk gas (heavy particles) temperature remains approximately constant (hence the name Nonthermal Discharge).

It is important to note that under optimum operating conditions, *more than 98% of the energy is coupled directly to the electrons; consequently, the process is very efficient compared to bulk gas heating.* The excited electrons collide with the gas molecules resulting in the formation of excited atomic/molecular states and other highly reactive species (Step #3), driving the desired chemical reactions and destroying the hazardous compounds. It is important to remember that the reactive species are a result of energetic-electron/molecule collisions, and hence, they are formed only within the microdischarges. After a discharge extinguishes, the created reactive species diffuse into the remainder of the gas and they collide with the hazardous compounds chemically altering them into simpler compounds (Step #4). Thus, NTD effectively exploits the unique characteristics of non-equilibrium plasmas (gases with highly excited free electrons) to drive desired chemical reactions, destroying hazardous compounds that are difficult to remediate with existing technologies.

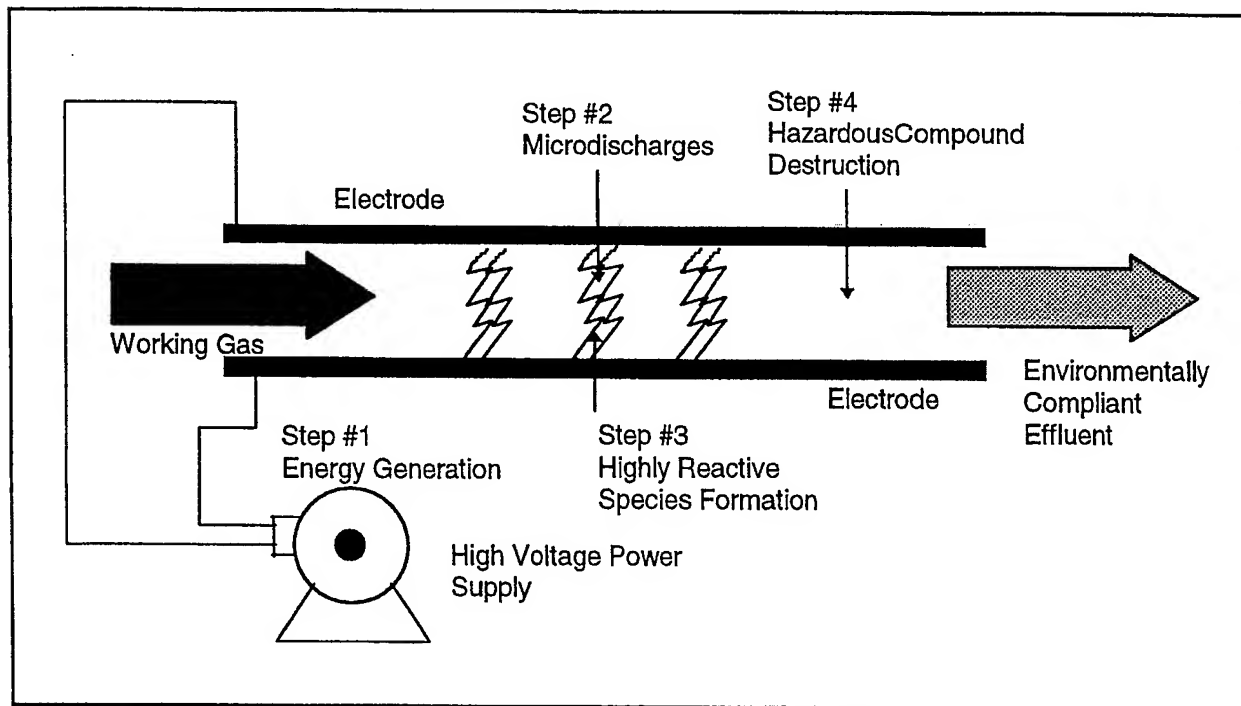


Figure 1. Schematic of a generic NTD system.

OBJECTIVE

The objective of this study is to undertake a combined experimental/theoretical program that will perform the basic research and provide the database to support the development of optimized design for Air Force and Wright Laboratory applications. Specifically, the study will:

- Develop a versatile NTD testbed for pollution;
- Conduct parametric and optimization experiments to determine the conditions that minimize the energy dissipation of NTD;
- Determine the exhaust stream composition at various experimental conditions, and
- Develop a reaction pathway and mechanistic model of the NTD process.

Another major objective of the proposed project is to educate and train minority students in the area of advanced emission control technologies. This will provide a pool of future minority engineers and scientists capable of assisting the Air Force, other federal agencies/departments, and industry with their programs on pollution prevention and treatment of exhaust gases.

APPROACH

The study will involve both experimental and theoretical studies. The experimental phase will involve the design and fabrication of an NTD testbed and the use of the testbed to study the effects of process variables such as inlet gas composition, power level and gap spacing on energy consumed per molecule of hazardous species removed, effluent composition and NO_x removal efficiency.

The modeling effort will involve the development of a reaction pathway and mechanistic model that will provide insight into the fundamental understanding of the electron-impact and subsequent chemical kinetics.

ACCOMPLISHMENTS

- All the major equipment and facilities of this new project were ordered and received.
- The condition and testing of the experimental setup has been completed
- Preliminary data collection has begun

EDUCATION AND TRAINING

- A summer internship award by SAIC was made to Iskil Soyinka, a junior in engineering, to participate in the project for the summer of 1996.
- Mr. Z. Wang is a graduate student in chemistry has decided to pursue his Ph.D. in chemistry in the project.

PUBLICATIONS AND PRESENTATIONS

- A project kickoff meeting was held on June 13, 1996 at Clark Atlanta University between representatives of Clark Atlanta University, SAIC, Eglin Air Force Base (Wright Laboratory, Armament Directorate) and Tyndall AFB (Armstrong Laboratory, Environics Directorate). Presentations were made by the CAU Principal Investigator and the Eglin AFB Project Program Manager.



**ENHANCING CLARK ATLANTA UNIVERSITY
PARTICIPATION IN DEFENSE RESEARCH**

VOLUME II

FINAL RESEARCH PROJECT REPORT

PROJECT DIRECTOR: DR. KOFI B. BOTA

SEPTEMBER 1, 1992 – JUNE 30, 1997

CONTRACT NUMBER DAAL03-92-G-0380

**CLARK ATLANTA UNIVERSITY
223 JAMES P. BRAWLEY DRIVE, SW
ATLANTA, GEORGIA 30314**

TABLE OF CONTENTS

SECTION 1: EXECUTIVE SUMMARY.....		3
1.1	Objectives	3
1.2	Research Programs	3
 SECTION 2:		
2.1	Research Project.....	5
2.2	Elastically Tailored Composite Design.....	13
2.3	Long Term Durability of Polymer Matrix Composites for High Temperature Applications	20
2.4	Blended-Wing-Body Structural Technology Study	23
2.5	Finite Element and Analytical Cross-Sectional Analysis of Composite Rotor Blades for Nonclassical Beam Formulation.....	27
2.6	Finite Deformation Response of Unsymmetric Composite Laminates in the Presence of Damage	29
2.7	High Performance Computing Techniques in Fluid Structure Interactions Problems	30
2.8	Constitutive Modeling and Testing of Polymer Matrix Composites Incorporating Physical Aging at Elevated Temperatures	33
2.9	Modeling and Testing of Hybrid Titanium Composite Laminates at Normal and Elevated Temperatures	37
2.10	Low Density, Low Conductivity Pan Ablative Optimization and Nozzle Fabrication	41
2.11	Compressive Creep of IM7/K3B Composite and the Effects of Physical Aging on Viscoelastic Behavior	45
2.12	Characterization and Mechanical Testing of a Polarization-Maintaining Optical Fiber – Phase II	49
2.13	Micromechanics Modeling of Fiber Reinforced Composites Incorporating Distinct Interface Properties	53
2.14	Sol-Gel Based Mullite Ceramics	57
2.15	Zirconia-Toughened Alumina Ceramics	66
2.16	Mechanical and Physical Testing of a Polarization-Maintaining Optical Fiber.....	75
2.17	Superconducting Materials Processing	83
2.18	Investigation of Front Frame Failure in High Performance Aircraft Engines	87
2.19	Research in Structural Dynamics and Control and Aeropropulsion	96
2.20	Unsteady Aerodynamics of Rotor-Stator Interactions	105
2.21	An Adaptive Flow Solver for Air-Borne Vehicles Undergoing Time-Dependent Motions/Deformation	122
2.22	Unsteady Aerodynamics of Airfoils Undergoing Large Amplitude Motions/ Deformations-Parallel Implementation of Incompressible Viscous Flows.....	125
2.23	High Frequency Response of a New Fiberoptic Probe for Temperature Fluctuation Measurement.....	128
2.24	Experimental Investigation of Flow Disturbances in Constricted Arteries.....	130
2.25	Thermal Analysis of a Novel Axial Power Monitor For Nuclear Reactors.....	131
2.26	Model Studies of Heart Valve Motion Under Pulsatile Flow	133

SECTION 1: EXECUTIVE SUMMARY

1.1 Objectives

The Army-supported research program entitled "Enhancing Clark Atlanta University Participation in Defense Research" (Grant #DAA203-92-9-03890), focused on interdisciplinary research areas in environmental technologies: flow, structures and materials; and software engineering. The program aimed at enhancing CAU's research capabilities, through development of resources and facilities (including equipment and personnel) in areas relevant to the Department of Defense. Several projects were executed and several faculty members were supported to develop expertise and research programs that fall within the mission goals and program objectives of the Department of Defense.

1.2 Research Programs

This final report is organized into two volumes. Below is a listing of the research projects covered by each volume:

Volume I

- Groundwater Flow and Contaminant Transport Modeling
- Development of a Pulsating Medical Waste Incinerator
- Study of the Effects of Ambient Conditions Upon the Performance of Fan Powered, Infrared Natural Gas Burners
- Development of a Two Stage, Pulse Combustion, VOC Destruction Technology
- Preliminary Study of Droplet Behavior Under Various Pressures
- Waste Form Development for Use with ORNL Waste Treatment Facility Sludge
- The Application of Plasma ARC Torch in the Vitrification of Hazardous and Simulated Radioactive Mixed Waste
- The Application of Geographic Information Systems (GIS) in Environmental Assessment, Restoration, Modeling and Management
- Atlanta Electronic Commerce Resource Center Integrating Computer-Based Distance Learning
- Turbulent Premixed Methane-Air Combustion
- Optimization of Non-Thermal Discharge (NTD) Electrochemical Systems

Volume II

- Health Monitoring of Concrete Structures Using Distributed Time Domain Reflectometry (ETDR) Sensors
- Elastically Tailored Composite Design

- Long term durability of polymer matrix composites for high temperature applications
- Blended-wing-body structural technology study
- Finite element and analytical cross-sectional, analysis of composite rotor blades for nonclassical beam formation
- Finite deformation response of unsymmetric composite laminates in the presence of damage
- High performance computing techniques in fluid structure interaction problems
- Constitutive modeling and testing of polymer matrix composites incorporating physical aging at elevated temperature
- Modeling and testing of hybrid titanium composite laminates at normal and elevated temperatures
- Low density, low conductivity PAN ablative optimization and nozzle fabrication
- Compressive creep of IM7/K3B composite and the effects of physical aging on viscoelastic behavior
- Characterization and mechanical testing of a polarization maintaining optical fiber - Phase II
- Micromechanics modeling of fiber reinforced composites incorporating distinct interface properties
- Sol-gel based mullite ceramics
- Zirconia-toughened alumina ceramics
- Mechanical and physical testing of a polarization-maintaining optical fiber
- Superconducting materials processing
- Investigation of front frame failure in high performance aircraft engines
- Research in structural dynamics and control and aeropropulsion
- Unsteady aerodynamics of rotor-stator interactions
- An adaptive flow solver for air-borne vehicles undergoing time-dependent motions/deformation
- Unsteady aerodynamics of airfoils undergoing large amplitude motion/deformations: Parallel implementation of incompressible viscous flows
- High frequency response of a new fiberoptic probe for temperature fluctuation measurements
- Experimental investigation of flow disturbances in constricted arteries
- Thermal analysis of a novel axial power monitor for nuclear reactors
- Model studies of heart valve motion under pulsatile flow

2.1 HEALTH MONITORING OF CONCRETE STRUCTURES USING DISTRIBUTED TIME DOMAIN REFLECTOMETRY (ETDR) SENSORS

OBJECTIVES

The long-term objective of this research project is to establish a practical technology using embedded electrical time domain reflectometry (ETDR) sensors for the application of in-service health monitoring of concrete structures. Specifically, the research effort will develop a new technique using ETDR sensors to measure structural stress/strain state and to detect the growth of crack damage in civil concrete structures. This health monitoring scheme can monitor in-service loading condition of the structure as well as locate the on-set of crack damage and initiate an early repair to prevent the growth of the damage. It will enhance the benefits of more commonplace, routine maintenance and repair programs and significantly reduce the cost of routine inspection and extend the service life of the nation's civil infrastructure.

APPROACH

Electrical time domain reflectometry (ETDR) is a well-developed technique and has been widely used to locate and evaluate discontinuities in coaxial power transmission cables. The ETDR technique can be best described as "closed-loop radar," where the information is derived from the reflections of a voltage pulse sent through a transmission medium. A typical ETDR system uses a transmission medium, e.g., a transmission cable, a step generator, and an oscilloscope, as shown in Figure 1.1. A voltage step sent by the step generator propagates along the transmission cable. When electric impedance discontinuities are present at any locations along the cable due to external disturbance, some of the electric step pulse is reflected at the point of discontinuity. The reflected step signal carries the information about the characteristic impedance of the transmission cable and shows both the position and the nature (resistive, inductive, or capacitive) of each discontinuity along the line. All of the information (position, nature, and extent of each discontinuity) is immediately available from the oscilloscope display. Figure 1.2 shows the sensor deformation and the corresponding ETDR output. The ETDR is a well-established technique and hardware equipment is commercially available. Benefits of using the ETDR technique as distributed sensor in smart structures have been addressed by Stastny (1992).

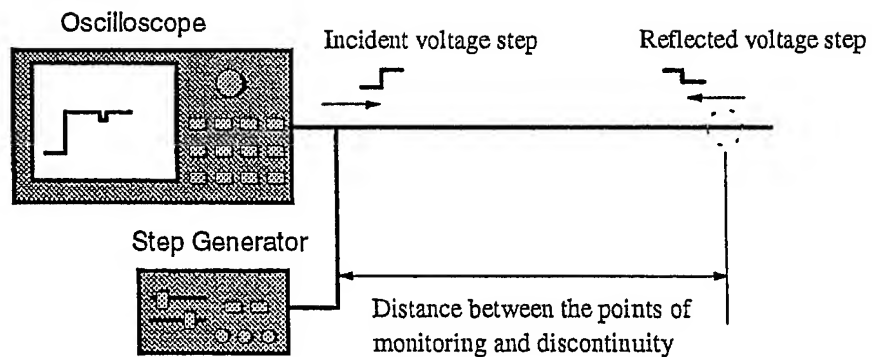


Figure 1.2 Typical ETDR system

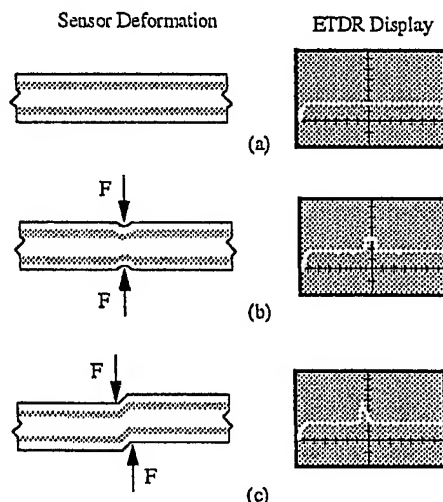


Figure 1.2. Typical sensor deformation and the corresponding ETDR output: (a) undeformed configuration, (b) radial normal compression, and (c) shear deformation.

To use the ETDR technique for health monitoring of concrete structures, ETDR sensors will be embedded in the concrete to serve as distributed stress/strain sensors and damage detectors. The envisioned embedding scheme is shown in Figure 1.3. The ETDR sensing cable is prestrained before it is embedded in concrete. During the forming (curing) process of the concrete, the cable remains strained. After the forming, both the cable and the concrete structure are in a state of prestress, i.e., the cable is in tension and the concrete in compression. Since the sensing cable is much smaller in size and compliant in material property relative to the concrete host material, this prestress state may not affect the overall structural performance. After the forming of the concrete the embedded ETDR sensing cable is therefore a part of the structure. It will deform with the structure as the structure is subjected to external loading, such that the cable can serve as an on-line stress/strain sensor to quantitatively measure structural internal stress state. Moreover, when a crack damage occurs in the concrete at a location along the sensing line, the prestress of the cable at this location will be released, resulting in a significant impedance discontinuity in the sensing cable. The location of the crack damage and even the magnitude of the crack can therefore be easily detected.

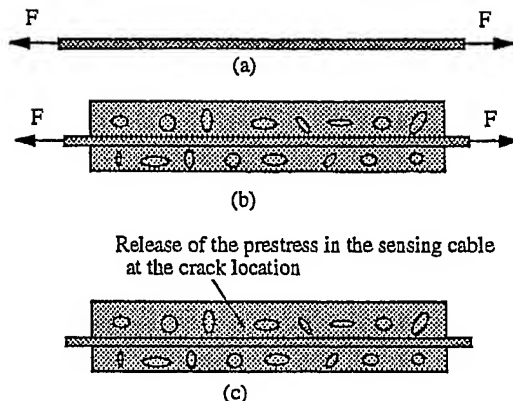


Figure 1.3. Proposed embedding scheme of ETDR sensing cable in a concrete structure: (a) prestress of the cable, (b) forming of the concrete, and (c) crack detection.

The utilization of the ETDR sensing cable for health monitoring of concrete structures presents a number of challenges. The issues related to the choice of ETDR sensor materials and mathematical algorithms to quantitatively correlate ETDR signal to stress/strain and crack damage measurement have to be determined. It is also essential to understand and model the mechanism of the mechanical interaction between the embedded ETDR sensors and host concrete material and the resulting ETDR output signal. In addition, the reliability of the sensing technique and long-term durability of the sensors in the application of large-scale concrete structures also need to be assessed.

ACCOMPLISHMENTS

Technical Results and Discussion

Research tasks in the first phase of this project are (1) experimental characterization of ETDR sensors and (2) analytical modeling of the ETDR signal response of sensing cables. The experimental set-up for characterizing ETDR signal response of coaxial sensing cables to external loading has been accomplished and preliminary test results have been obtained. A finite element analytical scheme has also been developed to model the ETDR signal response. The technical accomplishments of the research project to date are reported in the sections that follow.

Finite Element Modeling

A finite element analysis (FEA) method has been developed to model TDR signal response of coaxial sensing cables subject to external loading. The FEA procedure involves the determination of the capacitance of the originally undeformed cable and that of the deformed cable when subject to external loading. Since the ratio of the capacitance of the deformed and undeformed cables can be related to the change of the characteristic impedance of the cable as:

$$Z_1 / Z_0 = C_0 / C_1, \quad (1)$$

the TDR signal response of the cable can be determined in terms of reflection coefficient as:

$$\rho = \frac{Z_1 / Z_0 - 1}{Z_1 / Z_0 + 1} = \frac{C_0 / C_1 - 1}{C_0 / C_1 + 1}. \quad (2)$$

In the above expressions, Z and C are the characteristic impedance and the capacitance of cable and the subscript "0" and "1" indicate the quantities before and after deformation, respectively.

Coupled-field finite elements with structural nodal degree-of-freedom (displacements) and electrical nodal degree-of-freedom (voltage) are used to model the structure of the coaxial cable. The dielectric energy U_e is first calculated for the undeformed cable by applying a unit electrical voltage difference across the electrodes. Then, the equivalent capacitance of the cable is determined by

$$C = 2U_e. \quad (3)$$

After obtaining the capacitance of the undeformed cable, C_0 , finite element structural analysis procedure is performed to determine the cable deformation due to applied loads. Non-linear procedure using Newton-Raphson algorithm is employed to carry out the analysis. This procedure updates incremental change of the finite element shape functions on each increment of the load. Thus, the structural stiffness matrix and dielectric conductivity matrix are updated for the deformed cable geometry when the structural equilibrium is achieved. The equivalent capacitance of the deformed cable is then determined by calculating the dielectric energy of the deformed cable through Eq. (3).

Finite element modeling of TDR signal response of a typical coaxial cable subject to tension and compression loading, respectively, have been performed. The cable is constructed by polyethylene dielectric, aluminum outer conductor and copper inner conductor. The axisymmetric coupled-field finite elements with the structural and electrical material properties shown in Table 1 for each constituent were used.

Table 1.1 Material Properties

	Young Modules E (msi)	Poisson's Ratio ν	Relative Dielectric Constant ϵ
Aluminum	10	0.33	
Copper	15.6	0.355	
Polyethylene	0.017	0.3	2.26

The finite element model mesh with structural and electrical boundary conditions for the cable subject to tension is shown in Figure 1.4. Symmetric structural boundary condition was imposed on the left end of the model and an uniform displacement was applied on the mid section of the model. The nodal voltage on the outer and inner conductors were set to one and zero volt, respectively.

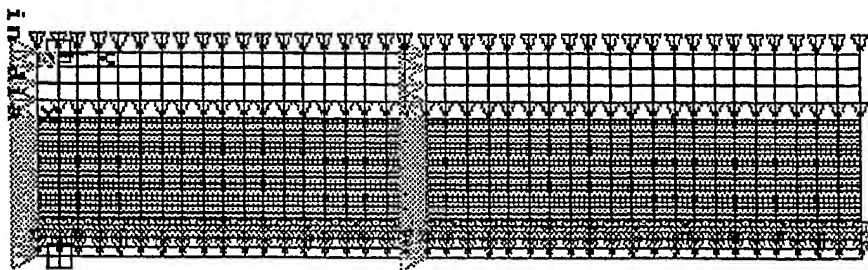


Figure 1.4 Finite element mesh and boundary conditions for the coaxial cable subject to axial tension.

The resulting cable deformation and the TDR signal response are shown in Figure 1.5. It is apparent that the reflection coefficient of the TDR signal is able to represent the “necking” effect of the cable deformation. The trend of the TDR signal response from the finite element analysis appears to be similar as those of experimental results reported in the literature (Su, 1987).

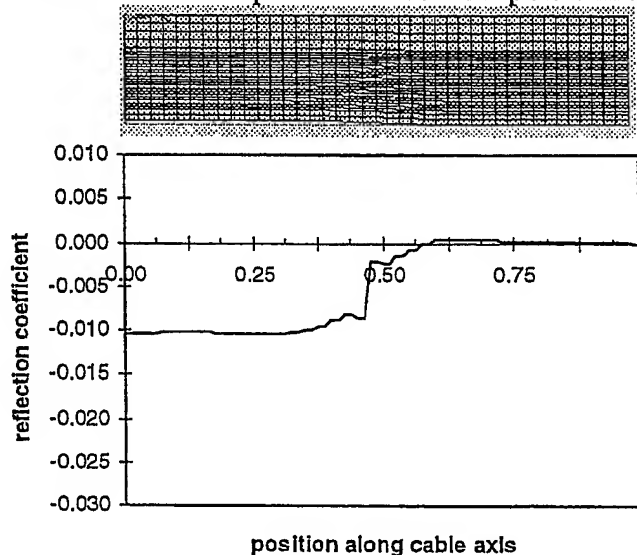


Figure 1.5. Cable deformation and the corresponding TDR signal response.

The finite element model mesh with structural and electrical boundary conditions for the cable subject to axisymmetric compression is shown in Figure 1.6. Axisymmetric compression loading was applied at the mid-section of the model. The nodal voltage on the outer and inner conductors were set to one and zero volt, respectively.

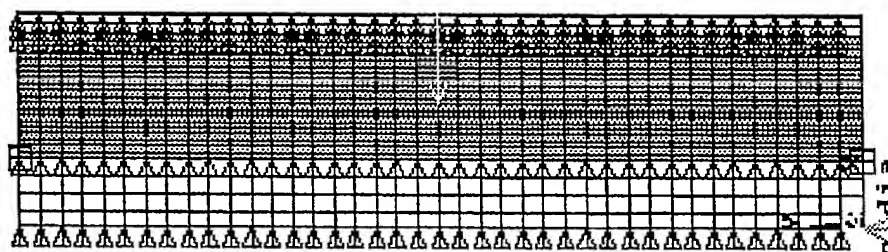


Figure 1.6. Finite element mesh and boundary conditions for the coaxial cable subject to axisymmetric compression.

The resulting cable deformation and the TDR signal response for the axisymmetric compression loading condition are depicted in Figure 1.7. It is shown again that the TDR signal response can also represent the compression deformation of the cable.

The preliminary results of the analysis show that the developed finite element analytical method can model the TDR signal response of the cable due to external loading. It was shown that the nature of the loading type, the location, and the magnitude regarding to the applied load can be represented by the TDR signal response. Three-dimensional finite element models are currently being developed for non-axisymmetric loading cases. The FEA results will be compared and correlated with experimental measurements conducted in the course of this project.

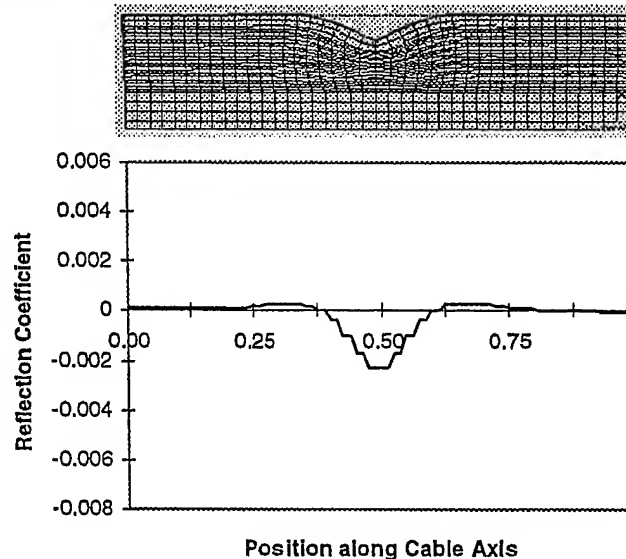


Figure 1.7. Cable deformation and the corresponding TDR signal response.
Experiments

To experimentally characterize TDR signal response of sensing cables, a comprehensive test program is being carried out. The set-up of the test apparatus has been completed. It includes an Instron screw-driven 4505 test frame, an HP 54124T digitizing oscilloscope, and an IBM-Compatible PC with HP-VEE data acquisition system. Four types of loading, i.e., axial tension, transverse compression, transverse shear, and spatial resolution, tests will be performed. During the tests the load level, displacement, and TDR signal will be recorded and analyzed. Coaxial cables of various sizes and dielectric materials will be tested.

Test fixtures to be used to carry out experimental characterization of ETDR stress/strain sensing cables have been designed, fabricated, and installed. The schematics of the transverse compression, transverse shear and spatial resolution test fixtures are shown in Figure 1.8.

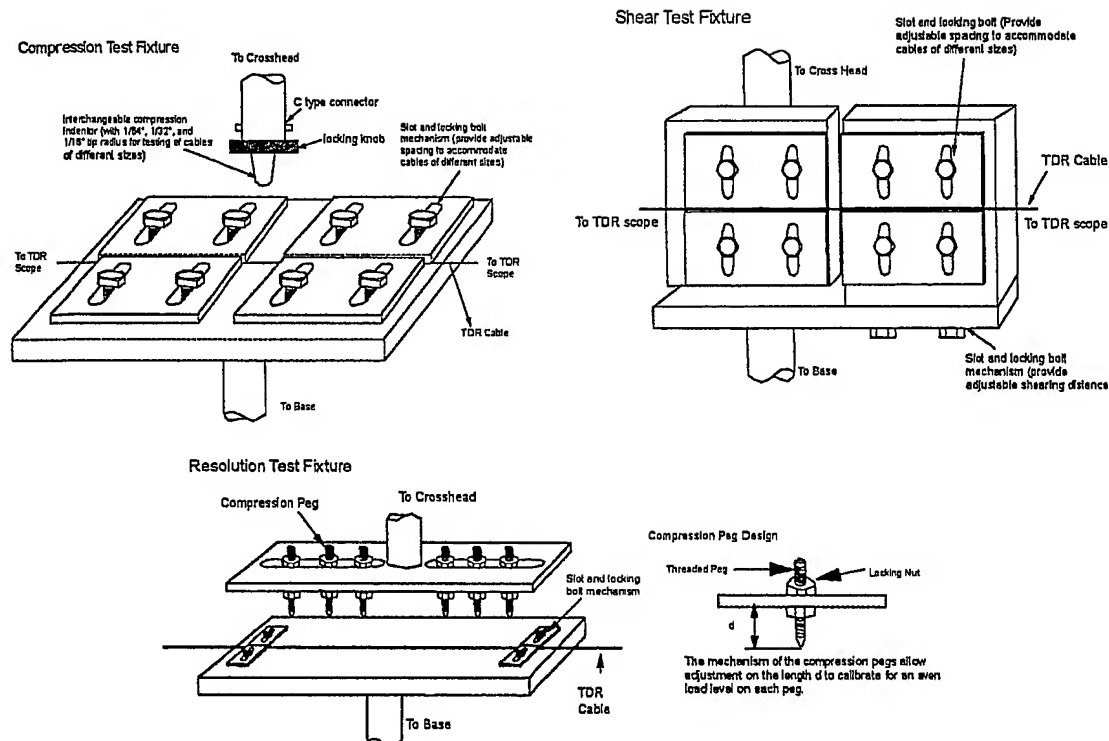


Figure 1.8 Schematic of test fixtures.

Preliminary results of the TDR signal response to transverse compression of a 1/4" 50 ohm coaxial cable have been obtained. The cable was compressed at the location 2-1/4 feet from the end connection of the signal generator by a peg with 1/16" tip radius. TDR signal data were acquired at no-load and 165 N compression load conditions. The measured electrical potentials as a function of wave reflection time is depicted in Figure 1.9. It shows no apparent TDR signal change along the cable length except at the location of the compression load. The preliminary results confirm that the TDR sensing cable respond to the localized external loading and this technique can be used for stress/strain measurements.

Comprehensive tests will be conducted throughout the course of this project. The relation between the magnitude of the load and corresponding TDR signal response will be established. The experimental results will also be used to verify the finite element scheme developed in this project.

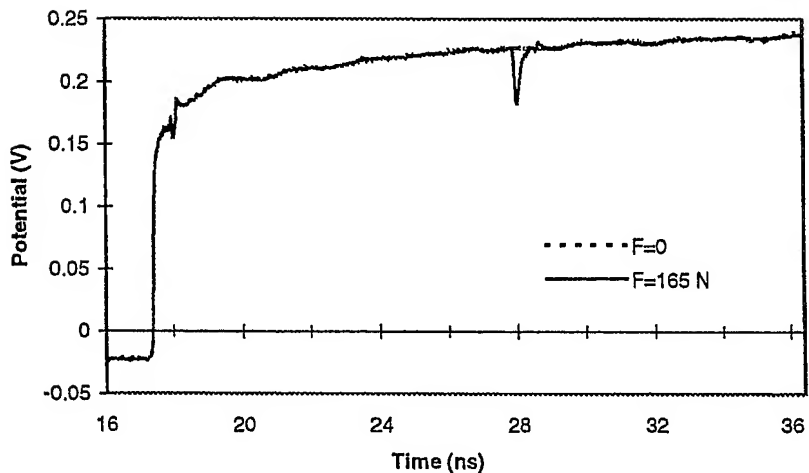


Figure 1.9. TDR signal response of 1/4' 50 ohm coaxial cable subject to transverse compression.

EDUCATION AND TRAINING

This project has provided a good opportunity for CAU students to involve in engineering research in both hands-on experiments and numerical modeling. Two undergraduate students majoring in engineering and one graduate student in computer science have been trained to conduct the research tasks. Information about these students are listed in the followings.

Ms. Funmilola Awoniyi	Junior in Engineering
Mr. Johnny Washington	Junior in Engineering
Mr. Dejun Chu	M.S. Student in Computer Science

PUBLICATIONS AND PRESENTATIONS

Lin, M. W., Abatan, A. O., and Danjaji, M. B., 1997, "The Use of Time Domain Reflectometry Sensing Cables as Stress/Strain Sensors in Smart Material Systems," SPIE's Annual Symposium on Smart Structures and Materials, San Diego, CA, March 3-6, 1997 (in preparation).

REFERENCES

Escobar, P., Gusmeroli, V., and Martinelli, M., 1992, "Fiber-Optic Interferometric Sensors for Concrete Structures," *Proceedings, First European Conference on Smart Structures and Materials*, Glasgow, May, 1992, pp. 215-218.

Feng, M. Q., and Suzuki, H., 1994, "An Optical Fiber Sensor for Monitoring Civil Infrastructure," *Proceedings, International Conference on Intelligent Materials, ICIM '94*, June 1994, pp. 498-509.

Krushchwitz, B., Claus, R. O., Murphy, K. A., May, R. G., and Gunther, M. F., 1992,

"Optical Fiber Sensors for the Quantitative Measurement of Strain in Concrete Structures," *Proceedings, First European Conference on Smart Structures and Materials*, Glasgow, May, 1992, pp. 241-244.

Su, M.-B., 1987, "Quantification of Cable Deformation with Time Domain Reflectometry Techniques," Ph.D. Dissertation, Department of Civil Engineering, Northwestern University, Evanston, Illinois, June 1987.

Stastny, J. A., 1992, "Time Domain Reflectometry (TDR) Techniques for the Design of Distributed Sensors," M.S. Thesis, Virginia Polytechnic Institute and State University, Blacksburg, Virginia, October, 1992.

2.2 "ELASTICALLY TAILORED COMPOSITE DESIGN"

Investigator: A. Badir, Assistant Professor, Clark Atlanta University

Collaborator: E. Armanios, Georgia Institute of Technology

BACKGROUND

Elastically tailored composite designs are being used to achieve favorable deformation modes under a given loading environment. Coupling between deformation modes such as extension-twist or bending-twist is created by an appropriate selection of fiber orientation, stacking sequence and materials. A prerequisite for the implementation of an elastically tailored concept, is the development of analytical models which accurately predict their structural response and isolate the material and geometrical parameters controlling their behavior. The research outlined in the next sections address this issue.

OBJECTIVES

The goal of this research is to understand the role of the material's anisotropy on the structural behavior of elastically tailored composite structures. This goal has been achieved by developing different analytical models for anisotropic beams. Accurate closed form solutions, simple enough to save the time and money consumed in running finite element programs, have been developed. The derived closed form expressions are an indispensable tool at a preliminary design stage where practical analyses capable of screening different candidate configurations and selecting best mixture of material and stacking sequence are highly demanded. Moreover, the analytical expressions are an essential tool in optimization problems.

APPROACH

The structural modeling of the anisotropic material represents the building block towards a qualitative comprehension of the response in addition to quantitative results. The major advantages and features of the analysis are briefly outlined in the following sections.

A variationally and asymptotically consistent anisotropic thin-walled beam theory (Badir 1992) constitutes the building block of the structural modeling. The theory is based on an asymptotical analysis of two-dimensional anisotropic shell energy. Closed-form expressions for the beam stiffness coefficients, stress and displacement fields are provided. The major advantage of this study is that the displacement field is not assumed *a priori* and emerges naturally as a result of the asymptotical analysis of the shell energy. The out-of-plane warping due to extension, torsion and bending are determined in closed form in terms of the 21 independent Hookean's material constants, the stacking sequence and the cross-sectional geometry.

ACCOMPLISHMENTS

A theory for anisotropic thin-walled closed section beams which enable the prediction of their response under hygrothermal loadings has been developed (Badir, 1994a). Closed-form expressions for the beam stiffness coefficients, equivalent hygrothermal loads, stress and displacement fields are obtained in terms of the 21 independent Hookean's material constants. The analysis is applied to predict the response of composite beams under thermomechanical loading. An extension to the theory to predict the mechanical response of two-cell composite beams has also been developed (Badir 1994b, 1995)

Equations of motion for the free vibration analysis of anisotropic thin-walled closed section beams has been derived (Armanios and Badir, 1994 and 1995) using a variational asymptotic approach and Hamilton's principle. The analysis is applied to two laminated composite constructions. The developed model enables the analytical evaluation of the effect of the elastic coupling mechanisms on the vibration behavior.

A constrained optimization scheme has been developed (Lentz *et al.* 1996) in order to construct unsymmetric laminates which exhibit extension-twist coupling under mechanical loading while minimizing hygrothermal warping. The optimum designs were fabricated and compared with the hygrothermally stable laminates obtained by stacking a set of rotated [0/90] plies. It was found that the laminate configurations resulting from the optimization scheme have improved coupling. A parallel effort aiming at low cost manufacturing of elastically tailored composite was performed. The reduction in cost is a result of using flat molds as a substitute to complex three-dimensional ones. The manufacturing technique uses the residual hygrothermal stresses resulting from the curing cycle to create laminated plates with prescribed three-dimensional warping. This approach was used to produce laminated plates with initial twisting curvature, saddle and spherical shapes from flat molds.

A brief summary of these accomplishments is outlined in the following sections. More details are found in the publications.

Modeling of Thin-Walled Beams Subjected to Hygrothermal Loads

Thermal and moisture stresses are induced in anisotropic materials as a result of the mismatch in the thermal expansion and moisture swelling coefficients of their constituents. A prerequisite for the implementation of an elastically tailored concept, is the development of an analytical model which accurately predicts the hygrothermal effect and isolate the material and geometrical parameters controlling the behavior.

A theory for anisotropic thin-walled closed section beams which enables the prediction of their response under hygrothermal loadings has been developed under this research work (Badir, 1994a, 1996). The theory is an extension of the work of Badir (1992) and Berdichevsky *et al.* (1992), and considers thin-walled beams with circumferentially varying thickness and stiffness. It is based on an asymptotical expansion of two dimensional anisotropic shell energy. The major advantage of this approach is the fact that the displacement is not assumed *a priori* and emerges as a result of the analysis. Closed-form expressions for the beam stiffness coefficients, equivalent hygrothermal loads, stress and displacement fields are obtained in terms of the 21 independent Hookean's material constants. The influence of material anisotropy and hygrothermal coefficients on the displacement field is identified. Their contribution to the out-of-plane warping is determined. The analysis is applied to predict the response of composite beams under thermomechanical loading. The constitutive relationships are found as

$$\begin{Bmatrix} T \\ M_x \\ M_y \\ M_z \end{Bmatrix} = \begin{Bmatrix} C_{11} & C_{12} & C_{13} & C_{14} \\ C_{12} & C_{22} & C_{23} & C_{24} \\ C_{13} & C_{23} & C_{33} & C_{34} \\ C_{14} & C_{24} & C_{34} & C_{44} \end{Bmatrix} \begin{Bmatrix} U_1' \\ \varphi' \\ U_3'' \\ U_2'' \end{Bmatrix} - \begin{Bmatrix} T^{(nm)} \\ M_x^{(nm)} \\ M_y^{(nm)} \\ M_z^{(nm)} \end{Bmatrix} \quad (1)$$

where T , M_x , M_y and M_z represent the axial load, torsional moment, bending about y and x -axes, respectively. Explicit expressions of the stiffness coefficients C_{ij} ($i, j = 1, 4$) were derived. The equivalent non-mechanical loads $T^{(nm)}$, $M_x^{(nm)}$, $M_y^{(nm)}$ and $M_z^{(nm)}$ were derived in closed form expressions as integral of material properties and cross sectional geometry. Using Eq. (1), the deformation due to hygrothermal stresses are predicted. Following the cure cycle, the drop in temperature causes the extension-twist configuration to twist. This pretwist of the beam can be predicted by considering the mechanically applied load to be zero in Eq. (1).

The tip twist for an antisymmetric box cantilevered beam made of a $[\theta]_6$ layups due to a drop in temperature, ΔT , of 280°F was investigated (Badir, 1996). The tip twist tends to increase with θ and reaches its maximum when the plies are oriented at 45 degrees. Thermal pretwist may reach 12° for a $[45]_6$ lay-up, while moisture content tends to alleviate thermal effects. The specific moisture content for total alleviation from the thermal effect is about 0.8%.

The induced tip twist for a bending-twist coupled configuration subjected to a unit temperature rise and drop on the top and bottom walls, respectively is calculated (Badir, 1996). Excellent correlation with numerical analyses is obtained.

Free Vibration Analysis Of Anisotropic Thin-Walled Closed-Section Beam

The equations of motion for the free vibration analysis of anisotropic thin-walled closed section beams have been derived under this research work (Armanios and Badir 1994), using a variational asymptotic approach and Hamilton's principle. The analysis is applied to two laminated composite constructions: The Circumferentially Uniform Stiffness which produces extension-twist coupling and the Circumferentially Asymmetric Stiffness producing bending-twist coupling. The effect of the elastic coupling mechanisms on the vibration behavior of thin-walled composite beams are evaluated analytically. The influence of fiber orientation on the frequencies associated with coupled vibration modes is investigated.

For a cantilevered beam of length L , the natural frequencies of the extension-twist vibration modes are derived as

$$\omega_n = \frac{n\pi\lambda}{2L} \quad (n = 1, 3, 5, K) \quad \text{where} \quad \lambda^2 = \frac{2\alpha}{\beta \pm \sqrt{\beta^2 - 4\alpha m_c I}} \quad (2)$$

with

$$\alpha = C_{11}C_{22} - (C_{12})^2 \quad \text{and} \quad \beta = C_{11}I + C_{22}m_c \quad (3)$$

where C_{11} , C_{22} and C_{12} are the extension, twist and extension-twist coupling stiffnesses, respectively. The parameters m_c and I are associated with the inertia terms. The predictions are validated by comparison with a finite element simulation and experimental work. Good correlation is obtained.

Analysis Of Two-Cell Composite Beams

The most significant difference between single-cell and multi-cell isotropic sections is in the analysis of torsion. Torsion of a multi-cell beam is a statically indeterminate problem. Independent shear flow associated with multi-cells exist and cannot be determined by static equilibrium equations. However, for anisotropic beams, the difference is more pronounced since torsion is coupled with other deformation modes. Moreover, the influence of the material's anisotropy on the displacement is too complex to cast in a kinematic assumption similar to classical theory of extension-bending and torsion. A consistent approach to account for the various behavioral modes associated with anisotropic two-cell beams is developed (Badir, 1995). Explicit closed-form expressions for the beam stiffness coefficients, the stress, strain and displacement fields are provided.

Constrained Optimization Of Thin-Walled Composite Beams With Coupling

A constrained optimization scheme has been developed for obtaining the optimum coupling in thin walled, closed section composite beams (Lentz *et al.*, 1996). The stacking sequence for producing the maximum extension-twist and bending twist coupling have been

determined. Constraints have been imposed using the Sequential Unconstrained Minimization Technique. The hygrothermal deformation of the beam is minimized through the use of an external penalty function. A second constraint imposed is that the first two natural frequencies of each mode shape are distinct from a single specified frequency. This constraint has been implemented by the use of an extended interior penalty function.

The results of the optimization show that the constrained optima is very close to the unconstrained optima, so that the magnitude of coupling obtained drops only by approximately three percent. In each case of wall thickness varying from two to eight plies, the global solution incorporates two ply angles. A local optimum exists using only one ply angle. The difference in coupling magnitude is about ten percent. Depending on the associated manufacturing cost, this local optimum may be a viable solution. The coupling and hygrothermal twist of the beam show most sensitivity to the Young's modulus and shear modulus of the material because the beam coupling results from local extension-shear coupling. As expected, variations in the thermal and hygroscopic properties of the composite effect the resultant twist without changing the coupling produced.

PUBLICATIONS

Armanios, Erian A. and Badir, Ashraf M. (1995) "Free Vibration Analysis of Anisotropic Thin-Walled Closed-Section Beams," *AIAA Journal*, Vol. 33, No. 10, pp. 1905-1910.

Armanios, E. and Badir, A. (1994), "Free Vibration Analysis of Anisotropic Thin-Walled Closed-Section Beams," *Proceedings of the 35th AIAA/ASME/ASC/AHS/ ASC Structures, Structural Dynamics and Materials (SDM) Conference*, Hilton Head, South Carolina, April 18-20, pp. 164-171.

Badir, Ashraf and Erian Armanios (1996), "On The Significance of Extension And Bending-Related Warping Effects in Thin Walled Composites," submitted to the *International Journal Of Solids and Structures*.

Badir, Ashraf (1996), "Theory of Anisotropic Thin-Walled Closed-Section Beams With Hygrothermal Effects," submitted to the *Journal of Applied Mechanics*.

Badir, Ashraf (1995a), "Stiffness Matrix Formulation For Anisotropic Beams," *Proceedings of the ASCE Engineering Mechanics Conference*, Boulder, Colorado, May 21-24, pp. 257-260.

Badir, Ashraf (1994a), "Structural Modeling Of Multi-Cell Composite Beams," *Proceedings of International Conference on Composites Engineering*, New Orleans, Louisiana, August 28-31, pp. 31-32.

Badir, Ashraf (1995), "Analysis of Two-Cell Composite Beams," *Proceedings of the 36th AIAA/ASME/ASC/AHS/ ASC Structures, Structural Dynamics and Materials (SDM) Conference*, New Orleans, LA, April 10-13, pp. 419-424.

Badir, Ashraf (1994b), "Analysis of Composite Beams Under Mechanical And Hygrothermal Loads," *Proceedings of the Second Annual Engineering and Architecture Symposium*, Prairie View, Texas, March 21-22, pp. 327-332.

Lentz, K., Armanios, E. and Badir, A. (1996), "Constrained Optimization Of Thin-Walled Composite Beams With Coupling," *Proceedings of the 37th AIAA/ASME/ASC/AHS/ ASC Structures, Structural Dynamics and Materials (SDM) Conference*, Salt Lake City, Utah, pp. 2326-2334.

PRESENTATIONS

Armanios, E. and Badir, A. (1994), "Free Vibration Analysis of Anisotropic Thin-Walled Closed-Section Beams," *Presented at the 35th AIAA/ASME/ASC/AHS/ ASC Structures, Structural Dynamics and Materials (SDM) Conference*, Hilton Head, South Carolina, April 18-20, pp. 164-171.

Badir, Ashraf (1995a), "Stiffness Matrix Formulation For Anisotropic Beams," *Presented at the ASCE Engineering Mechanics Conference*, Boulder, Colorado, May 21-24, pp. 257-260.

Badir, Ashraf (1994a), "Structural Modeling Of Multi-Cell Composite Beams," *Presented at the International Conference on Composites Engineering*, New Orleans, Louisiana, August 28-31, pp. 31-32.

Badir, Ashraf (1995), "Analysis of Two-Cell Composite Beams," *Presented at the 36th AIAA/ASME/ASC/AHS/ ASC Structures, Structural Dynamics and Materials (SDM) Conference*, New Orleans, LA, April 10-13, pp. 419-424.

Badir, Ashraf (1994b), "Analysis of Composite Beams Under Mechanical And Hygrothermal Loads," *Presented at the Second Annual Engineering and Architecture Symposium*, Prairie View, Texas, March 21-22, pp. 327-332.

Lentz, K., Armanios, E. and Badir, A. (1996), "Constrained Optimization Of Thin-Walled Composite Beams With Coupling," *Presented at the 37th AIAA/ASME/ASC/AHS/ ASC Structures, Structural Dynamics and Materials (SDM) Conference*, Salt Lake City, Utah, pp. 2326-2334.

REFERENCES

Armanios, Erian A. and Badir, Ashraf M. (1995) "Free Vibration Analysis of Anisotropic Thin-Walled Closed-Section Beams," *AIAA Journal*, Vol. 33, No. 10, pp. 1905-1910.

Armanios, E. and Badir, A. (1994), "Free Vibration Analysis of Anisotropic Thin-Walled Closed-Section Beams," *Proceedings of the 35th AIAA/ASME/ASC/AHS/ ASC Structures, Structural Dynamics and Materials (SDM) Conference*, Hilton Head, South Carolina, April 18-20, pp. 164-171.

Berdichevsky, V. , Armanios, E. and Badir, A. "Theory of Anisotropic Thin-Walled Closed-Cross-Section Beams", *Composite Engineering*, Special Issue on the Use of Composites In Rotorcraft and Smart Structures, Vol. 2, Nos. 5-7, 1992, pp. 411-432.

Badir, Ashraf and Erian Armanios (1996), "On The Significance of Extension And Bending-Related Warping Effects in Thin Walled Composites," submitted to the *International Journal Of Solids and Structures*.

Badir, Ashraf (1996), "Theory of Anisotropic Thin-Walled Closed-Section Beams With Hygrothermal Effects," submitted to the *Journal of Applied Mechanics*.

Badir, Ashraf (1995), "Analysis of Two-Cell Composite Beams," *Proceedings of the 36th AIAA/ASME/ASC/AHS/ ASC Structures, Structural Dynamics and Materials (SDM) Conference*, New Orleans, LA, April 10-13, pp. 419-424.

Badir, Ashraf (1994a), "Analysis of Composite Beams Under Mechanical And Hygrothermal Loads," *Proceedings of the Second Annual Engineering and Architecture Symposium*, Prairie View, Texas, March 21-22, pp. 327-332.

Badir, Ashraf (1994b), "Structural Modeling Of Multi-Cell Composite Beams," *Proceedings of International Conference on Composites Engineering*, New Orleans, Louisiana, August 28-31, pp. 31-32.

Badir, Ashraf (1992), "Analysis of Advanced Thin-Walled Composite Structures," *Ph.D. thesis*, School of Aerospace Engineering, Georgia Institute of Technology.

Lentz, K., Armanios, E. and Badir, A. (1996), "Constrained Optimization Of Thin-Walled Composite Beams With Coupling," *Proceedings of the 37th AIAA/ASME/ASC/AHS/ ASC Structures, Structural Dynamics and Materials (SDM) Conference*, Salt Lake City, Utah, pp. 2326-2334.

2.3 LONG TERM DURABILITY OF POLYMER MATRIX COMPOSITES FOR HIGH TEMPERATURE APPLICATIONS

Investigator: A. Badir, Assistant Professor, Clark Atlanta University

Collaborator: R. Talreja, Georgia Institute of Technology

BACKGROUND

Structural applications of polymer matrix composites (PMCs) at high temperatures, e.g., in the 21st century subsonic civil transport propulsion systems will only be affordable when their long term durability and lifetime assessment can be reliably made. This has been identified by the industry as a major barrier. This project will develop mechanisms-based methodologies for lifetime assessment of PMCs under tension-tension fatigue. The investigations will form the bases for developing microstructure-property relationships for fatigue mechanisms including the effects of thermal aging and other environmental effects relevant to high temperature applications. Concepts and analyses of damage mechanics are being applied to describe degradations of stiffness and strength and their criticalities toward developing a life prediction methodology.

OBJECTIVES

The objectives of this research are as follows.

1. To clarify the mechanisms of damage operating in tension-tension fatigue of PMCs with advanced polyimide matrices.
2. To develop microstructure-property relationships and evolution of damage using damage mechanics concepts.
3. To develop life prediction methodologies for stiffness-critical and strength-critical cases.
4. To verify the models for a biaxially loaded (axial load and internal pressure) cylindrical pressure vessel.

APPROACH

The fatigue life diagram for tension-tension loading of unidirectional fiber composite is plotted as strain vs. logarithm of the load cycles to failure. Although fatigue testing is done under controlled load, the variable on the vertical axis of the diagram is the maximum strain attained in

the first load cycle. The significance of the maximum strain is that this quantity represents the state of damage reached in the first load cycle and it is reasonable to expect that any progression of damage in subsequent load cycles will be determined by this state of damage. Furthermore the two extreme states in fatigue, i.e. the static failure and the fatigue limit, are given generically in terms of strain. The static failure occurs at the strain to failure of fibers irrespective of the fiber volume fraction and the fatigue limit is governed by the matrix which is undergoing strain-controlled fatigue.

ACCOMPLISHMENTS

Technical Results and Discussion

The test program consists of tension-tension fatigue in the following conditions.

- a. Fatigue Testing Under Constant Room Temperature:
- b. Fatigue Testing Under 120 Degree Centigrade:
- c. Fatigue Testing Under Glass Transition Temperature minus 50 Degrees Centigrade:

Experimental study has been conducted and still is in progress to investigate the mechanical behavior of a T650-35/AMB21 unidirectional polymer composite system. Emphasis is placed on the development and refinement of techniques used in elevated temperature uniaxial PMC testing. Issues such as specimen design, grippings, strain measurement, and temperature control and measurement are addressed. Fatigue experiments at room temperature have been conducted for several unidirectional samples at different levels of maximum stress, S_{max} , with $R_s = 0.1$ (s_{min}/s_{max}). The S_{max} values were based on the average ultimate tensile strength, s_{ult} , obtained from the static tensile test. A cyclic load frequency with a sinusoidal command wave form is employed. Two inch long tabs have been bonded to all laminates using epoxy paste. The strain is being continuously monitored throughout the test by recording the strain (using extensometer or strain gages) and the associated load during the cycling to assess stiffness reduction.

All specimens failed suddenly in a fiber broom failure type associated with "popping" sounds caused by the fiber bundles fracturing. Failure at the tabs has been experienced. Adhesive tape will be used instead of the epoxy paste in an attempt to overcome this problem.

Some preliminary testing results are listed below.

**STATIC TENSILE PROPERTIES OF UNIDIRECTIONAL LAMINATE AT ROOM TEMPERATURE
(Load Control)**

Specimen	E_{11} (psi)	σ_{ult} (psi)	ε_{ult}	v_{12}
1	$23.84*10^6$	$222.45*10^3$	0.933%	0.295
2	$23.25*10^6$	$251.80*10^3$	1.08%	0.31
3	$21.06*10^6$	$227.61*10^3$	1.08%	
4	$21.18*10^6$			
5	$23.82*10^6$			
6	$23.00*10^6$			
Average	$22.7*10^6$	$234*10^3$	1.03%	0.303
Standard deviation	1.26	15.67	0.084	0.01

TENSION-TENSION FATIGUE OF T650-35/AMB-21 UNIDIRECTIONAL LAMINATE AT ROOM TEMPERATURE (10 Hz, R=0.1, Load Control)

Specimen	S_{max} (psi)	Nf	Remarks
4	0.84 sult	127	
5	0.86 sult	151	
1	0.85 sult	66	
6	0.77sult	348	
3a	0.75 sult	3251	
2a	0.70 sult	145	Failure initiated at tabs
2b	0.70 sult	8	Failure initiated at tabs
4a	0.70 sult	33	Failure initiated at tabs
5a	0.70 sult	128	Failure initiated at tabs
6a	0.70 sult	118	Failure initiated at tabs

**STATIC TENSILE PROPERTIES OF AMB-21 AT ROOM TEMPERATURE
(Strain Control)**

Specimen	Initial E_{11} (psi)
1	$0.384*10^6$
2	$0.406*10^6$
Average	$0.395*10^6$

EDUCATION and TRAINING

Graduate Student: Mesfien Mehreteab

Undergraduate Student : Iskil Soyinka (Sophomore, Engineering)

OUTREACH AND TECHNOLOGY TRANSFER

Collaborative R&D activities with NASA Lewis Research Lab.

Point of contact:

Dr. Ken Bowles
MS 49-1
NASA/LeRC, 21000 Brookpark Rd., Cleveland, OH 44135

PUBLICATIONS AND PRESENTATIONS

Badir, A., Mehreteab, M. and Soyinka, I. (1996), "A Study of Elevated Temperature Testing Techniques for the Fatigue Behavior of PMCs", to appear in the *Proceedings of the 9th Annual HITEMP Review*, sponsored by NASA Lewis Research Center, Cleveland Ohio, October 1996.

Badir, A., Mehreteab, M. and Soyinka, I. (1996), "A Study of Elevated Temperature Testing Techniques for the Fatigue Behavior of PMCs", to be presented at the *9th Annual HITEMP Review*, sponsored by NASA Lewis Research Center, Cleveland Ohio, October 1996.

2.4 BLENDED-WING-BODY STRUCTURAL TECHNOLOGY STUDY

Investigator: A. Badir, Assistant Professor, Clark Atlanta University

BACKGROUND

Future air travel market competition mandates the introduction of Very-Large-Aircraft (VLA) to accommodate the ever increasing number of national and international passengers. The Blended-Wing-Body (BWB) is a long range 800 passenger VLA designed to enter service in the year 2020 with a 2015 technology level. Such an aircraft is envisioned to fill a market estimated at roughly 300,000 seats or 375 aircrafts. This research work addresses the structural issues regarding the choice, analysis and design of the BWB's airframe to achieve maximum cost effectiveness, a large part of which relates to weight reduction.

OBJECTIVES

The objective of this research is to apply analytical methods to investigate the structural response of the Blended Wing Body in an attempt to validate and interpret results obtained from Finite Element Analyses. Stability of the outer wing panel is examined analytically for the local as well as the overall stability.

APPROACH

A skin plate with end compression varying linearly in the direction of loading, equilibrated by shear stress along the longitudinal edges is studied. This stress condition is found in the wing skin in bending, and a solution is being sought starting from the energy of the plate and using Ritz method.

ACCOMPLISHMENTS

Technical Results and Discussion

Figure 4.1 shows the skin plate under a load gradient. The compressive stress varies linearly from one edge to the other, and the difference in stress is equilibrated by shear stresses along the longitudinal edges. The stability of the rectangular skin is considered. The expression for the energy of the skin is given by

$$U = \frac{1}{2} \int_a^b \int_a^b \left\{ D_{11} \left(\frac{\partial^2 w}{\partial x^2} \right)^2 + 2D_{12} \frac{\partial^2 w}{\partial x^2} \frac{\partial^2 w}{\partial y^2} + D_{22} \left(\frac{\partial^2 w}{\partial y^2} \right)^2 + 4D_{14} \frac{\partial^2 w}{\partial x^2} \frac{\partial^2 w}{\partial x \partial y} + 4D_{24} \frac{\partial^2 w}{\partial y^2} \frac{\partial^2 w}{\partial x \partial y} + 4D_{44} \left(\frac{\partial^2 w}{\partial x \partial y} \right)^2 + \sigma_x t \left(\frac{\partial^2 w}{\partial x^2} \right)^2 + \sigma_y t \left(\frac{\partial^2 w}{\partial y^2} \right)^2 + 2\tau_{xy} t \frac{\partial w}{\partial x} \frac{\partial w}{\partial y} \right\} dy dx \quad (1)$$

The expressions for the mid-plane stresses are obtained from the plane stress equilibrium equations

$$\frac{\partial \sigma_x}{\partial x} + \frac{\partial \tau_{xy}}{\partial y} = 0 \quad (2)$$

$$\frac{\partial \sigma_y}{\partial y} + \frac{\partial \tau_{xy}}{\partial x} = 0 \quad (3)$$

while considering a linear variation of compressive stress σ_x from σ_{\min} to σ_{\max} given by

$$\sigma_x = -\sigma_{avg} \left[\left(\frac{1-\eta}{1+\eta} \right) \frac{2x}{a} + \frac{2\eta}{1+\eta} \right] \quad (4)$$

where

$$\sigma_{avg} = \frac{1}{2} (\sigma_{max} + \sigma_{min}) \quad (5)$$

$$\eta = \frac{\sigma_{min}}{\sigma_{max}} \quad (6)$$

a = plate length

Substituting Eq. (4) into Eq. (2) and integrate with respect to *y* using the condition of zero shear stress τ_{xy} at $y = \frac{b}{2}$ leads to the following expression of τ_{xy}

$$\tau_{xy} = \frac{\sigma_{avg}}{\phi} \left(\frac{1-\eta}{1+\eta} \right) \left(\frac{2y}{b} - 1 \right) \quad (7)$$

and from Eq. (3), σ_y is a constant (zero for our case), i.e.

$$\sigma_y = 0 \quad (8)$$

The deflection surface of the simply supported skin in bending may be represented by a double Fourier series

$$w = \sum_{m=1}^{\infty} \sum_{n=1}^{\infty} a_{mn} \sin \frac{m\pi x}{a} \sin \frac{n\pi y}{b} \quad (9)$$

Substituting Eq. (4) and (7-9) into the energy expression (1) and performing the indicating integration, we obtain the energy in terms of the deflection coefficients a_{mn} . Minimizing the energy with respect to these coefficients will lead to a set of simultaneous homogeneous equations

$$\frac{\partial U}{\partial a_{mn}} = 0 \quad (10)$$

to be solved for the *a*'s. Setting the determinant of this system of equations to zero, the characteristic equation is obtained from which the critical stress will be calculated.

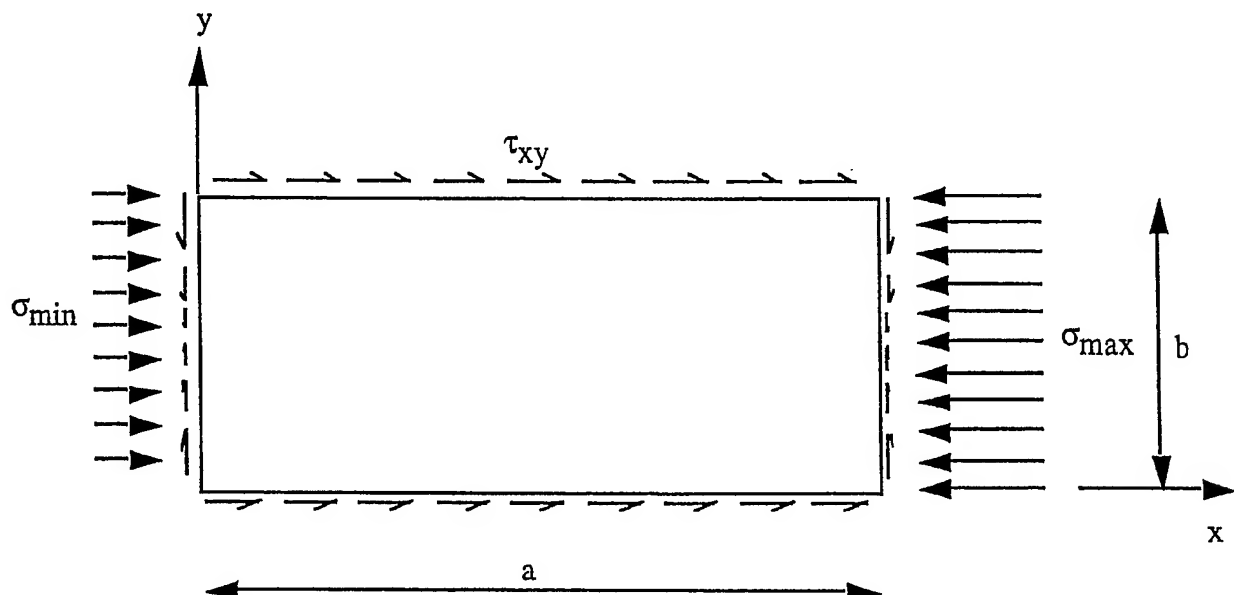


Figure 4.1. Plate subjected to end compression varying in the direction of loading, equilibrated by shear stress along the longitudinal edges (Skin of BWB in bending)

OUTREACH AND TECHNOLOGY TRANSFER

Dr. Badir is presently engaged in a 3 year Blended Wing Body (BWB) technology development study as a member of a NASA/Industry/University team. This team includes NASA Langley and NASA Lewis Research Centers, McDonnell Douglas Aerospace, Clark Atlanta University, Stanford University, University of Southern California and University of Florida.

Points of Contact:

Dr. James H. Starnes, Jr.
 Head, Structural Mechanics Branch
 Structures Division
 NASA Langley Research Center

Mark A. Page
 BWB Technical Program Manager
 Advanced Systems and Technology
 McDonnell Douglas Aerospace

Mail Code 71-35, 2401 E. Wardlow Rd.
 Long Beach, CA 90807-5309

PUBLICATIONS AND PRESENTATIONS

Team Presentation (1996), "NASA /McDonnell Douglas BWB Advanced Design Review", hosted by McDonnell Douglas Aerospace, Long Beach, Ca., April 24-25.

2.5 FINITE ELEMENT AND ANALYTICAL CROSS-SECTIONAL ANALYSIS OF COMPOSITE ROTOR BLADES FOR NONCLASSICAL BEAM FORMULATION

Investigator: A. Badir, Assistant Professor, Clark Atlanta University

Collaborator: D. Hodges, Georgia Institute of Technology

OBJECTIVES

The major objective of the proposed research is the development of a body knowledge suited for efficiently screening candidate structural configurations during the early design stages of composite blades. The findings of this research will have significant impact on the design of advanced composites by providing an optimum compromise between accuracy and computational effort. The developed theories will provide accurate closed form solutions to predict the blade cross-section stiffness properties, yet simple enough to save the time and money consumed in running finite element programs at a preliminary design stage.

TASKS

This research will utilize variational-asymptotical method in order to solve the composite rotor blade cross-sectional problem. Analytical solutions will be derived as detailed in the following schedule

- Year 1 : Derive an analytical stiffness model for thin-walled beams with arbitrary cross-sectional geometry, including trapeze effects.
- Year 2 : Extend model to include initial curvature, twist, oblique cross section, and arbitrary choice of reference line
- Year 3 : Extend model to include Timoshenko and Vlasov Effects
- Year 4 : Extend the model to include non-homogeneous boundary conditions
- Year 5 : Extend the model to provide an analytical model for integrated stiffeners

ACCOMPLISHMENTS

This is a new project which was recently started.

OUTREACH AND TECHNOLOGY TRANSFER

Collaboration between Clark Atlanta University, Georgia Institute of Technology and Bell Helicopter Textron (BHT) is identified. The work is tailored so that the results are useful within the technical community, specifically at BHT. BHT agrees to allow the PI's to visit their facility at regular intervals, to present their latest results, and to engage in technical interactions with the BHT engineers.

Point of Contact: C. Rousseau
Bell Helicopter Textron

Collaboration between Clark Atlanta University, Georgia Institute of Technology and the Aeroflightdynamics US Army Aviation & Troop Command is also identified. The work is tailored so that the results are useful within the Army's comprehensive computer program, originally called the second generation comprehensive helicopter analysis system or 2GCHAS. AFDD agrees to use reasonable efforts to provide the PI's information needed to create a software that works with 2GCHAS and allow the PI's to visit Bob Ormiston and his group at regular intervals, to present their latest results, and to engage in technical interactions with his group.

Point of Contact: Bill Bousman
Aeroflight dynamics
US Army Aviation & Troop Command

2.6 FINITE DEFORMATION RESPONSE OF UNSYMMETRIC COMPOSITE LAMINATES IN THE PRESENCE OF DAMAGE

Investigator: A. Badir, Assistant Professor

Collaborator: E. Armanios, Georgia Institute of Technology

OBJECTIVES

The successful implementation of composites in rotorcraft structures hinges on ensuring their damage tolerance and affordability. The objective of this research is to develop efficient testing method for measuring the coupled response of damaged unsymmetric composites.

TASK

Selected unsymmetrical hygrothermally controlled laminates with and without initial twist will be subjected to extensional loads using an MTS hydraulic Axial/Torsional load unit with 22 Kips axial load capacity and 10,000 in-lbs torsional capacity. Comparison of experimental results, such as extension-twist response, with the test data obtained based on the improved transducer design built at Georgia Tech will be performed. Moreover, test data will be correlated with analytical predictions for unsymmetrical laminates with and without embedded free edge and internal delaminations.

ACCOMPLISHMENTS

This project recently began.

OUTREACH AND TECHNOLOGY TRANSFER

Collaboration with Army Labs and NASA Langley Research Center (Kevin O'Brien) for the assessment of the test methods provided by using a biaxial load frame and the tension-torsion testing machine at Clark Atlanta University.

Point of Contact: Dr. T. Kevin O'Brien
Senior Research Scientist
U.S. Army Research Laboratory
Vehicle Structures Directorate
MS 188E
NASA Langley Research Center
Hampton, VA 23604

2.7 HIGH PERFORMANCE COMPUTING TECHNIQUES IN FLUID STRUCTURE INTERACTION PROBLEMS

Investigators: O. Olatidoye, G. Jones, and S. Sarathy

Collaborators: T. Tezduyar (Univ. of Minn), S. Aliabadi (Univ. of Minn)

INTRODUCTION

Most real life problems involve the commingling of several disciplines, however, most modeling and analysis procedures seek to isolate specific causal relationships within a particular domain, in order to make the model amenable to analytical treatment. This general approach has persisted even with the onset of advanced computational methods, which do allow different facets of the problems to be treated together in a multi-disciplinary manner. However, this approach has a cost, namely the extremely large computational cost associated with these *mega-analyses* and the associated long turnaround times, make these less useful for practical applications. Foremost among these, are problems related to the interaction of fluids and structural components, wherein the structural behavior of the structure is closely related to the fluid phenomenon. Many real life situations fall under this broad category. However, this problem is especially critical for large buildings and off-shore structures, as well as vehicles in the presence of explosive detonations, and waterways under flooding conditions. High performance computing technologies, that make use of vector supercomputing and massive parallel processing, can be used to substantially reduce the burden of such mega analyses, allowing realistic solutions to real problems.

OBJECTIVES

The objective is to apply high performance computing (HPC) methods and technologies to solving complex real life problems involving fluid-structure interactions. This effort aims at developing a common methodology wherein various problems, in this broad category, of interest

to the Army, can be tackled and solved using the Army High Performance Computing Research Center HPC resources.

METHODOLOGY AND APPROACH

The methodology being developed, makes use of the most popular class of computational methods available to solve flow problems, namely Computational Fluid Dynamics (CFD) formulations, using an appropriate form of the Navier-Stokes equations, with automatic mesh generation and remeshing when necessary. The structural analysis methods include Finite Element Methods (FEM) as well as other semi-analytic methods used to predict elasto-dynamic behavior. The approach we are using is to identify the critical analysis components of the physical problem, both fluid-flow and structural, develop consistent level formulations for both the fluid and structural domains, define the interaction in terms of problem parameters, develop a sensitivity analysis of the these parameters with respect to the desired solution, and develop appropriate visualization techniques to incorporate results in both domains. This approach has been applied to the problem of large structures under the action of fluid motion, such as off-shore structures under tidal action, skyscrapers under wind loads, vehicles in the vicinity of explosive detonation, waterway structures under flooding conditions, among others.

ACCOMPLISHMENTS

Results and Discussions

The first problem tackled deals with the analysis of skyscrapers under wind loads. The methodology described above was used to develop a method specific to this problem. A CFD scheme was chosen to predict the wind loading on the building under gusting conditions. The flow was treated as incompressible and was solved using a modified form of Navier-Stokes equations, using automatic mesh generation around the building exterior. The CFD computations were performed on a Cray J90 vector machine, involving several man-weeks to complete and requiring two or more hours per execution on the Cray J-90 supercomputer.

EDUCATION AND TRAINING

A primary mandate of the AHPCRC has been to foster awareness and develop educational thrusts, in order to expose a larger number of undergraduate students to HPC related research experiences. A central program meeting this goal, has been the Summer Institute at University of Minnesota, where undergraduate students from CAU and other member schools, learn various aspects of supercomputing and take part in research projects using HPC techniques. As a part of this effort, we have initiated a series of workshops on HPC, featuring speakers from University of Minnesota Supercomputer group, as well as from within CAU. We are currently developing an undergraduate curriculum to provide CAU students with a unique training opportunity, to acquire the skills related to HPC.

Students	Classification	Major	Graduate/Undergraduate
Gary Jones	Junior	Civil Eng.	Undergraduate
LaKeitha Gilbert	Junior	Mechanical	Undergraduate
Stephanie Elder	Junior	Computer Science	Undergraduate
Leon Thomas	Junior	Computer Science	Undergraduate
Oghie Ojior	2 nd Year	Computer Science	Graduate
Eddie Mason	Sophomore	Computer Science/ Mathematics	Undergraduate
Veda Chandler	Junior	Electrical Engineering/ Mathematics	Undergraduate

OUTREACH AND TECHNOLOGY TRANSFER

While the primary research effort has been in the use of HPC in the solution of fluid structure interaction problems, several discussions have conducted on utilizing similar approaches in solving complex dynamic simulation problems. In particular, Michael Letherwood and David Gunter of the U.S Army Tank Automotive Command in Warren MI, have expressed some interest in pursuing such a HPC approach to solving nonlinear simulations of multi-vehicle dynamics. A similar discussion is under way with AEDAR Corporation and Dr. Fabunmi, in using some these methods in complex simulations of weapon systems.

PUBLICATIONS AND PRESENTATIONS

S. Sarathy, and O. Olatidoye, "Parallel Physical Object Oriented Simulation", in *Jan'1996 Winter Simulation Multiconference*, LaJolla CA, Society for Computer Simulation.

REFERENCES

S. Sarathy and V.R. Murthy. An Advanced Parallel Rotorcraft Flight Simulation Model: Parallel Implementation and Performance Analysis. In AIAA Flight Simulation Technologies Conference, Monterey, CA, August 1993.

Olatidoye, O.A., Abu-Saba, E.G., Fobbes, V. and Dixon, N., "Dynamic Analysis of the Joint Dominated Beam", NASA Langley Research Center, Hampton, Virginia, October 1986.

Olatidoye, O.A., Chiang, R.N. and Wang, J.C., "The Design and Application of an Optimization Model for Thermal Performance of Atrium Buildings",

ASHRAE/DOE/BTECC Thermal Performance of the Exterior Envelopes of Buildings III,
Clearwater Beach, Florida, December 2-5, 1995.

**2.8 CONSTITUTIVE MODELING AND TESTING OF POLYMER MATRIX
COMPOSITES INCORPORATING PHYSICAL AGING AT ELEVATED
TEMPERATURES**

Investigators: D. R. Veazie

Collaborators:

T. S. Gates
NASA Langley Research Center
M.S. 188-E
Hampton, VA 23681

L. C. Brinson
Northwestern University
2145 Sheridan Road
Evanston, IL 60208

INTRODUCTION

Long term durability is an important issue in the selection and design of high temperature polymer matrix composites (PMC's) for structural applications in the next generation commercial aircraft. This high speed civilian transport for the post-2000 marketplace is expected to be a supersonic aircraft capable of Mach 2+ cruise while carrying 300 passengers. This sustained cruise will result in skin temperatures near 200°C, a high temperature environment for polymeric composites that are expected to exhibit time dependent, viscoelastic properties. In order to screen materials for selection in long term tests, accelerated test methods and associated analytical models must be developed which provide the means for characterizing the time dependent properties and predicting the long term behavior from short term test data. Due to the explicit time dependence of viscoelasticity, creep and creep recovery tests are a natural choice for studying the time dependent aging process.

A possible disadvantage of polymer-based composites is that the physical and mechanical properties of the matrix often change significantly over time due to exposure to elevated temperatures and environmental factors. This problem has resulted in an extensive research initiative to develop comprehensive material property characterization techniques and analytical modeling methods aimed at predicting the long term mechanical response of polymer matrix composites at elevated temperatures. The ultimate goal is to develop accurate analytical models and accelerated test methods needed to engineer advanced polymer matrix composites to ensure long-term structural integrity over the design life-time.

The three basic constituents of advanced PMC's are fiber, interphase, and matrix. In many circumstances the polymeric matrix can be the major constituent that contributes to degradation or changes in durability of PMC's. Changes in composite stiffness, strength and fatigue life can all be related to changes in the mechanical properties of the polymer matrix. As shown in Bank, et al.

Linear viscoelastic behavior during creep compression can be assumed if sufficient testing is performed to confirm the validity of Boltzman's superposition principle and proportionality. Aside from the obvious sign differences from tensile creep testing, compressive testing can take advantage of established procedures. Care must be taken however, to pick a stress level which gives linearity over the complete range of temperatures yet also provides enough creep strain to develop the compliance curves.

Time/temperature and time/aging time superposition techniques developed for characterizing physical aging during tensile creep work equally as well with compressive creep. Shifting and collapsing creep compliance curves was a straightforward process and lent itself well to the formation of master curves and the three parameter characterization. The momentary master curves show the clear temperature dependency of short term creep compliance. The ordering of the curves was as expected with the highest temperatures resulting in the highest creep compliance. The directional dependency of the PMC is also evident by noting the differences in the compliance between the transverse and shear tests.

Master curve parameters combined with aging shift rates, effective time theory, and lamination theory should allow for the prediction of long term compressive creep compliance behavior of thin composite laminates under elevated temperature. Verification of this will require long term data for a variety of laminates.

Experiments were also performed to determine the effects of physical aging on creep compliance of IM7/K3B composite laminates loaded in tension or compression. Experimental results and established analytical methods were used to investigate the similarities and differences of tension and compression for both the shear and transverse loading modes.

The short term (96 hour) tests, run over a range of sub- T_g temperatures provided material constants, material master curves and aging related parameters. The test data was consistent and repeatable over the entire range of test temperatures. Comparing results from the short term behavior indicated that although trends in the data with respect to aging time and aging temperature are similar, differences exist due to load direction and mode. Temperature has a similar effect on tension and compression loading with the compression loading producing more exponential long term behavior as compared to the tension cases.

The long term (1500+ hour) predictions compared favorably to the long term test data with the model demonstrating more accuracy in the shear mode as compared to the transverse mode. The sensitivity of the long term predictions to aging shift rate imply that the predictive model must account for both loading mode and loading direction. This implication would also hold true when considering development of accelerated test methods based upon the changes in physical aging due to temperature.

In other results, the IM7/K3B composite shows evidence of a small, non-aging, stress relaxation. Attributing this phenomenon to thermal residual stresses might not be conclusive here, however assessing this effect on the time dependent properties and prediction of the long term behavior of PMC's may prove useful.

EDUCATION AND TRAINING

Two undergraduate students were supported as research assistants on this project. **Mr. Ronald O. Grover** is a junior dual-degree Mathematics and Mechanical Engineering major. He is presently attending the Georgia Institute of Technology. **Ms. Charmin Roundtree** is a sophomore dual-degree Mathematics and Civil Engineering major. She is completing her last year at Clark Atlanta University and plans to attend the Georgia Institute of Technology in Fall 1997.

PUBLICATIONS

- Gates, T. S., Veazie, D. R., and Brinson, C. (1996), Creep and Physical Aging in a Polymeric Composite: Tension versus Compression, *Paper Submitted: Proceedings of the American Society of Mechanical Engineers*.
- Veazie, D. R., and Gates, T. S. (1996) Compressive Linear Viscoelastic Creep and the Effects of Physical Aging on the IM7/K3B Composite, *Paper Accepted: Experimental Mechanics*.
- Gates, T. S., Veazie, D. R., and Brinson, C. (1996), Tension versus Compression Effects on the Creep and Physical Aging in a Polymeric Composite, *Paper Submitted: ASTM STP*.
- Veazie, D. R. (1996), The Effects of Residual Stress on the Physical Aging of a Thermoplastic Composite, *Proceedings of the VIII International Congress on Experimental Mechanics*, 1, 407.

PRESENTATIONS

1. VIII International Congress on Experimental Mechanics and Experimental/Numerical Mechanics in Electronic Packaging, Nashville, TN, June 10-14, 1996. (Effects of Residual Stress on the Physical Aging of a Thermoplastic Composite)
2. ASTM Second Symposium on High Temperature and Environmental Effects on Polymeric Composites, Norfolk, VA, November 13, 1995. **Session Chair** - Durability of Composites.
3. ASTM November Meeting, Norfolk, VA, November 12-17, 1995. Member - Committee D-30 High Modulus Fibers and Their Composites (Editorial Subcommittee, Lamina/Laminate Properties - Compression, Research Subcommittee, Thermophysical Properties Subcommittee)

REFERENCES

1. Bank, L. C., Gentry, T. R. and Barkatt, A., "Accelerated Test Methods to Determine the Long-Term Behavior of FRP Composite Structures: Environmental Effects," *Journal of Reinforced Plastics and Composites*, Vol. 14, June, 1995, pp. 559-587.

2.9 MODELING AND TESTING OF HYBRID TITANIUM COMPOSITE LAMINATES AT NORMAL AND ELEVATED TEMPERATURES

Investigators: D. R. Veazie, A. Abatan (P.I.), and Dr. M. Lin

Collaborators:

T. L. St. Clair	S. Johnson
NASA Langley Research Center	CERC
M.S. 188-E	Georgia Tech
Hampton, VA 23681	Atlanta, GA 30309

INTRODUCTION

The next generation military and commercial aircraft requires applications for high strength, low weight structural components subjected to elevated temperatures. The hybrid titanium composite laminate (HTCL) is a material system that merits attention because of its capability to operate in structures at higher temperatures. In this system, thin plies of titanium are adhesively laminated together using a high temperature resin with high modulus fibers included in the bondline. Material systems such as the ARALL (Aramid Reinforced Aluminum Laminates) and GLARE laminates have essentially the same concept of the HTCL's and are now flying on several commercial and military aircraft. The history of laminated metals has shown definite mechanical advantages that can translate to weight savings in commercial and military aircraft applications (Miller et al., 1994) and (Schijve, 1993).

OBJECTIVES

This experimental study will investigate the laminated/hybrid technology applied to high temperature titanium alloys, and a graphite fiber reinforced high temperature thermoplastic polyimide adhesive, in hopes of demonstrating that these systems will be useful in the next generation high speed aircraft. Four unidirectional hybrid titanium composite systems were fabricated with different titanium alloys and titanium layer thicknesses. The results were compared to each other to assess laminate strength, load-deformation behavior, and failure modes.

APPROACH

Monotonic tensile tests were conducted in accordance with ASTM Specification D3552-77 on the HTCL specimens. From the limited supply of material manufactured, twelve HTCL specimens were fabricated, three from each panel. Each specimen was tested statically to failure at room temperature to examine the tensile strength and load-deformation behavior.

Prior to testing, all specimens were dried for at least 24 hours at 110°C in a convection oven (Veazie and Gates 1995). Following the drying, the specimens were stored inside a desiccator until the start of the tests. The tensile response was evaluated using dog-bone straight-sided specimens in laboratory air on a 100 kN servo-hydraulic test frame equipped with digital controller and data acquisition. A crosshead displacement rate of 2 mm/min was used to effect a constant strain rate. Hydraulic grips incorporating flat-faced wedges with a non-aggressive surface finish were used to allow for firm gripping of the composite without grip-induced failures. Uniaxial strain was measured on the surface of the specimen using clip-on extensometers with a 25 mm gage section. Stress was calculated based upon the applied load and the specimen cross-section before testing. This stress, along with the corresponding average measurement of two back-to-back extensometers aligned longitudinally on the specimen flats, was used to compute the mechanical properties of the HTCL's.

ACCOMPLISHMENTS

Technical Results

Four HTCL systems were fabricated as 17.8 cm by 17.8 cm panels in a hydraulic press with load cell and 30.5 cm by 30.5 cm induction heated platens. Two of the four HTCL systems were fabricated with the titanium Ti-15-3 alloy, while the other two systems were fabricated with the titanium Timetal b-21S alloy for the metal portion of the laminated panels. Prior to laminating, the titanium alloys were given a surface treatment available from Semco and designated Pasa-Jell 107.

A high temperature polyimide resin obtained from Imitec, designated LARCTM-IAX {a version of LARCTM-IA 4 mole % offset [8 mole % phthalic anhydride (PA) end cap] in N-methyl-2-pyrrolidone (NMP) in which the backbone was modified slightly with 10 mole % of a more rigid diamine, p-phenylenediamine, to improve solvent resistance}, was used as the adhesive (Progar and St. Clair 1990). The fiber, IM7, was an intermediate modulus carbon fiber manufactured by Hercules. Each panel was prepared using LARCTM-IAX, 30 wt. % solids solution in NMP with a viscosity of 30,400 cp and 29 vol. % IM7 fibers solution coated as a unidirectional prepreg (adhesive tape) approximately 0.18 mm thick. The prepreg was made by the Composites and Polymers Materials Branch (CPB) of the NASA Langley Research Center on a multipurpose prepegging machine. The primer, which was also prepared by the CPB, was applied to the titanium sheets as a 7.5 wt. % solution of LARCTM-IAX in NMP and air dried for one hour after which they were placed in a convection oven and heated for one hour each at 150°C and 230°C.

The laminate assembly was arranged in an open-ended matched-die mold by alternating layers of titanium sheets with layers of adhesive tape. High temperature tape was used to hold the assembly and to prevent the laminate from sticking to the mold. A thermocouple was attached to the end of the laminate to provide feedback to the platen temperature controller. Panel 1 was prepared with three plies of the adhesive tape and four plies of the titanium Ti-15-3 alloy measuring 5 mils thick. Panel 2 was prepared with three plies of adhesive tape and four plies of the titanium Timetal b-21S alloy measuring 5 mils thick. Panel 3 was prepared with two plies of tape and three plies of the titanium Ti-15-3 alloy measuring 11 mils thick. Panel 4 was prepared with two plies of the adhesive tape and three plies of the titanium Timetal b-21S alloy measuring 10 mils thick.

Each laminate assembly was arranged in the bottom part of the die mold, placed in a forced-air oven without the top part of the die mold, then heated for 30 minutes each at 150°C, 175°C and 230°C. This staged process, approximately one hour before applying pressure, was used to remove some of the volatiles prior to the bonding procedure. The laminates were further processed under a pressure of 6.89 MPa at 360°C for one hour.

Dog-bone test specimens similar to those described in ASTM Specification D3552-77 (Standard Test Method for Tensile Properties of Fiber-Reinforced Metal Matrix Composites) measuring 15.2 cm. in length were machined from the laminated panels. Three replicates of each specimen were used for each test.

In a comparison with the monolithic titanium sheets, all HTCL systems showed a significant improvement in the elastic modulus, as well as improved yield strength. The laminates that contained the titanium b-21S alloys approximately doubled the elastic modulus of the monolithic b-21S. Comparable mechanical properties were observed in laminates with equivalent titanium ply thicknesses, however the laminates that contained the titanium Ti-15-3 alloys experienced lower ultimate strength and failed at a lower strain. HTCL systems that contained the four 5 mils thick titanium plies showed a significant strength-to-weight-ratio improvement in elastic modulus and ultimate strength than those that contained three of the thicker titanium ply systems; however, these systems failed at a lower strain.

The fracture modes of the four HTCL's varied greatly. The 10 mils thick b-21S alloy specimens experienced very little delamination damage, mostly localized. All HTCL's, except the 10 mils thick b-21S alloy specimens, suffered severe delamination damage that extended throughout the specimen length. The 5 mils thick titanium plies fractured throughout the gage length of the specimens, while the thicker titanium plies experienced more localized fracture. In the Ti-15-3 alloy specimens, the IM7 fiber breakage was extensive throughout the specimen length; whereas fiber breakage was more localized in the b-21S alloy specimens. Ti-15-3 alloy specimens experienced considerably more fiber matrix debond damage than b-21S alloy specimens.

This investigation evaluated the tensile response of four HTCL systems at room temperature. Results of these test were compared to assess the improvement in mechanical properties achieved by the influence of the titanium layer. Four laminates were fabricated from

two different titanium alloys with varying thicknesses, then tested statically to failure in tension. Results included stress-strain curves, ultimate strength, strain-to-failure, initial modulus of the HTCL's, and the description of the observed failure modes.

The experiments showed that the titanium layer in these HTCL systems influences the mechanical properties. Higher yield strength in the titanium alloys, in this case the b-21S alloy, results in HTCL's with greater ultimate strength. However, the stiffer Ti-15-3 titanium alloy did not result in a HTCL with a higher elastic modulus. If systems with higher strength-to-weight-ratios are of primary concern, as in applications for future high speed aircraft, HTCL systems that are fabricated with many thinner titanium plies show improvement over systems with fewer, thicker titanium plies. Overall, the HTCL systems presented here provide stronger and stiffer alternatives to their corresponding monolithic metals.

EDUCATION AND TRAINING

Genine I. Bryant is a second year dual degree student at Clark Atlanta University. She is currently pursuing a B.S. in Mathematics, and plans to continue her studies at the North Carolina A&T State University in Mechanical Engineering. She plans to receive B.S. degrees from both institutions in May of 1999. As a student researcher, she has participated in research relating to the mechanics of polymer matrix composites. She is from Cleveland, Ohio.

PUBLICATIONS

- Veazie, D. R., Badir, A. M., and Grover, R. O. (1996), Effects of Titanium Plies on the Strength of a Hybrid Titanium Composite Laminate, *Paper Accepted: Proceedings of the American Society for Composites*.
- Veazie, D. R., Grover, R. O., and Bryant, G. I. (1996), Titanium Layer Influence on the Strength of a Hybrid Titanium Composite Laminate, *Proceedings of the First National Students' Conference*, NASA University Research Centers at Minority Institutions, March 31 - April 2, 1996.

PRESENTATIONS

1. First National Student's Conference NASA University Research Centers at Minority Institutions, Greensboro, NC, March 31 - April 2, 1996. (Titanium Layer Influence on the Strength of a Hybrid Titanium Composite Laminate)
2. American Society for Composites 11th Technical Conference on Composite Materials, Atlanta, GA, October 7 - 9, 1996. (Effects of Titanium Plies on the Strength of a Hybrid Titanium Composite Laminate)

REFERENCES

1. Miller, J. L., Progar, D. J., Johnson, W. S., and St. Clair, T. L., "Preliminary Evaluation of Hybrid Titanium Composite Laminates," NASA TM 109095, April 1994.
2. Schijve, J., "Development of Fibre-Metal Lam-inates, ARALL and GLARE, New Fatigue Resistant Materials," *FATIGUE '93*, May 3-7, 1993, pp. 3-20.
3. Progar, D. J. and St. Clair, T. L., "A New Flexible Backbone Polyimide Adhesive," *Journal of Adhesion Science and Technology*, Vol. 4, No. 7, 1990, pp. 527-549.
Veazie, D. R. and Gates, T. S., "Compressive Creep of IM7/K3B Composite and the Effects of Physical Aging on Viscoelastic Behavior," *SEM Spring Conference on Experimental Mechanics*, June 12-14, 1995, pp. 491-498.

2.10 LOW DENSITY, LOW CONDUCTIVITY PAN ABLATIVE OPTIMIZATION AND NOZZLE FABRICATION

Investigators: D. R. Veazie, A. Abatan (P.I.) and M. Lin

Collaborators:

G. Wendell
Project Manager
Thiokol Corporation
Brigham City, UT 84302

R. Harwell
Marshall Space Flight Center
M.S. PT21
Marshall, AL 35812

INTRODUCTION

Concerns about the stability of the domestic supply of carbonizable aerospace grade rayon for ablative composites have led to interest in an alternate carbon fiber precursor. Polyacrylonitrile (PAN) based carbon fibers have been shown through various studies to be an acceptable alternative. Another approach to developing a replacement for rayon is to reduce the thermal conductivity and density of the composite by the inclusion of filler ceramic microballoons to the PAN prepreg. These microballoons are an evolution from previous rayon low density materials which used carbon microballoons, but provide cost and thermal conductivity advantages.

The ply lift anomaly which occurs in ablative composites causes erratic erosion and spallation, leaving large multiple voids between plies of the material. This can lead to loss of the thermally protective char cap and result in increased heat-affected depth of the material. The fiber/matrix bond strength in low-density PAN based carbon fiber reinforced phenolic composites

is believed to influence this event. In particular, higher cross-ply tension and interlaminar shear strength properties are necessary to accommodate the high cross ply thermal expansion (cool-down dilation) experienced in ablative applications.

OBJECTIVES

An experimental study was undertaken to investigate the mechanical properties believed to influence ply lifting in ablative, PAN composite liner materials, in hopes of demonstrating that these systems will be useful as viable substitutes for rayon-based ablative composites. Four PAN fiber ablative composite systems were fabricated with different ceramic microballoon levels and cure pressures. The results were compared to each other to assess laminate strength, load-deformation behavior, and failure modes.

APPROACH

Monotonic tensile tests were conducted in accordance with ASTM Specification D3039M-95 on the PAN composite specimens. From the limited supply of material manufactured, 16 PAN composite specimens were fabricated, four from each panel. Each specimen was tested statically to failure at room temperature to examine the tensile strength and load-deformation behavior.

The tensile response was evaluated using rectangular specimens in laboratory air on a 100 kN servo-hydraulic test frame equipped with digital controller and data acquisition. A loading rate of 150 N/sec was used to effect a constant strain rate. Hydraulic grips incorporating flat-faced wedges with a non-aggressive surface finish were used to allow for firm gripping of the composite without grip-induced failures. Fine grit abrasive paper, held in place by the pressure of the grip, was used as friction tabs between the wedges and the specimen. Uniaxial strain was measured on the surface of the specimen using clip-on extensometers with a 25 mm gage section. Stress was calculated based upon the applied load and the specimen cross-section before testing. This stress, along with the corresponding average measurement of two back-to-back extensometers aligned longitudinally on the specimen edges, was used to compute the mechanical properties of the PAN composites.

ACCOMPLISHMENTS

Technical Results

Four PAN ablative composite systems were autoclave cured as 35.56 cm. long by 44.64 cm. wide by 10.16 cm. thick panels. Two of the four PAN composite systems were fabricated with 20% ceramic microballoon filler content, while the other two systems were fabricated with 15% microballoon content. Optical microscopy and vibrational spectroscopy were used to study the size, size distribution and integrity of the virgin microballoons prior to layup.

The prepreg broadgoods, obtained from ICI Fiberite and designated MX-134 LDR, included the ceramic microballoon fillers in SC-1008 Phenolic Resin, along with the T300 PAN fibers. Normal certification testing of the prepreg including a minimum of volatile content, resin content, filler content and flow was performed by ICI Fiberite. In addition, flow and Differential Scanning Calorimetry (DSC) testing of the prepreg was performed by Thiokol. The composite panels were fabricated at Thiokol and the Productivity Enhancement Center of the NASA Marshall Space Flight Center (MSFC).

From the as-received rolls, 35.56 cm. long by 44.64 cm. wide plies were cut and piled into 8 stacks of 32 plies per stack. Each stack was double sealed in foil bags and placed in cold box storage until layup. After warming to ambient (approximately two hours), these 8 "sub-stacks" were preheated in a convection oven at 60°C for 30 min. To simulate tape wrap debulk, the stacks were then arranged in a hydraulic press with load cell and induction heated platens to form a 256 ply composite. Teflon tape and high temperature, non-perforated release film was used to hold the assembly and to prevent the laminate from sticking to the tool surfaces, respectively. Thermocouples attached to the center of each platen provided feedback to the platen temperature controller. A maximum pressure of 2.76 MPa was applied to the stacks at 60°C for 30 min.

Following the press, the panels were bagged and placed under a minimum of 24.0 in. Hg vacuum for 1 hour. Each panel was monitored to assure that the vacuum drop did not exceed 1.0 in. Hg within 15 min. and held to a minimum of 21.0 in. Hg for a period of 15 min. Each bagged panel was then placed in a programmable temperature and pressure cycle autoclave. Autoclave pressure was held constant throughout the cure cycle. Thermocouples placed directly on top and under the center of the first debulk stack was used to monitor the composite temperature.

Panel 1 was prepared with 20% ceramic microballoon filler content and cured at a pressure of 1.65 MPa. Panel 2 was prepared with 20% microballoon content and cured at 0.35 MPa. Panel 3 was prepared with 15% ceramic microballoon filler content and cured at a pressure of 1.65 MPa. Panel 4 was prepared with 15% microballoon content and cured at 0.69 MPa. The microballoon filler contents selected were based on the widest range that are of interest and are predicted to result in composite bulk densities from 1.1g/cc to 1.4 g/cc. The skewed distribution to the higher process pressures is prompted by the desire to be able to co-process these materials with standard density materials to further reduce cost.

Rectangular test specimens similar to those described in ASTM Specification D3039M-95 (Standard Test Method for Tensile Properties of Polymer Matrix Composite Materials) measuring 25.4 cm. in length, 2.54 cm. wide, and approximately 0.3175 cm. thick were machined from the laminated panels. Four replicates of each specimen were used for each test.

In a comparison with the specimens from panels that were cured at lower pressures, the specimens from panels cured at 1.65 MPa showed an improvement in the initial modulus. Comparable initial moduli were observed in laminates with equivalent cure pressures, however the laminates that contained 20% ceramic micro-balloon filler content experienced lower ultimate strength. All PAN specimens showed little plastic deformation and failed at similar strains.

The fracture modes of the four PAN composites varied greatly. The specimens from Panel 1, prepared with 20% ceramic micro-balloon filler content and cured at a pressure of 1.65 MPa, experienced very little delamination damage, mostly localized. All PAN composites, except the specimens from Panel 1, suffered severe delamination damage that extended throughout the specimen length. The PAN fibers in specimens prepared from panels with 15% ceramic micro-balloon filler content experienced more distortion at fracture. In the specimens from panels that were cured at a pressure of 1.65 MPa, the PAN fiber breakage was more localized; whereas fiber breakage was extensive throughout the specimen length in the specimens that were cured at lower pressures. Specimens from panels cured at lower pressures also experienced considerably more fiber matrix debond damage and crumbling than specimens cured at 1.65 MPa.

This investigation evaluated the tensile response of four PAN composite systems at room temperature. Results of these test were compared to assess the improvement in mechanical properties achieved by the influences of the ceramic microballoon content and the cure pressure. Four laminates were fabricated with two microballoon contents and varying cure pressures, then tested statically to failure in tension. Results included stress-strain curves, ultimate strength, strain-to-failure, initial modulus of the PAN composites, and the description of the observed failure modes.

The experiments showed that the ceramic microballoon content and the cure pressure in these PAN composite systems influences the mechanical properties. If systems with higher moduli are of primary concern, PAN composites that are fabricated with higher cure pressures show improvement over systems cured at lower pressures. If higher tensile strength is necessary to accommodate the high cross ply thermal expansion causing ply lift in ablative applications, PAN composites fabricated with a lower ceramic microballoon filler content yield stronger composites.

EDUCATION AND TRAINING

Keva Vaughn is a third year dual degree student at Clark Atlanta University. She is currently pursuing a B.S. in Mathematics, and plans to continue her studies at the Georgia Institute of Technology in Civil Engineering. She plans to receive B.S. degrees from both institutions in May of 1998. As a student researcher, she has participated in research relating to the mechanics of polymer matrix composites.

PUBLICATIONS AND PRESENTATIONS

- Veazie, D. R., and Vaughn, K. (1996), Preliminary Evaluation of Low-Density, Low-Conductivity PAN Ablative Composites, *Proceedings of the First National Students' Conference*, NASA University Research Centers at Minority Institutions, March 31 - April 2, 1996.

PRESENTATIONS

1. First National Student's Conference NASA University Research Centers at Minority Institutions, Greensboro, NC, March 31 - April 2, 1996. (Preliminary Evaluation of Low-Density, Low-Conductivity PAN Ablative Composites)

2.11 COMPRESSIVE CREEP OF IM7/K3B COMPOSITE AND THE EFFECTS OF PHYSICAL AGING ON VISCOELASTIC BEHAVIOR

Investigators: D. R. Veazie (P.I.)

Collaborators:

T. S. Gates	C. E. Harris
NASA Langley Research Center	NASA Langley Research Center
M.S. 188-E	M.S. 188-E
Hampton, VA 23681	Hampton, VA 23681

INTRODUCTION

Advanced polymer matrix composites (PMC's) are desirable for structural materials in diverse applications such as aircraft, civil infrastructure and biomedical implants because of their improved strength-to-weight and stiffness-to-weight ratios. The development of analytical and experimental tools to aid in the study of composite durability is the impetus for intensive design and development studies at NASA and major industry based airframe developers (Brinson and Gates, 1995).

When a polymer matrix is cooled to below its glass transition temperature, T_g , the material does not achieve instantaneous thermodynamic equilibrium. Instead the free volume, enthalpy and entropy evolve over time toward their hypothetical equilibrium values. Physical aging is the change in the mechanical and physical properties of the material during this time. Physical aging occurs when a polymer is subjected to a temperature bounded by T_g above, and the temperature of the highest secondary transition below. Struik (1978) showed that it was possible to isolate the physical aging process in polymers from other behaviors by performing isothermal creep compliance tests and using superposition techniques to establish the aging related material constants. Several experimental studies have illustrated that the matrix dominated composite properties of continuous fiber reinforced PMC's, namely the shear and transverse response, are affected by physical aging in a manner similar to pure polymers (Sullivan, 1990) and (Gates and Feldman, 1995) and (Veazie and Gates, 1995).

OBJECTIVES

It is the intent of this work to establish unique experimental techniques to accurately measure the compressive creep strain and recovery strain as a function of test time and aging time for the time dependent response of fiber reinforced polyimide composites. Resulting compressive creep compliance master curves, physical aging shift factors and shift rates for inclusion in Struik's effective time theory are used to model the physical aging effects in the composite.

APPROACH

The material system chosen for this study was a continuous carbon fiber reinforced thermoplastic polyimide fabricated by DuPont and designated IM7/K3B. The fiber, IM7, was an intermediate modulus carbon fiber manufactured by Hercules. The unaged T_g in the composite as measured by Dynamic Mechanical Analyzer (DMA) G'' peak was 240°C. Change in the T_g from the unaged condition over extended aging times was measured by industrial studies and found to remain within 3°C over 10,000 hours of isothermal aging at 170°C (Brinson and Gates, 1995). For this study, it was therefore assumed that chemical aging of the composite would not occur and the T_g would remain constant over the duration of the tests.

This research presents unique experimental techniques and apparatus used to measure the viscoelastic behavior of PMC's in compression at elevated temperatures. Isothermal, constant load, creep compliance measurements were performed on the matrix dominated transverse and in-plane shear behavior of IM7/K3B in compression. Linear viscoelasticity was used to characterize the creep and superposition techniques were used to establish the physical aging related material constants. The resulting creep compliance master curves, physical aging shift factors and shift rates can be used as input data to a viscoelastic creep compliance procedure to establish time dependent behavior and predict long term response. The observed differences in the time dependent behavior in the transverse and in-plane shear directions along with the effects of elevated temperature are discussed.

ACCOMPLISHMENTS

Technical Results

The range of linear viscoelastic behavior was experimentally determined to satisfy the conditions of proportionality. Experiments were also conducted to assure that the linear Boltzman's superposition condition was met for all tests. Using the test and data reduction procedures, the short term sequenced creep compliance data for IM7/K3B was found as a function of aging time over a range of five temperatures. Isothermal momentary master curves for the transverse (S_{22}) and shear (S_{66}) terms were generated to show the temperature dependency of short term creep compliance and the directional dependency of the PMC.

To evaluate the proportionality criteria, creep tests were run at 230°C and 225°C, representing the maximum test temperatures used for transverse and shear compliance respectively. The applied stress levels were between 3.56 MPa and 1.81 MPa for the transverse compliance proportionality tests and between 8.34 MPa and 5.59 MPa for the shear compliance proportionality tests. Coincidence of the transverse compliance and the shear compliance curves indicated that the different stress levels caused little variation in compliance on the log scale although there was some small trend in location of the curves in relation to the applied stress. Based upon these results and the fact that the same applied stress level was to be used at all temperatures, proportionality was met for all tests.

The strain history of a typical creep/recovery sequence for a $[\pm 45]_{2s}$ specimen was shown. The condition of linear Boltzman's superposition is assumed to be satisfied because of the good correlation between the predicted recovery strain and the measured recovery strain. It was recognized that the assumption of linear viscoelastic behavior based upon these results might not be conclusive, however it was felt that deviations from linearity were small enough to confidently proceed with linear modeling. The final applied stress levels chosen for the creep tests were 2.68 MPa and 6.97 MPa for the transverse and shear tests, respectively.

Three replicate specimens were used over a range of five temperatures to generate the isothermal momentary master curves for transverse (S_{22}) and shear (S_{66}) terms. The momentary master curves parameters (S_0, τ, β) were found by a parameter fit to the combined data sets from all replicates. It should be noted that even though only one set of momentary master curve parameters was given, each of the replicate tests had their own shift rate (μ). Therefore, the shift rates are average values. The standard deviation of μ was also provided. The average shift rates are plotted versus test temperature in for the transverse and shear compliance. The data points were connected with a smooth curve to illustrate the trends. These tests show that the transverse direction shift rate falls continuously, while the shear shift rate is fairly level until 225°C.

For comparison purposes, the resultant momentary master curves for each temperature which correspond to the data are plotted together for the transverse and shear compliance. These master curves represent the sum of all the short term sequenced creep compliance data.

PUBLICATIONS

- Veazie, D. R., and Gates, T. S. (1995) Physical Aging Effects on the Compressive Linear Viscoelastic Creep of IM7/K3B Composite, *NASA TM 110224*, December, 1995.
- Veazie, D. R., and Gates, T. S. (1995), Compressive Creep of IM7/K3B Composite and the Effects of Physical Aging on Viscoelastic Behavior, *1995 Proceedings of the SEM Spring Conference on Experimental Mechanics*, 1, 491.

- Veazie, D. R. (1995), Numerical Modeling of Advanced Composites for Space Applications, *Proceedings of the 67th Annual Conference of the National Technical Association - Global Information: Space and Education*, 13.

PRESENTATIONS

1. National Technical Association 67th Annual Conference, Houston, TX, July 20-22, 1995. **Session Chair** - Aerospace II (Paper - Numerical Modeling of Advanced Composites for Space Applications)
2. High Speed Research Composites, Adhesives, and Sealants Interim Review, NASA Langley Research Center, Hampton, VA, June 28-29, 1995.
3. Society for Experimental Mechanics (SEM) Spring Conference and Exhibit, Grand Rapids, MI, June 12-14, 1995. (Compressive Creep of IM7/K3B Composite and the Effects of Physical Aging on Viscoelastic Behavior)
4. High Speed Research Materials Durability Semi-Annual Review, NASA Langley Research Center, Hampton, VA, May 9-10, 1995.
5. Advances in Smart Materials for Aerospace Applications, NASA Langley Research Center, Hampton, VA, May 4-5, 1995. (**Session Chair** - Thermophysical Properties)
6. AIAA/ASME Adaptive Structures Forum, New Orleans, LA, April 13, 1995.
7. Computational Materials Research Workshop, NASA Langley Research Center, Hampton, VA, January 5-6, 1995. (Micro/Macro Mechanics of Time Dependent Behavior in Composites)
8. National Research Council Annual Review, NASA Langley Research Center, Hampton, VA, September 1-2, 1994.

REFERENCES

1. Brinson, L. C. and Gates, T. S., "Effects of Physical Aging on Long-Term Creep of Polymers and Polymer Matrix Composites," *INT. J. SOLIDS STRUCTURES*, **32**, (6), 827-846, (1995).
2. Struik, L. C. E., *Physical Aging in Amorphous Polymers and Other Materials*, Elsevier North-Holland Inc., New York, NY, (1978).
3. Sullivan, J. L., "Creep and Physical Aging of Composites," *Composite Science and Technology*, **39**, 207-232, (1990).

4. Gates, T. S. and Feldman, M. "Time-Dependent Behavior of a Graphite/Thermoplastic Composite and the Effects of Stress and Physical Aging," *Journal of Composites Technology & Research*, 17, (1), 33-42, (1995).
5. Veazie, D. R. and Gates, T. S., "Physical Aging Effects on the Compressive Linear Viscoelastic Creep of IM7/K3B Composite," *NASA-TM 110224*, December (1995).

2.12 CHARACTERIZATION AND MECHANICAL TESTING OF A POLARIZATION-MAINTAINING OPTICAL FIBER - PHASE II

Investigators: D. R. Veazie and L. Moeti

Collaborators:

E. Cuddihy
Jet Propulsion Laboratory
M.S. 188-E
Pasadena, CA 23681

INTRODUCTION

Polarization-maintaining (PM) optical fibers are increasingly being considered for new applications in, for example, advanced space craft inertial reference units as fiberoptic rotation sensors. Applications where volume is a consideration have used PM fibers wound onto small spools (Perlmutter, 1993). These new PM fibers, often referred to as PANDA fibers, are significantly different from commercial optical fibers in two major ways. First, commercial optical fibers generally consist of a wave guide surrounded by an acrylic jacket. In the PANDA fiber, there exists a silicone layer between the wave guide and the jacket. Secondly, the PANDA fiber contains two beryllium oxide stress rods around the wave guide core that produces a stressed wave guide core specific for polarized light.

Technical literature exists on the physical and mechanical properties of commercial optical fibers which can be used for engineering design. Development of theories to predict fiber lifetime for commercial optical fibers using fiber parameters have been established (Kapron and Yuce, 1991). Literature reports on the temperature-dependent behavior of highly birefringent optical fibers are available (Barlow, 1985). For the case of PANDA fibers the temperature dependence of fibers wound onto different diameter cylinders has been measured (Ruffin, 1995). The modeling and prediction of mechanical properties of optical fibers based on material properties is not available in the open literature. The ability to predict mechanical properties of optical fibers for design applications where testing may not be practical would be of great use.

OBJECTIVES

Micromechanical modeling of the composite mechanical properties of optical fibers was conducted. Good agreement was obtained between the values of Young's modulus obtained by micromechanics modeling and those determined experimentally for a single mode optical fiber where the wave guide and the jacket are physically coupled. The modeling was also attempted on a polarization-maintaining optical fiber (PANDA) where the wave guide and the jacket are physically decoupled, and found not to applicable since the modeling required perfect bonding at the interface. The modeling utilized constituent physical properties such as the Young's modulus, Poisson's ratio, and shear modulus to establish bounds on the macroscopic behavior of the fiber.

APPROACH

In this research, the modeling of the mechanical properties of optical fibers based on micromechanics is presented. The properties predicted by micromechanical modeling are compared to experimental values determined earlier (Moeti et al., 1996).

Micromechanical modeling is often used to quantitatively characterize the effects of constituent properties on the macroscopic behavior of composite materials. The effects of the arrangement of the constituents, as well as the distribution of stresses and deformations among the constituents, can be studied using micromechanical modeling. In the micromechanical self-consistent field methods, approximations of phase geometries are made and a simple representation of the response field is obtained. The phase geometry is represented by one single fiber embedded in a matrix cylinder. This outer cylinder is embedded in an unbounded homogeneous material whose properties are taken to be equivalent to those of the average composite properties. The matrix under a uniform load at infinity introduces a uniform strain field in the fiber. Elastic constants are obtained from this strain field. The results obtained are independent of fiber arrangements in the matrix and are reliable at low fiber volume fractions V_f , reasonable at intermediate V_f , and unreliable at high V_f (Chawla, 1987).

ACCOMPLISHMENTS

Technical Results

In this research, micromechanical analyses was used to estimate the composite properties of a single mode optical fiber. As in the context of continuum mechanics, it is assumed that the interface between the glass fiber (wave guide) and the polymeric matrix (jacket) is perfect. Therefore throughout the entire loading application, the interface is a mathematical surface across which material properties change discontinuously, while the interfacial traction and displacements are continuous across the interface. When perfect bonding is assumed, the macromechanical properties and strength of the composite (wave guide plus jacket) are determined solely by the properties of the constituent materials. For the control fiber as described earlier, the interface

between the wave guide and the jacket can be regarded as being perfect, i.e., physically coupled. In the case of the PANDA fiber, the wave guide and the jacket are physically decoupled.

The micromechanical method used here focuses on the upper and lower bounds on the elastic constants. This method does not predict the properties directly, however, if the upper and lower bounds coincide, then the property is determined exactly. Frequently, the upper and lower bounds are well separated. When these bounds are close enough they can be used as indicators of the material behavior. This is the case for the longitudinal properties of a unidirectional system as considered here. Hill (1965) derived rigorous bounds on the longitudinal Young's modulus, E_{11} , in terms of the bulk modulus in plane strain (k_p), Poisson's ratio (ν), and the shear modulus (G) of the two phases. For the glass wave guide of the optical fiber system, E_f , G_f and ν_f were 1.04×10^7 Psi, 6.07×10^6 , and 0.16, respectively which are known published values for glass. The polymer jacket used on the single mode optical fiber is an acrylic polymer, believed to be similar to polymethyl methacrylate (PMMA). The published value for the modulus E_m of PMMA is given as 4.79×10^5 Psi, which was used for micromechanical modeling. The compressibility of PMMA, $\xi_m = 0.0355$ Psi, was used to derive the shear modulus for the jacket, G_m , as

$$G_m = \frac{3(1-2\nu_m)}{2\xi_m(1+\nu_m)}. \quad (1)$$

The volume fractions for the wave guide and the jacket, V_f and V_m , were 0.25 and 0.75, respectively. Calculations to determine E_{11} of the optical fiber system were made by varying the Poisson's ratio (ν_m) and Young's modulus (E_m) of the jacket, separately. No restrictions were made on the core form or packing geometry. The term k_p is the modulus for lateral dilatation with zero longitudinal strain and is given by

$$k_p = \frac{E}{2(1-2\nu)(1+\nu)}. \quad (2)$$

The bounds on the longitudinal modulus, E_{11} , are

$$\frac{4V_f V_m (\nu_f - \nu_m)^2}{(V_f/k_{pm}) + (V_m/k_{pf}) + 1/G_m} \leq E_{11} - E_f V_f - E_m V_m \leq \frac{4V_f V_m (\nu_f - \nu_m)^2}{(V_f/k_{pm}) + (V_m/k_{pf}) + 1/G_f} \quad (3)$$

The bounds were shown for the longitudinal modulus of the composite optical fiber, E_{11} , for a Young's modulus (E_m) of the jacket equal to 4.79×10^5 Psi, and a range of values of the Poisson's ratio (ν_m) of the jacket. A composite modulus, E_{11} , in the order of 2.96×10^6 Psi is estimated, for the single mode optical fiber used in this study. The bounds were also shown for E_{11} for a given Poisson's ratio $\nu_m = 0.37$ and a range of values for E_m . These results show good agreement with the measured values.

The modulus of the optical fiber determined from static loading was shown. A value of 2.87×10^6 Psi for the modulus was obtained which is consistent with the value predicted from micromechanical modeling (2.96×10^6 Psi). Good agreement is observed in the values of modulus from micromechanical modeling and static loading, for the single mode optical fiber

where the glass wave guide and the polymeric jacket are physically coupled. For the case of the PANDA fiber where the glass wave guide and the polymeric jacket are decoupled, the micromechanical modeling was not applicable.

It should be noted that this type of micromechanical analysis is limited by the assumption of a perfect interface between the wave guide and the jacket. However, the assumption of perfect bonding is sometimes inadequate, as in the case of the PANDA fiber where the wave guide and the jacket are physically decoupled thus providing a distinct interfacial zone (interphase) between the core and the jacket. This weak, compliant interphase has lower strength and stiffness than those of the wave guide and the jacket. Recently, Veazie and Qu (1995) obtained micromechanical solutions for the nonlinear inelastic behavior of composites with weak, compliant interphases using the Mori-Tanaka method as a building block. New micromechanical analyses such as these may find utility in predicting the macromechanical properties of advanced optical fiber systems such as PANDA fibers.

Micromechanical modeling was used to predict the composite modulus of a single mode optical fiber. The micromechanical analysis was limited to the case of a perfect interface between the glass wave guide and the polymeric jacket of the optical fibers. The modeling worked well in the case of the single mode optical fiber where the glass wave guide and the polymeric jacket are physically coupled. The micromechanical modeling did not work for the polarization-maintaining PANDA fiber where the glass wave guide and the polymeric jacket are physically decoupled. Good agreement for the single mode optical fiber was obtained for the modulus predicted by micromechanical modeling and values measured experimentally.

PUBLICATIONS

- Moeti, L., Moghazy, S., Veazie, D., and Cuddihy, E., (1996), Constitutive Modeling of the Mechanical Properties of a Polarization-Maintaining Optical Fiber, *Paper Submitted: Optical Engineering*.

REFERENCES

1. Perlmutter, "A tactical fiber optic gyro with all-digital signal processing," Proc. 16th Biennial Guidance Test Symposium, AFDTC-TR-93-06, pp. 337-350, 46th Guidance Test Squadron/CC (AFMC), Holloman AFB, NM (1993).
2. Kapron and H.H. Yuce, "Theory and measurement for predicting stressed fiber lifetime," Optical Engineering 30(6), pp. 700-708 (1991).
3. Barlow, "Optical fiber birefringence measurement using a photoelastic modulator," J. Lightwave Technol., vol LT-3, pp135-145 (1985).
4. Ruffin, J. Sawyer, and C.C. Sung, "Effect of spool diameter on the temperature-dependent extinction ratios of polarization-maintaining fibers," Optical Engineering 34 (1), 56-57 (1995).

5. Moeti, S. Moghazy, A. Ally, S. Barnes, A. Abhiraman, P. Desai, and E. Cuddihy, "Mechanical and Physical Testing of a Polarization-Maintaining Optical Fiber," *J. of Lightwave Technology*, Paper submitted.
6. Veazie, and Qu, J., Effects of Interphases on the Transverse Stress-Strain Behavior in Unidirectional Fiber Reinforced Metal Matrix Composites, *Composites Engineering*, 5, No. 6, 597-610, (1995).
7. Chawla, *Composite Materials*, Springer-Verlag, New York, (1987).
8. Hill, A Self Consistent Mechanics of Composite Materials, *Journal of Mechanics and Physics of Solids*, 13, 189, (1965).

2.13 MICROMECHANICS MODELING OF FIBER REINFORCED COMPOSITES INCORPORATING DISTINCT INTERFACE PROPERTIES

Investigators: D. R. Veazie

Collaborators:

J. Qu
Micromechanics Laboratory
Georgia Tech
Atlanta, GA 30309

INTRODUCTION

Fiber reinforced composites posses general advantages because they are lightweight and strong materials, and they have high temperature capability. Proven and potential applications in automotive, nuclear, and aerospace industries have been discussed extensively (Chawla, 1987). For example, unidirectional continuous fiber reinforced composites such as Al_2O_3 /Al have been used as connecting rods in automotive engine applications. Similarly, Al_2O_3 /Mg composites have been used as turbine blades and shafts in the aeronautical industry. In these examples, reduced weight and reciprocating mass result from the use of these ceramic fiber reinforced metal matrix composites. Potential applications such as these have indicated a need for a fundamental understanding of the mechanical properties of these materials.

Metal matrix composites are under rapid development for use in propulsion and structural systems of space technology. But a crucial problem in their use is the presence of high residual (internal) stress induced during the fabrication process. Residual stresses are the self-equilibrating internal stresses existing in a free body which has no external constraints acting on its boundary. Residual stresses arise from the elastic response of the material to an inhomogeneous distribution

of inelastic strains such as plastic strains, phase transformations, misfit, thermal expansion strains, etc. This process-induced residual stress in composites is essentially thermal in nature, and is caused by a significant mismatch in the coefficients of thermal expansion between the fiber and the matrix with large temperature differential during the cooling process. Large temperature changes occurring in these materials during processing often lead to undesirable reduction of strength and stiffness.

When certain composites are fabricated and subsequently heat treated, the material may be in a stress-free state at an elevated temperature. However upon cooling to room temperature, residual stresses develop due to thermomechanical mismatch. Residual stresses may lead to the development of matrix cracking, and may also have adverse effects on the macromechanical properties of the composite. In this research, micromechanical analyses have been employed to determine the effects of interphase parameters on fiber reinforced composites under process-induced residual stress.

In the context of continuum mechanics, the interfaces between the fiber and matrix are often assumed to be perfect. That means that throughout the entire loading application, the interface is a mathematical surface across which material properties change discontinuously, while interfacial traction and displacements are continuous across the interface. When perfect bonding is assumed, the macromechanical properties and strength of the composite are determined solely by the properties of the constituent materials. However, the assumption of perfect bonding is sometimes inadequate. In many fiber reinforced composites, the bond between the fibers and the matrix material is not of the perfect kind that can be modeled by a continuity of traction and displacements across the fiber-matrix interface. Instead, the bond is affected across a thin interfacial zone, an interphase, which has distinct properties from the fiber and matrix.

An interphase which has distinct properties from the fiber and matrix, or a distinct interphase, can be compliant, weak, or both. A compliant interphase is one in which the interphase material has lower stiffness than those of the matrix and/or the fibers. A weak interphase however, means that the strength of the interphase is lower than that of the matrix and fibers. This can occur with interphases that behave in a rigid-perfect plastic manner, for example. An interphase can also be both compliant and weak. An elastic-perfect plastic interphase for example, may behave in this manner. The macromechanical properties of composites, such as the stiffness and the strength are significantly affected by the nature of the bond (the interphase) between the fiber and matrix material (Achenbach and Zhu, 1989).

OBJECTIVES

In this research, the focus is on the nonlinear, inelastic behavior of composites with a distinct interphase between the fiber and the matrix. The transverse properties of unidirectional continuous fiber reinforced composites are of particular interest. The Al_2O_3 / Al system is used as a model material. It is assumed that the interphase between the matrix and the fiber is due to a thin layer of carbon coating of the fibers. Carbon coatings on ceramic fibers can be accomplished by chemical vapor deposition (CVD), a process involving the decomposition and reaction of gases

in a chamber in order to deposit the solid coatings. The carbon coatings deposited are in the form of highly anisotropic layered graphite (Ning et al., 1990). Because the precise in-situ properties of carbon coatings are not well known, the elastic properties of carbon in its most common form are used in this research. The coating (interphase) is modeled as a layer of elastic-perfect plastic springs with its yield strength as the interphase strength. In the study, the fibers are modeled as isotropic, linear elastic solids. The matrix is modeled as an elastic-plastic solid with its plastic behavior following the Ramberg-Osgood equation, or as an elastic-plastic solid using Mises or Hill yield surfaces with associated plastic flow rule. Consequently, the overall effective stress-strain curve will become non-linear as soon as either the interphase yields (fiber debonding) or the matrix yields.

APPROACH

A unidirectional Al_2O_3 /Al composite is chosen as the model material. In this study, square array packing of circular cross-section fibers is assumed. A schematic of the cross-section of the unidirectional fiber reinforced composite can be shown, where a Cartesian coordinate system $x_1x_2x_3$ can also be shown. For normal load applied in the x_2 -direction, the composite is subjected to plane strain deformation. Furthermore, due to symmetry and the periodicity of fiber spacing, the state of stress and deformation in the composite can be completely defined by the stresses and strains in a quarter region of a unit cell.

It can be easily verified that the proper boundary conditions on the quarter unit cell are given by

$$u_2(x_1, 0) = 0, \quad \tau_{12}(x_1, 0) = 0, \quad \text{for } 0 \leq x_1 \leq b \quad (1.1a,b)$$

$$u_2(x_1, b) = d_2, \quad \tau_{12}(x_1, b) = 0, \quad \text{for } 0 \leq x_1 \leq b \quad (1.2a,b)$$

$$u_1(0, x_2) = 0, \quad \tau_{12}(0, x_2) = 0, \quad \text{for } 0 \leq x_2 \leq b \quad (1.3a,b)$$

$$u_1(b, x_2) = d_1, \quad \tau_{12}(b, x_2) = 0, \quad \text{for } 0 \leq x_2 \leq b \quad (1.4a,b)$$

where d_1 and d_2 are constants that need to be determined from the solution procedure. Of course, the stresses and displacements in the quarter unit cell must satisfy the equilibrium, compatibility and the constitutive equations. In addition, the interface conditions must be considered.

ACCOMPLISHMENTS

Technical Results

In this research, a framework has been established to characterize the effects of distinct interphases in the study of fiber reinforced composites. On the basis of this framework, a rigorous analysis has been carried out for the transverse normal loading of a unidirectional fiber reinforced composite, and for the loading of a composite under process-induced residual stresses.

Through the use of finite element method, the stress fields near the fiber/matrix interface are obtained. It is found that to prevent matrix cracking, the fibers should be at least three times as rigid as the matrix. Furthermore, for the Al_2O_3 /Al composites considered here, higher transverse strength of the composite may be achieved by coating the fiber with a material whose

yield strength is about 80% of the yield strength of the matrix. It is also found that very weak interphases can reduce interfacial damage caused by the relative sliding between the fiber and the matrix.

Also in this research, a Mori-Tanaka secant (tangent) approach is developed to predict the transverse effective stress-strain curve of the composite. This Mori-Tanaka approach yields satisfactory solutions at fiber volumes below 50%. Since it requires only the numerical solution of a single fiber in a matrix, this approach can be used by design engineers for design optimization.

Finally, it is concluded that magnitude of the interphase stiffness does not seem to play a significant role. This can be seen by comparing the results for the perfect interface to the results for compliant but strong interphases are finite. This conclusion justified the somewhat arbitrary selection of the carbon coating's elastic properties used in this research.

PUBLICATIONS

- Veazie, D. R., and Qu, J. (1996), Effects of Interphases on Fiber Reinforced Composites Under Process Induced Residual Stress, *Paper Accepted: Journal of Composites Technology and Research*.
- Veazie, D. R., and Qu, J. (1995), Effects of Interphases on the Transverse Stress-Strain Behavior in Unidirectional Fiber Reinforced Metal Matrix Composites, *Composites Engineering*, 5, No. 6, pp. 597-610.
- Veazie, D. R., and Qu, J. (1995), Process Induced Residual Stress Effects on Fiber Reinforced Composites Incorporating Distinct Interphases, *Proceedings of the Second International Conference on Composites Engineering*, 1, 775.
- Veazie, D. R., and Qu, J. (1994), Interphase Effects on the Macromechanical Behavior in Unidirectional Fiber Reinforced Metal Matrix Composites, *Proceedings of the First International Conference on Composites Engineering*, 1, 543.
- Veazie, D. R. (1994), An Approximate Analytical Solution for Composites Incorporating Distinct Interface Properties, *E&A '94 Conference Proceedings - PVAMU*, 2, 802.

PRESENTATIONS

1. International Conference on Composites Engineering (ICCE/2), New Orleans, LA, August 21-24, 1995. Session Chair - Metal Matrix Composites (Effects of Interphases on Fiber Reinforced Metal Matrix Composites Under Process Induced Residual Stress)
2. International Conference on Composites Engineering (ICCE/1), New Orleans, LA, August 28-31, 1994. (Effects of Interphases on the Transverse Stress-Strain Behavior in Fiber Reinforced Metal Matrix Composites)

3. Engineering & Architecture '94 Symposium, PVAMU, Prairie View, TX, March, 21-22, 1994. (An Approximate Analytical Solution for Composites Incorporating Distinct Interface Properties, - 2, 802.)

REFERENCES

1. Achenbach, J. D. and Zhu, H. (1989), Effect of Interfacial Zone on Mechanical Behavior and Failure of Fiber-Reinforced Composites, *J. Mech. Phys. Solids*, **37**, 381-393.
2. Chawla, K. K. (1987), *Composite Materials*, Springer-Verlag Pub., New York.

Ning, X. J., Pirouz, P., Lagerlof, K. P. D., and DiCarlo, J., (1990), The Structure of Carbon in Chemically Vapor Deposited SiC Monofilaments, *J. Mater. Res.*, **5**, 2865-2876.

2.14 SOL-GEL BASED MULLITE CERAMICS

Investigators: L. Moeti and E. Karikari

INTRODUCTION

The use of sol-gel techniques has become an important route in the preparation of high purity ceramics. The poor high temperature mechanical properties of existing ceramics can generally be traced to a variety of undesirable microstructural features, such as large grain sizes, residual porosity, glassy phases, and the presence of impurities, Romine (1987). Many bulk ceramics with vastly improved microstructures have been produced in recent years by sol-gel processing methods. The advantages of sol-gel processing include the making of new materials of greater purity, new compositions, and lower processing temperatures compared to conventional melt techniques. Sol-gel processing is useful for the development of coatings, powders, and monolithic materials of compositions that cannot be made by conventional techniques because of problems such as phase separation during melting, Pouuxviel et al., (1987). Oxide ceramics have been available for some time but have primarily been produced by colloidal as opposed to sol-gel processing, Johnson, et al., (1987) until recent years.

Considerable attention has focused on the preparation of mullite, $3\text{Al}_2\text{O}_3 \bullet 2\text{SiO}_2$, Aksay, et al. (1991), Sacks, et al., (1990). Most of the literature covering mullite is focused on the synthesis from alkoxides involving the hydrolysis and condensation reactions. One of the significant limitations in producing good chemical homogeneity using aluminum and silicon alkoxides is the different rates of reactivity between the two. Numerous techniques have been used in an attempt to overcome this problem. Prehydrolysis of the silicon alkoxide, Yoldas, et al., (1988), very low hydrolysis, Colomban (1989), and the use of chelating complexes, Heinrich, et

al., (1994) to reduce the reactivity of the aluminum alkoxide have been used. In the present research the use of prehydrolysis of the silicon alkoxide was used.

Most techniques to prepare mullite have been conducted in anhydrous alcohols where careful control of the water used for hydrolysis is performed. The use of aqueous routes to prepare mullite precursors has also been used. In most of the techniques, Sacks, et al., (1982), Ismael, et al., (1987) colloidal sols of silica and alumina are used. However, the chemical homogeneity in these systems is not as good as the alkoxide based approach.

OBJECTIVES

In this research, FTIR and rheological characterization were used to follow the hydrolysis and condensation, and structure buildup in alkoxide based mullite precursors to determine the impact of the starting chemistry and processing conditions on the final mullite ceramic. Heat treatment and microstructural analysis were conducted to correlate the final grain sizes in the mullite ceramics to the chemistry approach used.

APPROACH

The precursor sols were prepared using Aluminum tri-sec butoxide (ATSB) and Tetraethylorthosilicate (TEOS) as the primary reagents. The TEOS was prehydrolyzed before the addition of the ATSB. Hydrochloric (HCl) acid was used as the catalyst and 2-propanol was used as the solvent in all experiments conducted. Three molar ratios of water to TEOS were used to perform the hydrolysis (1.5, 2.5, and 3.0). The prehydrolyzed TEOS was allowed to react for 24 hours at which point the ATSB dissolved in 2-propanol was then added. Two temperatures were used for aging (40 and 65°C). FTIR analysis and rheology were used to monitor the sol to gel transition. TG/DTA was conducted to determine heating profiles of the gels to prepare final ceramic powders. X-ray analysis and Scanning Electron Microscopy (SEM) were performed to identify crystalline phases and examine the microstructure, respectively.

QA/QC PROCEDURES

The equipment used for characterization in this research was calibrated as per manufacturer specifications to ensure reliable results. Standard samples were used, for example, to calibrate the rheology experiments and conform to QA/QC protocols and standards. All compounds used for synthesis were reagent certified and stored in parafilm sealed bottles.

ACCOMPLISHMENTS

Technical Results and Discussion

Tables 14.1 and 14.2 show the synthetic condition used to prepare the mullite precursors and the gelation conditions, respectively. From Table 14.2 it is observed that the variation in temperature had the greatest effect on the time to gelation. For the sols aged at 65°C, the time to gelation was shorter when compared to sols aged at 40°C. In addition, the increased molar water to TEOS ratio decreased the time required for gelation. Figure 14.1 shows a plot of the molar water to TEOS ratio versus gelation time for the aging temperatures used.

Figure 14.2 shows the rheological properties of a typical sol during the aging process, indicating increasing viscosity with aging time, which is consistent with the changing structure as shown by the FTIR plot in Figure 14.3. The condensation reactions are seen to increase as a function of aging as observed by the decreasing presence of the C-O bond at 2200 - 2300 cm^{-1} . Attempts to identify Si-O-Al bridging were not successful since the Si-O and Al-O bonds occur at about the same wavenumber (800-900 cm^{-1}). The viscoelastic properties measured during the sol-gel transition for a typical sample agreed with the FTIR characterization. The increasing elastic component or storage modulus (G') compared to the viscous component or loss modulus (G'') as a function of aging were consistent with the FTIR plots. In the early portion of the aging process the loss modulus was more dominant than the storage modulus. Thermal analysis (TG/DTA) to monitor the conversion of the mullite precursor gel to the mullite ceramic was conducted where it was observed that mullitization occurred at 980°C which was confirmed by x-ray analysis which showed fully crystalline mullite at 1100°C with fine grain size determined from SEM. The material yields as observed from the TGA plot are very low, approximately 50% by mass from the precursor gel. This is due to the nature of the sol-gel process where the yield is dictated by the starting materials - ATSB and TEOS. This low materials yield is one of the drawbacks of the sol-gel process. However, the ability to control the formation of mullite at the molecular level using sol-gel processing allows for better control in the properties of the final mullite when compared to powder processing techniques. The mullite powders prepared from the sol-gel approach can be used for matrices, since at this point there would be no materials shrinkage. The limitation from the sol-gel approach would be in trying to do near net shape sintering of the precursor gel. In the present research the focus was on the former not the latter. The low materials yield observed from the TGA plot is due to the solvents that the reagents are dissolved in and the requisite chemistry of the sol-gel process coupled to the sintering requirements to form mullite. The composition used in the starting materials is set to prepare stoichiometric mullite and is confirmed in the final mullite by both DTA and X-ray analysis.

EDUCATION AND TRAINING

The following students were involved in the mullite based ceramics projects:

Name	Classification	Status
Omoyele Oluwa	M.S. Chemistry	Graduated May 1996
Shari Ernest	B.S./M.S. Chemistry	Graduate Student
Arun Kori	B.S. Chemistry	Graduated August 1995

Name	Classification	Status
Suzette Nubie	B.S. Chemistry	Graduated May 1996
Keisha Sopher	B.S. Chemistry	Graduated May 1996

Gel #	Amount of various chemicals used					Temp (°C)	TEOS/water(r)	Gel time days	Appearance (physical)
	TEOS(ml)	2Propanol(ml)	HCl(v)	H ₂ O(ml)	Altrsx(ml)				
1-1	5ml	17	3	0.6	25	40	1.5	*	viscous with solvent
1-2	5ml	17	3	0.6	25	65	1.5	*	Thick/clear
1-3	5ml	17	2	0.6	25	40	1.5	*	Solution
1-4	5ml	17	2	0.6	25	65	1.5	10	clear, transparent
1-5	5ml	17	1	0.6	25	40	1.5	26	clear, transparent
2-1	5ml	17	3	0.8	25	40	2	21	clear, transparent
2-2	5ml	17	3	0.8	25	65	2	24	clear, transparent
2-3	5ml	17	1	0.8	25	40	2	45	clear, transparent
2-4	5ml	17	1	0.8	25	65	2	11	clear, transparent
3-1	5ml	17	3	1.2	25	40	3	35	clear, transparent
3-2	5ml	17	3	1.2	25	65	3	8	clear, transparent
3-3	5ml	17	2	1.2	25	40	3	13	still solvent
3-4	5ml	17	2	1.2	25	65	3	10	clear, transparent
3-5	5ml	17	1	1.2	25	40	3	21	clear, transparent
3-6	5ml	17	1	1.2	25	65	3	9	clear, transparent

* represents 32days, *13 represents 45days, Altrsx Repls. (C₂H₅CH(CH₃)O)₃Al (80%v/v)

Table 14.1 Effect of Synthesis Conditions on Gelation Time.

Table 14.2 Effect of Reaction Conditions on Gelation Time.

Gel #	Temperature °C	Gellation time
1-2	65	*
1-4	65	10 days
2-2	65	24 days
2-4	65	11 days
3-2	65	8 days
3-4	65	10 days
3-6	65	9 days

Gel #	Temperature °C	Gellation time
1-1	40	*
1-3	40	*
1-5	40	32 days
2-1	40	36 days
2-3	40	45 days
3-1	40	35 days
3-3	40	* ¹³
3-5	40	21

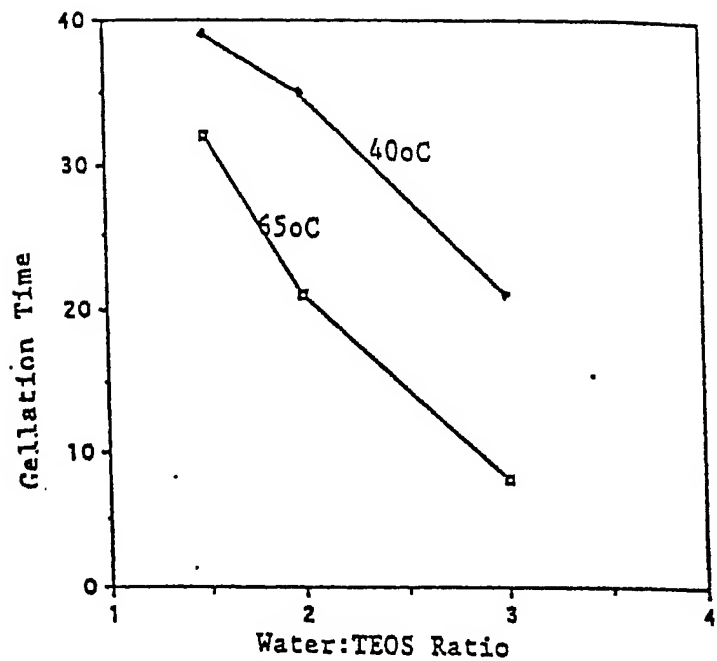


Figure 14.1 Effect of Molar Water to TEOS Ratio on Gelation Time for 40 and 65°C.

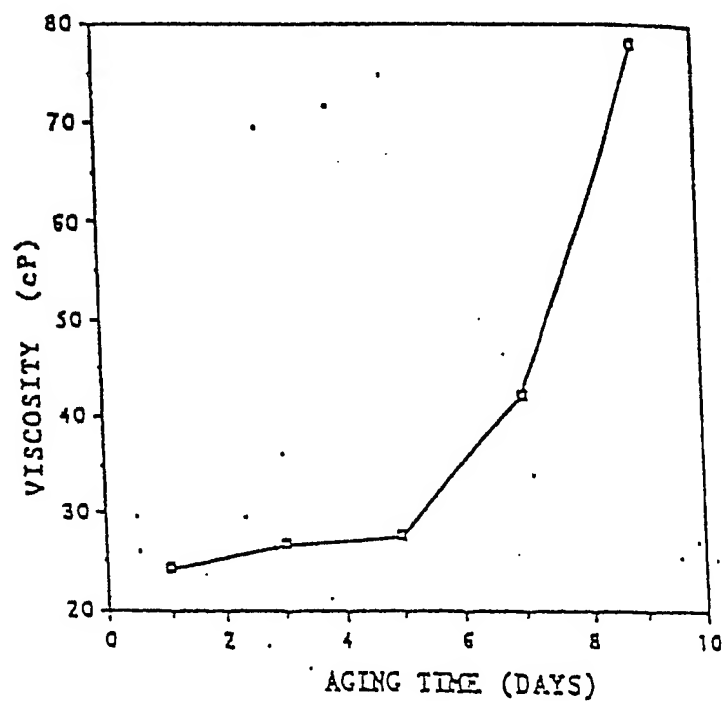


Figure 14.2 Viscosity as a Function of Aging for Precursor Sol Sample 2-1.

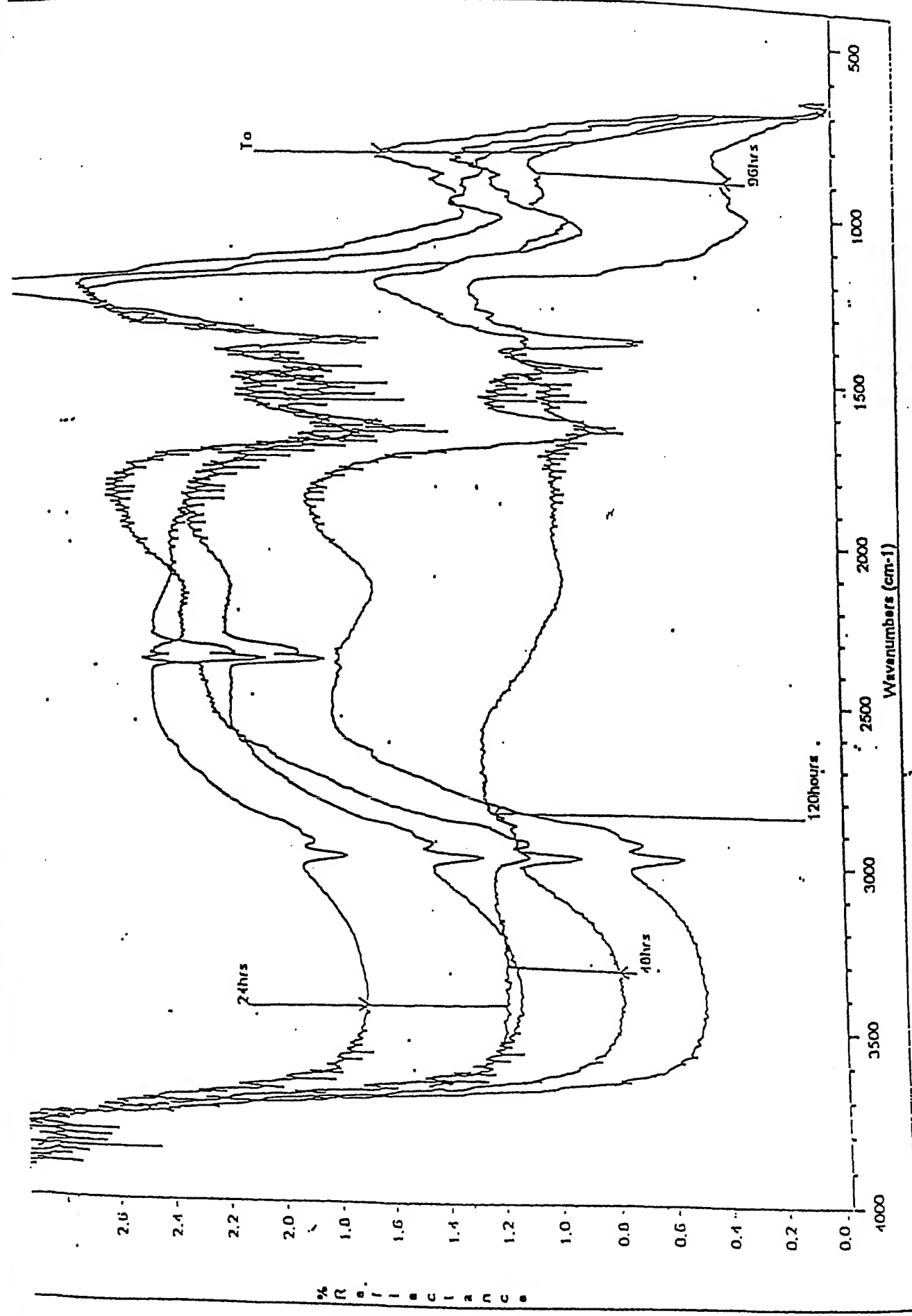


Figure 14.3. FTIR of Mullite Precursor During Aging.

OUTREACH AND TECHNOLOGY TRANSFER

Existing collaborations involve technology transfer with NASA-Lewis. The interaction with NASA-Lewis is on preparing oxide/oxide mullite ceramic composites using the mullite powders synthesized in our laboratory as matrix materials. Following the completion of hot pressing composite samples they will be sent to Drs. Serene Farmer and Ali Sayir at NASA-Lewis for interfacial characterization and high temperature mechanical testing.

PUBLICATIONS AND PRESENTATIONS

1. "Mullite-Based Ceramics Formed by the Sol-Gel Inorganic Polymer Precursor Route", L. Moeti, E. Karikari, and O.Oluwa, *Polymer Preprints*, accepted.
2. "FTIR and Rheological Characterization of Sol-Gel Based Mullite Ceramics", L. Moeti, E. Karikari, and O.Oluwa, *Journal of the American Ceramic Society*, submitted.
1. "Rheological and Microstructural Characterization of Sol-Gel Based Mullite", L. Moeti, E. Karikari, O. Oluwa, 47th Southeast/51st Southwest Joint Regional Meeting of the American Chemical Society, Nov 29, Dec 1, 1995 Memphis, TN.
2. "²⁹Si NMR Characterization of the Sol-Gel Transition in Mullite Precursors", L. Moeti, Y. Pang, E. Karikari, S. Earnest, K. Sopher, 47th Southeast/51st Southwest Joint Regional Meeting of the American Chemical Society, Nov 29, Dec 1, 1995 Memphis, TN.
3. "Oxide/Oxide Mullite Composites Derived from Sol-Gel Processing" L. Moeti, E. Karikari, S. Earnest, 47th Southeast/51st Southwest Joint Regional Meeting of the American Chemical Society, Nov 29, Dec 1, 1995 Memphis, TN.
4. "Chemically Derived Zirconia Toughened Alumina via Sol-Gel Processing" L. Moeti, E. Karikari, J. Chen, S. Nubie, 47th Southeast/51st Southwest Joint Regional Meeting of the American Chemical Society, Nov 29, Dec 1, 1995 Memphis, TN.

REFERENCES

J.C. Romine, *Ceram. Eng. Sci. Proc.*, **8** [7-8], 755 (1987).

J.C. Pouxviel and J.P. Boilot, *J. of Non-Cryst. Solids*, **89**, 345 (1987).

D.D. Johnson, A.R. Holtz, and M.F. Grether, *Ceram. Eng. Sci. Proc.*, **8** [7-8], 744 (1987).

I.A. Aksay, D.M. Dabbs, and M. Sarikaya, *J. Am. Ceram. Soc.*, **74**, 2343 (1991).

M.D. Sacks, H.W. Lee, and J.A. Pask, in *Ceramic Transactions*, vol 6, Mullite and Mullite Matrix Composites, edited by S. Somiya, R.F. Davis, and J.A. Pask (American Ceramic Society, Westerville, 1990), p. 167

B.E. Yoldas and D.B. Partlow, *J. Mat. Sci.*, **23**, 1895 (1988).

P. Colombar, *J. Mat. Sci.*, **24**, 3002 (1989).

T. Heinrich, F. Raether and H. Marsmann, *J. of Non-Crystalline Solids*, **168**, 14 (1994).

M.D. Sacks and J. A. Pask, *J. Am. Ceram. Soc.*, **65**, 70 (1982).

M.G.M.U. Ismael, Z. Nakai, and S. Somiya, *J. Am. Ceram. Soc.*, **70**, C-7 (1987).

2.15 ZIRCONIA-TOUGHENED ALUMINA CERAMICS

Investigators: L. Moeti and E. Karikari

INTRODUCTION

There is currently a great interest in the development of new materials for advanced structural applications, for example engine components in high technology aerospace applications. These new materials should have improved properties such as strength, toughness, and wear resistance. Ceramic oxide composites are increasingly becoming desirable as materials for these applications. Tetragonal zirconia (ZrO_2) - toughened alumina (Al_2O_3) has become an area of increased technical interest in recent years, Classen (1976), Claussen et al., (1977), Becher (1981). By the introduction of dispersed ZrO_2 into an alumina matrix the resulting zirconia-toughened alumina (ZTA) has demonstrated improved toughness and strength when compared to pure alumina, Kamiya (1990). The stress induced tetragonal-to-monoclinic ($t \rightarrow m$) phase transformation and the stress induced microcracking, Evans et al., (1986), McMeeking et al., (1982), Evans et al., (1986) are the principal toughening mechanisms in ZTA ceramics. Factors such as particle size, particle size distribution, and the nature of the polymorph contribute to the toughening mechanisms and strength enhancement. These factors can be modified by the processing techniques used in the fabrication of ZTA ceramics.

The sliding wear resistance of ZTA ceramics, Kamiya et al., (1990) have shown improved properties when compared to Al_2O_3 or tetragonal ZrO_2 ceramics. An extensive amount of research has been conducted on the solid particle erosion wear of brittle materials such as Al_2O_3 , silicon carbide/silicon nitride (SiC/Si_3N_4) composites, tetragonal zirconia, and whisker-reinforced composites, Lange et.al., (1979), Wada et al., (1988). However, the erosion wear resistance of ZTA has only recently been investigated in a systematic fashion.

OBJECTIVES

Most of the research conducted in the development of ZTA ceramics has been either by colloidal/powder processing or by partial chemical routes. The disadvantages of these methods include the impurities in the starting materials and the difficulty in achieving good uniform distribution of the zirconia dispersed in the alumina matrix. In the present research a chemically based approach using high purity starting materials consisting of zirconium and aluminum metal alkoxides were used to control the precursor chemistry and particle sizes and also achieve improved uniform distributions of ZrO_2 dispersed in the Al_2O_3 matrix. By carefully controlling the precursor chemistry high purity ZTA ceramics with smaller grain sizes were prepared which should improve the toughness and wear erosion properties of ZTA ceramics.

APPROACH

High purity starting materials were used to synthesize ZTA ceramics with 7, 15, and 22 volume percent of zirconia. Aluminum tri-sec butoxide (ATSB), zirconium propoxide, and yttrium isopropoxide were the reagents used. Triethanolamine (TEA) was also used to stabilize the ATSB by the formation of chelating complexes between the ATSB and the TEA which reduced the reactivity of ATSB to water. The solvent used for all experiments done was sec-butanol (2-butanol). Precursor sols both with and without yttria to stabilize the zirconia were prepared. Hydrolysis conditions were established such that sols could be gelled in several hours or days depending on water content and amount of TEA used. Table 15.1 shows the synthetic conditions used to prepare the ZTA precursors. Figure 15.1 shows the synthesis process used to prepare the ZTA ceramic precursors. FTIR spectroscopy was used to follow the structural evolutions in the precursor sol to gel transition. Rheological properties of the precursor sols and gels were also monitored and correlated to the synthesis conditions. ZTA precursor gels obtained were heated to temperatures up to 1300°C and the crystallinity and microstructure of the final ceramics were examined by X-ray analysis and Scanning Electron Microscopy (SEM), respectively.

QA/QC PROCEDURES

The equipment used for characterization in this research was calibrated as per manufacturer specifications to ensure reliable results. Standard samples were used, for example, to calibrate the rheology experiments and conform to QA/QC protocols and standards. All compounds used for synthesis were reagent certified and stored in parafilm sealed bottles.

Table 15.1 Effect of Synthesis Conditions on Gelation Time

Sample	ATSB (mol 10 ⁻³)	ZRP (mol 10 ⁻¹)	YIP (mol 10 ¹)	sec-butanol (mol 10 ¹)	H ₂ O/Total Alkoxide (ml)	TEA/Total Alkoxide (molar ratio)	ZrO ₂ (volume percent)	Gel Time (hours)
1	4.75	2.231	0	30	2	0.302	7	8
2	6.09	2.856	0	40	2	0.321	7	24
3	6.09	2.856	0	40	2	0.332	7	48
4	6.09	6.693	0	40	2	0.333	15	10
5	6.09	6.693	0	40	2	0.344	15	24
6	3.81	6.827	0	30	2	0.284	22	1
7	3.81	6.827	0	30	2	0.301	22	6
8	3.81	6.827	0.804	30	2	0.328	22	10
9	3.81	6.827	0.804	30	2	0.345	22	40
10	6.09	6.693	0	40	4.5	0.388	15	192
11	4.75	2.231	0	30	4.5	0.347	7	0.5

ATSB Aluminum tri-sec butoxide
 ZRP Zirconium propoxide
 YIP Yttrium isopropoxide
 TEA Triethanolamine

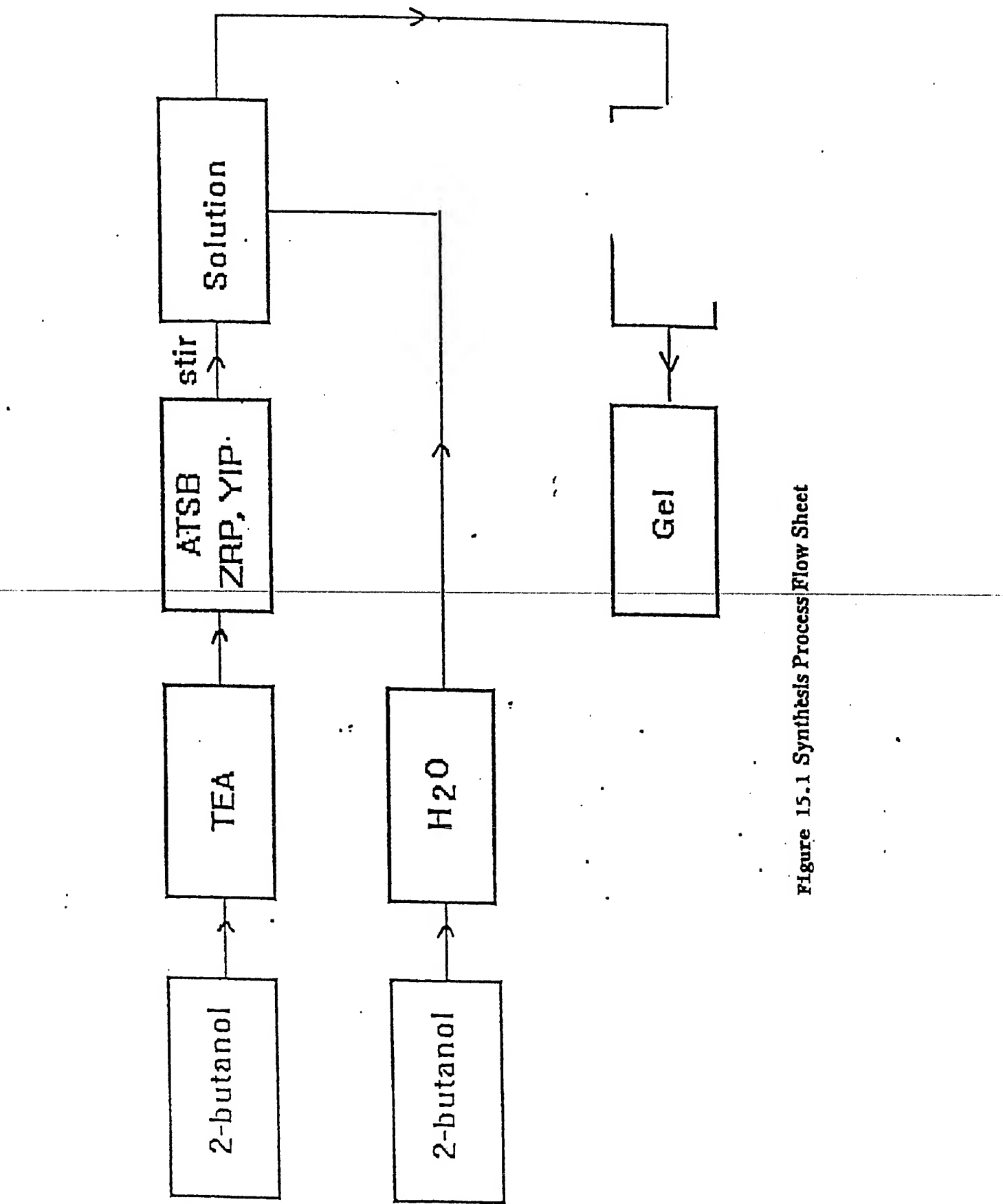


Figure 15.1 Synthesis Process Flow Sheet

ACCOMPLISHMENTS

Technical Results and Discussion

Figures 15.2 and 15.3 show the FTIR spectra of a ZTA (with 22 volume percent zirconia) precursor sol and gel, respectively, both with yttria (6 mol percent to zirconia) precursor after 2 hours of aging. The greater extent of hydrolysis of the gel in comparison to the sol is observed by the larger peak at 3100 cm^{-1} wave numbers. This is consistent with the further extent of reactions and the build-up of structure in the gels as compared to the sols. The rheological properties of the sol to gel transition were followed using both steady shear and dynamic viscosity. From steady shear experiments it was observed that the sols in the initial stages show slightly shear thinning behavior. As the gelation point is approached the sols begin to exhibit a slight yield stress and shear thinning with a hysteresis loop which indicates the break down of structure as the shear rate is increased. Figure 15.4 shows a plot of viscosity versus shear rate for a ZTA precursor sol with 22 volume percent zirconia and 6 mol percent yttria to zirconia. From dynamic viscosity measurements the sols show a small elastic component during the early stages of aging. Aged viscous sols and the gels are observed to have a larger elastic component which is again consistent with the build up of structure. The rheological data is in agreement with the observations of structural change as observed from FTIR characterization of the aging sols and gels. Heat treatment was conducted to prepare ZTA powders. A weight loss of 50% from the gel to the final ZTA ceramic was observed. The microstructure of the ZTA powders was examined using SEM and the crystalline phases were examined using x-ray analysis. Small grain size, fully crystalline high purity ZTA ceramics were produced. From x-ray phase analysis α alumina and tetragonal zirconia were the phases identified, indicating that tetragonal zirconia is retained even without the presence of yttria.

EDUCATION AND TRAINING

The following students were involved in the ZTA ceramics projects:

Name	Classification	Status
Jun-Li Chen	M.S. Chemistry	Graduated August 1996
Suzette Nubie	B.S. Chemistry	Graduated May 1996

OUTREACH AND TECHNOLOGY TRANSFER

As part of the technology transfer with NASA-Dryden the synthesis of zirconia toughened alumina powders has been completed. Two (2) research papers have resulted from this effort. We are now beginning to prepare for mechanical testing at NASA-Dryden in conjunction with the hot pressing being done at Georgia Tech to determine mechanical properties for inclusion in material property codes. The point of contact at NASA-Dryden is Dr. Kajal Gupta.

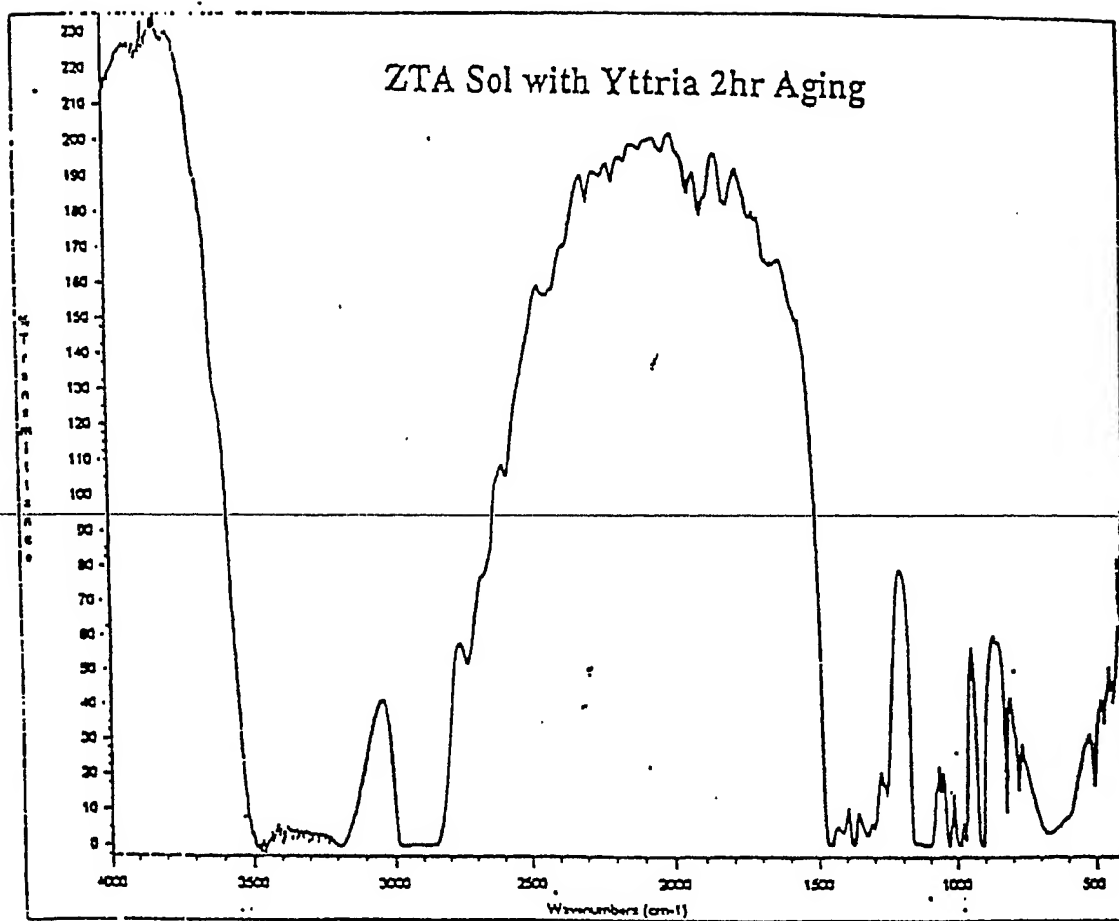


Figure 15.2 FTIR Spectra of ZTA Precursor Sol

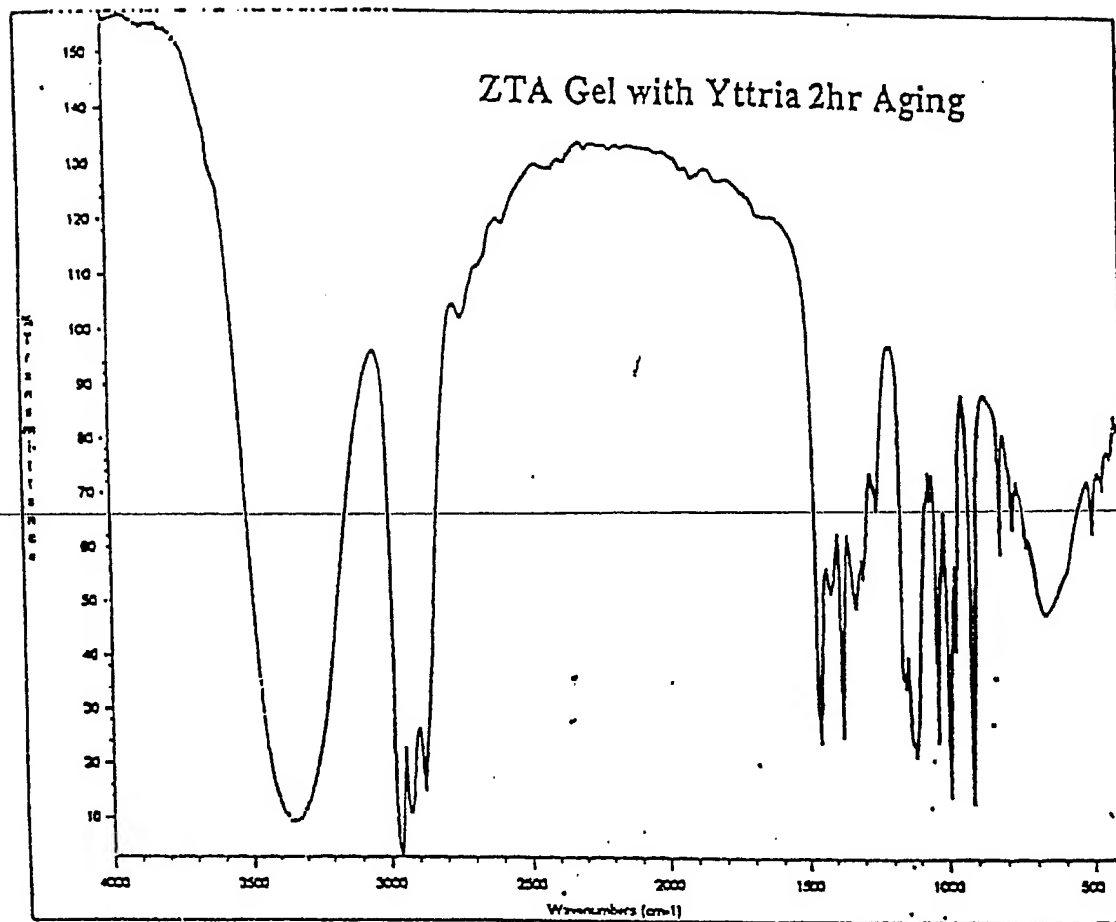
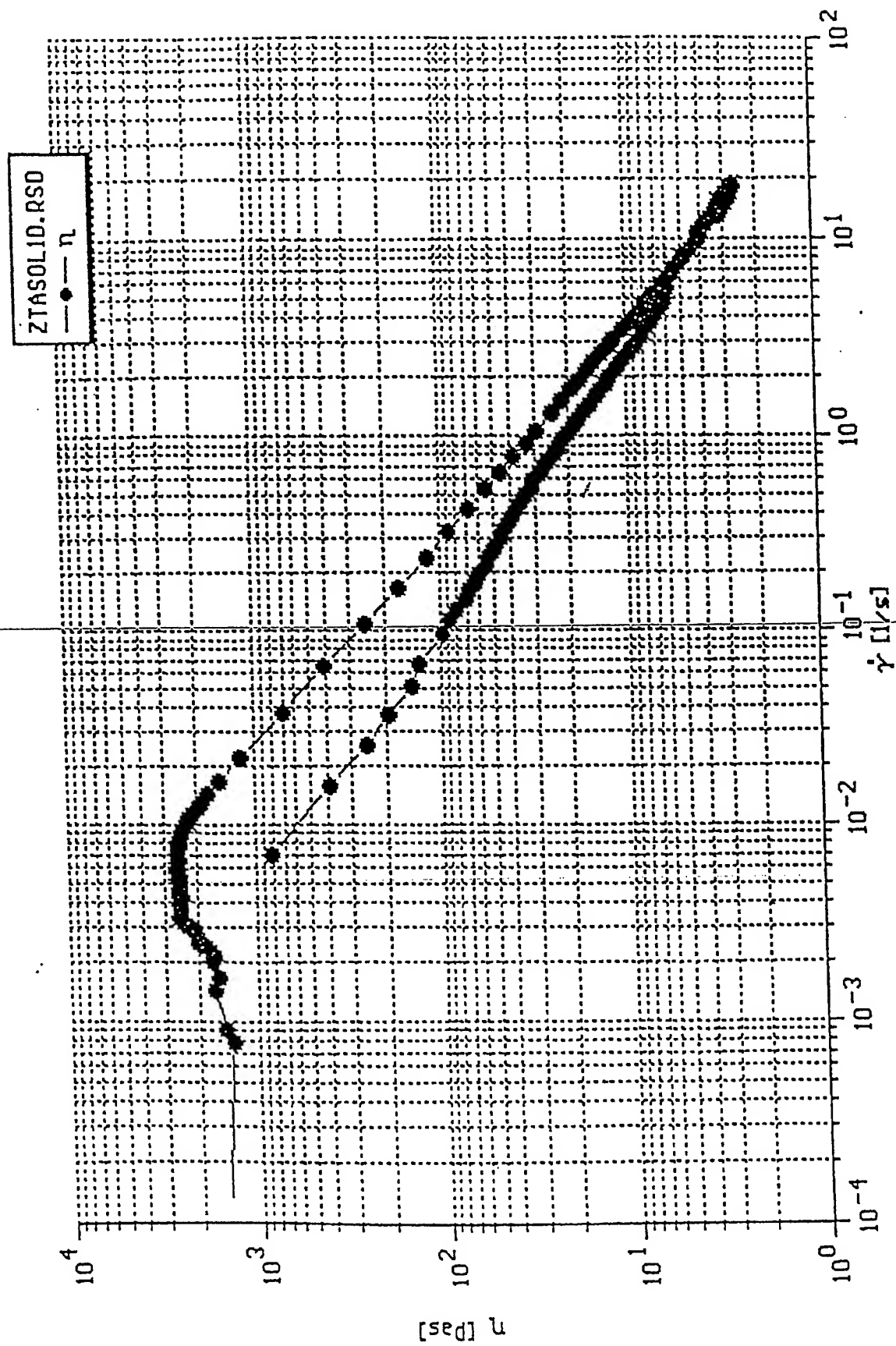


Figure 15.3 FTIR Spectra of ZTA Precursor Gel



PUBLICATIONS AND PRESENTATIONS

1. "Inorganic Sol-Gel Polymer Precursor Routes for the Formation of Zirconia Toughened Alumina Ceramics", L. Moeti, E. Karikari, and J. Chen, *Polymer Preprints*, accepted.
2. "Characterization of the Sol-Gel Transition for Zirconia-Toughened Alumina Precursors", L. Moeti, E. Karikari, and J. Chen, *Journal of Materials Research*, submitted.
3. "Chemically Derived Zirconia Toughened Alumina via Sol-Gel Processing" L. Moeti, E. Karikari, J. Chen, S. Nubie, 47th Southeast/51st Southwest Joint Regional Meeting of the American Chemical Society, Nov 29, Dec 1, 1995 Memphis, TN.

REFERENCES

N. Claussen, *J. Am. Ceram. Soc.*, 59 [1-2] 49-51 (1976).

N. Claussen, J. Steeb, and R.F. Pabst, *Am Cer. Soc. Bull.*, 56 [6] 559-62 (1977).

P.F. Becher, *J. Am. Ceram. Soc.*, 64 [1] 37-39 (1981).

H. Kamiya, M. Takatsu, and A. Hattori., *J. Ceram. Jpn.* 98 [5] 456-63 (1990).

A.G. Evans and K.T. Faber, *J. Am. Ceram. Soc.*, 64 [7] 394-98 (1981).

R. McMeeking and A.G. Evans, , *J. Am. Ceram. Soc.*,65 [5] 242-46 (1982).

A.G. Evans and R. M. Cannon, *Acta. Mettal.*, 34 [5] 761-800 (1986).

H. Kamiya and M. Takatsu, *J. Ceram. Soc. Jpn.* 98 [1]13-21 (1990).

F.F. Lange and A.G. Evans, , *J. Am. Ceram. Soc.*, 62 [1-2] 62-65 (1979).

S. Wada and N. Watanabe, *J. Ceram. Soc. Jpn.* 96 [5] 599-602 (1988).

2.16 MECHANICAL AND PHYSICAL TESTING OF A POLARIZATION-MAINTAINING OPTICAL FIBER

Investigators: L. Moeti and S. Moghazy

INTRODUCTION

Polarization-maintaining (PM) optical fibers are increasingly being considered for new applications in, for example, advanced spacecraft inertial reference units as fiberoptic rotation sensors. In such applications the PM fiber would be wound on a spool under some state of mechanical stress combining both a winding tension and a bending stress. The wound spool could be expected to generate additional thermally induced stresses from thermal expansion and contraction effects during service where it could be expected to experience extremes of temperature ranging from -50°C to $+85^{\circ}\text{C}$. Other applications where volume is a consideration have also used PM fibers wound onto small spools, Perlmutter (1993).

These new PM fibers, often referred to as PANDA fibers, are significantly different from commercial optical fibers in two major ways. First, commercial optical fibers generally consist of a wave guide surrounded by an acrylic jacket. In the PANDA fiber, there exists a silicone layer between the wave guide and the jacket. Secondly, the PANDA fiber contains two beryllium oxide stress rods around the wave guide core that produces a stressed wave guide core specific for polarized light. Technical literature exists on the physical and mechanical properties of commercial optical fibers which can be used for engineering design. Development of theories to predict fiber lifetime for commercial optical fibers using fiber parameters have been established, Kapron et al., (1991). Literature reports on the temperature-dependent behavior of highly birefringent optical fibers are available, Ramaswamy et al., (1979), Ourmazd et al., (1983), Rashleigh et al., (1983), Barlow (1985). For the case of PANDA fibers the temperature dependence of fibers wound onto different diameter cylinders has been measured, Ruffin et al., (1995). However, no open literature exists on the physical and mechanical properties of PANDA fibers, which is herein reported.

OBJECTIVES

The objectives for this project was to determine mechanical and physical properties of polarization-maintaining optical fibers that can be used for design applications. In this research, a commercial single-mode optical fiber was used as a control to establish and validate test criteria which the PANDA fiber was subjected to.

APPROACH

The modulus of PANDA fibers was determined by three techniques. In the first, the engineering modulus was obtained from mechanical testing using an Instron Model 4505. In the second technique, sonic modulus was measured using a Morgan Instruments Model PPM-5R Dynamic Modulus Tester, which is a nondestructive test technique. The third technique used involved static loading to generate stress-strain curves from incrementally increased loads on suspended fiber samples. A commercial single mode optical fiber, Corning SMF-28, was used as a control to establish the testing protocols. In addition, the modulus of stripped PANDA and control fibers was measured. The acrylic jackets of the fibers were removed using sulfuric acid at 90°C. For the PANDA fiber a hexane rinse was used to remove the silicone layer following the removal of the acrylic jacket. For consistency the hexane rinse was also used to clean the surface of the stripped control fiber. The relative cross-sectional areas of both the control and PANDA fibers are 1/4 for the glass wave guide and 3/4 for the plastic jackets.

The coefficient of thermal expansion (CTE) for both the PANDA and control fibers was measured using a Perkin-Elmer Series 7 Thermal Analysis System. The CTE was measured over a range of 25 to 100°C. X-ray analysis of the PANDA fiber was conducted using a Rigaku X-ray Diffractometer to determine if any change in the amorphous/crystalline content occurred due to stress induced crystallization during loading.

QA/QC PROCEDURES

The equipment used for characterization in this research was calibrated as per manufacturer specifications to ensure reliable results. Standard samples were used, for example, to calibrate the sonic modulus tester and conform to QA/QC protocols and standards.

ACCOMPLISHMENTS

Technical Results and Discussion

Modulus Measurements. Figure 16.1 shows a comparative plot of stress versus strain of the intact PANDA and control fiber with jackets. The stress-strain curves do not intersect the origins of the strain and stress axes due to the fact that both the PANDA and control optical fibers have a curvature from being wound on a spool. This caused the inability to reach a true zero on the Instron during the testing (zero load and zero slack).

The modulus of the control fiber without jacket was found to be 8.49×10^6 Psi, which is close to the published value for fused quartz (10.4×10^6 Psi), the material used for the control fiber wave guide. From mechanical testing, it is observed that the modulus for the whole control fiber with jacket is 2.10×10^6 Psi, or 8.4×10^6 Psi when stress is calculated from measured load using the glass wave guide's cross-sectional area (a 4/1 ratio). Comparing with the measured

modulus of 7.10×10^6 Psi for the wave guide alone reveals that the acrylic jacket has a minor contribution to the modulus.

The load that the PANDA fiber could be subjected to was limited because of slipping during testing due to the silicone layer. Slippage began at a strain level of about 0.015 %. Above this strain, the grips used would tear through the acrylic jacket thus exposing the silicone layer. From the initial portion of the stress-strain curve before slipping occurred, the modulus of the PANDA fiber was found to be 6.10×10^6 Psi based on total fiber area, or 6.40×10^6 Psi based on the cross-sectional area of the glass wave guide only.

Figure 16.2 is a comparison stress-strain plot of the stripped PANDA fiber and the stripped control fiber. The removal of the jacket was done in an attempt to prevent the slippage occurring in testing the PANDA fiber due to the silicone layer. However, both stripped PANDA and control fibers were very brittle and broke at very low loads. The modulus determined from the initial portion of the stress-strain curves are shown in Table 16.1 and compared to modulus values of the fibers with acrylic jackets.

Sonic modulus was used as a nondestructive technique to determine the modulus of both the PANDA and the control fiber. Table 16.2 shows the sonic modulus values obtained for both fibers with and without jackets. The sonic modulus measurements were made at low loads below the slippage threshold. Two methods were used to calculate the sonic modulus, the first being the most frequent velocity of sound waves traveling through the sample and the second being the average velocity of the sound waves traveling through the sample. No significant difference between the methods was observed in the values of the sonic modulus obtained.

A static loading technique was also used to measure the modulus of both the PANDA and control fiber. In this method the elongation of the fiber for incremental increases in load was monitored and a stress-strain curve was generated from which the modulus was determined. Figure 16.3 shows the stress-strain plots of both the PANDA and control fibers. Table 3 shows the modulus values of both fibers determined from the static loading technique.

From an analysis of both the engineering and sonic modulus of the control fiber (Tables 16.1 and 16.2), the acrylic jacket had some detectable influence on the composite modulus. In the case of the PANDA fiber, the acrylic/silicone jacket had no apparent influence on the composite modulus, being that primarily of the glass wave guide with or without jacket. The stripped fibers were very brittle and broke at low loads. The moduli in these cases were calculated from the initial portion of the stress-strain curve. It should be noted that in the PANDA fiber the glass core and the acrylic jacket are physically decoupled by the silicone layer. The values of modulus for both PANDA and control fibers with jacket are in good agreement with those obtained by mechanical and sonic techniques.

When comparing the sonic modulus to the engineering modulus good agreement is observed. This result is important for research or engineering studies desiring to measure the engineering modulus of optical fibers without destroying the test samples.

TABLE 16.1
Engineering Modulus of PANDA and Control Fibers

	Modulus (Psi)		
	with jacket (glass area)	with jacket (whole fiber area)	without jacket (glass area)
PANDA	6.52×10^6	1.60×10^6	6.50×10^6
Control	8.49×10^6	2.10×10^6	7.14×10^6

TABLE 16.2
Sonic Modulus of PANDA and Control Fibers

	Sonic Modulus (Psi)		
	with jacket (glass area)	with jacket (whole fiber area)	without jacket (glass area)
PANDA	7.80×10^6	1.86×10^6	7.80×10^6
Control	8.80×10^6	2.24×10^6	8.30×10^6

TABLE 16.3
Static Loading Modulus of PANDA and Control Fibers
(Psi)

	with jacket (whole fiber area)
PANDA	2.17×10^6
Control	2.87×10^6

FIGURE 16.1

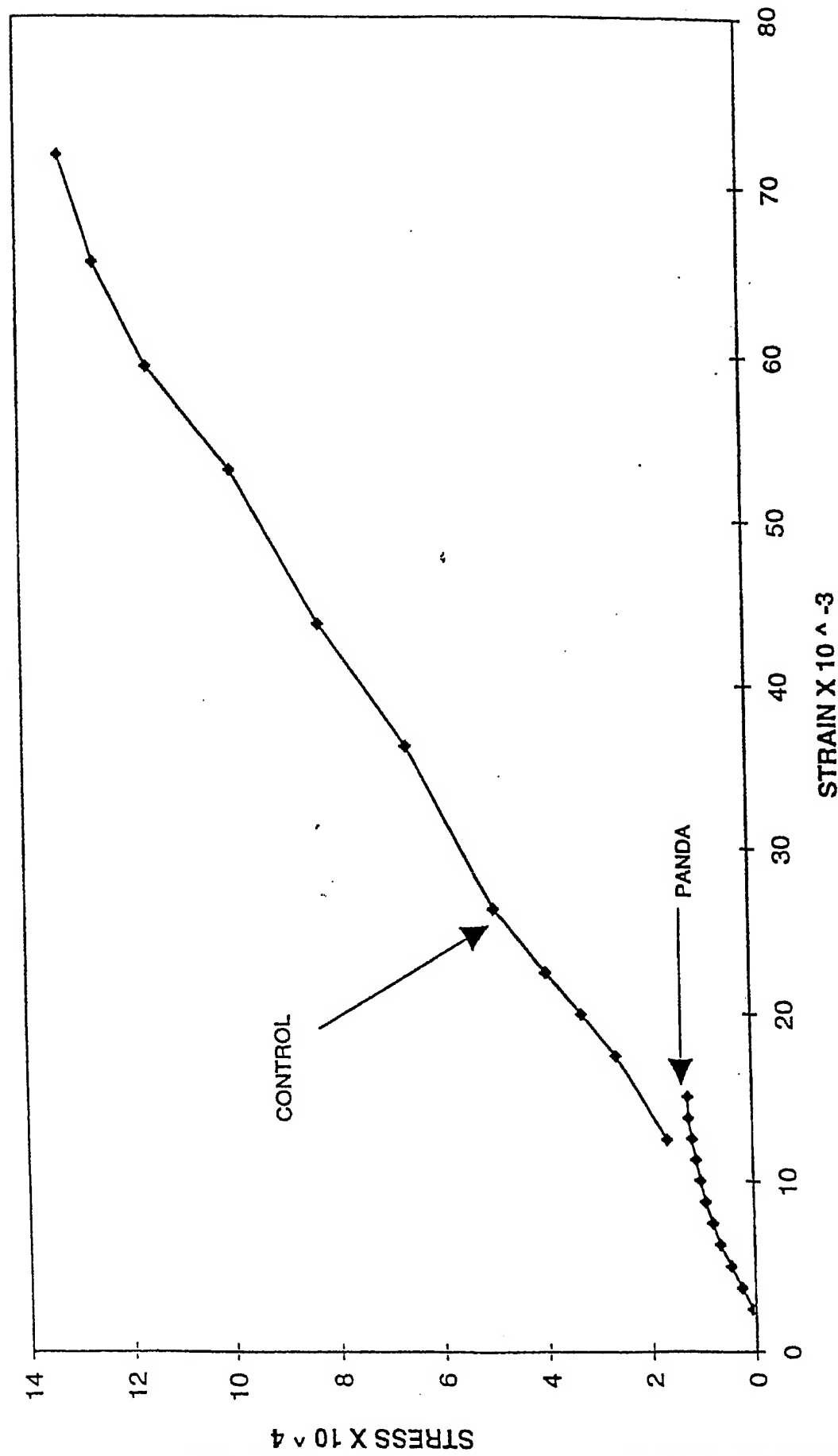


FIGURE 16.2

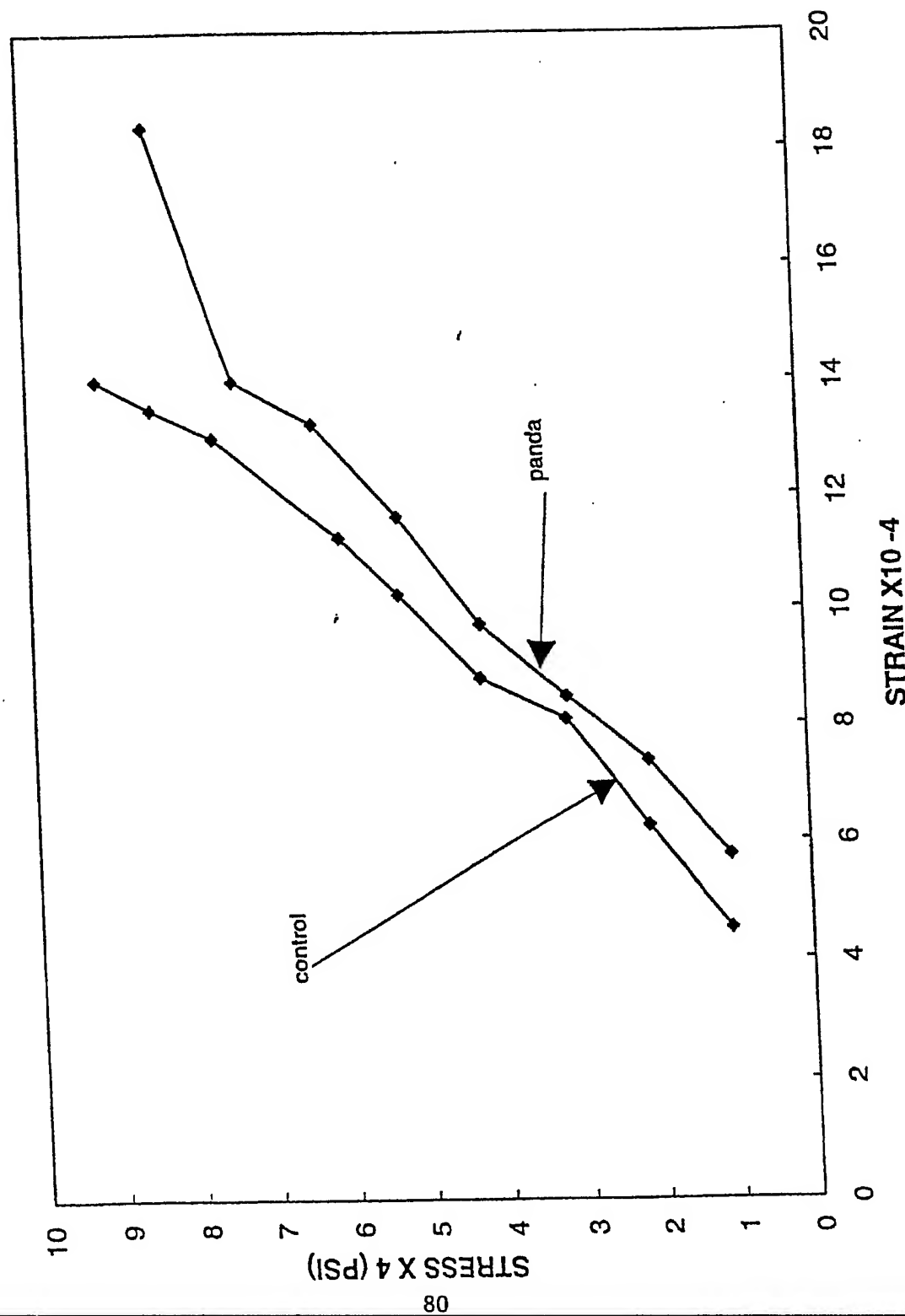
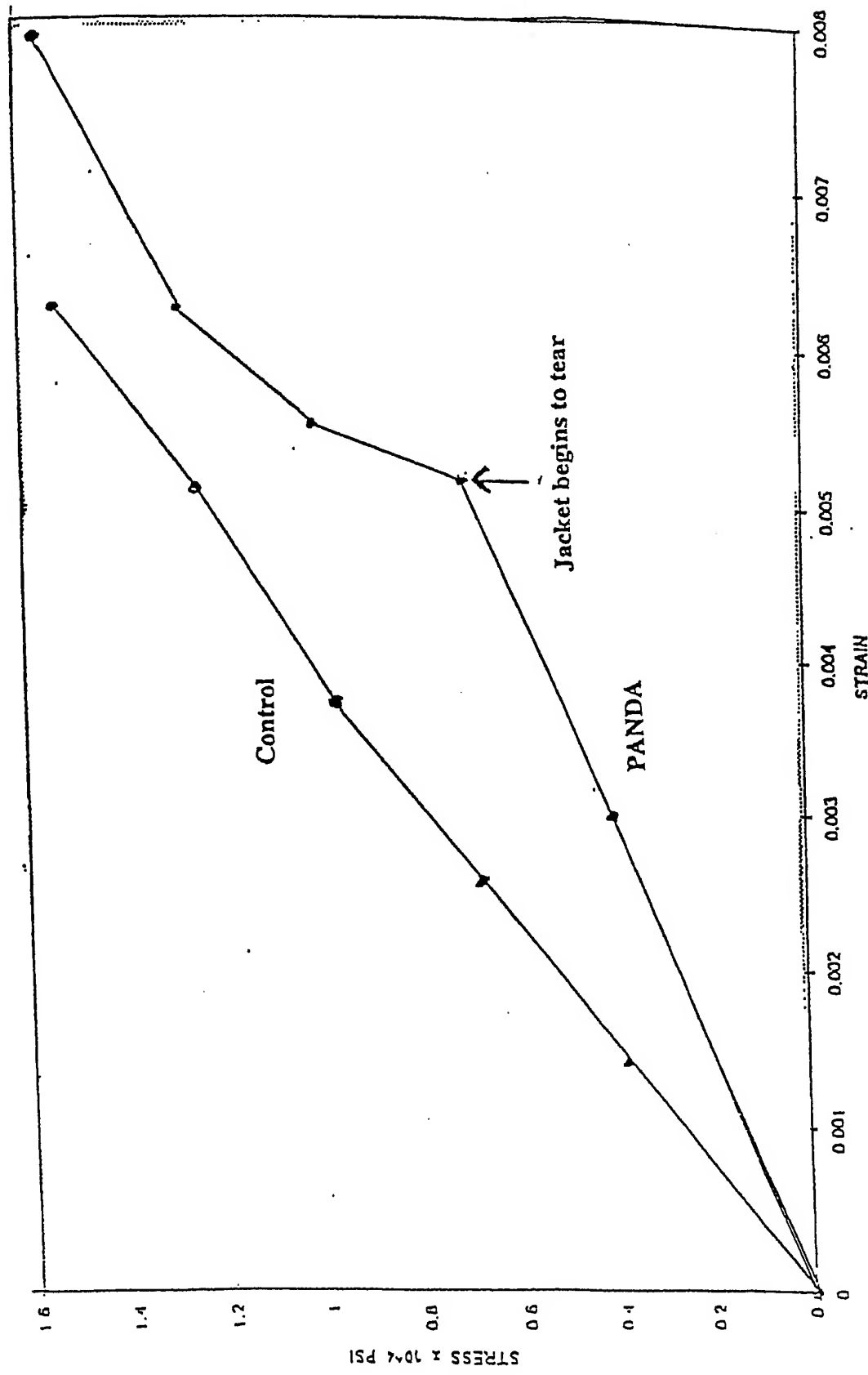


FIGURE 16.3

STATIC LOADING FOR PANDA AND CONTROL WITH JACKET



EDUCATION AND TRAINING

The following students were involved in the optical fiber project:

Name	Classification	Status
Samesha Barnes	B.S./B.S. Chem/Chem.Eng	Graduated October 1996
Al-Amin Ally	B.S./B.S. Physics/Civil Eng	Graduated May 1996
Kariema Smith	B.S./B.S. Chem/Chem.Eng	Graduate Student
Lanier Watkins	B.S./M.S. Physics	Graduate Student

OUTREACH AND TECHNOLOGY TRANSFER

The collaboration with NASA-JPL on optical fiber research has resulted in two (2) submitted papers and two (2) papers in preparation for submission in June 1996. The contact at NASA-JPL is Edward Cuddihy who is also a co-author on all the papers. Based on the expertise we have developed in testing optical fibers nondestructively, we have submitted a proposal to NASA-JPL to test Long Duration Exposure Flight (LDEF) optical fibers.

PUBLICATIONS AND PRESENTATIONS

1. "Mechanical and Physical Testing of a Polarization-Maintaining Optical Fiber", L. Moeti, S. Moghazy, A. Ally, S. Barnes, A. Abhiraman, P. Desai, and E. Cuddihy, Journal of Lightwave Technology, submitted.
2. "Long Term Reliability Prediction of Polarization-Maintaining Optical Fibers", L. Moeti, S. Moghazy, A. Ally, S. Barnes, and E. Cuddihy, Optical Engineering, submitted.
3. "Constitutive Modeling of the Mechanical Properties of Optical Fibers", L. Moeti, S. Moghazy, D. Veazie, and E. Cuddihy, Optical Engineering, submitted.

REFERENCES

M.S. Perlmutter, "A tactical fiber optic gyro with all-digital signal processing," Proc. 16th Biennial Guidance Test Symposium, AFDTC-TR-93-06, pp. 337-350, 46th Guidance Test Squadron/CC (AFMC), Holloman AFB, NM (1993).

F.P. Kapron and H.H. Yuce, "Theory and measurement for predicting stressed fiber lifetime," Optical Engineering 30(6), pp. 700-708 (1991).

V. Ramaswamy, R.H. Stolen, M.D. Divino, and W. Pleibel, "Birefringence in elliptically clad borosilicate single-mode fibers," Appl. Opt., vol. 18, pp. 4080-4084 (1979).

A. Ourmazd, M.P. Varnham, R.D. Birch, and D.N. Payne, "Thermal properties of highly birefringent optical fibers and preforms," *Appl. Opt.*, vol. 22, pp. 2374-2379 (1983).

S.C. Rashleigh and M.J. Marrone, "Temperature dependence of stress birefringence in an elliptically clad fiber," *Opt. Lett.*, vol 8, pp.127-129 (1983).

A.J. Barlow, "Optical fiber birefringence measurement using a photoelastic modulator," *J. Lightwave Technol.*, vol LT-3, pp 135-145 (1985).

P.B. Ruffin, J. Sawyer, and C.C. Sung, "Effect of spool diameter on the temperature-dependent extinction ratios of polarization-maintaining fibers," *Optical Engineering* 34 (1), 56-57 (1995).

2.17 SUPERCONDUCTING MATERIALS PROCESSING

Investigators: J. Hurley, E. Karikari, and M. Danjaji

OBJECTIVE

Develop an understanding of the operation and functionality of a Philips X'Pert MPD diffractometer and its applicability in optimizing process parameters to obtain single phase $\text{YBa}_2\text{Cu}_3\text{O}_7$ powder. The process parameters include time, temperature, particle size, and oxygen partial pressure.

BACKGROUND

Commercially available $\text{YBa}_2\text{Cu}_3\text{O}_7$ powders are increasingly being used in the development of electrical and optoelectronic systems. As we learn more about the properties of 1237 yttrium barium copper oxide (YBCO) superconducting systems, we gain insight into ways to ultimately extend present application boundaries. The powders, though often advertised as single phase (pure) materials, generally are marked by inconsistent levels of impurities [1-3]. As applications move toward more quality-sensitive systems, powder purity will increasingly gain attention as we seek to meet new technological challenges.

In our study, powder impurities will be based upon (i) YBCO phases different from (1237), and (ii) extraneous contaminants inherent in the preparation of the $\text{YBa}_2\text{Cu}_3\text{O}_7$ powders such as carbon and moisture. Sample purity is determined from X-ray diffraction (XRD) peak measurements. X-ray diffraction is widely accepted in the evaluation of structural transformations due XRD's ability to clearly identify phases at temperatures above and below the temperature of a

particular phase transition [4,5]. A known strong peak, unique to the target material, $\text{YBa}_2\text{Cu}_3\text{O}_7$, can be monitored for changes, including peak growth or reduction in terms of transitions between superconducting and non-superconducting states.

In analyzing the reactions using X-ray diffraction, the procedure begins with the identification of a specific reaction temperature, followed by the powders undergoing. The percent transformation is determined by dividing the integrated peak intensity of the reaction product at $t_i < t < t_f$ by the integrated peak intensity at $t > t_f$, then plotting this quantity as a function of time from t_i to t_f .

Common practice enlists defining the time for 50% transformation as

$$t(50\%) = t, \quad (1)$$

which leads to a reaction rate (R.R.) such that

$$\text{R.R.} = 1/t \propto a \exp(-DQ/RT), \quad (2)$$

in which

$\text{R.R.} \equiv$ reaction rate,

$t \equiv$ time @ 50% transformation,

$DQ \equiv$ reaction activation energy,

$a, b \equiv$ reactants,

$g \equiv$ reaction products,

$R \equiv$ expansion constant, i.e., a single number describing thermal expansion behavior.

Theoretical equations are used to establish good mathematical fit to experimental data, including:

$$a + Da = a(1 + R)^{(1+T/273)1.5}, \quad (3)$$

wherein,

$a \equiv$ initial lattice constant @ approximately 25 °C,

$Da \equiv$ change in lattice constant when T is changed by an amount DT,

$a \equiv$ fractional change in lattice constant per unit temperature change (thermal expansion coefficient)

$$= 1/a (Da/DT).$$

It is worth noting that the behavior of the isotherms at high and low temperatures serves as the basis for our evaluation. Lower temperature isotherms will approach 100% peak growth much more slowly than higher temperature isotherms. Instead of this phenomenon, the goal is to isolate conditions, temperature and time, under which 100% peak growth occurs most rapidly.

METHODS AND APPROACH

Superconducting and non-superconducting YBCO (1237) powders were scanned at a rate of 0.5°/min. over a diffraction angle range of 5-85° (2q) with and without magnified intensities for peaks possibly masked by the background. Although both sample types showed the similar diffraction profiles, noticeable differences in the intensity and d-spacing of some reflections were observed. Peak assignments and phase identification were accomplished with the Total Diffraction Database TADD). The superconducting powder revealed an absence of a low intensity peak at 11.75 Å which corresponds to a 2q value of 7.52 ° and was shown to correspond to either a 001 or 010 YBCO (1237) non-superconducting peak.

RESULTS AND DISCUSSION

Stecura [1] identified impurity phases in superconducting YBCO (1237) powders after being heat-treated at various times in oxygen, including:

YBa ₂ Cu ₄ O ₈	YBa ₂ Cu ₃ O _{6.56}
YBa ₂ Cu ₃ O ₆	Y ₂ BaCuO ₅
Ba ₂ CuO ₃	Y ₄ Ba ₃ O ₉
Y ₄ Ba ₄ O ₇	Y ₂ Ba ₂ O ₃
Y ₂ BaO ₄	YC _u O ₂
BaCuO ₂	Y ₂ Ba ₄ O ₇
Y ₂ Cu ₂ O ₅	

The TADD revealed the presence of Y₂Cu₂O₅, BaCuO₃, Y₂Ba₂O₃, YC_uO₂, Ba₂CuO₃, BaCu₃O_{6.56}, BaCu₂O₂ phases in the powders. These impurity phases were detected at high diffraction angles from ~ 50 °C < 2q < 85 °C. A relatively strong peak at 1.58 Å was indexed as either an 116 or 123 reflection from YBCO (1237). Although some impurity phases [viz. (1236.8), (1236), Y2Cu2O5, and BaCu2O2] also show a peak at 1.58 Å, the intensity of the peak from 1237 is significantly higher (~ 10 - 15 X). Hence, it can be concluded that this peak might be a true YBCO (1237) peak. The 1.57 and 1.91 Å peaks, likely to come from the (1237) phase, were not detected in the non-superconducting powder.

Diffraction peaks were magnified around the 320 (2q) split peak and indexed as 013 and 103 peaks from YBCO (1237). Although the superconducting and non-superconducting samples revealed peak splitting, the intensities of the peaks were reversed. The PC-Identity package of the Philips X'Pert MPD APD software was used to identify the phases present in the powders. All the peaks in the superconducting and nonsuperconducting powder samples were consistent with standard peaks from YBCO (1237). The following impurity phases were determined through the PC-ID software to be:

YBa ₂ Cu ₄ O ₈	YBa ₂ Cu ₃ O _{6.56}
YBa ₂ Cu ₃ O ₆	Y ₂ BaCuO ₅
Ba ₂ Cu ₂ O ₂	Ba ₂ CuO ₃
BaCuO ₂	Y ₂ Ba ₄ Cu ₇ O

$Y_2Ba_4Cu_7O_{15}$

Impurity phases with elemental composition $Y_xBa_yO_z$ or $Y_xCu_yO_z$ were not detected through available methods. All measurements were accomplished at room temperature due to the unavailability of the furnace.

CONCLUSIONS

The results indicate that although superconducting and non-superconducting powders showed similar diffraction patterns at room temperature; noticeable differences in the intensity and d-spacing were observed for some reflections. A low intensity peak expected at ≈ 11.75 Å for a 2θ value of 7.52° in the YBCO (1237) superconducting powder was missing. The TADD program revealed a peak that could correspond to either an 001 or 010 reflection of the $YBa_2Cu_3O_7$ non-superconductor. Additional tests must be included to distinguish reflection assignment.

Contributions from impurity phases played a much stronger role than originally anticipated. Reflections that were too closely coupled to other impurity phases were often indiscernible from the 237 phase. Results were limited by an inability to make measurements at varied temperatures to correlate theoretical and experimental isotherms. Such measurements will be continued in future studies.

ACCOMPLISHMENTS

- Theoretical Results and Discussion (See above)
- Education and Training

The following students were mentored and trained in this project:

Name	Major	Classification
Affiong Bassey	Engineering (Electrical)	Junior
Amira Sa'Di	Computer Engineering	Junior
Mitchell Smith	Chemistry	Graduate Student
Sandra Sutten	Mathematics/Computer Science	Senior

- Outreach and Technology Transfer
 - Collaborations: University of Florida, Department of Materials Science and Engineering, Dr. Stan Bates
University of Florida, Department of Materials Science and Engineering, Dr. Rajiv Singh
Philips Electronics, Inc.
- Bob Westerdale, Ray Gest, and Pat Cole

REFERENCES

- [1] S. Stecura and W.H. Philipp, Journal of Materials Synthesis and Processing V. 1, No.5, 359-375 (1993)
- [2] S. Stecura, Journal of Materials Synthesis and Processing, V. 2, No. 3, 169-177 (1994)
- [3] D.M. Leeuw et al, Physica C 152, 39-49 (1988)
- [4] D.D.L. Chung et al, "X-Ray Diffraction at Elevated Temperatures", Chapter 5, VCH Publishers, p. 189 (1992)
- [5] W.J. Clegg et al, Nature 322, 58-59 (1988)

2.18 INVESTIGATION OF FRONT FRAME FAILURE IN HIGH PERFORMANCE AIRCRAFT ENGINES

Investigators: Tiejun Bai, Jatinder Singh
Collaborator: James Fabumi, AEDAR Corporation

INTRODUCTION

There are several basic research issues which are being examined in this project. The manner in which the interactions between the duct acoustic modes and the front frame resonant modes affect the effective damping of the strut vibrations is of interest. The effective damping of the front frame struts include the inherent structural damping, as well as the energy exchange between the vibrating struts and the unsteady pressure field. Several basic issues are raised in connection with the computation of the unsteady pressure field itself, since the boundary conditions which have to be imposed on the unsteady fluid equations, are themselves time dependent.

OBJECTIVES

The objective of this research program is to develop a better understanding of the possible causes of unstable vibration of the stationary components in the engine front frame. The long range goal is to develop a methodology for predicting the possible occurrence of unstable vibrations of engine stationary components due to the interaction between the component vibrations and the duct acoustic modes.

APPROACH

The approach of this project is both experimental and theoretical. First of all, experimental results obtained by AEDC have been reduced and analyzed. Then, theoretical model

for damping identification from experimental data has been formulated and implemented into computer programs. The model is then used to analyze the data and obtain damping information.

ACCOMPLISHMENT

Technical Accomplishment

The data reduction and analysis for the available data tapes obtained from full-scale engine tests which were conducted by Arnold Engineering Development Center (AEDC). The results obtained provide considerable insight into the problem under investigation, and help to identify the important parameters in modeling of the problem.

To effectively process the tape recorded data, a new data acquisition and analysis system, including hardware installation and software has been development. The new system consists of a Intel 80486 DX 66MHz based computer, data acquisition boards and necessary software. It uses two data acquisition boards. The first one is a National Instrument EISA-A2000 High Performance Data Acquisition board which is a 12 bit resolution A/D plug-in board for the EISA bus with a 1 MHz sampling rate. The second board is National Instrument AT-MIO-16X. It contains a 16 bit, 100KHz, sampling ADC with up to 16 analog inputs.. The primary software for instrument control and data acquisition is Laboratory Virtual Instrument Engineering Workbench (Lab VIEW) developed by National Instruments Corporation.

The single most significant accomplishment under this program is the work on identification of modal damping coefficients from forced response measurements. Formulation, algorithms and all necessary computer programs have been developed and implemented. Results have been obtained from available tapes. Techniques which will be used to connect the effective modal damping of the front frame struts to the engine operating conditions have also been developed. However, since the limited operating conditions which the data tapes provide, we are unable to conduct trend analysis from the damping identification results. The formulation and algorithms are described in details as follows:

This work is motivated by efforts to understand the causes of excessive vibration stresses which have resulted in premature failures of the front frame struts of the engine. In order to isolate the trends in the occurrence of these unusually high stresses, it is necessary to obtain estimates of the effective damping of the structure at different engine operating conditions. The conventional processing of engine aeromechanical data e.g., Campbell diagrams etc., do not provide this information. However, it is evident that the forced response data measured while the engine is undergoing aeromechanical testing, may contain sufficient information to estimate the effective damping of the resonant modes. A study of the trends in these damping factors should reveal the possible conditions under which the struts can be expected to experience increased vibrational stresses. Under certain assumptions which appear valid for the operation of jet engines, the techniques which have previously been used to identify modal damping from measurements of structural transfer functions can be applied to estimate the effective damping from the forced response measurements. The key idea is to recognize that although the measured responses themselves are not transfer functions, if the spectra of the excitation forces are nearly

uniform, the nature of the forced response spectra in the complex plane, is very similar to that of transfer functions. This requirement is met by the fact that the forced responses of the engine stationary components are derived from engine order excitations whose spectra vary with the engine rotor speed. Therefore, as the rotor speed is steadily increased from low to high, the effective excitation of the engine components are similar to that of a swept sine excitation in modal testing. In the complex plots of the linear forced response spectra, the role of modal constant is played by an unknown quantity (which combines the modal constant and the unknown excitation) which needs not be determined in order to extract the modal damping factor.

The analysis of frequency response data to obtain modal properties was first developed by Kennedy and Pancu (1947) in their work on aircraft flutter testing. Advances made in this field in recent years have been due to the ready availability of powerful computational resources for the rapid analysis of Fast Fourier Transform. The detailed theory of modal testing and analysis have been presented in several publications i.e., [Lang, 1975], [Brown et al, 1977], [Ewins, 1984], [Flannelly et al, 1981], and [Fabunmi et al, 1977]. By starting with the forced responses in the frequency domain, expressed in terms of the mobility functions and the excitation forces, the equations which have previously been used to analyze frequency response functions, can be applied to the linear spectra of the forced responses themselves, in order to yield the modal damping factors. As a result, equations which can be used to develop algorithms for reducing forced response data from engine aeromechanical tests, have been derived. A computer program has also been developed to implement the algorithms.

The linear spectra of the forced responses of a damped structure can be related to the spectra of the excitation forces via the frequency response functions:

$$\{y(\omega)\} = [Y(\omega)]\{f(\omega)\} \quad (1)$$

where $\{y(\omega)\}$ is the $N \times 1$ vector of the forced response, $\{f(\omega)\}$ is the $M \times 1$ vector of the excitation forces, and $[Y(\omega)]$ is the $N \times M$ matrix of the structural frequency response functions. In other words, the response spectra at coordinate "i" due to forces at all the M excitation coordinates is given by:

$$y_i(\omega) = \sum_{j=1}^M Y_{ij}(\omega) f_j(\omega) \quad (2)$$

For a fairly general class of damping mechanisms, the expression for the matrix $[Y(\omega)]$ has been shown to be [Fabunmi, 1985]:

$$\{Y(\omega)\} = \sum_{n=1}^{N \rightarrow \infty} \left[\frac{\{\phi\}_n \{\phi\}_n^T}{m_n} \right] \frac{1}{\Omega_n^2 (1 - (\omega^2 / \Omega_n^2) + i g_n(\omega))} \quad (3)$$

where $\{\phi\}_n$ is the n -th orthonormal mode vector of the structure, $\{\phi\}_n^T$ is its transpose, m_n is the n -th modal mass, Ω_n is the frequency of the n -th mode, and $g_n(\omega)$ is the frequency dependent

damping coefficient of the n-th mode. demoted by A_{ijn} , then:

$$Y_{ij}(\omega) = \sum_{n=1}^{N \rightarrow \infty} \frac{A_{ijn}}{\Omega_n^2(1 - (\omega/\Omega_n)^2 + ig_n(\omega))} \quad (4)$$

and the forced response at coordinate i become:

$$y_i(\omega) = \sum_{j=1}^M \sum_{n=1}^{N \rightarrow \infty} \frac{A_{ijn}f_j(\omega)}{\Omega_n^2(1 - (\omega/\Omega_n)^2 + ig_n(\omega))} \quad (5)$$

Further, let:

$$B_{in}(\omega) = \sum_{j=1}^M \frac{A_{ijn}f_j(\omega)}{\Omega_n^2} \quad (6)$$

and,

$$G_n(\omega) = \frac{1}{1 - (\omega/\Omega_n)^2 + ig_n(\omega)} \quad (7)$$

then the forced response at coordinate i can be written as:

$$y_i(\omega) = \sum_{n=1}^{N \rightarrow \infty} B_{in}(\omega)G_n(\omega) \quad (8)$$

At frequencies close to the resonance of mode n, the forced response is dominated by the contribution of that made to the series in Eq. 8. In the neighborhood of this frequency, following the assumption that the spectra of the excitation forces does not vary sharply with frequency, the forced response can therefore be approximated by the following expression:

$$y_i(\omega) \approx B_{in}(\omega)G_n(\omega) + \varepsilon_n \quad (\Omega_n - \Delta < \omega < \Omega_n + \Delta; \Delta \rightarrow 0) \quad (9)$$

where ε_n is a complex valued residual due to the contributions of the remaining truncated modes. All the quantities in Eq. 9 are complex valued, and in the neighborhood of the resonant frequency Ω_n , the frequency behavior of $G_n(\omega)$ governs the frequency behavior of the forced response. It will further be assumed that the damping function $g_n(\omega)$ appearing in the definition of $G_n(\omega)$ is approximated by its value at $\omega = \Omega_n$, thus:

$$G_n(\omega) \approx \frac{1}{1 - (\omega/\Omega_n)^2 + ig_n(\omega)} \quad (10)$$

In the subsequent discussions, $g_n(\omega)$ will be referenced simply as g_n , the damping coefficient of the n-th mode. The function represented by Eq. 10 has been the subject of

extensive analysis in publications on the subject modal testing and analysis. The following is a brief review of its more relevant properties. The real and imaginary parts of $G_n(\omega)$ are:

$$\operatorname{Re}(G_n(\omega)) = \frac{1 - (\omega^2/\Omega_n^2)}{(1 - (\omega^2/\Omega_n^2))^2 + g_n^2} \quad (11)$$

$$\operatorname{Im}(G_n(\omega)) = \frac{-g_n}{(1 - (\omega^2/\Omega_n^2))^2 + g_n^2} \quad (12)$$

It follows that:

$$\operatorname{Re}(G_n(\omega))^2 + \operatorname{Im}(G_n(\omega))^2 = -\frac{\operatorname{Im}(G_n(\omega))}{g_n} \quad (13)$$

or,

$$\operatorname{Re}(G_n(\omega))^2 + \left(\operatorname{Im}(G_n(\omega)) + \frac{1}{2g_n}\right)^2 = -\frac{1}{4g_n^2} \quad (14)$$

On a Nyquist plot of $G_n(\omega)$, with $\operatorname{Im}(G_n(\omega))$ as ordinate and $\operatorname{Re}(G_n(\omega))$ as abscissa and frequency as parameter, according to Eq. 14, a circle will be obtained. Its center will be at coordinate $(0, -\frac{1}{2g_n})$, and its radius will be $\frac{1}{2g_n}$. For any pair of points on the circle, lying on opposite sides of the resonant frequency, the damping coefficient can be expressed as follows:

$$g_n = \frac{\omega_+^2 - \omega_-^2}{\Omega_n^2(\tan(\theta_+) + \tan(\theta_-))} \quad (15)$$

From Eq. (9), the arc of the Nyquist plot of the forced response spectra will be part of a circle which has been amplified by a factor of $|B_{in}(\omega)|$, rotated about the origin through an angle of $\arg(B_{in}(\omega))$ and then shifted from the origin by the complex residual ε_n . The circle that is fitted to the data in the neighborhood of the resonant frequency will have an origin at some coordinate (a, b) . The point on this circle, diametrically opposite the resonant frequency will have coordinate (e, f) . If the forced response data in the neighborhood of the resonant frequency are represented by an ordered set of numbers denoted by:

$$(\omega_i; \operatorname{Re}(y(\omega_i)); \operatorname{Im}(y(\omega_i))); \quad i = -L, -(L-1), \dots, -1, 0, 1, \dots, L-1, L; \quad \omega_0 = \Omega_n;$$

then following are the necessary formulas needed to identify the modal damping from the forced response spectra:

For each data point i that lies on the circle, we must have:

$$(\operatorname{Re}(y(\omega_i)) - a)^2 + (\operatorname{Im}(y(\omega_i)) - b)^2 = R^2 \quad (16)$$

which expands to:

$$\operatorname{Re}(y(\omega_i))^2 + \operatorname{Im}(y(\omega_i))^2 - 2a\operatorname{Re}(y(\omega_i)) - 2b\operatorname{Im}(y(\omega_i)) = R^2 - a^2 - b^2 \quad (17)$$

For $i=0$, $\omega_0 = \Omega_n$, we have:

$$\operatorname{Re}(y(\Omega_n))^2 + \operatorname{Im}(y(\Omega_n))^2 - 2a\operatorname{Re}(y(\Omega_n)) - 2b\operatorname{Im}(y(\Omega_n)) = R^2 - a^2 - b^2 \quad (18)$$

From above two equations, by subtracting one from another we can have:

$$\begin{aligned} & (\operatorname{Re}(y(\omega_i))^2 - \operatorname{Re}(y(\Omega_n))^2) + (\operatorname{Im}(y(\omega_i))^2 - \operatorname{Im}(y(\Omega_n))^2) \\ &= 2a(\operatorname{Re}(y(\omega_i)) - \operatorname{Re}(y(\Omega_n))) + 2b(\operatorname{Im}(y(\omega_i)) - \operatorname{Im}(y(\Omega_n))) \end{aligned} \quad (19)$$

Because the actual data points will not lie exactly on the circle, the error is defined as:

$$\begin{aligned} \varepsilon_i &= (\operatorname{Re}(y(\omega_i))^2 - \operatorname{Re}(y(\Omega_n))^2) + (\operatorname{Im}(y(\omega_i))^2 - \operatorname{Im}(y(\Omega_n))^2) \\ &\quad - 2a(\operatorname{Re}(y(\omega_i)) - \operatorname{Re}(y(\Omega_n))) - 2b(\operatorname{Im}(y(\omega_i)) - \operatorname{Im}(y(\Omega_n))) \end{aligned} \quad (20)$$

To find (a, b) which minimizes the sum of the squared error, we define:

$$s = \sum_i \varepsilon_i^2 \quad (21)$$

For s with respect to (a, b) , we require:

$$\frac{\partial s}{\partial a} = \sum_i 2\varepsilon_i \frac{\partial \varepsilon_i}{\partial a} = 0 \quad (22)$$

and,

$$\frac{\partial s}{\partial b} = \sum_i 2\varepsilon_i \frac{\partial \varepsilon_i}{\partial b} = 0 \quad (23)$$

which gives:

$$\begin{bmatrix} A & C \\ C & B \end{bmatrix} \begin{bmatrix} a \\ b \end{bmatrix} = \begin{bmatrix} E \\ F \end{bmatrix} \quad (24)$$

where:

$$A = \sum_{i=-L}^L 4[\operatorname{Re}(y(\omega_i)) - \operatorname{Re}(y(\Omega_n))]^2 \quad (25)$$

$$B = \sum_{i=-L}^L 4[\operatorname{Im}(y(\omega_i)) - \operatorname{Im}(y(\Omega_n))]^2 \quad (26)$$

$$C = \sum_{i=-L}^L 4[\operatorname{Re}(y(\omega_i)) - \operatorname{Re}(y(\Omega_n))][\operatorname{Im}(y(\omega_i)) - \operatorname{Im}(y(\Omega_n))] \quad (27)$$

$$E = \sum_{i=-L}^L 2[\operatorname{Re}(y(\omega_i)) - \operatorname{Re}(y(\Omega_n))][\{\operatorname{Re}(y(\omega_i))^2 - \operatorname{Re}(y(\Omega_n))^2\} + \{\operatorname{Im}(y(\omega_i))^2 - \operatorname{Im}(y(\Omega_n))^2\}] \quad (28)$$

$$F = \sum_{i=-L}^L 2[\operatorname{Im}(y(\omega_i)) - \operatorname{Im}(y(\Omega_n))][\{\operatorname{Re}(y(\omega_i))^2 - \operatorname{Re}(y(\Omega_n))^2\} + \{\operatorname{Im}(y(\omega_i))^2 - \operatorname{Im}(y(\Omega_n))^2\}] \quad (29)$$

so that:

$$a = 2 \left(\frac{BE - CF}{AB - C^2} \right) \quad (30)$$

$$b = 2 \left(\frac{AF - CE}{AB - C^2} \right) \quad (31)$$

The coordinate (e,f) is:

$$e = 2 \left(\frac{BE - CF}{AB - C^2} \right) - \operatorname{Re}(y(\Omega_n)) \quad (32)$$

$$f = 2 \left(\frac{AF - CE}{AB - C^2} \right) - \operatorname{Im}(y(\Omega_n)) \quad (33)$$

Now, the modal damping coefficient can be calculated as follows:

$$g_n^{i,j} = \frac{\omega_{+i}^2 - \omega_{-i}^2}{\Omega_n^2(\tan(\theta_{+i}) + \tan(\theta_{-i}))} \quad (34)$$

where:

$$\theta_{+i} = \arccos \frac{[\operatorname{Re}(y(\omega_{+i})) - e][\operatorname{Re}(y(\Omega_n)) - e] + [\operatorname{Im}(y(\omega_{+i})) - f][\operatorname{Im}(y(\Omega_n)) - f]}{\sqrt{\{[\operatorname{Re}(y(\omega_{+i})) - e]^2 + [\operatorname{Im}(y(\omega_{+i})) - f]^2\}\{[\operatorname{Re}(y(\Omega_n)) - e]^2 + [\operatorname{Im}(y(\Omega_n)) - f]^2\}}} \quad (35)$$

$$\theta_{-i} = \arccos \frac{[\operatorname{Re}(y(\omega_{-i})) - e][\operatorname{Re}(y(\Omega_n)) - e] + [\operatorname{Im}(y(\omega_{-i})) - f][\operatorname{Im}(y(\Omega_n)) - f]}{\sqrt{[\operatorname{Re}(y(\omega_{-i})) - e]^2 + [\operatorname{Im}(y(\omega_{-i})) - f]^2} \{[\operatorname{Re}(y(\Omega_n)) - e]^2 + [\operatorname{Im}(y(\Omega_n)) - f]^2\}} \quad (36)$$

The superscript "i,j" in Eq. 16 has been used to underscore the fact that due to the imperfection of measured data, and the approximate nature of the circle fit technique, the value of the damping coefficient calculated using different pairs of points on either side of the resonant frequency, will differ slightly from each other. If all possible combinations of i,j are used, then a statistical technique can be used to determine the mean value of the damping coefficient, as well as its standard deviation.

The software package that came with the Multi-channel Spectrum/Network Analyzer--HP 3566A does not provide the feature to conduct the curve fitting. In addition, the raw data and the results from the FFT routine of the software package are stored in the SDF format. Therefore, to use the data acquired by the HP analyzer and the measurement results from the provided software, the data must be converted into ASCII format so that computer programs written in languages such as Quick Basic, FORTRAN and/or C can be used to further analyze the data. After careful examination of the SDF format and the data storage structure used in the provided software, utility softwares have been used to convert the needed data into ASCII format and then a program has been used to re-arrange the data into a multi-column structure which is convenient to future analysis. Then, a program which conducts circle fitting and calculates the modal damping coefficient is developed. The algorithm and the developed software have been used on the available data tapes to obtain some preliminary results. However, since a complete damping coefficient survey would require data recorded under different engine operating conditions and these additional data tapes have not been made available to CAU, only limited preliminary damping coefficient results are obtained and reported.

Under this program, work on the a concept for on-line damage detection has also been started. To start, AEDAR researchers have chosen a simple system of lumped masses, connected by lumped stiffness and damping elements. The concept is to use data from a number of locations to train a neural network to predict the data at another location. When the system is undamaged, the neural network will show good accuracy of prediction. As soon as a damage occurs in the system, the network to generate an error signal because of the mismatch between its predictions and the actual measurements. This work will be continued in the future.

EDUCATION AND TRAINING

Following students participated in the research program:

1. Corey Echols (Graduate Student, graduated)
2. Dolon Silimon (Junior, Engineering program at CAU)
3. Paceon Walker (Undergraduate Student, Sophomore)

PUBLICATIONS AND PRESENTATIONS

- Corey Echols, Dolon Silimon, Paceon Walker, Jatinder Singh, and Tiejun Bai, "Vibration Analysis of Aircraft Engine Component Using FFT," Mechanical Engineering Symposium, Prairie View A&M University, October, 1994.
- Frederick Ferguson, James A. Fabunmi, and Tiejun Bai, "An Intergro-differential Scheme for the Navier-Stokes Equations," 1994 Winter Annual Meeting of the American Society of Mechanical Engineers (ASME), Chicago, November, 1994.
- Frederick Ferguson, James A. Fabunmi, and Tiejun Bai, "An Analysis of the Aeroelastic Response of Vibrating Surfaces," the 33rd AIAA Aerospace Sciences Meeting, January 9-12, 1995.

REFERENCES

Brown, D., Carbon, G. and Ramsey, K. 1977. "Survey of Excitation Techniques Applicable to the Testing of Automotive Structures," Proceedings SAE, No. 770029.

Capace, V.R. and Fleeter, S. 1987. Unsteady aerodynamic interactions in a multi-stage compressor. *Journal of Turbomachinery*, Transactions of the ASME, Vol. 109, No.3, pp.420-428.

Chi, R.M. 1980. Unsteady aerodynamics in stalled cascade and stall flutter prediction. ASME Paper No. 80-C2/Aero-1.

Ewins, D.J. 1984. "Modal Testing: Theory and Practice," Research Studies Press.

Fabunmi, J.A. 1985. "Extended Damping Models for Vibration Data Analysis," Journal of Sound and Vibration (1985) 101(2), pp. 181-192.

Fabunmi, J.A. and Tasker, F.A. 1988. "Advanced Techniques for Measuring Structural Mobilities," Proc. ASME Journal of Vibration, Acoustics, Stress, and Reliabilities in Design, Vol. 110, pp. 345-349.

Flannelly, W.G., Nagy, E.J. and Fabunmi, J.A. 1981. "Analytical Testing," NASA CR 4329, May 1981.

Giles, M.B. 1990. Stator-rotor interaction in a transonic turbine. *Journal of Propulsion and Power*, Transactions of the ASME, Vol.6, No.5, pp. 621-627.

Kennedy, C.C. and Pancu, C.D.P. 1947. "Use of Vectors in Vibration Measurement and Analysis," Journal of the Aeronautical Sciences, Vol. 14, No. 11, Nov. 1947.

Kerrebrock, J.L. 1977 Aircraft Engines and Gas Turbines. The MIT Press.

Lang, G.F. 1975. "Understanding Vibration Measurements," Application Note No. 9, Nicolet Scientific Corporation.

Morfey, C.L. 1964. Rotating pressure patterns in ducts: Their generation and transmission, *Journal of Sound and Vibration*, (1964) 1, 60-87.

Namba, M. 1977. Three dimensional analysis of blade force and sound generation for annular cascade in distorted flows. *Journal of Sound and Vibration*, (1977) 50(4), 479-508.

Oates, G. C., Aerothermodynamics of Gas Turbine and Rocket Propulsion, AIAA Education Series, Washington, DC, 1988

2.19 RESEARCH IN STRUCTURAL DYNAMICS AND CONTROL AND AEROPROPULSION

Investigators: O. Puri, Tiejun Bai, J. Singh
Collaborator: J. Fabumi, AEDAR Corporation

INTRODUCTION

Forced response problems in high performance aircraft engines have remained major obstacles which must be overcome. Over the past several decades, considerable research effort has been devoted to the forced response and fluid-structural instabilities of rotating components such as fan, compressor and turbine rotor systems. Rotating component, such as compressor blade, are susceptible to nonuniform flows generated by inlet distortion, wakes, and pressure disturbances from adjacent blade rows. Large unsteady aerodynamic loads can be experienced by the blades when they pass through these flow nonuniformities or flow defects. When the frequency of these unsteady aerodynamic loads matches the blade natural frequency, blade failures can occur. However, although non-rotating components can also be subjected to unsteady aerodynamic loads which result in high dynamic stress level in the component, the non-rotating components such as stators and the engine front frame have been validated mainly on the bases of their structural stability and integrity. Little consideration has been given to fluid-structural interactions.

The excessive vibration and the resulting high stress experienced by the front frame struts of the F110-GE-129 caught many people by surprise. At certain conditions, stress on some of the struts significantly exceeded the scope limit for the material, 39.6 KSI, P-P. This limit is fatigue limit based on 10^7 cycles. For the highest stress which occurs at a frequency of 3475 Hz, 10^7 cycles will be exceeded in just 48 minutes. To solve the problem, a large number of experiments which included component test and full scale engine test have been conducted. Based on these tests, the excessive stress levels in the front frame of the F110-GE-129 were due to interactions between the strut's structure and the acoustic field in the duct. Engineering fix which focused on increasing the damping of the front frame strut has been proposed and experimentally validated. Although these measures have increased the structural damping and successfully reduced the

dynamic stress well below the scope limit, the physical mechanisms responsible for this problem is yet to be established.

OBJECTIVES

The objectives of this research project are to reduce and analyze aeromechanical test data obtained from full scale engine tests at AEDC, to investigate the causes for excessive vibration response of the front frame struts of the F110-GE-129 high performance turbofan engine, and to develop analytical and/or empirical models for predicting the conditions under which such high responses occur.

APPROACH

The research consists of two parts, namely 1). data processing and analysis, and 2). numerical modeling of fluid flow. Data analysis of existing tapes was completed and reported. We had waited for availability of geometric profile shapes for the front frame flap, and rotor of first stage of fan. Earlier we had received the geometric profile shapes for the front frame strut. But we did not receive complete information requested. Using the available information and assuming geometric shapes for the flap and rotor, we continued the process of flow analysis.

ACCOMPLISHMENT

Development of Data Processing Capabilities

The data processing equipment consisted of the data reproduction system and the data analysis system. Since the aeromechanical test data provided by AEDC are recorded on 14 tracks of 1 inch wide analog magnetic tapes, the data reproduction system utilized was a HONEYWELL Data Storage Model 101e Portable Tape System. The data analysis system is a 386sx based computer system with adequate software and a Multichannel Spectrum/Network Analyzer--HP 3566A. The tape recorded data were reproduced by the tape system and then acquired by the computer controlled analyzer. The latter then performed analog to digital data conversion, spectral analysis and other operation on the data. In the following, the data processing equipment and the data reduction procedure are discussed.

A HONEYWELL Data Storage Model 101e Portable Tape System was used in the data reproduction. The tape system was a high-performance, IRIG, portable, magnetic tape record/reproduce system with microcomputer control. The system used 1 inch wide magnetic tape with maximum reel size of 15 inches. It had a 14 track head configuration, among them 12 channels that could be set as FM channels and 2 as direct-record channels. It had a self-contained calibration system and could automatically conduct calibration verification. In this system, data electronics were designed for record/reproduce operation at all eight speeds, from 0.937 to 120 ips, without changing plug-ins. A full selection of FM and direct amplifiers was offered for IRIG intermediate band or wideband applications.

The core of the data analysis system was the Multichannel, Spectrum/Network Analyzer--HP 3566A. This analyzer is a powerful time and frequency domain measurement tool, which offers features for all types of mechanical testing, including rotating machinery analysis, vibration

test, structural analysis and acoustic noise testing. The analyzer is linked to a 386sx based computer, HP Vectra QS/16S, which controlled the operation of the analyzer and performed the data analysis and other operations. The analyzer had 8 channels that acquire data simultaneously, and it could expand to 16 channels if necessary. For fast measurement processing, a powerful hardware signal processor module converts time data to frequency data using the latest FFT technology. The analyzer had a dynamic range of 72 dB and maximum frequency span of 12.8kHz. It could acquire data at a maximum rate of 32,768 samples/sec per channel with a cross channel accuracy of 0.1dB (plus or minus).

This project processed a large amount of test data. A high speed, multichannel data acquisition and processing system was vital to this investigation. In addition, the system should offer flexibility to its users for post-processing of data during data analysis phase. The existing Spectrum and Network Analyzer was not designed for mass reduction and analysis of data. As a result, data processing by the existing system was basically manual, through a menu driven environment. It was extremely time consuming and labor intensive. For example, one data point (about 30 seconds recorded data) could take two to three weeks to process. Therefore, to speed up the data processing it was necessary to develop a new system which could acquire and analyze the data in a more efficient way.

Clark Atlanta University purchased the hardware and software for the development of the new data acquisition and analysis system. The system consisted of a Intel 80486 DX 66MHz based computer, data acquisition boards and necessary software. The system was a high speed multichannel data acquisition and processing system, which consisted of a based computer equipped with IEEE488 interface. It used two data acquisition boards. The first one was a National Instrument EISA-A2000 High Performance Data Acquisition board which was a 12 bit resolution A/D plug-in board for the EISA bus with a 1 MHz sampling rate. The board had four analog input channels, each with its own track-and-hold(T/H) circuitry. It could be used in laboratory and industrial environments for instrumentation, waveform recording, and electronic test and measurement applications. The fast 12 bit resolution analog input makes the board useful for high performance signal analysis, transient analysis, pulse-parameter measurement, and data logging. The second data acquisition board is National Instrument AT-MIO-16X. The AT-M10-16X is a high resolution, high performance, multifunction analog, digital, and timing I/O board for the PC AT and compatible computers. It contains a 16 bit, 100KHz, sampling ADC with up to 16 analog inputs, two 16 bit DACs with voltage outputs, eight lines of transistor transistor logic (TTL) compatible digital I/O, and three 16 bit counter/timer channels for timing I/O.

The primary software for instrument control and data acquisition is Laboratory Virtual Instrument Engineering Workbench (Lab VIEW) developed by National Instruments Corporation. LabVIEW is a software system for building high-performance instrumentation and analysis applications. It features a unique icon-based graphical compiled programming language and user interface that provides an integrated environment for engineering and scientific applications. Data can be acquired from GPIB, VXI, RS232 instruments or from National Instruments' plug-in data acquisition board. More than 1430 instruments can be controlled by the ready-to-use icons in the Instruments Library. Analysis functions in LabVIEW include statistical processing, array manipulation and digital signal processing. The graphical user interface includes color graphics with special pan and zoom features and picture import capabilities. To share resources and

exchange information with other research communities, this system is equipped with Ethernet interface.

Software was developed under LabVIEW for data processing. The program was used to acquire the data from an external source (the tape drive in our case) and run an FFT operation on the data acquired. The front panel provided a virtual instrument environment. Through the front panel, the data acquisition board (device), the channels, the amount of data point in each block for FFT, and the sampling frequency could be specified in the front panel. In addition, the windowing function and the low pass filter could be turned on or off, depending upon the needs. The spectrum of the signals were displayed with the time trace on the front panel. The peak value of the spectrum and the frequency at which the peak is located were also displayed.

Further more, the engine rotor speed, which is converted from the NL signals on the 12th track of the analog data tape, was shown graphically by a meter.

Reduction of Experimental Data

All the five data tapes which we received have been analyzed. The results obtained from the analysis include Campbell diagrams and damping identification. In addition, the effects of engine sweeping upon the vibrational response has also been studied. These analysis results will be briefly reviewed in the following.

Campbell Diagrams -- The data obtained from spectrum analysis have been used to construct the Campbell diagrams. These diagrams were constructed by programs developed at CAU, which generates the Campbell diagrams based upon the above mentioned FFT results. The computer code of this program has been reported. The data obtained revealed that all vibrations are forced vibrations which correspond to the 32 order excitations. Examinations of the Campbell diagrams confirm that all significant vibrations are order-related, and they are of the order 32, which is exactly the number of blades on the first stage of the fan. The first stage fan is located immediately down stream of the front frame struts. So far, all the results from various struts conclusively indicate that the excessive vibration of the front frame struts are caused by the downstream flow disturbance that is induced by the sweeping of the first stage fan of the compressor. Since the fan is at the downstream, this disturbance must have been propagated acoustically and exerted on the front frame struts. Therefore, the modeling of the fluid flow and acoustic field in the engine duct and investigation of the interaction among the acoustic waves, fluid flow and the strut structure are critical to the elucidation of the physical causes of the excessive vibrations.

Damping Identification -- This work is motivated by efforts to understand the causes of excessive vibration stresses which have resulted in premature failures of the front frame struts of the engine. In order to isolate the trends in the occurrence of these unusually high stresses, it is necessary to obtain estimates of the effective damping of the structure at different engine operating conditions. The conventional processing of engine aeromechanical data e.g., Campbell diagrams etc., do not provide this information. However, it is evident that the forced response data measured while the engine is undergoing aeromechanical testing, may contain sufficient information to estimate the effective damping of the resonant modes. A study of the trends in these damping factors should reveal the possible conditions under which the struts can be expected to experience increased

vibrational stresses. Under certain assumptions which appear valid for the operation of jet engines, the techniques which have previously been used to identify modal damping from measurements of structural transfer functions can be applied to estimate the effective damping from the forced response measurements. The key idea is to recognize that although the measured responses themselves are not transfer functions, if the spectra of the excitation forces are nearly uniform, the nature of the forced response spectra in the complex plane, is very similar to that of transfer functions. This requirement is met by the fact that the forced responses of the engine stationary components are derived from engine order excitations whose spectra vary with the engine rotor speed. Therefore, as the rotor speed is steadily increased from low to high, the effective excitation of the engine components are similar to that of a swept sine excitation in modal testing. In the complex plots of the linear forced response spectra, the role of modal constant is played by an unknown quantity (which combines the modal constant and the unknown excitation) which needs not be determined in order to extract the modal damping factor.

The analysis of frequency response data to obtain modal properties was first developed by Kennedy and Pancu (1947) in their work on aircraft flutter testing. Advances made in this field in recent years have been due to the ready availability of powerful computational resources for the rapid analysis of Fast Fourier Transform. The detailed theory of modal testing and analysis have been presented in several publications i.e., [Lang, 1975], [Brown et al, 1977], [Ewins, 1984], [Flannelly et al, 1981], and [Fabunmi et al, 1977]. By starting with the forced responses in the frequency domain, expressed in terms of the mobility functions and the excitation forces, the equations which have previously been used to analyze frequency response functions, can be applied to the linear spectra of the forced responses themselves, in order to yield the modal damping factors. As a result, equations which can be used to develop algorithms for reducing forced response data from engine aeromechanical tests, have been derived. A computer program has also been developed to implement the algorithms.

The software package that came with the Multi-channel Spectrum/Network Analyzer--HP 3566A does not provide the feature to conduct the curve fitting. In addition, the raw data and the results from the FFT routine of the software package are stored in the SDF format. Therefore, to use the data acquired by the HP analyzer and the measurement results from the provided software, the data must be converted into ASCII format so that computer programs written in languages such as Quick Basic, FORTRAN and/or C can be used to further analyze the data. After careful examination of the SDF format and the data storage structure used in the provided software, utility softwares have been used to convert the needed data into ASCII format and then a program has been used to re-arrange the data into a multi-column structure which is convenient to future analysis. Then, a program which conducts circle fitting and calculates the modal damping coefficient is developed. The algorithm and the developed software have been used on the available data tapes to obtain some preliminary results. However, since a complete damping coefficient survey would require data recorded under different engine operating conditions and these additional data tapes have not been made available to CAU, only limited preliminary damping coefficient results are obtained and reported.

The Effects of Engine Sweeping -- Since the signals were recorded when the engine was decelerating and accelerating respectively, it provides an opportunity to compare the Campbell diagrams for the same pressure probe or strain gauge to investigate the effect of the engine

acceleration or deceleration on the vibratory response of the front frame struts. Comparison of the Campbell diagram for the same pressure probe or strain gauge concludes that the measurement conducted in the deceleration and acceleration process produce same resonant frequencies, roughly the same amplitude of the resonance, and the similar overall trend of the response as the engine speed changes. However, these figures also indicate that although all of them show similar resonant peaks at the same frequencies, the magnitudes of the second peak at the higher frequency are different. It appears that when the engine was accelerating, the response is the highest, and the higher deceleration rate produced the lowest response level.

Computational Resources

Computational resources - hardware and software- required to perform numerical analysis of unsteady viscous flows through axial flow compressors/turbines depends largely on the level of approximations used. For two-dimensional analysis, current generation UNIX workstations give acceptable performance. A computer code (STAGE-2) developed at NASA Ames to perform 2-D viscous flow analysis through the rotor-stator combination was identified as a suitable candidate because a version of STAGE-2 existed which gave acceptable performance on UNIX workstation. Post processing software such as PLOT3D and FAST were also purchased. Also, a comparison of available workstations was done and Silicon Graphic Indigo with Elan Graphics option was purchased. This workstation had 64 MB of memory and 1 GB of disk space. Later, Clark Atlanta University also acquired an IBM Power Parallel system SP1 with 8 nodes and was used for flow analysis.

Modeling of the Fluid Flow in Front Frame/Fan Region

Unsteady flow analysis through a rotor-stator combination such as the IGV/rotor from first stage fan is complex and time consuming even for a 2-D case. In order to calculate time accurate flows, it was decided to do 2-D unsteady viscous flow analysis at several appropriate radial locations along the Front frame struts/rotor of the first stage of fan. This would provide time-accurate pressure distribution at specified operating conditions and result in an envelope of aerodynamic loading on the front frame strut which will then be used in the forced response analysis. With this in mind, hardware/software combination described above were acquired.

Calibration of the Code

STAGE-2 code obtained from NASA Ames was installed on Silicon Graphics Indigo, Elan Graphics Workstation. First step in using this code was to check if this code has been installed correctly. This was done by compiling this code and running it on a sample geometry provided with the code. Results obtained for first five time steps were compared with the results in a sample output provided with the code. This test case validated the installation of the code.

Next logical step was to run this code for a well known test case and see if this code reproduces results reported in published literature. This would also provide much needed practice and insight in using this code. Details of a test case and results obtained from it are described below.

Description of Test Case

Flow inside a two-stage axial-flow compressor with inlet guide vanes has been studied in aerodynamic tests at a low Mach number (Test Case E/CO-5 in AGARD Advisory Report No.

275). The inlet flow is drawn from ambient air and the flow field throughout out the facility is essentially incompressible, (relative Mach number being less than 0.14). The two-stage compressor model has a 5 ft. tip diameter and a hub/tip ratio of 0.8. The mid span wheel speed (at $r/R=0.9$) is $U_m = 153$ ft/sec and the nominal design flow coefficient is $C_x/U_m = 0.51$ where C_x is the average axial flow velocity. The flow path consists of a row of inlet guide vane (IGV) followed by two similar stages: Rotor 1, Stator 1, Rotor 2, Stator 2. The only difference between the stages is that the Rotor 1 stagger angle is increased by 3 degrees relative to the Rotor 2 stagger angle. There are 44 airfoils in the IGV and both stators and rotors.

Grid System

All blade geometries are defined by NACA 65 - series sections with circular arc mean camber lines. The geometry files was provided by Gundy-Burlet (NASA Ames Research Center) with permission from Robert P. Dring (United Technologies Research Center). Since there are 44 airfoils in each row, it was assumed that the flow is periodic from airfoil to airfoil in the circumferential direction, so the flow through only one airfoil-to- airfoil passage needs to be computed.

STAGE-2 code developed at NASA Ames by Gundy-Burlet and Rai (1987, 1988, 1989, 1991) is meant to be very flexible in accepting axial flow geometries with differing number of stages and airfoils in each row. A simple bookkeeping system exists which allows this flexibility. The grid system essentially consists of a system of patched and overlaid grids. If 'n' is the number of rows in the axial direction, then $2 \times (n+1)$ types of zones are used to discretize the flow field. The first and last zones are the inlet and outlet zones respectively. Each airfoil has an inner "O" grid and an overlapping outer grid. The inner and outer zones associated with the N^{th} airfoil are $(2xN)^{th}$ and $(2xN+1)^{th}$ zones respectively. Using this system, 12 grids are required to discretize the five-row system of the compressor. The grid and numbering system are as follows. The inner "O" grids (zones 2, 4, 6, 8, and 10) are generated by an elliptic grid generation process. The grid is densely packed close to surface to resolve viscous effects adequately. The grid size in inner "O" grid is 131 X 25. The grid size at inlet zone (zone 1) and exit zone (zone 12) are 28 X 51 each. The outer grids (zones 3, 5, 7, 9 and 11) are 80 X 51 each and are algebraically generated by shearing Cartesian meshes. Thus the total number of grid points in all 12 zones are 39,631.

Boundary Conditions

There are natural boundary conditions at the compressor inlet and exit as well as the airfoil surfaces. In addition, there are zonal boundary conditions because different zones are used to compute the flow at regions where viscous effects predominate (inner zones) and are important and far away from airfoils where viscous effects are not important (outer zones). These zones overlap at inner and outer zone boundaries and are explained in sufficient details in published works of Rai and Gundy-Burlet (1987, 1988, 1989, 1991). Data are transferred from the outer grid to the inner grid along the inner grid's outermost grid line. Information is then transferred back to the outer grid along its inner boundary. This is done using a nonconservative, linear interpolation technique. Stability is improved by increasing the overlap area. The patch boundaries are also treated in a nonconservative manner. Linear interpolation is used to reach over into the adjoining grid to integrate through the patch boundary.

The conditions throughout the compressor are subsonic. According to characteristic theory, three quantities are specified at the inlet, while one quantity is extrapolated from the interior of the compressor. The flow angle, upstream Riemann invariant, and average total pressure are specified while the downstream Riemann invariant is extrapolated from the interior of the inlet. At the exit, three quantities are extrapolated from the interior and one is specified. The average static pressure is specified, while the upstream Riemann invariant, circumferential velocity, and entropy are extrapolated from the interior. The exit static pressure is specified to be equal to the experimentally determined exit pressure.

The inner boundaries of the body-fitting "O" grids coincide with the airfoil surfaces. Adiabatic-wall, zero-normal-pressure-gradient, and no-slip boundary conditions are imposed on these body surfaces. In the case of the IGV and both stators, the no-slip condition implies specification of zero velocity. For the rotors, the no-slip condition requires that the fluid velocity vector of the surface be set equal to the rotor translation velocity vector. These boundary conditions are implemented implicitly within the iterative integration scheme. Additional details regarding both zonal and natural boundary condition can be found in Rai (1987).

Results

Results were presented for the 2-1/2 stage compressor geometry. Three iterations were performed at each time step, resulting in drop in residual. In the following discussion, a 'cycle' is

$$\frac{2\pi}{N}$$

defined as motion of the blade through an angle equal to $\frac{2\pi}{N}$, where N is the number of blades in stator airfoil following the rotor. Initially, computations were started with a relatively smaller time step (5000 time steps per cycle), and it was gradually increased to 500 time steps per cycle.

Computations for IGV/Rotor of First Stage of Fan

In order to initiate flow analysis in the front frame area of the engine under consideration, geometric data and flow conditions are needed. These were requested but only incomplete information was received about geometry and no flow condition data was provided. Thus the geometry and flow conditions were assumed to initiate computations. There are 13 struts/flaps and 32 rotor blades in the first stage of fan. To do the flow analysis, we chose to compute flow on 2 struts/flaps and 5 rotor sections. In the circumferential direction, we distributed seven such combinations, which meant flow simulation for a geometry of 14 strut/flaps and 35 rotor blades. To account for this and to keep the same blockage ratio, geometry had to be modified by factors of 13/14 for strut/flap and 32/35 for rotor in the circumferential direction. A grid was generated for such a combination.

STUDENT TRAINING AND EDUCATION

This project initiated and implemented a rigorous program of undergraduate and graduate student involvement in the project. These students were introduced to mathematical and mechanical vibration concepts so that they could understand the data reduction process.

Following students participated in the research program:

1. Corey Echols (Graduate Student, graduated)
2. Dolon Silimon (Junior, Engineering Program at CAU)
3. Paceon Walker (Undergraduate Student, Sophomore)

PUBLICATIONS AND PRESENTATIONS

During the period of the project, following presentations, and publications have been generated:

Presentations:

01	Project Briefing	Place - Wright Labs	April 15, 1992
02	Project Briefing	Place - Atlanta, GA	November 17, 1992
03	Presentation	Place - Orlando, FL	February 1993
04	Project Briefing	Place - Atlanta, GA	August 30, 1993

Fabunmi, J. A., Bai, T., Puri, O., Bota, K., and Sunderland, Lt. Carolyn, "Aero-Engine Component Damping Estimation From Full-Scale Aeromechanical Test Data," AIAA Paper 93-1873, AIAA/SAE/ASME/ASEE 29th Joint Propulsion Conference and Exhibit, June 28-30, 1993, Monterey, CA.

Ferguson, F., Fabunmi, J. A., and Bai, T., "An Analysis of Aeroelastic Response of Vibrating Surfaces," AIAA Paper 95-0724, 33rd AIAA Aerospace Sciences Meeting and Exhibit, January 9-12, 1995, Reno, NV.

Echols, C., Silimon, D., Singh, J., and Bai, T., "Application of FFT on Aero-Engine Data Analysis", Second Annual HBCU/Private Sector Energy Research and Development Technology Transfer Symposium, 1994.

2.20 UNSTEADY AERODYNAMICS OF ROTOR-STATOR INTERACTIONS

Investigator: J. Singh
Collaborator: J. Fabuni, AEDAR Corporation

INTRODUCTION

Turbomachinery flows are inherently unsteady and three-dimensional. They include some combination of laminar, transitional, turbulent, separated flows, and incompressible, subsonic, transonic, or supersonic flow regimes. Governing equations for the flow field are the Navier-Stokes equations and their numerical solution for the three-dimensional flow fields is prohibitively expensive and challenges the computing power of present computers in terms of storage and cost. To obtain details of the flow field with reasonable effort and resources, varying degrees of approximations are made to the Navier-Stokes equations for some flow situations. The approximated equations are solved numerically using finite-difference or finite-element methods. Depending on the flow situation and the desired accuracy of the numerical results, appropriate approximations of the Navier-Stokes equations are solved numerically. For a recent comprehensive review of the CFD techniques in the analysis of flow fields in the turbomachinery, see Lakshminarayana [1991].

For routine applications in the design cycle, invariably, potential flow/Euler equation solvers are used to calculate time-averaged pressure distributions on cascades or rotor-stator combination. Manwaring and Wisler (1992) have reviewed the current, unsteady potential flow and Euler equation solvers for routine prediction of unsteady aerodynamic loading on compressors and turbine blading. However, if interest lies in characterization of unsteady flow, specifically, temporal unsteady pressure distributions, then solution of two- and three-dimensional Navier-Stokes equations is required.

In general, for the rotor-stator interaction problem, flow is unsteady and periodic due to the passage of the rotor behind the stator. This coupled with non-uniform wake from the preceding struts/stators produces complex unsteady flow which is further complicated by potential interaction between rotor and stator. This interaction results in unsteady but periodic pressure fluctuations on the rotor and the inlet guide vanes (IGV)/struts. To accurately compute unsteady pressure distributions, viscous flow solvers are required. The flow is essentially three-dimensional, particularly, closer to the end wall and root regions. However, for majority of region surrounding mid span of rotor-stator combination, flow could be approximated as being two-dimensional. This enables one to use two-dimensional Navier-Stokes equation solvers resulting in considerable reduction in computer storage and time requirements, at the same time giving accurate temporal distribution of unsteady pressures. Significant effort has been spent at NASA and related industries in terms of developing CFD analysis capabilities for turbomachinery flows. The state of the art in viscous flow solvers for unsteady aerodynamic

analysis is reviewed first. That will be followed by selection of a particular flow solver for present work. Finally, results obtained so far are detailed and directions for future work is outlined.

Unsteady Viscous Flow Analysis Techniques for Rotor/Stator Interaction Problem: A state-of-the-art in computational fluid dynamic techniques in the analysis and design of turbomachinery is given by Lakshminarayana (1991) and another more recent review by Verdon (1992). Therefore no attempt is made to duplicate that effort. Among all the computer codes for unsteady viscous flow analysis of the rotor stator interaction described in the open literature, STAGE-2 was the only one that has been tested thoroughly against a benchmark test case and was available for use. It was acquired from NASA Ames Research Center.

Work done so far: STAGE-2 computer code has been developed by M. M. Rai and his coworkers at NASA Ames Research Center [Rai (1987), Rai and Madavan (1988), Gundy-Burlet et al. (1989, 1991)] to study unsteady viscous flow through the rotor-stator passage in the axial turbomachinery. Their earlier efforts resulted in the development of the two-dimensional, turbomachinery codes ROTOR-1 and ROTOR-2. These codes were modified later by Karen Gundy-Burlet to handle multistage, multairfoil turbomachinery flows (STAGE-2). In what follows, algorithm for STAGE-2 is described briefly.

Algorithm: In general, numerical solution of the Navier-Stokes equations by iterative techniques requires large amount of computer storage and time. As indicated before, the Navier-Stokes equations can be reduced to potential equation, boundary layer equation, Euler equation, and thin-layer Navier-Stokes equation. These approximations yield acceptable solutions to the flow problems under specific flow conditions. Also, the reduced equations are amenable to efficient computation. Unfortunately, these equations do not provide solutions to general viscous flows containing variety of flow zones that coexist, namely recirculating flow zones, potential flow zones and in some regions adjacent to the body - the boundary layer flow zone. To obtain numerical solution to this complex flow field, solution of the Navier-Stokes equations is prohibitively expensive. To overcome this problem, zonal techniques are used. In this, several zones are identified and the solution is obtained by using the appropriate equation in each zone and finally patching and integrating these regions to obtain a composite solution for the whole flow field.

STAGE-2 uses one such zonal scheme. Flowfield is divided into two basic types of zones. In an inner-zone close to the body where viscous effects are important, thin layer Navier-Stokes equations are solved in a closely spaced "O" grid that surrounds the IGV and rotor. In the outer zone, representing the passage between two blades, viscous effects are assumed small, and Euler equations are solved on a "H" grid that overlaps the inner "O" grid. This overlap allows for transfer of flow variables from one zone to another. Also, these "H" grids for stationary components (IGV, stator) and rotating components (rotors) are allowed to move relative to one another to simulate relative motion between them. This permits interaction problem to be modeled. In the following discussion, a 'cycle' is defined as motion of the blade through an angle

equal to $\frac{2\pi}{N}$, where N is the number of blades in rotor airfoil following the stator. Figure 1a-d shows the geometry under consideration along with the inner and outer grids for rotor and stator sections at quarter-cycle intervals. This highlights relative motion between the rotor and the stator to model the rotor-stator interaction.

The governing equations are cast in the strong conservative form. A fully implicit, finite-difference method is used to march the solution in time. The convection terms are evaluated using a third-order accurate upwind-biased Osher scheme [Rai and Chakravarthy (1986)]. The viscous terms are evaluated using second-order central differences. Flow is assumed fully turbulent and Baldwin-Lomax turbulence model is used to compute the turbulent eddy viscosity. Details of the zonal and natural boundary conditions, grid configurations are discussed by Gundy-Burlet et al (1989). Recently, this code has been adapted to work in a workstation environment [Gundy-Burlet (1991)]. This version is being used on the Silicon Graphic Workstation.

Application of STAGE-2: This code took a long time and effort of many researchers to develop and is very complex. To acquire facility in using this code, a well known test case was selected to gain much needed practice and insight in using this code. Remaining part of this section provides details of that test case and results obtained from that test case so far.

Description of Test Case: Flow inside a two-stage axial-flow compressor with inlet guide vanes has been studied in aerodynamic tests at a low Mach number (Test Case E/CO-5 in AGARD Advisory Report No. 275). The inlet flow is drawn from ambient air and the flow field throughout the facility is essentially incompressible, (relative Mach number being less than 0.14). The two-stage compressor model has a 5 ft. tip diameter and a hub/tip ratio of 0.8. The mid span wheel speed (at $r/R=0.9$) is $U_m = 153$ ft/sec and the nominal design flow coefficient is $C_x/U_m = 0.51$ where C_x is the average axial flow velocity. The flow path consists of a row of inlet guide vane (IGV) followed by two similar stages: Rotor 1, Stator 1, Rotor 2, Stator 2. The only difference between the stages is that the Rotor 1 stagger angle is increased by 3 degrees relative to the Rotor 2 stagger angle. There are 44 airfoils in the IGV and both stators and rotors.

Grid System: All blade geometries are defined by NACA 65 - series sections with circular arc mean camber lines. The geometry files was provided by Gundy-Burlet (NASA Ames Research Center) with permission from Robert P. Dring (United Technologies Research Center). Since there are 44 airfoils in each row, it was assumed that the flow is periodic from airfoil to airfoil in the circumferential direction, so the flow through only one airfoil-to-airfoil passage needs to be computed.

STAGE-2 code developed at NASA Ames by Gundy-Burlet and Rai (1987, 1988, 1989, 1991) is meant to be very flexible in accepting axial flow geometries with differing number of stages and airfoils in each row. A simple bookkeeping system exists which allows this flexibility. The grid system, essentially consists of a system of patched and overlaid grids. If ' n ' is the

number of rows in the axial direction, then $2 \times (n+1)$ types of zones are used to discretize the flow field. The first and last zones are the inlet and outlet zones respectively. Each airfoil has an inner "O" grid and an overlapping outer grid. The inner and outer zones associated with the N^{th} airfoil are $(2 \times N)^{th}$ and $(2 \times N+1)^{th}$ zones respectively. Using this system, 12 grids are required to discretize the five-row system of the compressor. The inner "O" grids (zones 2, 4, 6, 8, and 10) are generated by an elliptic grid generation. The grid is densely packed close to surface to resolve viscous effects adequately. The grid size in inner "O" grid is 131 X 25. The grid size at inlet zone (zone 1) and exit zone (zone 12) are 28 X 51 each. The outer grids (zones 3, 5, 7, 9 and 11) are 80 X 51 each and are algebraically generated by shearing Cartesian meshes. Thus the total number of grid points in all 12 zones are 39,631. Figures 20.1a-d show clearly the inner and outer grids (zones 2 through 11).

Boundary Conditions: There are natural boundary conditions at the compressor inlet and exit as well as the airfoil surfaces. In addition, there are zonal boundary conditions because different zones are used to compute the flow at regions where viscous effects predominate (inner zones) and are important and far away from airfoils where viscous effects are not important (outer zones). These zones overlap at inner and outer zone boundaries and are explained in sufficient details in published works of Rai and Gundy-Burlet (1987, 1988, 1989, 1991). Data are transferred from the outer grid to the inner grid along the inner grid's outermost grid line. Information is then transferred back to the outer grid along its inner boundary. This is done using a nonconservative, linear interpolation technique. Stability is improved by increasing the overlap area. The patch boundaries are also treated in a nonconservative manner. Linear interpolation is used to reach over into the adjoining grid to integrate through the patch boundary.

The conditions throughout the compressor are subsonic. According to characteristic theory, three quantities are specified at the inlet, while one quantity is extrapolated from the interior of the compressor. The flow angle, upstream Riemann invariant, and average total pressure are specified while the downstream Riemann invariant is extrapolated from the interior of the inlet. At the exit, three quantities are extrapolated from the interior and one is specified. The average static pressure is specified, while the upstream Riemann invariant, circumferential velocity, and entropy are extrapolated from the interior. The exit static pressure is specified to be equal to the experimentally determined exit pressure.

The inner boundaries of the body-fitting "O" grids coincide with the airfoil surfaces. Adiabatic-wall, zero-normal-pressure-gradient, and no-slip boundary conditions are imposed on these body surfaces. In the case of the IGV and both stators, the no-slip condition implies specification of zero velocity. For the rotors, the no-slip condition requires that the fluid velocity vector of the surface be set equal to the rotor translation velocity vector. These boundary conditions are implemented implicitly within the iterative integration scheme. Additional details regarding both zonal and natural boundary condition can be found in Rai (1987).

Results: Results are calculated for the 2-1/2 stage compressor geometry using STAGE-2. Three iterations were performed at each time step, resulting in drop in residual. Initially, computations were started with a relatively smaller time step (5000 time steps per cycle), and it was gradually increased to 500 time steps per cycle. Each time step took about 55.6 CPU seconds on SGI Indigo Elan with 64 MB of main memory. On Cray YMP, it took 3.9 CPU seconds per time step (Gundy-Burlet, 1991). Time-averaged quantities converged after 12 cycles and it took about 120 hours of CPU time for calculations on SGI Indigo Elan for present grid.

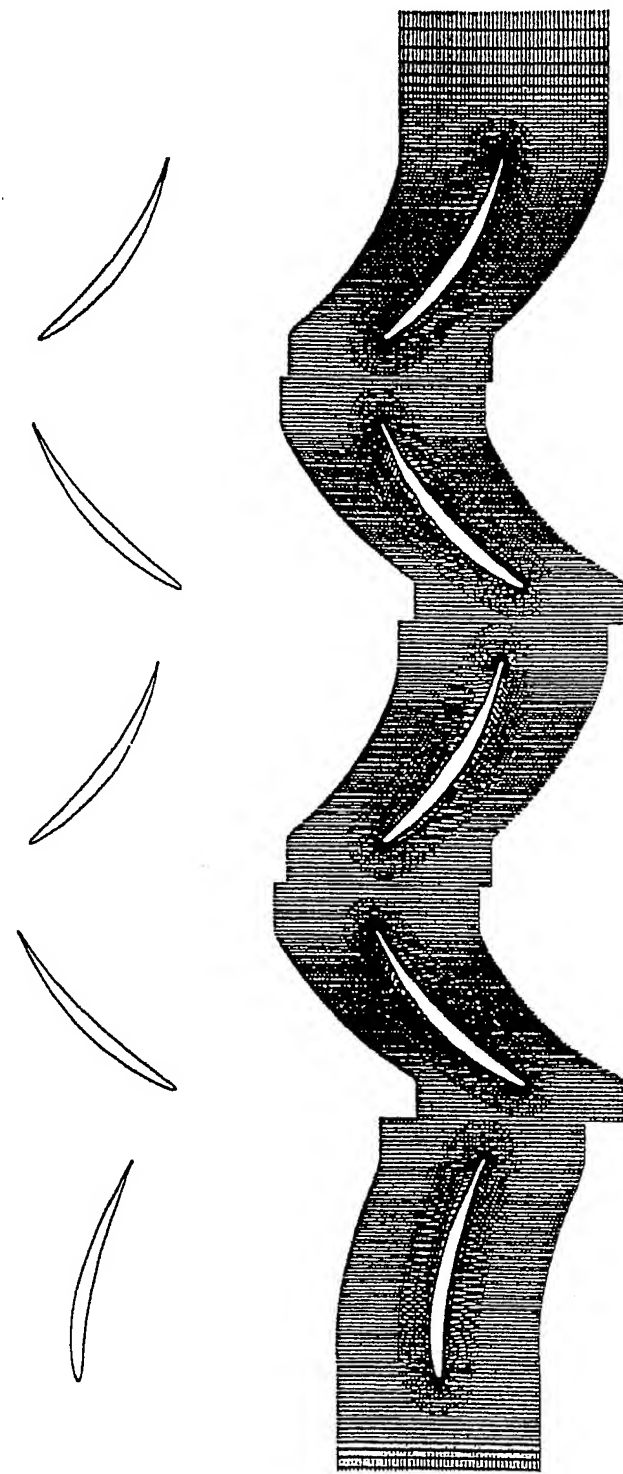


Figure 26.1. Geometry of 2¹/₂ stage compressor and grid around it for $\tau u = 0$

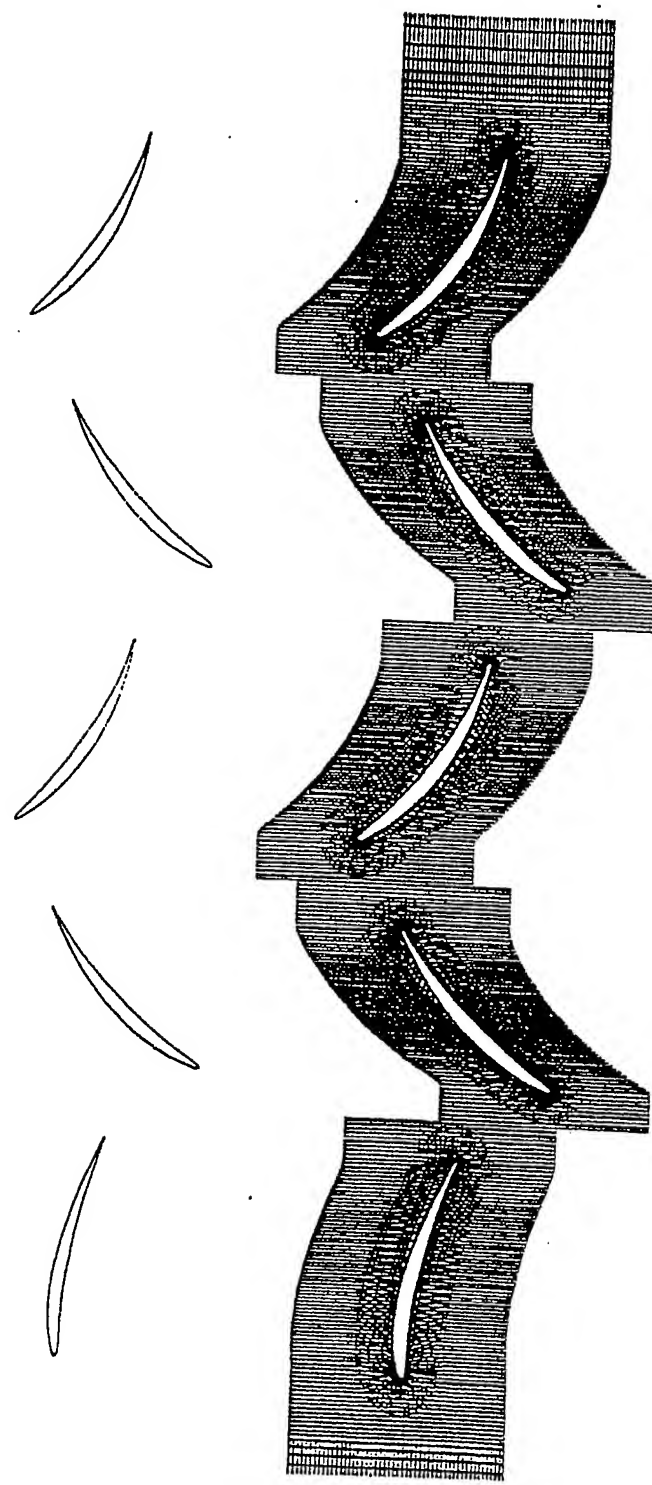


Figure 20.2 Geometry of 2 1/2 stage compressor and grid around it for $\tau_{u0}=0.25$

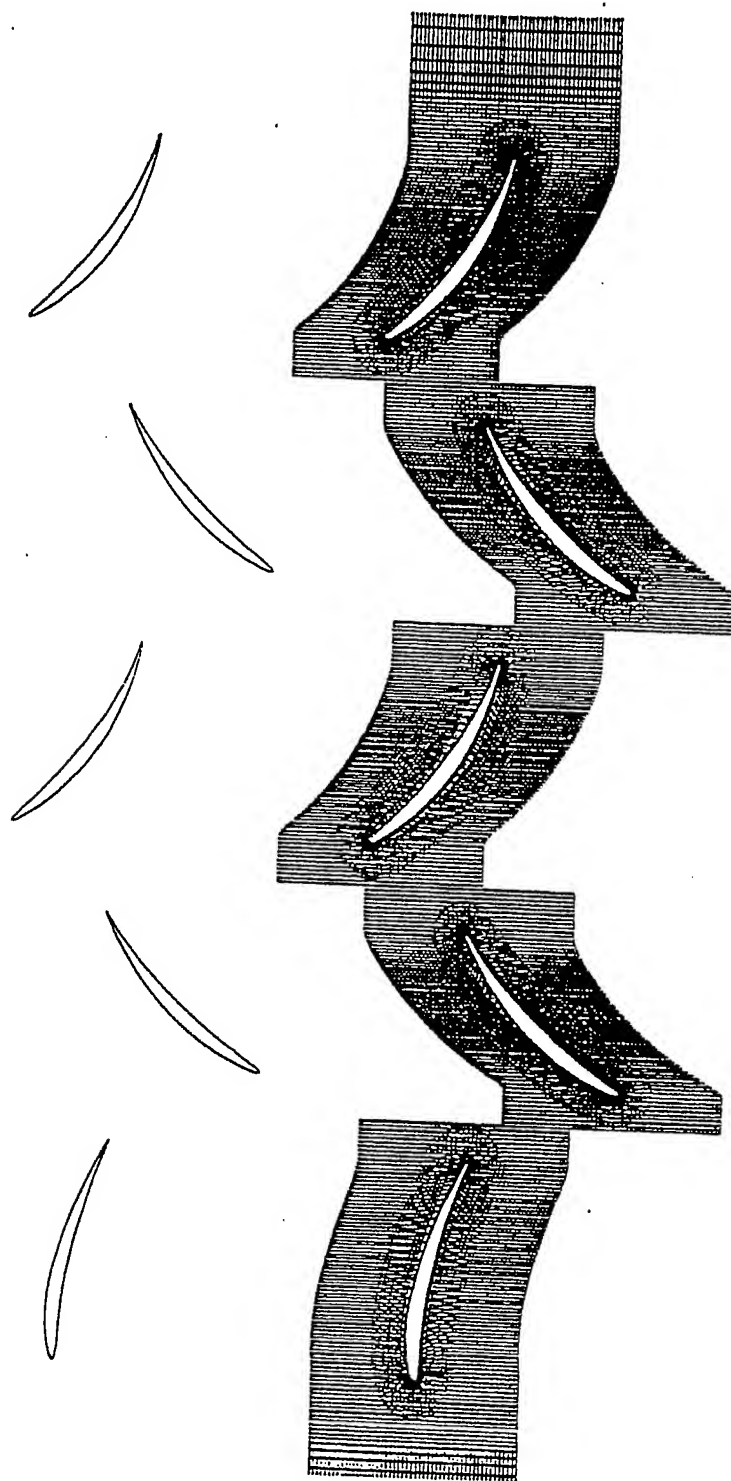


Figure 20.3 Geometry of 2 1/2 stage compressor and grid around it for $\tau_{u=0.50}$

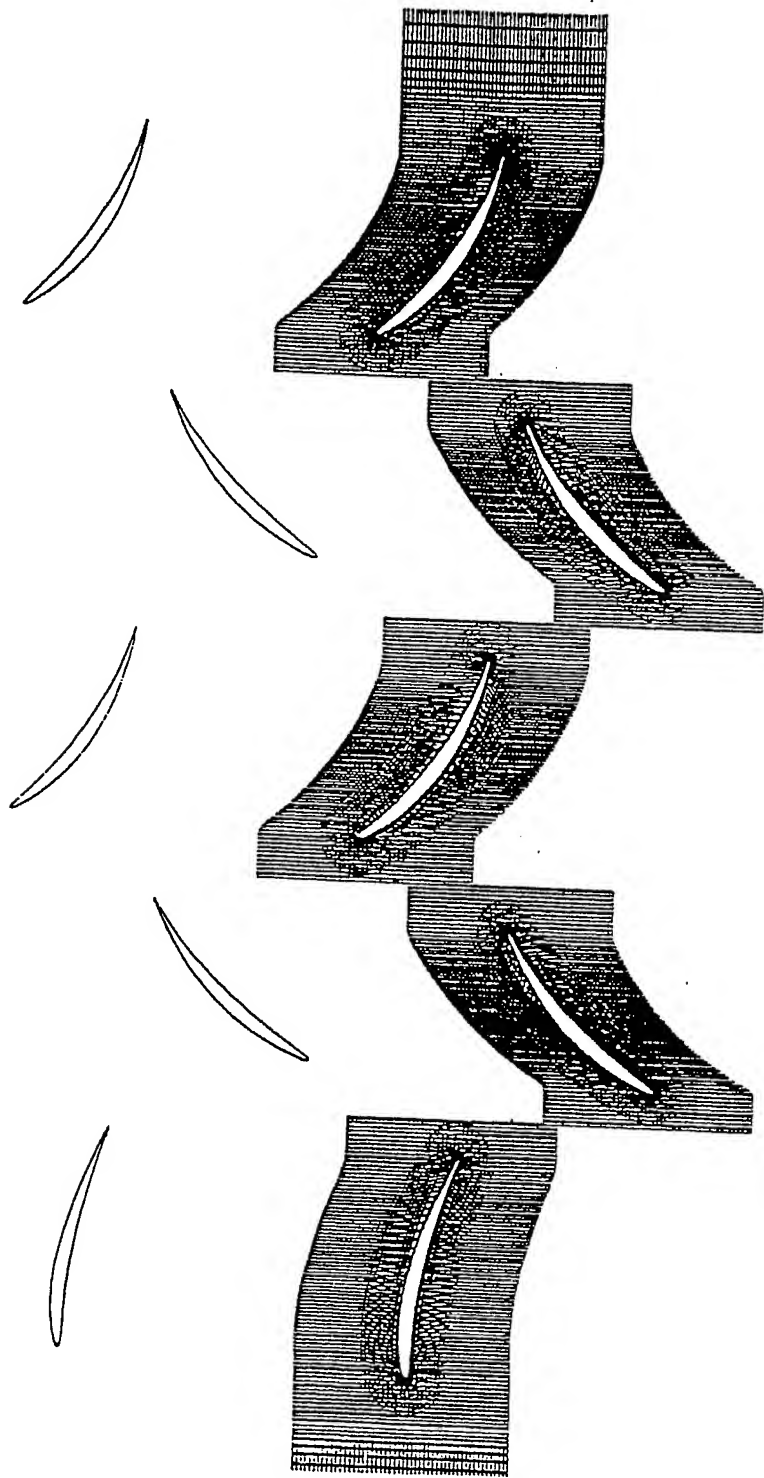


Figure 20.4 Geometry of $2\frac{1}{2}$ stage compressor and grid around it for $\tau_{u1}=0.75$

Figure 20.2 shows instantaneous pressure contours at $\tau\omega = 0$ during the twelfth cycle. Here $\tau\omega$ is the nondimensional time and varies between zero and one for a cycle. Although in this study the flow through only one passage of each row in the compressor is computed, for the sake of clarity, the periodicity condition has been used to generate additional passages. In this case, flow is essentially incompressible and there is insignificant flow separation. There is a small difference in pressure contours between the two stages. However in the case of off design operation, it is expected that there would be flow separation and the vorticity from upstream stages will interact with downstream row to produce much different pressure contours.

Figure 20.3a-d shows instantaneous entropy contours at quarter-cycle intervals. These entropy contours demonstrate that wake from the first rotor interacts with wake from second stator and with second stator as well causing the flow in the second stage to be more complex than through the first stage. It is also clear that wake convects downstream extending many chordlengths and causes fluctuations in surface pressure in the second stage.

Figure 20.4 shows pressure coefficients for the second stage rotor and stator in terms of the time-averaged surface pressures. The time-averaged static pressure is arrived at by averaging the instantaneous static pressures over one cycle. Pressure coefficient C_p is defined as

$$C_p = \frac{p_{avg} - (p_t)_{inlet}}{\frac{1}{2} \rho_{inlet} U_m^2}$$

where p_{avg} is the time-averaged static pressure, $(p_t)_{inlet}$ is the average total pressure at the inlet, ρ_{inlet} is the average density at the inlet and U_m is the rotor speed at the midspan of the blade. Pressure is plotted against axial position in the compressor. The axial gap between the pressure coefficient plots of rotor and stator represents actual axial gap. These values are in good qualitative agreement with the experimental values. Gundy-Burlet(1991) has reported these results but for a much finer grid and as expected results show excellent agreement with experimental values.

DIRECTIONS FOR FUTURE WORK

Lakshminarayana (1991) had reviewed the state-of-the-art in computational fluid dynamic techniques in the analysis of turbomachinery and made recommendations for future research. Two of these are

- a) Improved turbulence models to better account for flow unsteadiness for improved accuracy of numerical results, and
- b) adapting the code to massively parallel computers to cut down on computational time.

In consultations with the NASA Lewis scientists, where bulk of unsteady aerodynamic work for turbo machinery is being done in the US, these two topics will be pursued vigorously in the next two years.

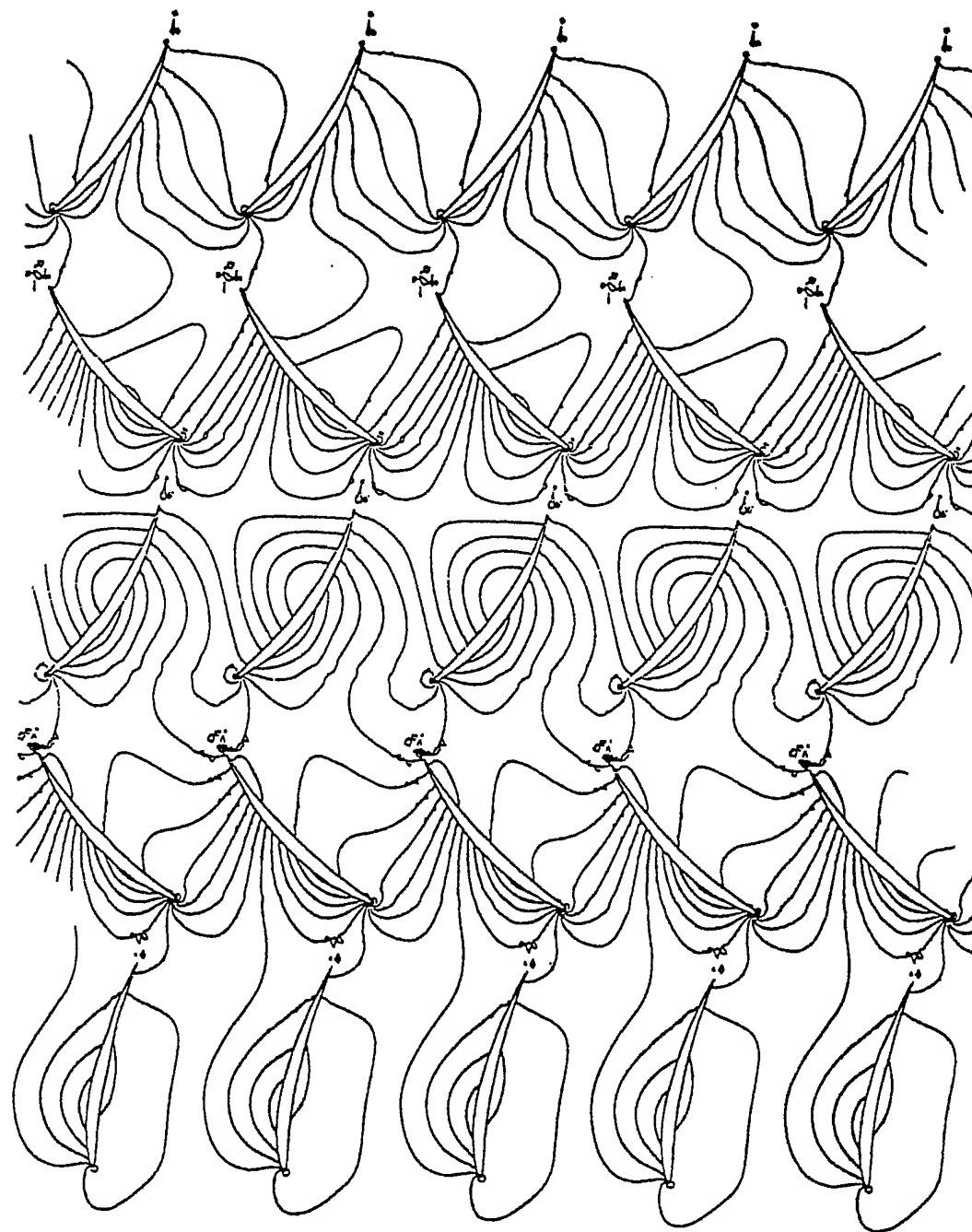


Figure 20.5 Instantaneous pressure contours for $\tau u=0$

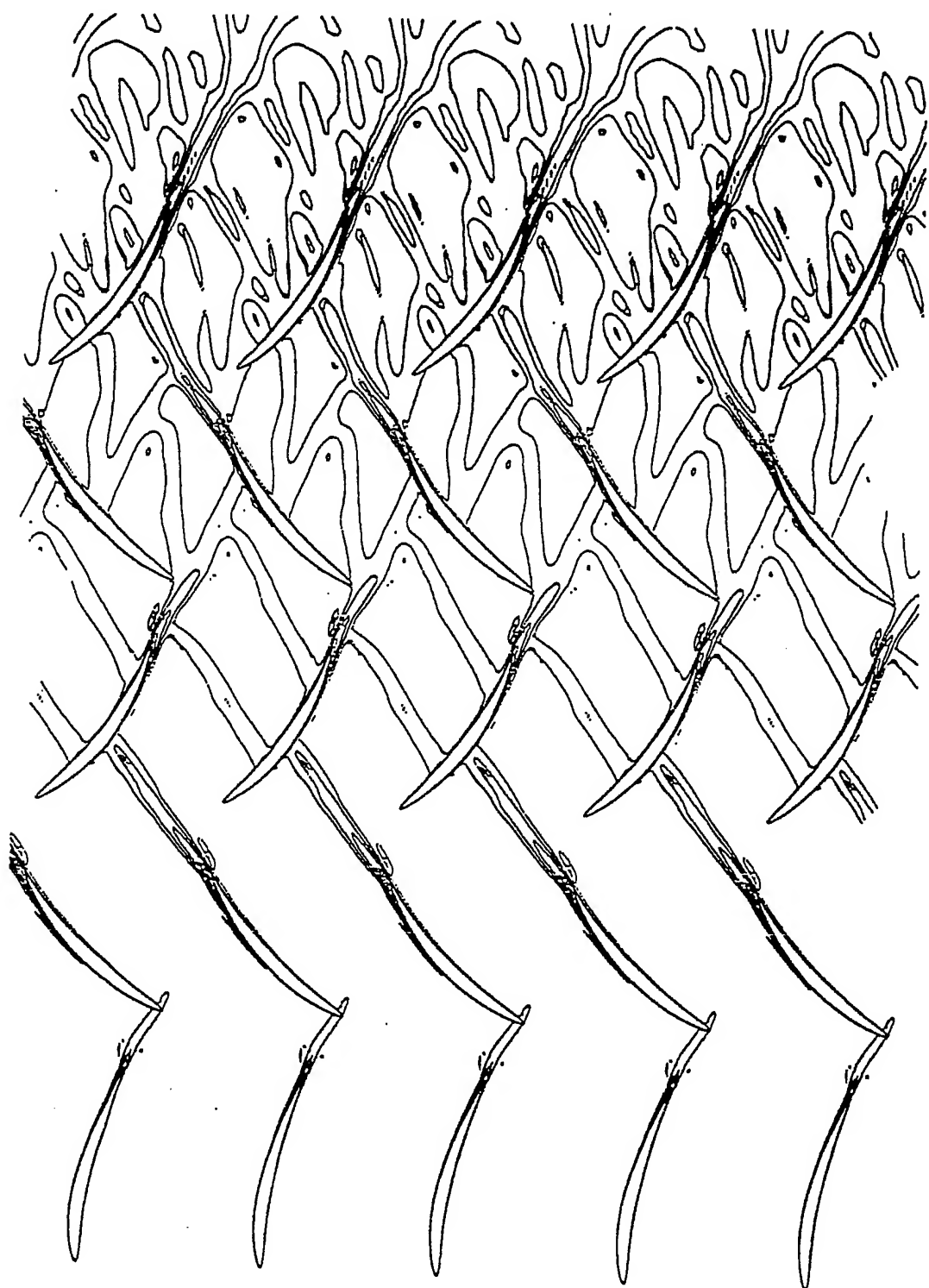


Figure 20.6 Instantaneous entropy contours for $\tau u = 0$

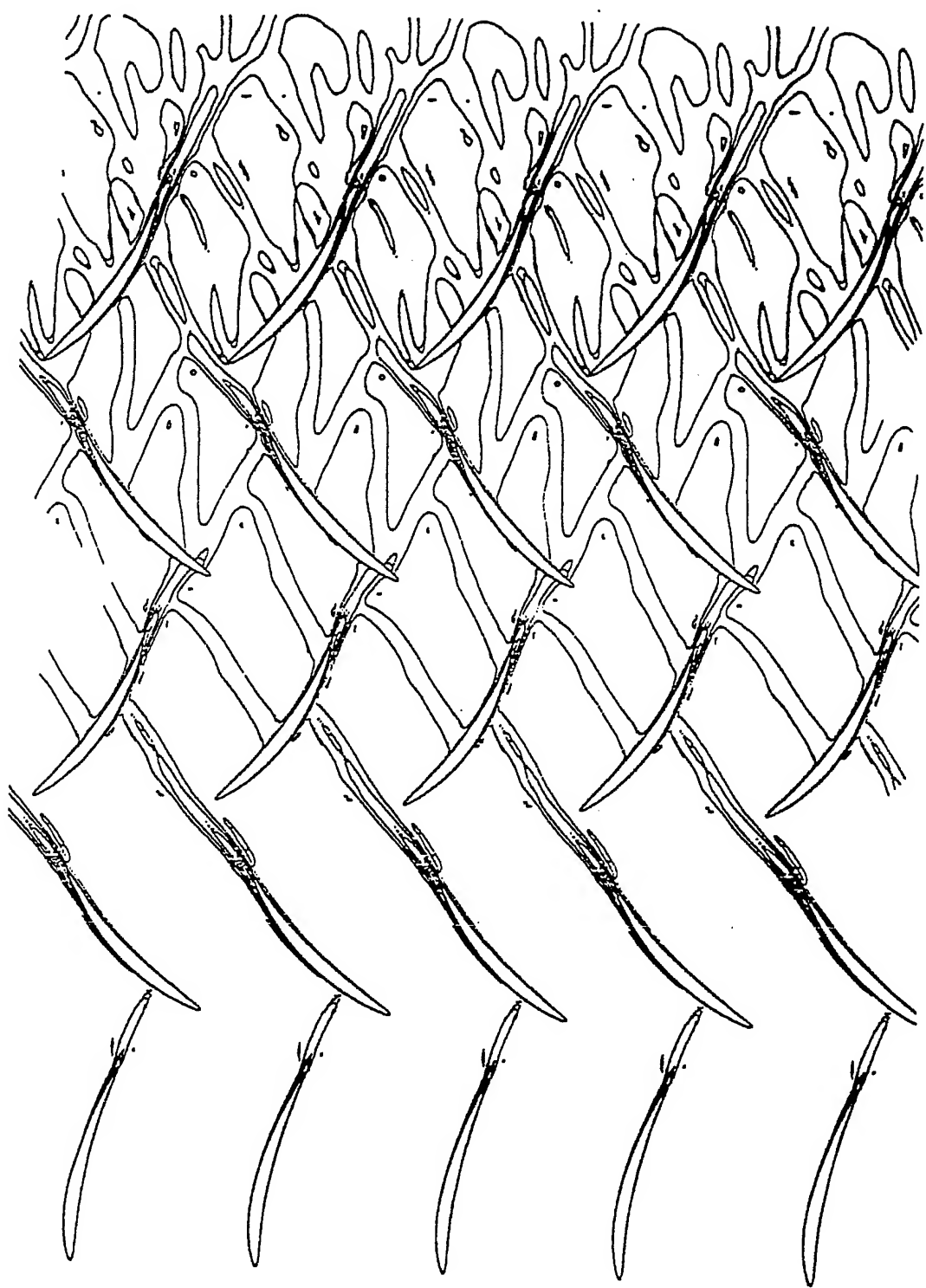


Figure 20.7 Instantaneous entropy contours for $\tau_{\text{in}}=0.25$

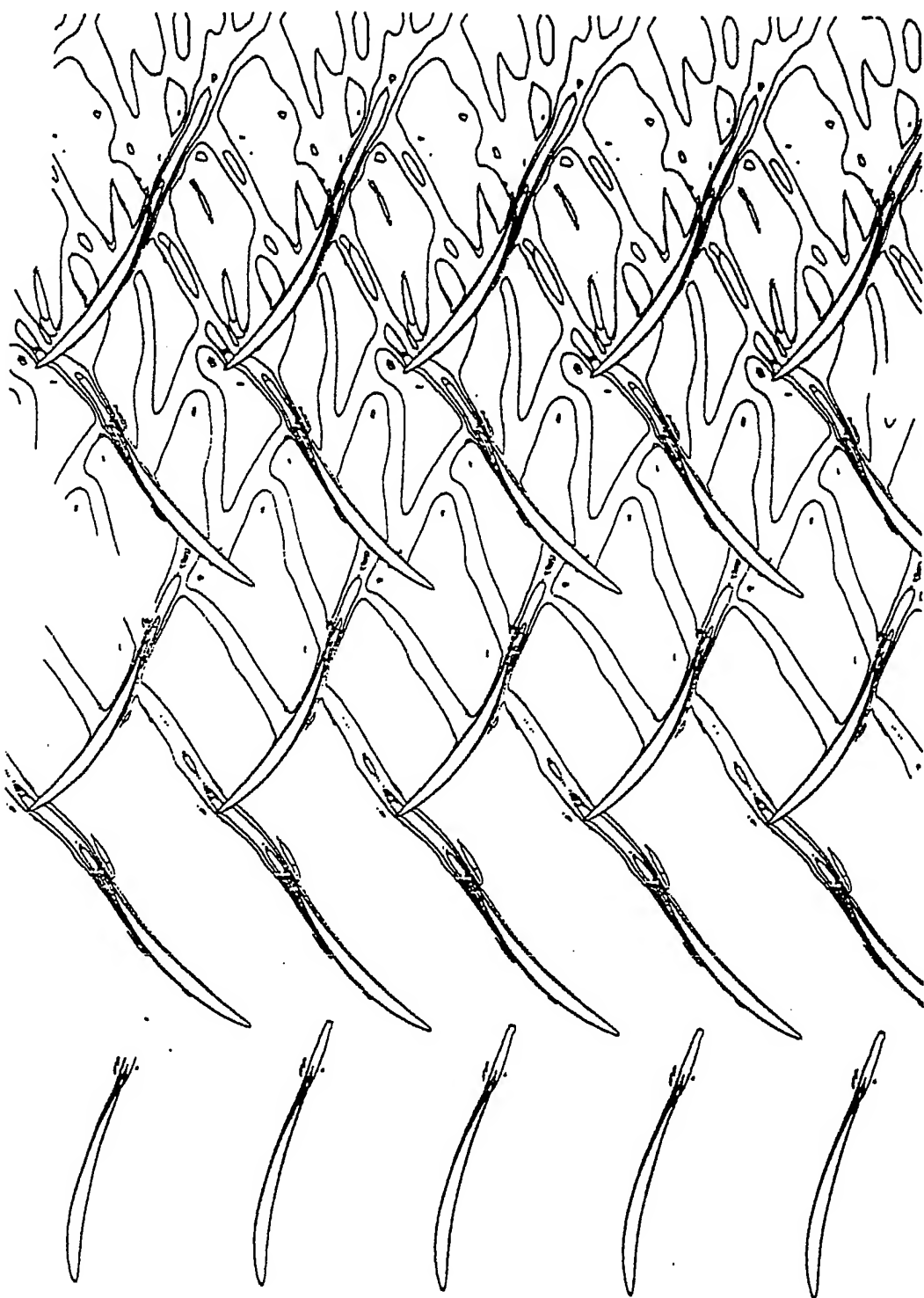


Figure 20.8 Instantaneous entropy contours for $\tau u = 0.50$

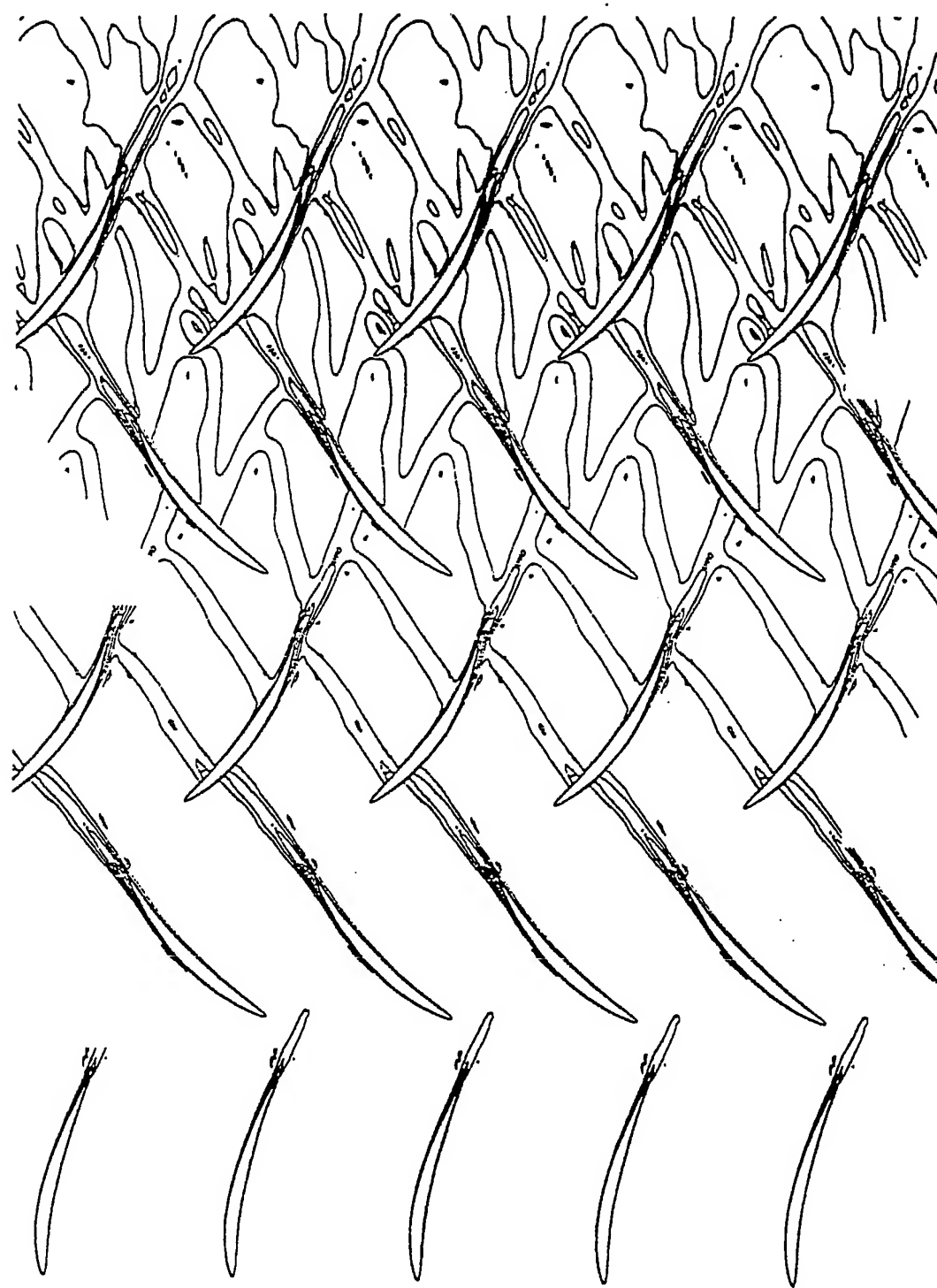


Figure 20.9 Instantaneous entropy contours for $\tau u=0.75$

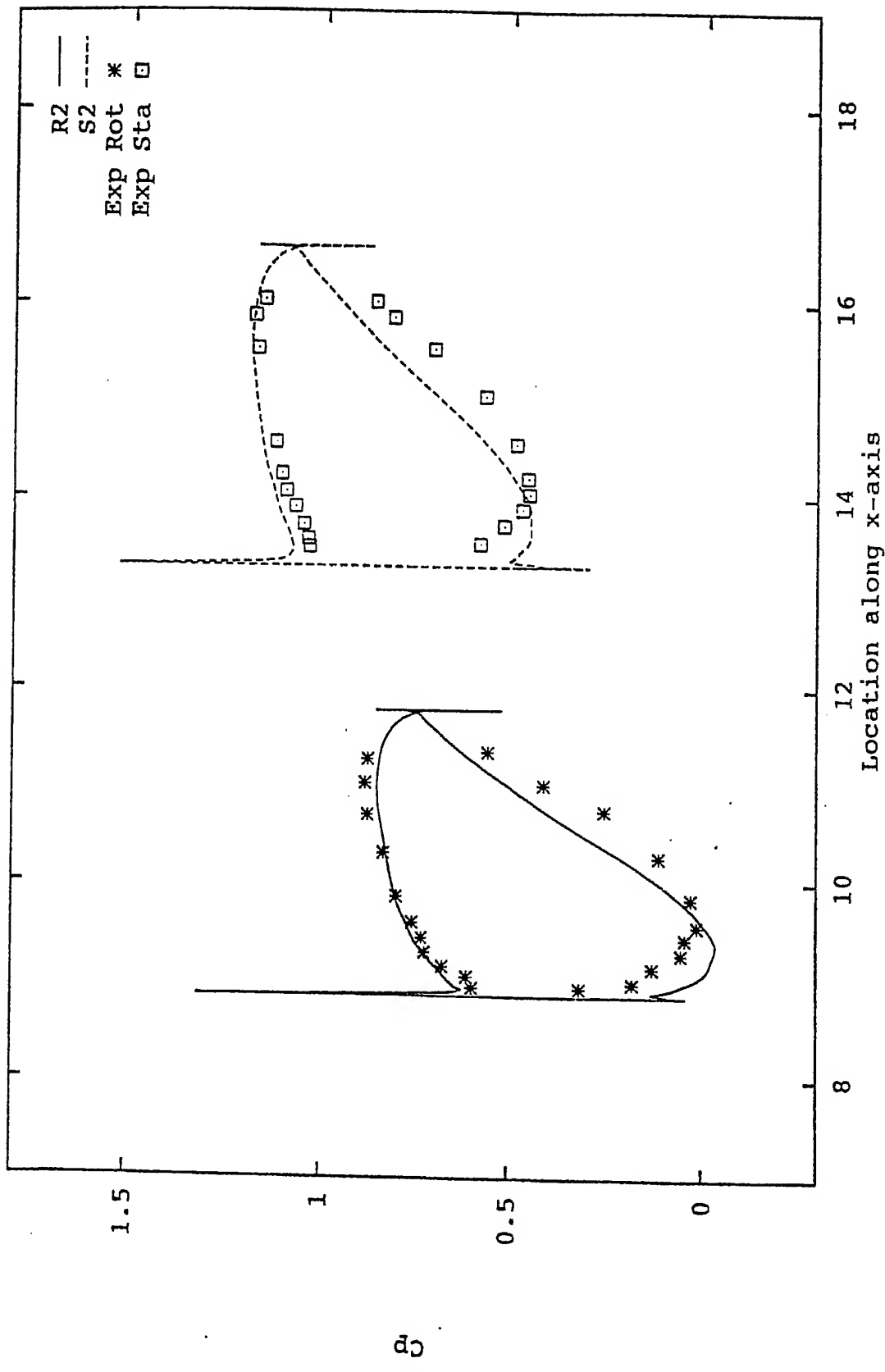


Figure 20.10 Time-averaged surface pressure coefficient for twelfth cycle.

REFERENCES

1. Gundy-Burlet, Karen L., Man Mohan Rai, and Robert P. Dring (1989), "Two-Dimensional Computations of Multi-Stage Compressor Flows Using a Zonal Approach," *AIAA Paper 89-2452*.
2. Gundy-Burlet , Karen L., (1991), "Computations of Unsteady Multistage Compressor Flows in a Workstation Environment," *ASME Paper 91-GT-336*.
3. Gundy-Burlet, Karen L., M.M. Rai, R.C. Stauffer, and R.P. Dring (1991), "Temporally and Spatially Resolved Flow in a Two-Stage Axial Compressor: Part 2 - Computational Assessment", *Journal of Turbomachinery*, April, Vol. 113, pp 227-232.
4. Lakshminarayana, B. (1991) , "An Assessment of Computational Fluid Dynamic Techniques in the Analysis and Design of Turbomachinery- The 1990 Freeman Scholar Lecture," *Journal of Fluids Engineering*, September, Vol. 113, pp 315-352.
5. Manwaring, S.R., and D. C. Wisler (1992), "Unsteady Aerodynamics and Gust Response in Compressors and Turbines," *ASME Paper 92-GT-422*.
6. Rai, Man Mohan, and Sukumar R. Chakavarthy (1986), "An Impact Form for the Osher Upwind Scheme," *AIAA Journal*, Vol. 24, No. 5, May 1986.
7. Rai, Man Mohan (1987), "Navier-Stokes Simulations of Rotor/Stator Interaction Using Patched and Overlaid Grids," *Journal of Propulsion*, Vol. 3, No. 5, pp 387-396.
8. Rai, M.M. and N. K. Madavan (1988), "Multi-Airfoil Navier-Stokes Simulations of Turbine Rotor-Stator Interaction," *AIAA Paper 88-0361*.
9. Verdon, J. M. (1992), "Unsteady Aerodynamic methods for Turbomachinery Aeroelastic and Aeroacoustic Applications", *AIAA Paper 92-0011*.

2.21 AN ADAPTIVE FLOW SOLVER FOR AIR-BORNE VEHICLES UNDERGOING TIME-DEPENDENT MOTIONS/DEFORMATION

Investigator:

J. Singh

Collaborator:

Stephen Taylor, California Institute of Technology

OBJECTIVES

The objectives of the research effort funded by NASA are to develop a flow solver for large-scale, three-dimensional simulations of flow around air-borne vehicles undergoing time-dependent motions/deformations, and to investigate computational science issues such as optimization techniques to improve memory and processor utilization of parallel machines. The intent is to identify a current flow solver algorithm that works and use this to write a flow solver that solves large scale industrial problems on parallel machines such as the Cray T3D and Intel Paragon, shared-memory multi-processors, and networked workstations. The outcome will be an efficient and versatile solver that is capable of solving flows around complex configurations undergoing time-dependent motions/deformations and will be capable of directly impacting NASA missions.

METHODOLOGY

The work is being carried out by a small multidisciplinary team consisting of an aerospace engineer at CAU (J. Singh - P. I.) with expertise in unsteady flows around nonrigid bodies and CFD and a computer scientist at Caltech (S. Taylor - Subcontractor) with extensive background in issues related to scalable parallel computations and large scale computations of unsteady flows around practical configurations. This effort also supports a group of graduate and undergraduate students at CAU and Caltech. At CAU, an Euler flow solver is being developed. The Euler Equations are being discretized spatially using a finite volume scheme, wherein the physical domain is subdivided into tetrahedral elemental volumes and the integral equations are applied to each volume. The algorithm is same as that of references [Frink (1992), Frink (1994)]. The goal is to have a second order accurate flow solver. At Caltech, emphasis is on enhancing the existing concurrent programming framework. Extensive amount of work in the area of large-scale concurrent simulations [Taylor et al., (1996)] utilizing novel dynamic load balancing algorithms has taken place at Caltech. These efforts have resulted in a set of Scalable Concurrent Programming libraries (SCPlib) that are portable to a wide range of high-performance multi-computers, shared-memory multiprocessors, and networked workstations. This library provides a framework for automatic load balancing, granularity control, interactive flow visualization and is being used in the current work.

ACCOMPLISHMENTS

At CAU: At the initiation of the project, SCPlib components were ported to the SGI workstation at CAU. SCPlib consists of a set of libraries that include the grid library, the structures library, and the part dealing with the concurrent graph abstraction, also known as the graph library. Initial focus was on developing understanding of these library components for parallel implementation and its use by writing simple programs. At the same time, details about the flow solver algorithm and its implementation were being finalized. Coding of the flow solver was initiated in November 19, 1995. Simultaneously, SCPlib components were being enhanced at Caltech (see next paragraph). With the release of newer SCPlib in March 19, 1996, the modifications were incorporated in the Euler flow solver being developed. The initial coding of the Euler flow solver has been completed. Currently we are working on solving flow through a rectangular pipe to checkpoint the grid data input and check various other components of the flow solver. Detailed validation of the code will be carried out by solving flow around ONERA M6 wing for $M=0.84$ and $\alpha=3.06^\circ$. Grid about this wing has been obtained from Dr. Neal T. Frink of NASA Langley Research Center. This grid data is currently being reformatted to be compatible with the input/output routines in the grid library part of SCPlib. This simulation will be completed before end of this summer.

At Caltech: Since the beginning of the project, the team at Caltech has completed integration of optimized load balancing strategies into the SCPlib and has quantified the performance improvements obtained using two large scale three-dimensional applications. One of these is related to a plasma simulation and the other a three-dimensional satellite simulation. This newer version of SCPlib incorporates major changes in the graph library component and simplifies the code development process. This library was transferred to CAU team in March 19, 1996 for integration into the Euler flow solver under development. Work is continuing to further develop the SCPlib and support development effort at CAU.

STUDENT TRAINING

In January 19, 1996, a graduate student - *Yudong Pang*, doing M.S. in Computer Sciences was identified and accepted to work on the project. Simultaneously, two undergraduate students also joined the research team at CAU - *William Slater* and *John Maweu*. Initially, these students were exposed to parallel programming framework and SCPlib by means of reading assignments followed by one on one sessions for answering any questions. One of the undergraduate student was very good resource to the group, having been exposed to the SCPlib concepts before joining this group while he did summer internship at Caltech. At Caltech, *Jerrell Watts*, the graduate student, also being supported by the project, has been a good resource person for answering many questions regarding SCPlib to both the P.I. and the students at CAU.

As an outcome of this research, a journal paper by *Jerrell Watts* and *Stephen Taylor* (1995) of Caltech has been submitted to the IEEE Transactions on Parallel and Distributed

Systems. It is anticipated that work on Euler flow solver will feature in the upcoming AIAA CFD Conference in 1997.

FUTURE WORK

To validate the Euler flow solver, following numerical experiments are planned for flow around ONERA M6 wing. First, flow will be solved using single partition on a single processor on the SGI workstation. This will be equivalent of a scalar run. Next, same case will be run on multiple partitions but on a single processor. This will ensure proper communication across partitions on a single processor. Finally, a run will be made for the case in which multiple partitions are mapped to more than one processor. This will be done on the SGI Power Challenge since it is available for use at the SCP Laboratory at Caltech. These runs will establish accuracy of the flow solver and at the same time validate the inter processor and inter partition communications. It is anticipated that this work will be completed before end of this summer. Once accomplished, we would be ahead of schedule on the tasks proposed in the project. Once the Euler flow solver is developed, extensions to a Navier-Stokes flow solver are straightforward since much of the ground work has already been done. Also, this flow solver is being developed using features such as ease of reuse between applications on widely different type of architecture and ease of extension to other related problems such as to aeroelastic problems in this case. This will entail writing a different module for the structures part and incorporating it in the current flow solver. SCPlib allows for such an integration by virtue of its design. Problems of interest to NASA will be identified and solved. As such this project is significant and will have a major impact on analysis of future air-borne vehicles that may deform during flight. Also the flow solver will have a potential to facilitate development of newer configurations that use unsteady aerodynamic forces advantageously in augmenting the performance while alleviating the undesirable effects associated with separated flows of unsteady origin.

REFERENCES

1. Frink, N. T., "Upwind Scheme for Solving the Euler Equations on Unstructured Tetrahedral Meshes," *AIAA Journal*, Vol. 30, No. 1, pp 70-77, January 1992.
2. Frink, N. T., "Recent Progress Towards a Three-Dimensional Unstructured Navier-Stokes Solver," *AIAA Paper 94-0061*, 1994.
3. Taylor, S., J. Watts, M. Rieffel, and M. Palmer, "The Concurrent Graph: Basic Technology for Irregular Problems," *IEEE Parallel and Distributed Technology*, Vol. 4, No. 2, pp 15-25, Summer 1996.
4. Watts, J. and Taylor, S., "A Practical Approach to Dynamic Load Balancing", Submitted to *IEEE Transactions on Parallel and Distributed Systems*, 1995.

2.22 UNSTEADY AERODYNAMICS OF AIRFOILS UNDERGOING LARGE AMPLITUDE MOTIONS/DEFORMATIONS-PARALLEL IMPLEMENTATION OF INCOMPRESSIBLE VISCOUS FLOWS

Investigator: Jatinder Singh

Performance Period: January 1996 - May 1996

OBJECTIVES

Numerical solutions to unsteady aerodynamic flows around airfoils undergoing time dependent motions/deformations will be studied using integral representation formulations. The objectives are to develop a code that will run on massively parallel machines, and to develop a time-accurate scheme such that the shed vorticity is tracked with minimal numerical diffusion and strength of the shed vorticity is also captured accurately. Computational results will be compared with those from experiments and other numerical studies for validation.

APPROACH

An alternate mathematical formulation, namely the Integral Representation approach for incompressible viscous flows will be used. Briefly, the kinematics of the flow governed by continuity and the definition of vorticity will be recast into an equivalent integral representation using fundamental solution. Also, for the kinetics part of the flow problem described by the vorticity transport equation, an equivalent integral representation will be used. These equations are described below.

Mathematical Formulation

It is well known that governing equations for the incompressible viscous flows are the continuity equation and the Navier-Stokes equation given by

$$\nabla \cdot \vec{V} = 0 \quad (1)$$

$$\frac{\partial \vec{V}}{\partial t} = -(\vec{V} \cdot \nabla) \vec{V} - \frac{1}{\rho} \nabla p + \nu \nabla^2 \vec{V} \quad (2)$$

where \vec{V} , p , ρ and ν are respectively velocity, pressure, density and kinematic viscosity of the fluid; and t is time. By defining vorticity $\vec{\omega}$ as

$$\vec{\omega} = \nabla \times \vec{V} \quad (3)$$

and taking curl of Equation (2) and after some simplifications, following is obtained

$$\frac{\partial \vec{\omega}}{\partial t} = -(\vec{V} \cdot \nabla) \vec{\omega} + (\vec{\omega} \cdot \nabla) \vec{V} + \nu \nabla^2 \vec{\omega} \quad (4)$$

Now Equations (1), (3) and (4) represent an alternate set of governing differential equations. There is an advantage in this formulation because it partitions the problem into a kinematic part and a kinetic part. Equations (1) and (3) represent kinematics of the flow problem dealing with instantaneous relationship between velocity and vorticity. These equations are linear. Equation (4) represents the kinetic aspect of the flow problem and describes the development or redistribution of vorticity in time. The terms on the right hand side represent respectively, convection, stretching and rotation, and diffusion of vorticity with time.

For numerical implementation, Equations (1) and (3) could be solved as a coupled system of linear equations or an equivalent Poisson's equation for the velocity vector given by

$$\nabla^2 \vec{V} = -\nabla \times \vec{\omega} \quad (5)$$

with appropriate boundary condition namely $\vec{V} = \vec{V}_B(t)$ on B (surface of the body).

Alternately, Equation (5) can be written as an equivalent integral representation form for the velocity vector as

$$\vec{V}(\vec{r}, t) = - \int_R \vec{\omega}_o \times \nabla_o P dR_o + \int_B [\vec{V}_o \cdot \vec{n}_o - (\vec{V}_o \times \vec{n}_o) \times] \nabla_o P dB_o, \quad (6)$$

where

$$P(\vec{r}; \vec{r}_o) = -\frac{1}{4\pi |\vec{r} - \vec{r}_o|}$$

This equation has a distinguishing feature in that it permits an explicit point by point evaluation of the \vec{V} everywhere in R , if $\vec{\omega}$ is known in R along with \vec{V} on B . This feature can be exploited fully on scalable parallel computers as follows. If there are ' n ' computational nodes in flow domain and ' p ' processors, then by assigning ' n/p ' nodes per processor, velocity in the flowfield could be computed in parallel.

In addition, the kinetic aspect described by Equation (4) is usually solved by either finite difference or finite element methods. Then Equations (4) and (6) represent an integro-differential approach. However, an integral representation for the vorticity vector can also be obtained and is given by

$$\begin{aligned} \vec{\omega}(\vec{r}, t) = & \int_R (\vec{\omega}_o Q)_{t=0} dR_o + \int_0^t \int_R (\vec{V}_o \times \vec{\omega}_o) \times \nabla_o Q dR_o \\ & - \nu \int_0^t \int_B [\vec{\omega}_o (\nabla_o Q \cdot \vec{n}_o) - Q_o (\vec{n}_o \cdot \nabla_o) \vec{\omega}_o] dB_o \end{aligned} \quad (7)$$

where the principal or fundamental solution Q is defined as solution to

$$\frac{\partial Q}{\partial t} - \nu \nabla^2 Q = 0 \quad (8)$$

and is given by

$$Q(\vec{r}, t; \vec{r}_o, t_o) = \frac{1}{[4\pi\nu(t - t_o)]^{\frac{3}{2}}} \text{Exp} \left\{ -\frac{(\vec{r} - \vec{r}_o)^2}{4\nu(t - t_o)} \right\}$$

In Equation (7), first integral on the right hand side gives the effect of the initial vorticity distribution on the flow. The second integral describes the redistribution of the vorticity by convection, stretching and rotation. The third integral gives the effect of the boundary values of $\vec{\omega}$ on the vorticity distribution at the time level t through diffusion. The distinguishing feature of the integral representation is that it expresses several kinetic processes for redistribution of vorticity as separate integrals. There also exists the possibility of using different numerical quadrature procedures for evaluation of different kinetic process characterized by different time scale and its implementation to scalable parallel computers will be studied in this research.

In order to carry out the kinematic part of the computation using Equation (6) and to advance the solution further, boundary values of vorticity must be determined. To determine the boundary vorticity uniquely, Equation (6) is particularized to boundary S and gives an integral equation with surface vorticity as an unknown and can be easily determined.

It should be noted that both of these are mathematically exact and no other approximations other than contained in the familiar Navier-Stokes equations are used. Underlying mathematical theory and numerical results for 2-D viscous flows have already been presented (see references). The kinematics part of the algorithm is well suited for implementation on parallel machines. Also, the velocity vorticity formulation is well suited for external flow applications because extent of vorticity field is confined to viscous zones only. This feature makes it very attractive to develop parallel implementation such that three-dimensional problems could be solved using current generation computers and parametric studies can be performed. Present effort is a step in that direction. This is an ambitious undertaking because numerical and experimental data on this subject is lacking. It is appropriate that some basework be done beforehand. As a first step, the theory presented before [Singh (1988), Singh and Wu (1994) and Singh (1995)] will be modified and the theoretical modeling work will be continued. Next, an existing viscous flow solver will be modified for comparison and validation. Finally, the parallel version of the viscous flow solver will be implemented.

ACCOMPLISHMENTS

In order to validate the new flow solver, a simpler theoretical analysis is required that yields accurate results under certain restrictive flow conditions. A simplified zonal approach has been developed to deal with deforming airfoils [Singh (1995)]. The theory was modified and explicit expressions for the unsteady aerodynamic forces and moments were derived. These results have been presented at a recent conference [Singh (1996)]. Next step is to develop viscous flow solver capabilities to solve flows around deforming airfoils by modifying an existing flow solver - ZETA. It is an efficient flow solver and provides quick turnarounds in workstation environments. Work is ongoing in that regard. Finally the parallel algorithm will be implemented.

REFERENCES

1. Wu, J. C., "Fundamental Solutions and Numerical Methods for Flow Problems", Int. J. Numerical Methods in Fluids, Vol. 4, 185-201, 1984.
2. Wu, Wang, and Gulcat, "Zonal Solutions of Unsteady Viscous Flow Problems", AIAA Paper 84-1637, June 1984.
3. Singh, Jatinder, "Unsteady Aerodynamics of Deforming Airfoils," AIAA Paper 95-1873, 13th AIAA Applied Aerodynamic Conference, June 19-22, 1995.
4. Singh, Jatinder, "Unsteady Aerodynamics of Deforming Airfoils - A theoretical and Numerical Study," AIAA Paper 96-2162, 1st AIAA Theoretical Fluid Mechanics Conference, New Orleans, June 1996.

2.23 HIGH FREQUENCY RESPONSE OF A NEW FIBEROPTIC PROBE FOR TEMPERATURE FLUCTUATION MEASUREMENT

Investigator: N. K. Talukder

Collaborator: G. Richards, Morgantown Energy Technology Center, Morgantown, WV

INTRODUCTION

A fiberoptic pyrometer capable of sensing high frequency (on the order of 100Hz) temperature fluctuation in gas flow was developed at the Sandia National Laboratories, Albuquerque, NM. Application of this pyrometer to temperature fluctuation measurement in the tail pipe of a pulse combustor was attempted at the Morgantown Energy Technology Center, Morgantown, WV. Although the fluctuating temperature of the probe tip which is a platinum thin film with low thermal mass could be determined accurately enough, the relationship between gas temperature fluctuation and the probe tip temperature fluctuation was not known. The ratio of the amplitudes of these temperature fluctuations, the transfer-function, depends on the unsteady heat convection between the flowing gas and the probe tip, unsteady heat conduction in the probe, and the unsteady heat radiation from the probe tip to the surrounding tube wall.

OBJECTIVE

The objective of this project is to determine the values of the transfer-function for a wide frequency range and for various radiation effects between the probe tip and the channel wall surrounding it.

APPROACH

The problem was approached analytically. A differential equation describing the heat transfer processes including convection, conduction and radiation was written and simplified under the assumption of low relative temperature fluctuation at the probe tip. An analytic solution of the differential equation was sought.

ACCOMPLISHMENTS

A closed solution of the differential equation describing the unsteady heat transfer processes determining the transfer function has been obtained. Transfer-function values for low radiation effects are presented graphically. The graphs are nearly linear and indicate that for practical measurements the gas temperature fluctuations depend on convection, conduction and radiation parameters and could be 100 times those of the probe tip temperature. This also validates the assumption of low relative temperature fluctuation at the probe tip. To determine the transfer-function under specific experimental conditions, the different parameters must be known.

PUBLICATIONS AND PRESENTATIONS

A seminar on this topic was given by N. K. Talukder at CAU Dept. of Physics. Two undergraduate students, Angel Torres and Troy Thompson, participated in these studies. The results were presented at the 10th International Heat Transfer Conference in Brighton, UK in 1994. The following paper was published:

Talukder, N.K.: Analysis of unsteady heat transfer determining high frequency response of a new fiberoptic temperature probe. Proceedings of the 10th International Heat Transfer Conference, Vol. 2, pp. 297-302, IChemE, Symp. Ser. 135, Taylor & Francis, London, 1994.

2.24 EXPERIMENTAL INVESTIGATION OF FLOW DISTURBANCES IN CONSTRICTED ARTERIES

Investigator: N. K. Talukder

Collaborator: A. B. Koblasz, School of Electrical Engineering, Georgia Institute of Technology, Atlanta, GA.

INTRODUCTION

A partial occlusion of an artery due to arterial diseases such as arteriosclerosis causes flow disturbances with certain characteristics depending on the severity of constriction. Analysis of the flow disturbances may lead to a disturbance index related to the degree of constriction. A noninvasive method of flow disturbance measurement combined with digital signal processing may lead to a powerful diagnostic tool aiding Vascular Surgeons in preoperative decision making as well as postoperative patient management.

Pulsed Doppler ultrasonic velocimetry is widely in use for noninvasive blood flow velocity measurement. Doppler signals from a sample volume in a flow field contain frequencies proportional to the flow velocity components along the ultrasonic beam. The velocity components in a fixed sample volume at a short distance (1-2 diameters) vary with the level of disturbance which in turn is expected to depend on the degree of constriction. Hence the power spectra of the Doppler signals should be related to the degree of vessel constriction.

OBJECTIVE

The objective of this project is to determine a correlation between a specifically defined disturbance index and the degree of constriction which may serve as a diagnostic aid in occlusive vascular diseases.

METHODOLOGY

A silicon rubber arterial model and a mechanical device to create variable degree of constriction were used in a pulsatile flow system in vitro. A range gated pulsed Doppler ultrasonic system and a pencil probe were used to obtain signals which were recorded by an audio cassette recorder, digitized using a sound card and analyzed using MATHCAD with the help of a PC.

ACCOMPLISHMENTS

Preliminary results show a distinct dependence of the power spectra obtained for short intervals of time (20 ms) in the deceleration phase of the pulsatile flow when the flow is expected to be unstable. The power spectra were found to become broader with increasing degree of constriction, as expected. A disturbance index was formulated on the basis of theoretical analysis to quantify the broadening of power spectra. This indicator of relative disturbance was found to clearly increase with increasing degree of constriction. However, further extensive studies including different constriction models, symmetric and asymmetric, as well as in vivo experiments using animal models are necessary to establish definite correlation curves that ultimately could facilitate noninvasive estimation of the severity of arterial occlusions in human patients.

PUBLICATIONS AND PRESENTATIONS

A seminar on this topic was given by N. K. Talukder at CAU Dept. of Physics. Two undergraduate students, Ronald Grover and Wendy Haugabrook, participated in these studies.

The results obtained were presented at the 3rd International Symposium on Biofluid Mechanics in Munich, Germany in 1994. The following paper was published:

Talukder, N and Talukder, K.: Doppler frequency spectral broadening as an indicator of the severity of arterial stenoses. Proceedings of the 3rd International Symposium on Biofluid Mechanics, Ser. 17, No. 107, pp 375-379, VDI, Duesseldorf, 1994.

2.25 THERMAL ANALYSIS OF A NOVEL AXIAL POWER MONITOR FOR NUCLEAR REACTORS

Investigators: N. K. Talukder and M. Danaji

Collaborators: H. W. Randolph and H. T. Sessions, Westinghouse
Savannah River Co., Aiken, SC.

BACKGROUND

A new type of axial power monitor was designed and manufactured by Delta-M Corp., Oak Ridge, TN. The thermal sensors of the power monitor are located near several coaxial recesses of a core rod distributed over its length. Calibration tests under steady electrical heating of some of these power monitors were carried out at the Savannah River Technology Center, Aiken, SC. These tests showed a good agreement between the results for two different methods

of electric heating. However, the reasons for the good agreement were not clear. Moreover, the applicability of the test results to actual reactor operation, whereby the heating process is by gamma and neutron irradiation, nedded a physical foundation.

OBJECTIVE

The objective of this project is to analyse the heat conduction in the core of the new axial power monitor and compare its thermal responses for the three different heating methods concerned on the basis of equal heating rates.

APPROACH

The problem was approached stepwise. First, analytic solutions were sought under the simplifying assumption of one-dimensional heat conduction (temperature at a point depends on one space coordinate only). Next a two-dimensional heat conduction analysis (temperature at a point depends on two space coordinate) was carried out taking into account the boundary conditions at the relevant segments of the power monitor, using a finite difference numerical method. In the third step which is underway, an axisymmetric heat conduction analysis is pursued in order to validate the results of the previous steps.

ACCOMPLISHMENTS

Axial (one-dimensional) and radial heat conduction in the respective relevant parts of the power monitor core were carried out for the three different heating methods. The results show good agreement among the thermal responses of the axial power monitor for the three different heating methods concerned. The theoretical results thus confirm the calibration test results and provide a physical basis for expecting the thermal response in actual reactor operation to lie between those for the two electric heating methods, for equal heating rates.

In one of the electric heating the heat source lies along the axis of the core rod and hence heat flow is nowhere purely axial. Although the heat conduction, strictly, is axisymmetric, a two-dimensional heat conduction analysis in rectangular slabs with length- to-width ratio corresponding to the relevant part of the power monitor core was carried out, as a second approximation. The results show only slight (<1%) difference from those of the analytic (one-dimensional) solutions.

EDUCATION AND TRAINING

Three undergraduate students, Quinton Watson, Dierdre Pinckney and Ronald Grover, as well as a graduate student, Donald Holloway, participated in these studies. Donald Holloway's master's Thesis entitled "Numerical Analysis of steady two-dimensional heat conduction with

heat source under various boundary conditions" was based on two-dimensional numerical analysis of heat conduction in rectangular slabs. The results were presented at the Engineering and Architecture '95 Symposium in Prairie View, TX. The following paper was published:

PUBLICATIONS AND PRESENTATIONS

N.K. Talukder and D.R. Holloway: Analysis of heat conduction in a novel axial power monitor for nuclear reactors. Proceedings of the Engineering and Architecture '95 Symposium, Vol. 1, pp 199-204, Prairie View, 1995.

A paper on the latest results of these studies was presented by N. K. Talukder at the 3rd Annual HBCU/Private Sector/Energy Research and Development Technology Transfer Symposium in Atlanta, GA in 1995. At this symposium a student poster presentation on this project was made by R. Grover.

2.26 MODEL STUDIES OF HEART VALVE MOTION UNDER PULSATILE FLOW

Investigator: N. K. Talukder

Collaborator: N. M. Komerath, School of Aerospace Engineering, Georgia Institute of Technology, Atlanta, GA.

BACKGROUND

The closure mechanisms of heart valves have been controversial for a long time. The primary importance of flow pulsation and the insignificance of the roles of vortices and real regurgitation were experimentally confirmed by Talukder et al. (1977) and Reul et al. (1981). The genesis of the apparent back flow or pseudo-regurgitation associated with heart valve closure was not clearly understood. It is important to gain a clearer understanding of the flow phenomena associated with the closure process of the natural heart valves, in order to be able to design more efficient prosthetic valves.

OBJECTIVES

The objectives of this project are to gain insight into the origin of pseudo-regurgitation and to investigate the presence or scope of real regurgitation during the closing movement of the heart valve leaflets.

METHODOLOGY

In these model studies a heart model consisting of a chamber and a verticle tube protruding into the chamber was used. The chamber simulates the left ventricle and the tube simulates the left atrium. Two short (2/3-1 tube diameter) pieces of thread simulating heart valve leaflets were suspended from two diametrically opposite points on the lower end of the tube. As model fluid, as well as a mixture of glycerin (40%) and water to which 200-micron amberlite beads were added for flow visualization. Pulsatile flow between the tube and the chamber was generated by pneumatically varying the pressure in the chamber which is partially filled with air. The plane in which the threads are suspended was illuminated using a laser light sheet. Movements of the threads and the beads in the illuminated layer were observed at right angle to the layer and recorded using a video camera (30 frames/s). Analysis of the video images were done by freeze-frame and split-frame (1/60 s) advance. For select pairs of consecutive images simultaneous velocity vectors in the illuminated plane were determined by applying Spatial Correlation Velocimetry (SCV).

ACCOMPLISHMENTS

The results obtained indicate forward movement of fluid in a central zone during closure movement of valve leaflets under pulsatile flow. Even when the net flow through the valve ring (lower end of the tube) reverses the flow in the diminishing zentral zone remain forward. The apparent back flow or pseudo-regurgitation is clearly due to backward movement of valve and fluid around a diminishing central zone of forward flow. The free ends of the threads indicate forward relative motion of fluid and no reversal of relative velocity of fluid until they touch each other (complete closure). The observations confirm the hypothesis that the heart valves may close without the least back flow through valve aperture.

Two undergraduate students, Allen Thomas and Loyal Christensen participated in these studies. A. Thomas made a student poster presentation at the 3rd Annual HBCU/Private Sector/Energy Research and Development Technology Transfer Symposium in Atlanta, GA in 1995. L. Christensen made a student poster presentation at the 4th Annual HBCU/Private Sector/Energy Research and Development Technology Transfer Symposium in Greensboro, NC in 1996. Some of the above results were presented by N. K. Talukder at the 4th International Conference on Physiological Fluid Dynamics in Gwalior, India in 1995. The following paper was published:

PUBLICATIONS AND PRESENTATIONS

N.K. Talukder and N.M. Komerath: Model studies of mitral valve motion under pulsatile flow. In Advances of Physiological Fluid Dynamics, M. Singh and V.P. Saxena, eds., Narosa Publ. House, New Delhi, pp. 217-221, 1995.

An abstract entitled "Model studies on the origination of pseudo-regurgitation during heart valve closure" was submitted to the ASME and has been accepted for presentation at the 1996 International Mechanical Engineering Congress and Exposition (IMECE) & ASME-Winter Annual Meeting to be held in Atlanta, GA in November, 1996.